UNIVERSITY OF NAPLES FEDERICO II

DEPARTMENT OF AGRICULTURAL SCIENCES

RESEARCH DOCTORATE IN AGRICULTURAL AND FOOD SCIENCES

XXIX CYCLE

PhD Research TOPIC:

AGROHYDROLOGICAL SIMULATION FOR MITIGATION AND MANAGEMENT OF SOIL MOISTURE DEFICIT IN RAINFED AGRICULTURE

Geoffrey OPENY
(MSc. Civil Eng. MAK, BSc. Agric.Eng. MAK)

Thesis submitted to the Department of Agricultural Science in partial fulfillment of the requirements for the award of degree of Doctor of Philosophy in Agricultural and Food Sciences of the University of NAPLES Federico II.

Tutor:	Prof. Mario PALLADINO	Coordinator:	Prof. Eng. Guido D'URSO
Co-Tutor	Prof. Eng. Guido D'URSO		

PORTICI February 2017

ABSTRACT

Drought is a natural disaster that occurs in all climatic regions, and is responsible for food insecurity in majority of developing countries. Globally, interventions to mitigate drought impacts have focused in semi-arid and arid areas. However, increased climatic variations have become more frequent in the recent past causing sporadic agricultural droughts with the end results being food shortages even in areas that receive relatively high rainfall. Many of such areas are occupied by vulnerable communities lacking strategic coping mechanisms for mitigation of drought impacts.

The aim of this study was to develop a simplified approach for computing a *Soil Moisture Deficit Index (SMDI)* that integrates limited climatic records common in developing countries together with freely available tools for supporting soil water management decisions under rainfed agriculture. Most soil moisture based drought indices are derived from long term records of measured soil moisture time series. However, such long-term soil moisture records are scarcely available in African countries where they could be of greatest benefit in designing techniques for mitigating drought impacts. Therefore, the main objective of this research was to evaluate the performance of simulated soil moisture time series to develop a SMDI with minimal requirements of input data.

To this aim, the study was organized in four consecutive objectives, namely: to identify and adapt a suitable drought indicator in relation to the data availability. Secondly, to assess the feasibility of using a calibrated agro-hydrological model for producing long time series of soil water dynamics and derive SMDI for monitoring agricultural droughts. The third objective was to upscale the SMDI through energy balance modeling using a case study in Northern Uganda. And the fourth objective was, to formulate a soil water management decision support scheme for mitigation of agricultural droughts in rain fed farming systems through application of SMDI.

The study is based on agro-hydrological data collected in a dairy farm of 10 ha in Northern Uganda equipped with Mateo station and low cost commercial soil sensors to monitor soil water dynamics in the root zone during two seasons under rain fed maize crops in 2015. Because of the importance of Evapotranspiration in agro-hydrological studies and limited reported research on it at the study site, 13 different simplified reference evapotranspiration (ET_0) models were compared with FAO-56 Penman-Monteith to select the best performing simplified model for application in the study area. Evaluation of the 13 ET_0 models showed

that the Makkink radiation model gave the best prediction of ET_0 with Root Mean Squared Error (RMSE) = 0.6 mm, Mean Absolute Error (MAE) = 0.4 mm, Nash Sutcliffe Efficiency (NSE) = 0.8, Coefficient of Agreement (d) = 0.90 and Coefficient of Determination (r^2) = 0.7. All temperature based models overestimated ET_0 with Thornthwaite giving the worst prediction in all the test statistics.

To address the first objective, the state of the art on soil moisture based drought indices were reviewed and the information gathered applied to formulate a new approach to define SMDI. The second objective was addressed through application of 1-dimensional water flow model (Hydrus 1D); firstly, in inverse mode to derive the soil hydraulic properties and secondly in direct mode to generate soil moisture time series by using the ET_0 model selected in the previous step in conjunction with gridded climatic data combined with limited weather observations. In the calibration phase, Landsat 8 OLI satellite images were used to estimate crop growth variables. In the second objective, published crop coefficients where used to generate continuous boundary conditions for 21-year agro-hydrological simulations. Calibration results showed good agreement between simulations and observations of water storage in the root zone with $r^2 = 0.73$ during calibration and $r^2 = 0.70$ during validation. The results of the long-time series simulations were used to derive threshold parameters for SMDI definition, following the statistical approach suggested by Hunt et al. (2009). Generation of the threshold parameters; i.e.: water content at field capacity (θ_{FC}) and water content at wilting point (θ_{WP}), through agro-hydrological simulations gave good comparison with the laboratory determined values through a pressure plate apparatus on undisturbed soil core samples; with $r^2 = 0.95$. Comparison between number of times SMDI<0, within a growing season and maize yields between 2007 to 2015, showed a negative linear correlation with $r^2 = 0.64$. Precipitation (P) and precipitation deficit (D) were fitted on theoretical probability distributions to calculate reference drought indices i.e. Standardized Precipitation Index (SPI) and Standardized Precipitation Evapotranspiration Index (SPEI). The fitting distributions (a 2-parameter gamma distribution for P, and a 3-parameter log-logistic distribution for D) gave an acceptable Kolmogorov-Smirnov goodness of fit test at 95% level of significance in both cases. All the reference indices [i.e. SPI, SPEI and Atmospheric Water Deficit (AWD)] showed positive correlation with SMDI demonstrating the robustness of SMDI for agricultural drought monitoring in the study area.

The third objective involved analysis of Landsat 8 thermal images to generate evaporative fraction (Λ) through energy balance modeling. A SMDI- Λ regression equation was developed

to spatialize SMDI. A comparison between SMDI and Λ through linear regression showed good agreement with $r^2 = 0.84$. An independent check with different sets of images were performed between the SMDI calculated using the SMDI-Λ regression equation and SMDI generated through agro-hydrological simulations provided a good agreement with $r^2 = 0.85$.

The last objective involved integration of the results obtained from objectives (i) to (iii) to formulate a decision support scheme. SMDI was found useful to delineate dry and the wet season in Northern Uganda; it showed that the dry season begins between November 25 to December 10 and the wet season begins between March 26 to April 5 of each year. A SMDI-based management decision support scheme was proposed, although it would need further investigations to verify its effectiveness. In conclusion, the approaches developed to define SMDI can easily be implemented in any developing country that experiences similar problems in rain fed farming.

ABSTRACT IN ITALIAN

La siccità è un fenomeno naturale tipico di qualunque area climatica, ed è responsabile dell'insicurezza alimentare nella maggior parte dei paesi in via di sviluppo. Dal punto di vista mondiale, gli interventi volti a mitigare gli impatti della siccità sono stati focalizzati sulle zone aride e semi-aride. Tuttavia, in tempi recenti, le crescenti alterazioni climatiche sono divenute più frequenti, causando sporadiche siccità agricole che hanno generato carenze alimentari anche in aree che ricevono precipitazioni relativamente elevate. Le popolazioni in molte di queste aree sono particolarmente esposte ai rischi derivanti da eventi siccitosi poiché sprovviste di meccanismi di adattamento che ne possano mitigare l'impatto.

Per valutare la vulnerabilità alla siccità si ricorre a valutazioni di indici basati su serie temporali di dati climatici e di umidità del suolo. Tuttavia, tali serie sono raramente disponibili in Africa, dove invece esse potrebbero essere di grande beneficio per orientare le strategie in campo agricolo e mitigare gli impatti della siccità. Di conseguenza, l'obiettivo principale di questa ricerca è stato la valutazione delle performance di serie temporali di misure simulate dell'umidità del suolo, al fine di sviluppare un SMDI avente minime necessità in termini di dati di input. Lo studio è stato focalizzato sullo sviluppo di un approccio semplificato per elaborare un indice del deficit di umidità del suolo (SMDI) che integri gli scarsi dati climatici comunemente reperibili nei paesi in via di sviluppo con altri strumenti e informazioni di libero accesso, al fine di supportare le decisioni della gestione delle coltivazioni dipendenti dalle precipitazioni.

Per questo scopo, lo studio è stato organizzato in quattro obiettivi consecutivi. In primo luogo, identificare e adattare un idoneo indicatore di siccità in relazione alla disponibilità di dati. In secondo luogo, verificare l'utilizzabilità di un modello calibrato agro-idrologico per produrre serie di lungo periodo delle dinamiche idriche del suolo e derivare un SMDI per monitorare le siccità agricole. Il terzo obiettivo è stato il miglioramento dello SMDI attraverso la modellistica di bilancio energetico, utilizzando un caso studio nel nord dell'Uganda. Infine, il quarto obiettivo è stato quello di formulare uno schema di supporto decisionale per la mitigazione delle siccità agricole in sistemi agricoli dipendenti dalle precipitazioni attraverso l'applicazione dello SMDI.

Lo studio è basato su dati agro-idrologici raccolti nel 2015 in un'azienda zootecnica-casearia di 10 ha nel nord dell'Uganda, ove è stata installata una stazione agro-meteorologica, corredata anche di sensori commerciali di costo ridotto per il monitoraggio del contenuto d'acqua nella zona radicale del suolo, per una coltivazione di mais durante due stagioni.

Innanzitutto si è proceduto ad un'analisi comparativa di tredici diversi modelli semplificati (basati su temperatura e/o radiazione solare) per la stima dell'evapotraspirazione di riferimento (ET_0) con il modello standard FAO-56 Penman-Monteith, al fine di selezionare il miglior modello semplificato da applicare nell'area di studio con dataset limitati. La valutazione comparativa ha mostrato che il modello radiativo di *Makkink* è quello che più si avvicina al valore fornito dal FAO-56, con RMSE = 0.6 mmm, MAE = 0.4 mm, NSE = 0.8, d = 0.90 e r^2=0.7. Tutti i modelli basati solo sulla temperatura sovrastimano ET_0; in particolare il modello di Thornthwaite è risultato quello con le peggiori performance.

Al fine di indirizzare il primo obiettivo, è stata operata una revisione della letteratura riguardante lo stato dell'arte circa lo sviluppo di indici di siccità basati dell'umidità del suolo, e le informazioni raccolte sono state usate per formulare un nuovo SMDI per applicazioni specifiche nel nord dell'Uganda. Il secondo obiettivo è stato indirizzato attraverso l'applicazione di un modello dinamico di bilancio idrologico del suolo unidimensionale (Hydrus 1D); l'applicazione è avvenuta prima in modalità inversa, al fine di derivare le proprietà idrauliche del suolo, e poi in modalità diretta, al fine di generare serie temporali di umidità del suolo, utilizzando il modello ET_0 selezionato nello step precedente insieme a dati climatici di tipo "grid" combinati con osservazioni climatiche limitate. In fase di calibrazione, immagini del satellite Landsat 8 OLI sono state utilizzate per la stima di variabili di crescita delle coltivazioni, Nel secondo obiettivo riguardante la simulazione delle serie temporali, coefficienti agronomici rilevati in lettaratura sono stati usati per generare condizioni di contorno continue per simulazioni agro-idrologiche di 21 anni. I risultati della calibrazione hanno mostrato buona correlazione tra le simulazioni e le osservazioni di immagazzinamento idrico nella zona radicale, con un coefficiente di determinazione (r^2 = 0.73) durante la calibrazione e (r^2 = 0.70) durante la validazione. I risultati delle simulazioni di serie di lungo periodo sono state usate per derivare dei parametri soglia per la definizione dello SMDI, seguendo l'approccio statistico suggerito da Hunt et al. (2009). I valori dei parametri soglia, riferiti al contenuto idrico alla capacità di campo (θ_{FC}) ed al contenuto idrico al punto di appassimento (θ_{WP}), ottenuti attraverso le simulazioni del bilancio idrologico effettuate su un arco temporale di circa dieci anni, sono stati confrontati con i valori risultanti da analisi di laboratorio su campioni di suolo indisturbato, ottenendo un'elevata correlazione (r^2=0.95). E' stato osservato come la frequenza di occorrenza di valori negativi dell'indice SMDI e la corrispondente produzione di mais, rilevata per i raccolti tra il 2007 e il 2015, abbiano una significativa correlazione negativa di tipo lineare (r^2=0.64). La precipitazione (P) e il deficit di precipitazione (D) sono stati adattati alle distribuzioni di probabilità teoriche al fine di calcolare

indici di siccità di riferimento, i.e. SPI e SPEI. Le distribuzioni adattate (una distribuzione gamma a 2 parametri per P e una distribuzione log-logistica a 3 parametri per D) hanno dato una risposta accettabile rispetto ai testi di Kolmogorov-Smirnov con adattamento al 95% di significatività i entrambi i casi. Tutti gli indici di riferimento (i.e. SPI, SPEI e AWD) hanno mostrato una correlazione positiva con lo SMDI dimostrando così la robustezza dello stesso per il monitoraggio della siccità agricola nell'area di studio.

Il terzo obiettivo ha riguardato l'analisi di immagini nell'infrarosso termico rilevate dal satellite Landsat 8 per stimare la frazione evaporativa (Λ) attraverso un modello semplificato di bilancio energetico delle superfici coltivate. Partendo dalla definizione di una relazione di correlazione lineare fra SMDI e corrispondenti valori di Λ (r^2 = 0.84), è stato possibile individuare una metodologia di spazializzazione dell'indice SMDI nell'intera zona agro-ecologica dell'area di studio. Un controllo indipendente con set di immagini differente effettuato tra lo SMDI calcolato usando l'equazione di regressione SMDI-Λ e lo SMDI generato tramite le simulazioni agro-idrologiche ha confermato la buona rispondenza.

L'ultimo obiettivo riguardava l'integrazione dei risultati ottenuti nei primi tre obiettivi per formulare uno schema di supporto decisionale. Lo SMDI è risultato utile a delineare le stagioni secca ed umida del nord dell'Uganda; esso ha mostrato che la stagione secca comincia tra il 25 novembre e il 10 dicembre e quella umida comincia tra il 26 marzo e il 5 aprile di ogni anno. Uno schema di supporto decisionale basato sullo SMDI è stato proposto, sebbene esso necessiterebbe ulteriori ricerche per dimostrare la sua efficacia. In conclusione, gli approcci sviluppati per definire lo SMDI possono essere implementati facilmente in ogni paese in via di sviluppo soggetto a simili problemi in ambito di agricoltura dipendente dalle precipitazioni.

ACKNOWLEDGEMENT

First of all, I would like to thank the ECART Project team for the financial support they provided and for the timely release of the funds whenever I needed it. I also would like to extend my sincere appreciation to the Vice Chancellor of Gulu University Prof. Jack Nyeko Penmogi, for granting me study leave at a time when the University depended more on visiting lecturers for implementation of the academic programs. I also would like to extend my appreciation to Prof. C.W. Baliddawa who encouraged and recommended me for the PhD program. I would also like to thank Gulu University for continuing to pay my salary that enabled me to support my family back in Uganda whenever I was away in Italy.

I would like in a special way to thank Prof. Eng. Guido D'Urso for providing me with the enabling environment whenever I was in Italy, and for being always ready to help whenever I needed it. I am grateful for especially guiding me in the application of open source tools for analysis of satellite remote sensing images that has been central in my study. I would like also in a special way to thank my supervisor Dr. Mario Palladino for introducing me in the field of soil hydrology and providing valuable guidance throughout my study in Italy.

Many individuals and friends contributed greatly to the success of this study. In this regard, I would like to extend my appreciation to Mrs. Paula Di Fiore who helped me to analyze soil data, especially the analysis of undisturbed soil core samples that I had brought from Uganda to the soil hydraulics laboratory of the Department of Agriculture. I would also like to thank Mr. Benedetto Sica, who guided me through the laboratory procedures to determine soil textural characteristics.

I cannot forget the company of Mr. Allesandro Mataffo and Mr. Massimiliano Borrello who picked me from the airport the first day I come to Italy and for the support they provided throughout the time I have been in Italy. They especially helped me adapt to living in Italy which was very challenging for me at the beginning. I would also like to thank Mr. Enrico Anzano for being helpful whenever I needed assistance in processing remote sensing images. I also extend my appreciation to Mr. Salvatore Falanga Bolognesi, who introduced me to R-programming language that greatly helped in implementation of the energy balance modeling and in handling large datasets. Mr. Salvatore Falanga Bolognesi also first guided me on how to access ECMWF resources.

I would like also to thank Dr. Collins Okello who gave me a very good orientation in Italy when I first came to Italy in May, 2014. I would also like to extend my appreciation to Dr. Nyeko Martine for providing the initial guidance on my research topic. Both Dr. Collins Okello

and Dr. Nyeko Martine have been pioneers from Gulu University in Italy for the PhD programs. The fact that you guys completed your PhDs from here in Italy encouraged me greatly to concentrate and also finish. I cannot forget Dr. Grace Okiror who provided assistance with downloading data from the data loggers. Many thanks also go to Dr. Tony Kidega and the entire GUCD team for the support they provided during installation of my research equipment in their farm and for providing security for the equipment.

I would also like to extend my sincere appreciation to my wife, Mrs. Ruth Ayee Openy, for taking care of our home in Uganda and taking good care of our two sons whenever I was in Italy. I appreciate your patience and for giving me time to always be away during my study.

Most of all, I would like to thank the Lord God Almighty for the gift of life and salvation that He has given me and for His constant protection. For I have always found comfort in His written word in the Bible during some of the most challenging of times.

SYMBOLS

Symbol	Description	Unit
d	Index of Agreement	(-)
E_s	Soil Evaporation	(m)
ET_c	Crop Evapotranspiration	(mm)
ET_o	Reference Evapotranspiration	(mm)
F_{AWC}	Fraction of available water content	(-)
F_r	Fractional vegetative cover	(-)
G_o	Soil Heat Flux	(Wm^{-2})
H	Sensible Heat Flux	(Wm^{-2})
h_c	vegetation/crop canopy height	(m)
k_1	the first calibration constant for estimation of land surface temperature	(-)
k_2	the second calibration constant for estimation of land surface temperature	(-)
$K^{\downarrow}$	down welling short wave solar radiant energy	(Wm^{-2})
$K^{\uparrow}$	upwelling long wave radiant energy	(Wm^{-2})
l	tortuosity factor of the soil water retention curve	(Wm^{-2} sr^{-2})
L_d	Downwelling radiance	(Wm^{-2} sr^{-2})
L_T	Surface radiance	(Wm^{-2} sr^{-2})
L_u	Up welling radiance	(Wm^{-2} sr^{-2})
L_λ	Surface radiance for a given wave length λ	(Wm^{-2} sr^{-2})
n	a scale parameter of the soil water retention curve	(-)
$NDVI_{min}$	Minimum value of the Normalized Difference Vegetation Index	(-)
$NDVI_{max}$	Maximum value of the Normalized Difference Vegetation Index	(-)
r^2	correlation coefficient	(-)
R_n	Net solar radiation	(Wm^{-2})
r_o	Surface reflectance	(-)
T_H	hot temperature from the temperature reflectance feature space	(^{o}c)
T_{lst}	Land surface temperature as estimated from satellite thermal bands	(^{o}c)
T_o	Pixelwise land surface temperature	(^{o}c)
T_p	Transpiration	(mm)
$T_{\lambda E}$	Cold temperature from the temperature reflectance feature space	(^{o}c)
α	The shape parameter of the soil water retention curve	(-)

β	Extinction parameter for the estimation of the leaf area index	(-)
δs	Change in soil water storage	(m)
δt	Change in time	(s)
ε	Land surface emissivity	(-)
λ	wave length (unless otherwise defined)	(µm)
λE	Latent heat flux	(Wm^{-2})
θ	water content	(m^3/m^3)
θ_{FC}	Soil Water content at field capacity	(m^3/m^3)
θ_{WP}	Soil water content at wilting point	(m^3/m^3)
θ_r	Residual water content	(m^3/m^3)
θ_s	Saturated water content	(m^3/m^3)
ϑ	The zenith angle	(^{o}c)
ρ_{nir}	Near infrared reflectance	(-)
ρ_r	Reflectance in the red band	(-)
ρ_{is}	Bare soil reflectance in the infrared band	(-)
ρ_{sr}	Bare soil reflectance at near infrared band	(-)
Λ	Evaporative fraction	(-)

ACRONYMS

AIC	Akaike's Information Criterion
AWD	Atmospheric Water Deficit
BIC	Bayesian Information Criterion
BRDF	Bidirectional Reflectance Distribution Function
CMI	Crop Moisture Deficit
CRED	Centre Of Research for Epidemiology of Disaster
ECMWF	European Centre for Medium-Range Weather Focus
ETDI	Evapotranspiration Deficit Index
EM-DAT	Emergency events Database
ET	Evapotranspiration
ETM+	Enhanced Thematic Mapper Plus
FAO	Food and Agricultural Organization of The United Nations
FAO-56	PM Reference Evapotranspiration as recommended in FAO drainage Paper No.56
FAPAR	Fraction of Absorbed Photosynthetically Active Radiation
GDP	Gross Domestic Product
GFDRR	Global Facility For Disastor Reduction And Recovery
GWD	Gridded Weather Data
GUCD	Gulu Uganda Country Dairy
GUI	Graphical User interface
GYGA	Global Yield Gap Atlas
ITCZ	Intertropical convergent zone
LAI	Leaf Area Index
LRA	Lord’s Resistance Army
MAE	Mean Absolute Error
NARO	National Agricultural Research Organization
NASA	National Aeronautics and Space Administration
NDPI	The first National Development Plan
NDPII	The second National Development Plan
NDVI	Normalized Difference Vegetation Index
NEMA	National Environment Management Authority
NGO	Non-Governmental Organization

NOAA	Northern Oceanic and Atmospheric Administration
NSE	Nash Sutcliffe Efficiency
NWSC	National Water and Sewage Corporation
OFDA	Office of Foreign U.S. Disaster Assistance
OLI	Operational Land Imager
OPM	office of the prime minister
OWD	Observed Weather Data
PDSI	palmer drought severity index
PM	Penman Monteith model
PAM	Plan for Modernization of Agriculture
PWMs	Probability Weighted Moments
PWD	Propagated Weather Data
RMSE	Root Mean Square Error
RZMS	Root Zone Moisture Stress
SC-PDSI	Self-Calibrating Palmer Drought Severity Index
SMAP	Soil Moisture Active Passive
SMARTS	Simple Model of the Atmospheric Radiative Transfer of Sunshine
SMDI	Soil Moisture deficit index
SMI	Soil Moisture Index
SMOS	Soil Moisture and Ocean Salinity
SPAC	Soil-Plant-Atmosphere Continuum
SPEI	standardized precipitation evapotranspiration index
SPI	standardized precipitation index
SSA	Sub-Saharan Africa
S-SEBI	Simplified Surface Energy Balance Algorithm
SVAT	Soil Vegetation Atmosphere Transfer model
SWDI	Soil Water Deficit Index
SWI	Soil Water Index
SWRC	Soil Water Retention Curve
SWAP	Soil Water Atmosphere Plant model
TIRS	Thermal Infrared Sensor
TM	Thematic Mapper
VCI	Vegetation Condition Index
VI	Vegetation Indices

WDVI	Weighted Vegetation Index
WMO	World Meteorological Organization
ZARDI	Zonal Agricultural and Development Institute

LIST OF FIGURES

LIST OF TABLES

CONTENTS

1 GENERAL INTRODUCTION

1.1 Motivation of The Study:

Rain-fed agriculture accounts for over 70% of the global crop production and is expected to rise as competing demands for global fresh water resources continue to increase (FAO, 2010; Nijbroek and Andelman, 2016; Biggs et al., 2008). It is estimated that the current food production will need to be increased by between 70% - 110% to feed the growing population projected to reach about 9 billion by 2050 (Nijbroek and Andelman, 2016). It is further projected that 80% of global food production will have to come from rain-fed farming system (Jägermeyr et al., 2016). This presents a critical set back in meeting global food needs as much of the areas under rain fed farming are concentrated in the poorer regions of the earth (Biggs et al., 2008). Besides, expansion of land area for food production is no longer sustainable as such, more food will have to be produced on less piece of land. This has been the basis for the agricultural intensification efforts by various development agencies emphasizing increasing food production per acre of land per unit of water (Godfray et al., 2010).

Water scarcity is perceived to be prominently responsible for food insecurity in developing countries especially in Sub-Saharan Africa (SSA), where agricultural productivity remains below the global average (Breman et al., 2003). Soil moisture deficit to crop moisture requirements is a common occurrence in rain-fed crop production systems. Its impact on crop yields varies depending on the phenological stage in which it sets in, during a growing season. Whenever rainfall varies abnormally such that the resulting soil moisture deficit leads to yield loss or complete crop failure the situation is termed *Agricultural drought* (Carolina, 2002; Stewart, 1988). A number of studies have shown that agricultural droughts have profound negative impacts on the livelihood of small holder farmers in SSA and that such negative impacts can be mitigated through proper understanding of soil water loss pathways which can in turn help to devise strategies to improve soil water retention (Makurira et al., 2011; Kongo and Jewitt, 2006; Ngigi et al., 2006; Rockström et al., 2004). However, water storage in the soil profile and its partitioning into the different paths it takes in the different flow regimes is the least understood aspect of hydrological cycle (Jewitt, 2006). This is so because soil hydraulic parameters that control moisture dynamics in unsaturated zone vary widely across scales (Montzka et al., 2011; Jhorar et al., 2004). The most contemporary methods for their estimation are laboratory based which a number of studies have demonstrated as not representative of the actual flow conditions at the scale of application (Shin and Mohanty,

2013; Dobriyal et al., 2012; Settin et al., 2007; Dirmeyer and Zhao, 2005; Rajkai et al., 2004; Espino et al., 1996). The laboratory method for the estimation of soil hydraulic properties relies on samples that are point based, as such their results are not easily transferable even across few meters at the field scale (Hopmans et al., 2002). The complexity in the variability of soil hydraulic parameters and the inability of the contemporary methods to provide estimates at the relevant scale of application is the main driver of research interests in soil hydrology and associated areas of study.

Soil moisture plays a central role in controlling ecosystem dynamics and is one of the key variables that integrates land surface hydrology, since it acts as water storage in the hydrological cycle (Li and Islam, 1999). It plays a central role in water balance studies across scales in: meteorology, hydrology, ecology and agronomy (Chen, et al., 2014; Lü et al., 2011; Montzka et al., 2011). Soil moisture in the root zone particularly regulates land surface-atmosphere interactions through modification of energy and moisture fluxes in the boundary layer (Ford, et al., 2014) and is also a very important variable in carbon cycle predictions (Friedlingstein et al., 2006). Improving estimates of soil moisture in the root zone is very critical in drought predictions, hydrological modeling and weather forecasting (Dobriyal et al., 2012; Dorigo et al., 2011; Dirmeyer and Zhao, 2005); which are important factors in agricultural water management. Acquisition of soil moisture data currently relies on three approaches, i.e.: in situ (generally point-scale) measurements, remote sensing observations and hydrological modeling (Romano, 2014). Continuous long-term ground-based measurements are greatly lacking, more so in developing countries. Remote sensing based acquisitions of soil moisture states are based on microwave sensors at about 25 km resolution and penetration depths of about 5cm that do not encompass the root zone (Fang and Lakshmi, 2014). Use of simulation models forced with climatic data when estimates of the soil hydraulic parameters can be obtained under certain assumptions presents a very viable option for soil moisture predictions especially in developing countries where networks of soil moisture measuring devices do not exist (Dorigo et al., 2011). The attractiveness of numerical modeling is that with the existing low cost soil sensors, soil hydraulic properties for a given support can be estimated through inverse simulations and sensitivity analysis as long as estimates of vegetation parameters can be obtained (Suhada et al., 2015). Current existence of free high resolution satellite images within the optical regions of electromagnetic spectrum (Ali et al., 2016; Vermote et al., 2016), such as Landsat and ASTER presents viable means of obtaining canopy

parameters for input into the simulation models which can be applied in almost any remote location.

1.2 Drought Definition, Classification and Impacts on Livelihood

1.2.1 Drought Definition and Classification

There is no agreement on a single definition of drought among the scientific community (Mishra and Singh, 2010). However, the general consensus is that a drought phenomenon starts with an extended period of persistent precipitation deficit leading to the following situations:

- seasonal alteration in soil water recharge leading to a reduction in soil water storage
- a sustained deficit in soil moisture to plants
- reduction in surface water supply and stream flows
- the combined effects of soil moisture deficit, reduced surface water and stream flows causing imbalance in demand and supply of public goods that depend on water.

Therefore, drought occurs whenever there is an abnormality in precipitation over an area characterized by an extended period of reduced precipitation amounts. The duration of the reduced precipitation over an area and the negative impacts it has on the normal functioning of the ecosystem form the basis for drought classification. According to Dai (2011) and Mishra and Singh (2010) drought is classified into four categories namely: meteorological drought, agricultural drought, hydrological drought and socio-economic drought.

(i) *Meteorological drought*; is defined by deficiency in precipitation over a region in a defined time period. Meteorological drought triggers all the other drought categories with negative impacts on ecosystem services.

(ii) *Agricultural drought***;** defined as a situation of sustained and declining soil moisture deficit leading to yield loss or complete crop failure and reduced pasture for range animals. the decline in soil moisture is based on evapotranspiration by a combined action of plant water uptake and soil evaporation and soil water drainage below the root zone. These factors that drive agricultural drought are not directly linked to precipitation so that agricultural drought normally lags meteorological drought. Agricultural drought is more prevalent in rain-fed farming system since reduction in rootzone moisture can only be replenished by subsequent precipitation event whose variability depends on natural factors. With observed changes in climate in most regions over the earth, agricultural drought has become more frequent over

the last two decades with devastating effects on livelihoods especially in developing countries.

(iii) *Hydrological drought***;** defined as a period of inadequate surface and subsurface water supply characterized by reduced stream flows, drop in lake water levels and reduction of water storage in aquifers. It is not quite straightforward to define the time period specifying the onset of hydrological drought because of the competing water supply needs such as irrigation, hydropower and municipal water needs. The onset of hydrological drought lags that of meteorological drought because a considerable amount of precipitation is required to restore stream flows, aquifer reservoirs and lake water levels.

(iv) *Socioeconomic drought*; is defined by a relationship between the demand and supply of an economic good (e.g. water, livestock forage and hydropower) in connection with drought impacts. For this reason, socio-economic drought involves the combined impacts of meteorological, agricultural and hydrological droughts on the economy of an area in such a way as to result in the demand of an economic goods exceeding supply as a result of water supply shortage.

1.2.2 Drought impacts on livelihood

Droughts account for about 8% of the global natural disasters and recent estimates on drought impacts for the period 1900 –2013, puts the number of drought events at 642 globally (Shiferaw et al., 2014). The reported drought events across the world resulted in deaths of about 12 million people and affecting over 2 billion causing an estimated economic loss of some USD135 billion (Masih et al., 2014). The vulnerability of a society to impacts of climatic variability such as drought depends on a number of factors such as: the level of technological development, the number of population, social behavior, land use pattern, the diversity of economic base, level of economic development and cultural practices (Naumann et al., 2014). Regions that are characterized by widespread poverty and whose economies depend on subsistence agriculture with little or no investments in irrigation infrastructure and where response to natural disasters are based on development aid are always the most affected.

Drought impacts on the African continent have been significantly worse than in other regions (Gautam, 2006). For instance, it is estimated that droughts within the African continent accounted for 25% of the natural disasters that occurred in the period 1960 – 2005, of which, 70% occurred in the eastern Africa (Gautam, 2006). Sub-Saharan Africa remains very

vulnerable to drought impacts because of its dependence on Agriculture which is very sensitive to climatic variability (Shiferaw et al., 2014). Subsistence farming on fragmented farmlands, predominantly rain-fed, put the population of the SSA in even greater risks due to the prevailing climatic variability which is projected to increase the number of natural disasters on the global scale.

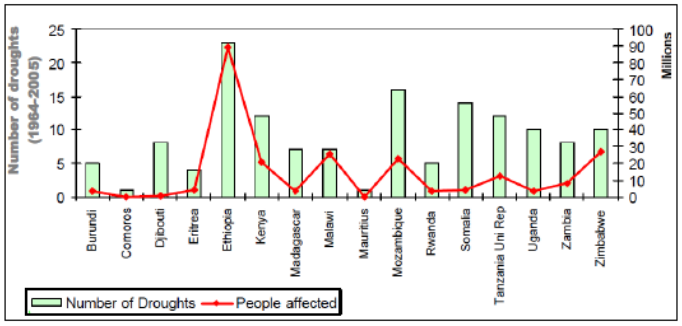

Figure 1.1 Number of droughts and people affected by country in Eastern African Countries: 1964 – 2005. Source: EM – DAT: the OFDA/CRED Internal Disaster Database ww.em-dat.net – Universite Catholique de Louvain – Brussels – Belgium

Droughts have had diverse impacts in SSA depending on the level of severity, spatial extent and duration. Some of these impacts include: crop failures, food shortages, famine, malnutrition, health issues, mass migration and loss of life (Naumann et al., 2014). Other drought impacts are associated with great damage to the environment, such as: land degradation posing many otherwise vegetated landscapes to the threat of aridity and desertification. These impacts have been observed at a range of geographical scales, affecting individual families and communities. In many instances the affected communities have lost their livelihoods and source of water, subjecting the entire population of a region to acute food shortages, nutrition related health issues with some countries' economy being severely impacted.

The Eastern African region in particular have had considerable drought impacts as depicted in Figure 1.1 for the period 1964 – 2005. Countries that experienced major drought impacts in order of being worst affected were: Ethiopia, Zimbabwe, Malawi and Kenya with droughts causing loss of human lives and livestock (Gautam, 2006). The least affected countries such as Uganda, Comoros and Burundi experienced a great deal of variability in crop yields within the same period. The major cause of these droughts in all cases are precipitation deficit causing meteorological drought with varying impacts (Nicholson, 2001). Drought impacts have been very severe on the eastern African countries because the economy of the region depends on precipitation (Ogallo, 1981). The mechanisms resulting into precipitation

and temperature variability that results in a number of climatic extreme events such as droughts and floods are still not well understood over the eastern Africa region. This is mainly because of large gaps in weather records (WMO, 2015). Many of the studies on the climatic factors controlling the extreme events over these regions are based on simulated regional data that provide lots of uncertainty when considering local impacts of the extreme events.

Uganda unlike many of the east African countries rarely experience extreme drought events because it receives relatively reliable rainfall compared to the rest of her neighboring countries (GFDRR-OPM, 2012). The number of major droughts recorded between 1900 and 2013, in EM-DAT website, (http://www.emdat.be/database) occurring in Uganda is 9, causing reported 194 deaths, affecting some 4,975,000 people and causing economic loss amounting to $1.8million. Thus, amounting to: 0.1%, of the total deaths, 76.8% of the total number of people affected and 2.3% of the total economic loss attributed to all the reported natural disasters during 1900 – 2013, (Masih et al., 2014). Therefore, by far extreme drought events are rare in Uganda but their impacts on the population are more widespread than any other natural disasters that are experienced (GFDRR-OPM, 2012). However, this in no way accounts for all the unreported deaths of both humans and livestock and the economic loss that actually occurred during the same period due to droughts. The complexity in understanding the onset of drought events, makes precious documentation of their impacts in a country such as Uganda not very possible given that reliable climatic data are very scanty (Nicholson, 2001). From time to time there are however newspaper reports on reduction of crop yields, famine and water for livestock that are attributed to droughts but such reports lack rigorous scientific scrutiny and cannot be relied on.

Mitigation strategies to counter the impacts of droughts are grouped in to what are referred to as *ex post* and *ex ante* responses to drought impacts (Shiferaw et al., 2014). The *ex post* and *ex ante* responses are aimed at minimizing shocks after droughts have occurred and minimizing the risks a priori to drought occurrence, respectively (Owens et al., 2003). In Uganda, *ex-post* mitigation strategies, have relied on development aid and migration for the case of cattle keepers. Whereas the *ex-ante* mitigation strategies have included: intercropping, promotion of drought tolerant varieties, some limited supplemental irrigation in few cases and diversification of income through engagement in other farming practices such as fish farming. However, these mitigation strategies can best be enhanced through development of appropriate indicators to analyze the onset and termination of drought events. Such indicators must take into account all the relevant factors responsible for understanding common drought types that affect specific

areas. For the case of Uganda in general and northern Uganda in particular focus must concentrate on analysis of short term agricultural droughts that are very common. This is due to the fact that short term agricultural droughts can be mitigated against locally through proper understanding of water loss pathways (Makurira et al., 2011).

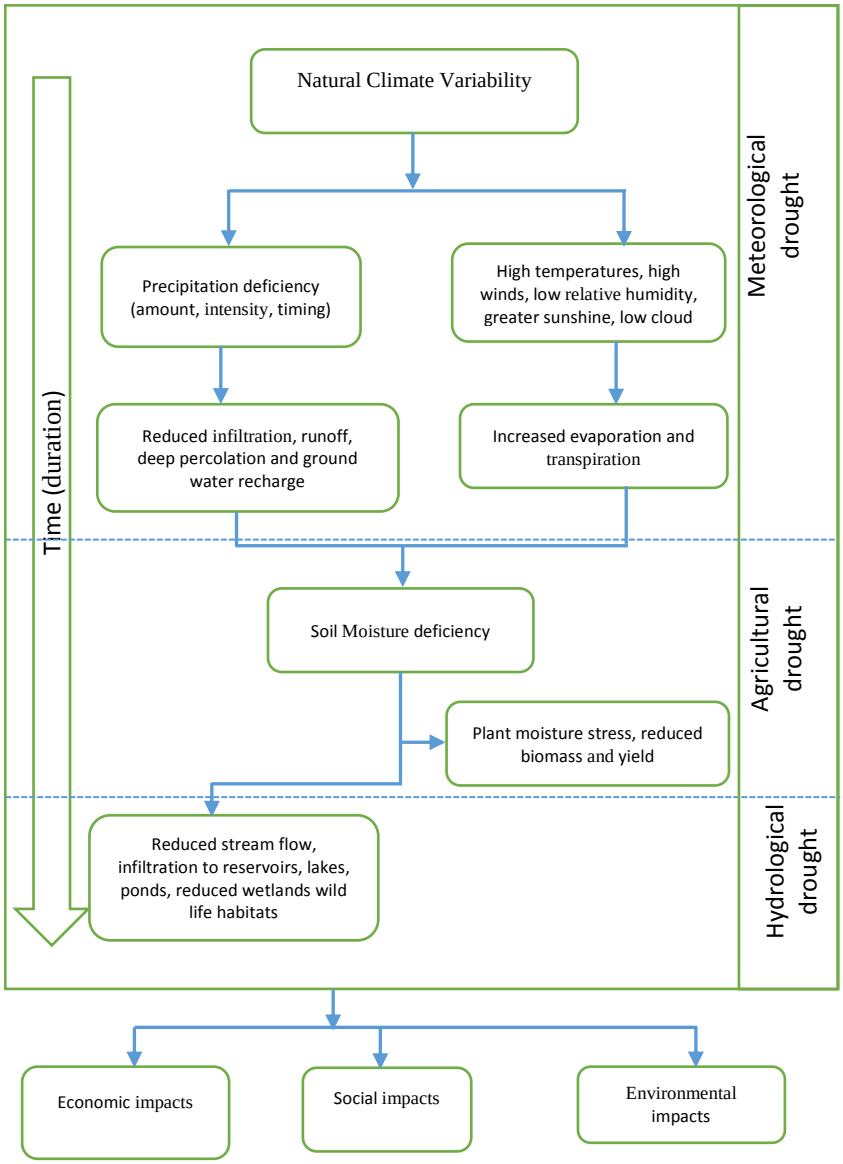

Figure 1.2 Drought Onset, Classification and Impacts

1.3 Soil and Water productivity in Uganda: current status and future perspective

Agriculture remains the backbone of Uganda's economy employing about 72 percent of the total formal and informal labour force. About 65% of Uganda's land mass is considered Agricultural land, relatively fertile and receives sufficient rainfall for rain-fed farming. However, it is estimated that only 49.2% of the agricultural land is considered arable land (World stat, 2014). According to FAO (2005), arable land refers to land under: temporary

crops, temporary fallow (less than 5 years), meadow for mowing or pasture, market & kitchen garden and land under permanent crops. Agricultural practices in Uganda are nearly 100% rain-fed, predominantly subsistence on highly fragmented lands. Arable land equipped for formal irrigation is estimated at 14,420 ha, accounting for only 0.1% of the total agricultural land, despite abundant fresh water resources (MW&E-Irrigation Master Plan, 2011).

Soil productivity refers to the ability of a soil to support crop production through the possible combination of its entire physical, chemical and biological characteristics (Dobriyal et al., 2012). The important attributes that determine soil productivity have not been generally studied in Uganda in the recent past (Myhill & Allen, 2002). Available comprehensive nation-wide soil surveys were done in the 1950s (Chenery, 1960). Most hydrological and crop modeling studies carried in Uganda have been based on approximate soil information estimates obtained from: consultation with soil scientists in the country, limited localized soil survey studies and from FAO database (Wart et al., 2013; Nyeko, 2010; Myhill and Allen, 2002). Water productivity is closely linked to soil productivity. Water productivity in its narrow sense, refers to the ratio of the net yield obtained from a given crop production system to the amount of water used to realize the yield (Makurira, 2010).

Soil and water productivity in Uganda is very low, due to a number of factors such as:

- Poverty and land fragmentation leading to over-exploitation of the land with inadequate soil and water conservation practices;
- Increasing rural population densities with few non-farm income opportunities;
- Low levels of commodity trade and the production of lower-value commodities, reducing incentives to invest in the soil;
- Little farmer knowledge of improved agricultural technologies, insufficient agricultural research that takes into account the needs and resource constraints of farmers, and a lack of effective agricultural extension;
- Inappropriate farming practices and systems including deforestation, bush burning and overgrazing (Olson, 1998; Zake et al., 1999; NEMA, 2001; Kazoora, 2002).

These negative trends continue to expose much of agricultural land areas to soil erosion and eventual land degradation. For these and other reasons, crop yields in farmers' fields in Uganda area estimated at 55% of the potential yields at research stations (Wart et al. 2013; Myhill & Allen, 2002). These factors, partly explain the reason Uganda is classified as the least developed country with an estimated per capita GDP of $572 as of 2013, (FAO, 2015). However, there is very high potential in rain-fed farming and agriculture is considered a key

determinant to alleviate the high poverty levels in the country if the Uganda's soil and water productivity can be enhanced.

Table 1.1 Major Drought on the African continent during the period of 1980 – 2010

Region	1980 – 89	1990 – 99	2000 – 09
East Africa	The lowlands of Ethiopia and the main productive areas of Kenya were affected by the 1984 drought (Gomess & Petrassi, 1994). In Ethiopia the 1984 drought caused the death of 1 million people and 1.5 heads of livestock. 8.7 million people were affected in total. In 1987 more than 5.6 million people in Ethiopia, 1 million in Eritriea and 200,000 in Somalia were severely affected (Drought monitoring centre, 2000)		Rainfall records indicate that in some parts of the sub-region the drought in 2000 was worse than that experienced in 1984(drought monitoring centre, 2002)
West Africa	The Sahel was hit by a severe drought in the early to mid-1980s (Brooks, 2004). The worst drought in this period occurred during the year 1984 affecting most of the countries in the Sahel (Gomess & Petrassi, 1994)		
North Africa		In Morocco, agricultural output recorded losses in 1992, 1995 and 1997 due to drought. In 1997 Algeria's cereal production decreased sharply as a result of severe drought (UNEP, 2002)	The most recent drought in Tunisia and Algeria (from 1999 – 2002) appears to be the worst since the mid mid-15th century, according to some researchers who analyzed tree-ring records from the region (http://environmental researchweb.org/cws.asticle/news/35673)
South Africa	In 1982/83 most parts of Southern Africa were severely affected (drought monitoring center, 2000)	Most south African countries were severely affected 1991/1992 drought. The 1991/1992 was the most severe drought recorded causing 54% reduction in grains harvest, exposing more 17 million people to the risks of starvation (Galliham et al., 1994, UNEP, 2002)	

Uganda has put in place various policies for enhancement of agricultural production. Some of which include:

- the first and second Uganda national development plans; (NDPI) and (NDPII) respectively whose vision is to transform Uganda's economy to middle income by 2020
- Plan for modernization of agriculture (PMA, that was enacted in 2010 and pledged to transform the subsistence agriculture to commercial farming by 2040
- The irrigation master plan.

These policies aim to transform the subsistence agriculture to a highly-commercialized profit making farming systems. Key constraints have been identified as lack of farm inputs, land fragmentation, high level of poverty in the country, soil degradation and climatic variability leading to frequent droughts (Kilimani et al., 2015). These research is meant to contribute towards achieving some of these goals by developing a method to support decision making at a farm level. Northern Uganda where the case study was conducted lags behind in all sectors of the economy in the country. This is due to the Lord Resistance Army (LRA) insurgency that grounded the region to a halt for 20 years. The 20-year insurgency, made collection of meteorological records impossible. Therefore, climate based studies to inform livelihood interventions in Northern region is almost nonexistent. The Acholi sub-region the worst affected by the LRA insurgency is endowed with large expanse of fertile agricultural land. However, crop production is still very limited compared to other parts of the country (Myhill and Allen, 2002). Tapping the agricultural potential of this region requires understanding the biophysical information in the region. These can be done through simulation models that once calibrated can be used to recreate past information that are missing and make predictions to enable planning to mitigate climate based risks such as droughts that are predicted to increase by 2050.

1.4 Statement of the Problem, Study Objectives and Summary of The Thesis

1.4.1 Problem Definition

Droughts are experienced in all climatic conditions on earth and have become more frequent in recent times. However, the focus of developing drought mitigation strategies has concentrated more in semi-arid and arid areas largely leaving out areas that receive reliable rainfall on average. Moreover, it is only the extreme drought events with devastating large scale impacts that draw attentions for intervention in such areas endowed with 'reliable rainfall' (Table 1.1). For this reason, it is recommended that drought should be studied within a regional context, because of their large scale characteristics (Mishra and Singh, 2010). However, this restriction limits the definition of droughts to refer only to large scale extreme events. This

perhaps explain the lack of agreement on a single definition of drought among the scientific community. It is however well known that agricultural drought characterized by a condition of declining moisture content in the soil has varying impacts from field scale to large areal extents. Agricultural drought at field scales would therefore require different mitigation measures from those having regional extents. Gaps still exists in addressing short term, field scale agricultural droughts that are more common in areas with predominantly rain fed farming systems. This is usually the situation in a country such as Uganda that receives on average 'abundant rainfall' but occasionally experiences crop failures due to pervasive weather variability. The problem in Uganda in general and Northern Uganda in particular are three-fold: Firstly, intra-seasonal agricultural droughts that occur randomly without known characteristics, secondly the inter-seasonal droughts that occur in known dry periods with 'little' or no rains but whose onset and termination are not clearly defined given the nature of rainfall variability and thirdly the limitation of soil and climatic data to delineate these periods. The problems are exacerbated by limited number of weather stations in operation in the region. The few available weather stations have data records with lots of gaps, in addition to the fact that the quality of the data collected in most cases are questionable. Consequently, rainfall variability analysis, soil, crop, vegetation and other biophysical information that can inform livelihood interventions are generally lacking. There are no reported field based water balance studies to inform farming practices. Earlier soil survey studies at scales of about 1:1,000,000 indicate that most of the areas especially in Northern Uganda have coarse textured soil which drains easily and as such the relatively high rainfall received does not ensure good yields. Crop failures related to moisture deficits in the soils are very common.

This study is therefore an attempt to apply available tools to *develop a soil moisture deficit indicator for field scale monitoring of agricultural droughts*. It is hoped that the resulting index will guide various on-farm decisions to enhance crop productivity and alleviate poverty which is very widespread in the area.

1.4.2 Study Objectives

(i) Overall objective:

The overall objective of this study was to develop a simplified approach to compute *Soil Moisture Deficit Index* (SMDI) for operational monitoring of the onset and termination of field scale agricultural droughts in areas with unreliable meteorological and soil moisture data records. The approach involved integration of limited climate and soil data in the study area

together with freely available tools such as gridded climatic data to fill gaps in observed weather records and satellite remote sensing images to derive crop growth variables for input in to a calibrated hydrological model to simulate soil moisture time series used for the computation of SMDI. The approach depends on application of low cost commercial soil sensors for the calibration of a 1-dimensional agro-hydrological model such as Hydrus 1D through numerical inversion for the subsequent direct simulation of long time soil moisture time series. The method was evaluated through a case study in Northern Uganda where 21-year soil moisture time series was generated through the calibrated model to define SMDI. This approach can be very useful for supporting soil moisture management decision in rain fed farming areas.

(ii) Specific Objectives

- *to identify and adapt a suitable drought indicator in relation to the data availability;*
- *to assess the feasibility of using a calibrated agro-hydrological model for producing long-term time series of soil water dynamics and derive SMDI for monitoring agricultural droughts;*
- *to upscale the SMDI through energy balance modeling using a case study in Northern Uganda;*
- *to formulate a soil water management decision support scheme for mitigation of agricultural droughts in rain fed farming systems through application of SMDI.*

1.4.3 Summary of the Thesis

The aim of this research was to develop a soil moisture deficit (SMDI) index for operational monitoring of the onset and termination of field scale agricultural droughts. The methodology is developed with an application focus for rainfed dominated farming system especially in developing countries, where reliable historical records of climate, soil and other biophysical variables are seldom available. Key concepts applied in developing the index include: satellite remote sensing image analysis to extract biophysical variables. Agro-hydrological simulations to generate soil moisture times series. derivation of reference indices through fitting key climatic variables such as precipitation on theoretical probability distributions, energy balance modeling to cross validate the index and gap filling climatic data through data propagation algorithms that utilizes regression analyses between observed climatic data and gridded weather data for gap filling and extending climatic records.

Chapter 1, which is the general introduction contains the background information, a brief summary of drought concepts, their characterization and impacts on livelihood. The Chapter concludes with problem definition leading to the objectives of the study and a summary of the thesis. Chapter 2 gives a general description of the study area and the data used in this study. It provides some details on climatic patterns over the entire Ugandan landmass, including factors that drive these climatic patterns. It also covers dominant soil characteristics and their relative productivity levels as reported by unpublished soil map that is under development by the National Agricultural Research Organization (NARO). It provides description of the main data sources applied in this research e.g. climatic data sources, satellite remote sensing images and yield data sources that were used to verify the new SMDI developed in this study.

Chapter 3 provides some reviews of the common drought indices used for monitoring agricultural drought. Key strengths and weaknesses of each of the common drought indices applied for agricultural drought monitoring are highlighted and their application gaps in especially developing countries identified.

Chapter 4 gives details of the core focus of this thesis, it provides description of the concepts applied to develop a new approach for the definition of the SMDI specifically for application in developing countries that depend solely on rain-fed agriculture. It provides a schematization that integrates all the concepts applied to develop the new approach to define SMDI as implemented in this thesis. It also covers algorithms for the calculation of key reference drought indices i.e. SPI (Standardized Precipitation Index) and SPEI (Standardized Precipitation and Evapotranspiration Index) that were applied to verify SMDI in the study area

Chapter 5 involved evaluation of the 12-common empirical reference evapotranspiration models in the study area. The 12-ET_0 models were grouped in to three categories i.e. Mass Transfer (MT) Based models, Temperature (T) based models and the Radiation (R) based model. Results of the evaluation reported and best performing category stated as supported by various test statistics with between each ET0 model and FAO-56PM as reference. The overall performing ET_0 model for the study area is identified. The chapter also covers algorithm for gap-filling climatic data using gridded weather data. Two sources of gridded weather data (i.e. ECMWF and NASA-P) were used in conjunction with a 4-year weather data collected from a digital weather station near the study site and main results of implementation of the algorithm presented.

Chapter 6 deals with the theoretical background that govern key concepts applied in calibration of water flow models as applied in agro-hydrological simulations. Different methods of soil hydraulic parameter estimation procedures are described and strengths and weaknesses highlighted. This chapter also deals with brief theoretical concepts that govern application of satellite remote sensing products for estimating crop growth variables such as, LAI and albedo. Detailed descriptions of the estimation procedures of each of these variables as applied in this study are provided. Chapter 7 deals with the case study of the calibration of Hydrus 1D in the study area. It covers the calibration steps and the presentation of key calibration and validation results obtained and their discussions.

Chapter 8 covers a case study that was conducted in Northern Uganda to test the core concepts developed in this thesis. It integrates information covered in chapters 4, 5,6 and 7 to generate a 21-year soil moisture time series for the calculation of the threshold parameters that were used to define the SMDI. Key results of the comparison between the threshold parameters generated through agro-hydrological modeling and those determined from the laboratory presented. The chapter also covers the results of the fitting distributions of the variables used to implement the algorithms for the calculation of the reference indices i.e. SPI and SPEI. Correlation analyses between SMDI and each of the reference indices and the results of regression analysis between SMDI and yield data obtained from the study area are reported. Chapter 8 also covers application of the energy balance model S-SEBI for calculation of the evaporative fraction in the study area applied for upscaling the developed SMDI. It was postulated that a linear relationship exists between SMDI and satellite derived evaporative fraction (Λ). The existence of this linear relationship means that SMDI can be obtained from SMDI- Λ regression equation to upscale it for application over the entire region with similar agro-meteorological and soil characteristics. Key results of the SMDI- Λ regression analysis presented. Chapter 8 concludes by application of the SMDI to formulate a decision support scheme for soil moisture management under rainfed farming system. the scheme is applied to delineate the study site's main growing season. Chapter 9 covers the general conclusion, future outlook and key innovative aspects of this research.

1.4.4 Limitation of this study

This study has been conducted mainly to address the problem associated with availability of climatic and soil data to formulate agricultural drought indicators in developing countries that solely depend on rainfall for crop growing. Therefore, the main limitation of this research was availability of reliable climatic and soil data. Soil map in the entire country is still being

developed, and it was not possible to get soil data that would cover a larger geographical area to help in verification of the SMDI that was developed using data only at one study site. Secondly most existing weather stations in the area have only precipitation and temperature data albeit with lots of gaps. There are only 3 operating weather stations in the study area covering the entire Northern region.

2 DESCRIPTION OF THE STUDY AREA AND DATA AVAILABILITY

Summary

This chapter presents a general description of the study area and data availability used in this research. It covers description of the climate of the study area and the major phenomena that drive them. The chapter also covers different data sets that were used for this study, which include soil and weather data sources, yield data and satellite remote sensing data that were used to estimate crop development parameters that facilitated the calibration of the agro-hydrological model as elaborated in chapter 6, and 7.

2.1 The Study Area

The case study area for this research, was Northern part of Uganda. Calibration of agro-hydrological model covered in chapter 8, was conducted in a small agricultural farm of approximately 10 acres about 7 km east of Gulu municipality in Gulu district. The farm was established in 2012 by a private individual in conjunction with some dairy farmers in the USA as a training farm for modern dairy production in Northern Uganda. It started with 20 dairy cows managed under zero grazing unit with Maize (*Zea mays*), Alfalfa (*Medicago sativa*) and Cowpea (*Vigna unguiculata*) being the main crops grown within the 10 hectares of land for cow feeds. Northern Uganda is believed to be unsuitable for Dairy industry because the region experiences relatively higher temperatures compared to most parts of the country and therefore considered unfavorable for dairy production. The development of the SMDI covered in chapter 4, involved upscaling the usability of the SMDI through the application of the energy balance model using Landsat 8 TIRS satellite images covering parts of Lake Albert, Lake Kyoga and the lower Aswa river basins shown in Figure 2.3. Figure 2.1 shows different farming practices in Uganda grouped into agro-ecological zones, the study area being indicated with the red rectangle.

2.2 Climate

Uganda lies in a relatively humid equatorial climate zone, but the differences in the topography, prevailing winds, water bodies and high mountains cause large variability in rainfall patterns across the country. Average annual rainfall ranges from 800 mm to 2500 mm falling into two seasons in the south and into one season in the North. Temperature varies with altitude and exhibit little change from season to season over many parts of the country, although

some areas such as the western, eastern, south-western parts of the country characterized by high elevations show significant variations (Basalirwa, 1995). The climatic sub-regions, the spatial patterns of the natural resources and land use in Uganda are largely determined by rainfall, as is the case in many tropical areas. Uganda's climate is generally more reliable for agricultural production when compared to the other East Africa regions (Griffiths, 1972).

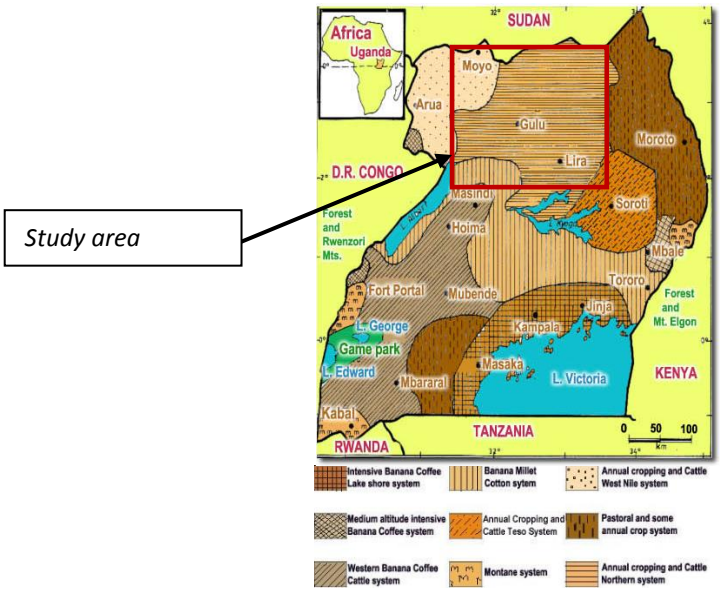

Figure 2.1 Agro-ecological zones in Uganda. The study area is shown. Source: Statistical Abstracts, MFP&ED, June 1997

Rainfall in Uganda is largely controlled by a number of climate phenomena such as: the inter-tropical convergence zone (ITCZ), the subtropical anticyclones, monsoon winds, and the moist westerlies from the Democratic Republic of Congo (DRC), locally termed 'Congo air mass', among several other regional and local factors (Basalirwa, 1995). The regional major features include the large water bodies and the complex topographic features. These features introduce significant modifications in the general wind- flow patterns over the region (Basalirwa, 1995).

Rainfall controlled activities fall under four seasons in Uganda. The first season is generally dry covering the months of December, January, February and Parts of March. During these months, covering December of the previous year in to the first two to three months of the next year, the ITCZ is far to the south outside the East African region (Basalirwa, 1991). Any rains falling during this season are associated with regional features mentioned above. The second season forms the main rainy season throughout Uganda, referred to locally as the 'long rains' lasting from March through May. This season coincides with the presence in the region

and the convergence into the ITCZ of the moist south-east monsoons from the Indian Ocean, controlled by the Mascarene anticyclone (Griffiths, 1972). The third season which is relatively dry except in parts of northern Uganda, lasts from June to the end of August. The rains in Northern Uganda during this season are associated with the influx of the moist westerly Congo air mass controlled by the St Helena heights centered off south-west Africa. Lastly, the fourth season is generally the second rainy season throughout the country and known locally as the 'short rains', lasting from September to the end of November. The rains of this season are associated with the convergence into the ITCZ of the north-east monsoons controlled by the subtropical anticyclones over the Azores and the Arabian Peninsula. Details of the climate of Uganda can be obtained from Basalirwa (1991) and Griffiths (1972).

Agricultural activities which are predominantly rainfall dependent as in many parts of East Africa fall under the two rainy seasons referred to as the 'long rains' and the 'short rains'. Recent droughts reported in parts of Northern Kenya, South Sudan and the Sahel are largely attributed to the climate perturbations over the region. Although such climate based major disasters have had minor impacts in Northern Uganda, they are projected to be more frequent (Nicholson, 2014). The structured preparation to absorb such large-scale shocks require interventions by the government and development partners. However, the short-term weather variations whose impacts are more locally confined are least reported. Such weather variability with local dimension triggers random field scale agricultural droughts in areas bordering the drought prune sub-regions such as Northern Uganda and they require insights into factors that drive them in order to devise appropriate strategies for their mitigation.

2.3 Description and summary of the data used in this study

Acquisition of metrological data in most developing countries is widely recognized as a major challenge (Wart et al., 2015; Nijbroek & Andelman, 2015; Nyeko, 2010). Considering this challenge, Northern Uganda is no exception, for instance within the annual cropping and cattle Northern system's agro-ecological zone, there are currently only three weather stations in operation. Moreover, reliable records can only be said of rainfall and air-temperature, albeit with lots of gaps. For this reason, meteorological data were obtained from three sources, namely: weather data records from the existing weather stations and two additional stations that were installed within Gulu district, one at Gulu University installed under the millennium science project in 2012. The second one being the automatic weather station procured for this research installed at the Dairy farm about 4km from Gulu University weather station. The

second source of the weather data were data records from the three operating weather stations in Northern Uganda i.e. weather station at Gulu Municipal, that at Lira Municipal and the one at Kitgum Town. The third source of weather data was the gridded weather data from European Centre for Medium Range Weather Forecast (ECMWF) reanalysis obtained at a 13km resolution covering the period 1979 – 2016 and the NASA-Power agro-climatic datasets. The gridded reanalysis data were used in conjunction with the data from FAO-Nile data base and the observed datasets from the existing weather stations, to generate what is referred to as propagated weather data.

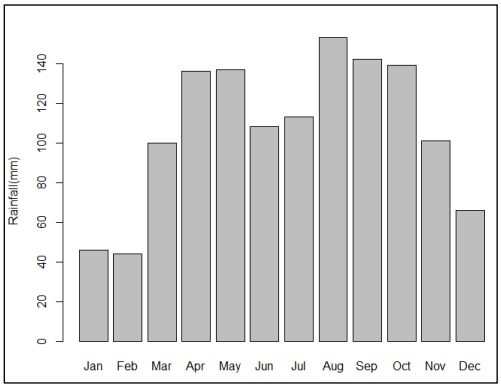

Figure 2.2 Monthly average rainfall from ECMWF reanalysis data (1979 - 2016) for a grid pixel corresponding to a location of Gulu Municipal weather station

2.3.1 Soils in Northern Uganda

The soils in northern Uganda are dominated by the ferralitic soils (Acric Ferralsols, Petric Plitnthosols, and Eutric Regosols of low to moderate agricultural productivity and Vertisols of moderate to high agricultural productivity. The ferralitic soils are rich in low activity clays (mainly kaolinite), which gives them low (<16 meq 100g-1) cation exchange capacity and hence are very poor at retaining cation nutrients. This implies that leaching loss of applied nutrients in form of mineral fertilizers is likely to be high. The dominant land preparation routines involve burning of vegetation and crop residues prior to primary tillage operations. This deprives the soils of the important organic matter inputs required to improving the CEC of the soils.

The ferralitic soils are also rich in sesquioxides, which increase the phosphorus fixation capacity, thus limiting availability of the nutrient for plant uptake. The Eutric Regosols on the other hand have high base saturation (and hence relatively more fertile than the ferralitic soils) but poor water retention capacity. Despite their relatively high agricultural productivity, the Veritisols are less used for arable farming due to their heavy texture, which presents major

challenges in the largely manual tillage operations characteristic of the farming systems in northern Uganda.

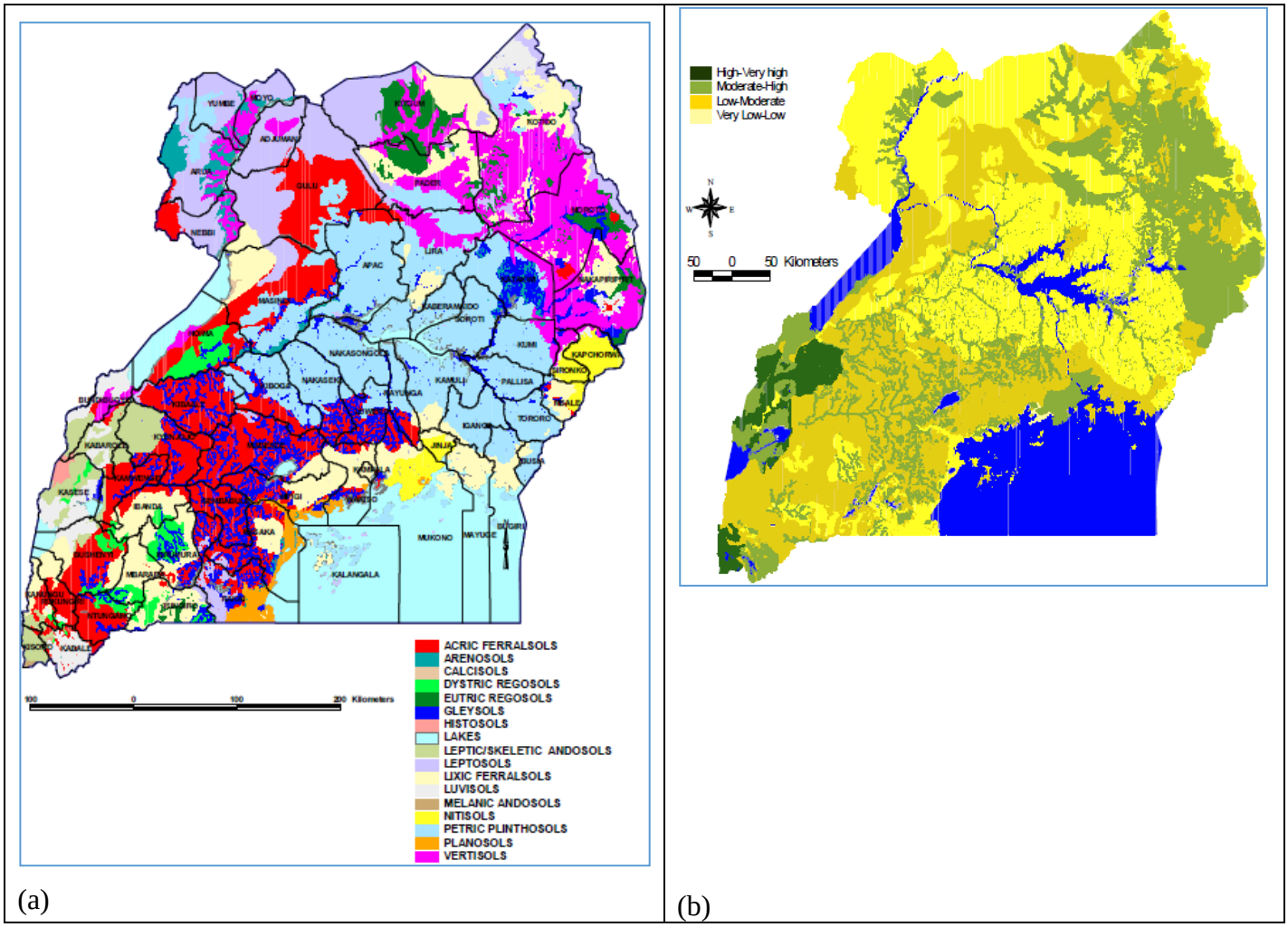

Figure 2.3 Maps showing (a) classification of Ugandan soils, and (b) Soil productivity in Uganda. Unpublished maps under development by NARO

2.3.2 Satellite Remote sensing data

The remote sensing estimation of the crop canopy parameters and the energy balance modeling were based on Landsat images that cover three agro-ecological zones (Figure 2.1 & 2.3), namely: (i) the annual cropping and cattle West Nile system, (ii) the banana Millet cotton system and (iii) the annual cropping and the northern cattle system. The Landsat 8 Operational Land Imager (OLI) and Thermal Infrared Sensors (TIRS) data are downloaded freely from United State Geological Survey website (https://earthexplorer.usgs.gov/). The images are identified by the paths of the imager and the rows of the images. For this study, image paths 171, 172 and row 58 were used. The Landsat 8 satellite carrying OLI and TIRS was launched in 2013 to extend the mission of Landsat 7 Enhanced Thematic Mapper Plus (ETM+) and Landsat 5 Thematic Mapper (TM) satellites (Loveland and Irons, 2016). The description of

Landsat 8 satellite, the OLI and TIR sensors and how it is different with the other Landsat 7ETM+ and Landsat 5TM sensors can be found in (USGS, 2016 and USGS, 2005).

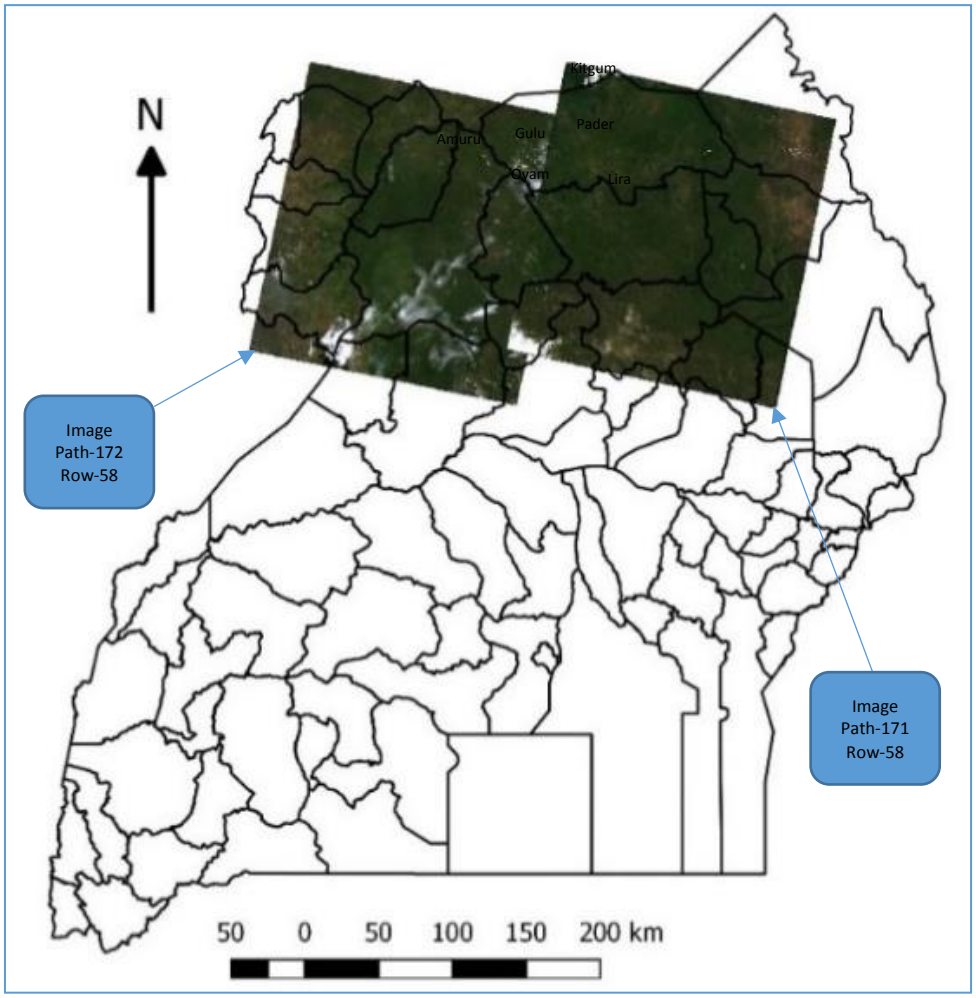

Figure 2.4 Map showing Landsat 8 images used in the analysis and the areal extent they cover Names of the focus districts for the case study are overlaid

2.3.3 Yield Data

Yield data are widely applied for validation of agricultural drought models, therefore yield data were obtained for the validation of the SMDI model developed and analyzed in this thesis. However, one of the limitation of this work was that it was not possible to obtain consistent yield records corresponding to the period propagated weather data were generated for the study area. For these reasons yield data were obtained from three sources: the first source was estimated from records of seasonal tonnage of silage made out of maize biomass for feeding dairy cows in the agricultural field in Northern Uganda used for the case study for the 2013 – 2015 period. The second source was yield records of seasonal maize production obtained from the National Agricultural Research Organization (NARO) for the study area. NARO considers

each agro-ecological zone in Uganda to have uniform agro-meteorological characteristics as such yield data obtained in one particular area within a given agro-ecological zone is considered representative for the entire agro-ecological zone. Yield data for maize production was therefore obtained only for the annual cropping and cattle Northern system agro-ecological zone (Figure 2.1) for 2007 – 2010 and 2014 – 2015 periods. the third source of yield data was obtained from Global Yield Gap Atlas (GYGA). GYGA has simulated yield data for grain production in most regions of the earth, Figure 2.5. The yields data in GYGA are simulated using calibrated crop growth model WOFOST based on propagated weather data and gridded global soil data. The simulated yields obtained cover 15 years from 1998 to 2012, although the GYGA yield datasets are rather based on coarse resolution simulation datasets.

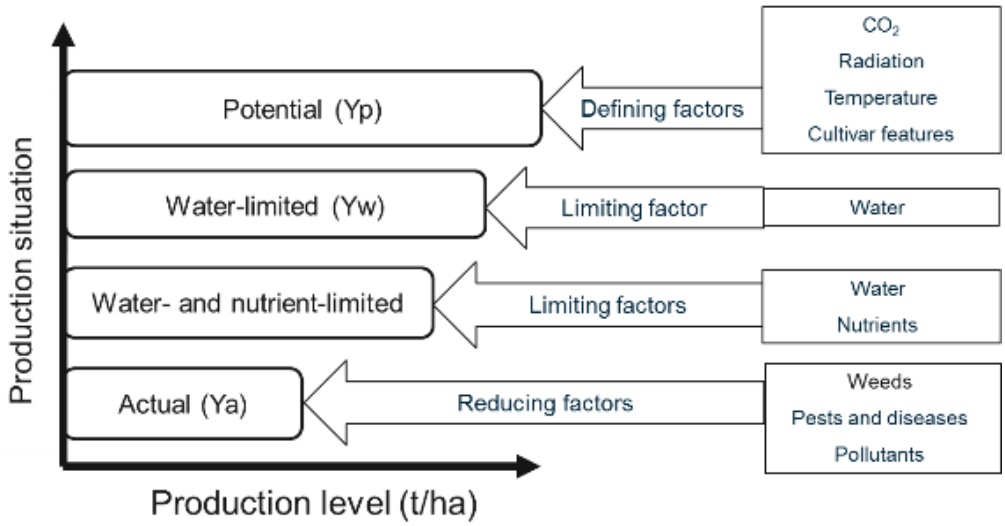

Figure 2.6 Generation of GYGA from crop growth model. Source: (Van Ittersum et al., 2013)

3 REVIEW OF DROUGHT INDICES APPLIED IN AGRICULTURAL DROUGHT MONITORING

Summary

In this chapter, some of the most common drought indices applied for agricultural drought monitoring are reviewed. It has been observed through the extensive body of literatures on drought monitoring that most of the drought indices in one way or the other are applied in monitoring agricultural drought. In most cases, meteorological droughts are applied because they are based mainly on precipitation and temperature data that are available in most weather stations. Because of this scenario, this chapter starts by reviewing meteorological drought indices and concludes with soil moisture based and remote sensing drought indices. Importance has not been placed on the order as they appear but emphasis is put on wide applicability of the drought indices. The soil moisture based indices that form the core of this research work are further elaborated in chapter 4.

3.1 Introduction

Drought indices are important metrics that are widely used for monitoring and assessment of drought characteristics. A drought index is a numerical indicator that is formulated by assimilating data from one or several variables such as precipitation, evapotranspiration, soil moisture etc. into a single numerical value (Zargar et al., 2011). Development of drought indices therefore depend strongly on the availability of suitable data (Niemeyer, 2008). Suitability of a given dataset for the development of a particular drought index is determined by some of the conditions that a good drought index must exhibit such as: statistical consistency across different spatial and temporal scales, comparability with other drought indices across different climatic regimes, connectedness to relative risks or historic conditions being assessed and should finally not be subjective, (Vicente-Serrano et al., 2009; Narasimhan and Srinivasan, 2005). There are over 150 documented drought indices that have been developed and more are being developed due in part to recent advancement in the satellite remote sensing technology (Zhang et al., 2017; Zargar et al., 2011; Niemeyer, 2008). A few of the drought indices in common use are listed in Table 2.1. Drought characteristics that are routinely monitored and assessed through application of drought indices are:

- *Duration*: refers to the length of time period that a given drought event takes. These can be some few weeks, several months to even years.

- *Severity*: this mainly refers to the degree of precipitation deficit or the degree of the resultant drought impact.
- *Spatial extent*: refers to the geographical area affected by a given drought event. This can vary from field scales, watershed to regional scale or even transboundary extent.
- *Magnitude*: refers to the accumulated water deficit which may be precipitation, soil moisture below some threshold during a drought period.
- *Frequency*: refers to also as the return period, it is defined as the average number of times a particular drought event with a severity or magnitude equal or greater than a given threshold.

The aim of this chapter is to review key drought indices that are used for monitoring agricultural drought.

3.2. Meteorological Drought Indices

Early development of drought indices depended on meteorological variables obtained from synoptic meteorological stations (Niemeyer, 2008). Essentially, these drought indices were classified as meteorological indices and are still currently referred to as such. The following are the most widely used meteorological drought indices:

3.2.1 Standardized Precipitation Index (SPI)

Developed by McKee et al. (1993), the SPI has gained wide acceptance in the past decade. SPI is primarily a meteorological drought index based on average precipitation amount in a 1, 3, 6, 9, 12, 24 or 48-monthly time step. In order to calculate SPI, the observed rainfall values for a given time step (usually in 1, 3, 6, 9, 12, 24 or 48-monthly period) are first fitted to a Gamma distribution. The Gamma distribution is then transformed to a Gaussian distribution (standard normal distribution with mean zero and variance of one), which gives the value of the SPI for the time step used. SPI is the recommended drought index by the world meteorological organization (WMO), for drought monitoring over diverse climatic conditions (Aghakouchak et al., 2015; WMO, 2009; Hayes et al., 1996) . More details on the computation of SPI are presented in chapter 4. The weakness of SPI has been attributed to two sources: i.e. the length of the precipitation records and the probability distribution on to which the precipitation is fitted for the calculation of SPI (Mishra and Singh, 2010). Since many regions do not have long term reliable precipitation records, computation of SPI for such areas are affected by short lengths of precipitation records. Secondly usually the probability distribution

on to which a given precipitation can be fitted differs from place to place. Therefore, it recommended that the precipitation of a particular area should first be fitted to an appropriate theoretical probability distribution, and the goodness of fit tested before applying SPI.

3.2.2 Standardized *Precipitation Evapotranspiration Index (SPEI)*

The SPEI was developed by Vicente-Serrano et al. (2010) and it compares the atmospheric demand, represented by the reference evapotranspiration (ET_0) with current water availability. The index has been applied in global drought studies (Spinoni et al., 2016; Vicente-Serrano et al., 2015; Beguería et al., 2014; Dai, 2011). SPEI has also been applied in diverse climatic regions for drought assessment such as in India: (Das et al., 2016); in China: (Xinyu et al., 2017; Yu et al., 2014), other regional applications were done in Europe: (Scaini et al., 2014; Törnros and Menzel, 2014; Vicente-Serrano et al., 2014) and in South Africa (Ujeneza and Abiodun, 2015).

The steps for the computation of SPEI are similar to those of the SPI; however, the SPEI uses the climatic water balance calculated from a difference between precipitation and reference evapotranspiration as input rather than precipitation alone (Beguería et al., 2014; Vicente-Serrano et al., 2010). Implementation of the SPEI algorithm involves calculation of the climatic water balance at various time steps, and fitting the resulting values to an appropriate probability distribution; usually the log-logistic probability distribution. This is done in order to transform the original values to standardized units that are comparable in space and time at different time steps (Beguería et al., 2014; Vicente-Serrano et al., 2010). More details of the SPEI algorithm is presented in chapter 4.

3.2.3 The Reconnaissance Drought Index (RDI)

The Reconnaissance Drought Index (RDI) developed by Tsakiris and Vangelis (2005) for regional drought severity assessment in South-Eastern-Europe (Vangelis et al., 2011; Tsakiris et al., 2007) in recent years, its use spread in European and global drought studies (Spinoni, 2016; Amin et al., 2015; Vicente-serrano et al., 2015; Shokoohi and Morovati, 2015). The index is calculated from precipitation (P) as a percentage of potential evapotranspiration (ET_0):

$$a = \frac{P}{ET_0} \qquad (3.1)$$

The reconnaissance drought index can be considered as an extension of SPI for more effective association with hydrological and agricultural drought (Niemeyer, 2008; Tsakiris and Vangelis, 2005). The index can be normalized as RDI_n , equation (3.2)

$$RDI_n = \frac{a_k}{\bar{a}_k} - 1 \qquad (3.2)$$

Where a_k is the value of the index for month k and $\bar{a}_k$ is the corresponding average value and the standardized value of the index can be written as:

$$RDI_{st}(k) = \frac{y_k - \bar{y}_k}{\hat{\sigma}_k} \qquad (3.3)$$

Where

$$y_k = \ln a_k \qquad (3.4)$$

And y_k is the arithmetic mean and $\hat{\sigma}$ is its standard deviation (Tsakiris et al., 2007; Tsakiris and Vangelis, 2005). The other commonly used meteorological drought indices include percent of normal and deciles.

3.2.4 Palmer Drought Severity Index (PDSI)

Palmer Drought Severity Index (PDSI) is one of the earliest and most widely used drought index (Alley, 1984; Palmer, 1965). It is formulated to evaluate prolonged periods of both abnormally wet and abnormally dry weather conditions. The index is based on a simple two-layer lumped parameter water balance model and is considered the most widely used drought index (Alley, 1984). The data input to calculate it include: precipitation, temperature, and average available water content of the soil for the entire climatic zone, although PDSI is considered a meteorological drought. Applying these inputs into a two-layer simple lumped parameter water balance model, various water balance components are calculated. These components include: evapotranspiration, soil recharge, runoff, and moisture loss from the surface layer. Then a 30-year historical weather data and the current water balance components are used to establish coefficients through which, a Climatically Appropriate for Existing Conditions (CAFEC) precipitation is computed. The precipitation deficit is then computed as the difference between the actual precipitation and the CAFEC. The precipitation deficit is then used to calculate the PDSI based on empirical relations.

The main criticism of the PDSI is that it is not comparable among diverse climatic regions (Wells et al., 2004; Alley, 1984). Another criticism of PDSI is that it is overly sensitive to

temperature changes (Feng et al., 2016). This is because ET_0 input as used in PDSI is calculated using the empirical Thornthwaite method which uses only the temperature input to calculate ET_0. More details on PDSI computations are presented in Palmer (1965), Alley (1984) and Akinremi and McGinn (1996). The limitation of PDSI led Wells et al. (2004) to develop a self-calibrating PDSI (SC-PDSI) that automate the constants used in the calculation of its empirical constants thereby enhancing its comparability across different climatic regions (Wells et al., 2004).

3.3. Agriculture Drought Indices

When soil moisture availability to plants drop to such a level as to disrupt the normal plant development and adversely affect crop yields, agricultural drought is considered to have set in. Generally, agricultural drought is defined through soil moisture deficit in relation to meteorological drought and its impact on agricultural production. Soil moisture times series provide the only realistic means of assessing agricultural drought (Mannocchi et al., 2004). However, availability of long term soil moisture time series is very limited in most regions especially in many developing countries where they are virtually non-existent. For this reason, some Agricultural drought indices were formulated on the basis of hydrological models (Narasimhan et al., 2005). The predictive values of such indices are therefore affected not only by the data accuracy and reliability but also by the assumptions embedded in the conceptualization of the hydrological model. In most cases, especially when applying distributed hydrological models, the limitations of the derived indices are linked to the soil water balance model formalization, its parameterization and its temporal and spatial resolution (Van Der Knijff et al., 2010). All drought indices including the meteorological, hydrological and remote sensing drought indices in one way or the other are used in agricultural drought monitoring. The following are the most widely used agricultural drought indices:

3.3.1 Crop Moisture Index (CMI)

Palmer (1968) developed CMI as an index for monitoring short term agricultural drought from the original procedure for calculating the PDSI. This was done to account for the time lag between the soil moisture available to plants and a precipitation events. This time lag has a buffering effect on the response of plants to precipitation deficit. The PDSI developed earlier by Palmer (1965) is useful mainly for monitoring long-term drought conditions as a result of precipitation deficit. However, agricultural crops are highly susceptible to short-term moisture

deficits during critical periods of crop growth stages. Whereas PDSI is calculated from precipitation deficits and is applied for monitoring long-term drought conditions, CMI is calculated from evapotranspiration deficits. CMI unlike PDSI is used for monitoring short-term agricultural drought conditions that are detrimental crop growth. More details on the use of the CMI algorithm are presented in Palmer (1968).

3.3.2 Drought indices based on transpiration

One of the truly agricultural drought index is the transpiration deficit (DT) index, developed by Marletto et al. (2005). The DT is calculated daily from a water balance model as the difference between the Potential and actual transpiration. Then the integrated transpiration deficit (DT_x), cumulated over x days is calculated as:

$$DT_x = \sum_{n-x}^{n} (T_m - T_e) \qquad (3.5)$$

Where *n* represent the current day on which the DT_x is being calculated and x = 30, 60, …, 180 days). The use of DT_x was assessed in comparison with SPI in the Emilia Romagna region the index demonstrated "noticeable differences" with SPI (Marletto and Zinoni, 2004; Marletto et al., 2005). The same authors stated that the difference resulted from the different procedures used to calculate each of the two indices. The DT_x is based on the adaptation mechanism plants have when experiencing moisture stress. The plant's water requirements depend on the prevailing atmospheric condition, the biological characterization of the plant species, its stage of development, the physical, chemical and biological properties of the soil and soil moisture content (Savva and Frenken, 2002; DeWitt, 1986). Whenever plants experience water stress such that the energy required to extract the limited water from the soil by the roots become ever greater, plants have mechanisms through the closure of stomatal pores to limit water loss through transpiration. In such a condition the plant's actual transpiration is less than potential, and this is the condition that the index captures (Marletto et al., 2005).

3.3.3 *Soil moisture based Agricultural drought indices*

Many other agricultural drought indices are based on Soil Water monitoring. These include the soil water index (SWI) and the soil moisture index (SMI) developed almost concurrently by Sridhar et al. (2008) and Hunt et al. (2009) and recently Soil water deficit index (SWDI) developed by Martínez-Fernández et al. (2015). These soil water based agricultural drought

Table 2.1 Current commonly used drought indices. Sources: Dai, (2011); WMO and global partnership (2016)

Type	Name of Index	Calculation method	Strengths	Weaknesses	References
Meteorological Drought	Standardized Precipitation Index (SPI)	Fitting a Long-term precipitation record into a normal distribution	Can be computed for different time scales Symmetric for both dry and wet periods Related to probability	Requires long term precipitation records No consideration of evapotranspiration	Mckee et al., 1994
	Reconnaissance Drought Index (RDI)	Fitting and transforming long term record into a normal distribution	Consider both precipitation and evapotranspiration Can be computed for different times scales Comparable to FAO aridity index	Requires long term meteorological data Sensitive to the method of calculating potential evapotranspiration	Asadi Zarch et al., 2015; Tsakiris and Vangelis, 2005; Tsakiris et al., 2006 Beguería
	Standardized Precipitation Evapotranspiration Index (SPEI)	Fitting and transforming a long- term deficit record into a normal distribution Calculating	Considers both water supply (precipitation) and demand (potential evapotranspiration) Can be computed for different time scales Considers both water supply (precipitation) and demand (potential evapotranspiration) Can be computed for different time scales	Requires long-term meteorological data Sensitive to the method to calculate potential evapotranspiration Seasonal Requires long-term meteorological data Sensitive to the method to calculate potential evapotranspiration Seasonal	Beguería et al., 2014; Vicente-Serrano et al., 2010 Alley, Beguería et al., 2014; Vicente-Serrano et al., 2010
	PDSI	Calculating the departure of moisture balance from the normal condition Based on a 2-layer bucket-water balance model	Uses a total water balance methods	Uses arbitrary rules for defining available water capacity in the soil	
Agricultural Drought	Soil Water Deficit Index (SWDI)	Comparison between actual soil water content, WCFC and WCWP	Can be determined by direct measuring or EO Implicitly accounts for precipitation and irrigation inputs	Assumes that the lag between meteorological and agricultural drought represents the response time for impact occurrence	Martínez-Fernández et al. 2015; Martínez-Fernández et al. 2016
	Integrated transpirative Deficit (TDx) pF	Cumulate difference between potential and actual transpiration	Has been developed and tested in northern Italy Accounts for hydrological balance Accounts	Sensitive to the assumptions of the hydrological model, its spatio-temporal resolution and its calibration Does not account for irrigation inputs	Marletto & Zinoni 2004; Marletto et al. 2005
	pF anomalies	Calculating the z-score of water potential derived from a hydrological model Linearly	Accounts for fully hydrological balance	Sensitive to the assumptions of the hydrological model, its spatio-temporal resolution and its calibration Does not account for irrigation inputs	Laguardia & Niemeyer 2008; Sepulcre-Canto et al. 2012
	Vegetation Condition Index (VCI)	Linearly scale of NDVI derived from remote sensing	Identifies drought impact on vegetation Identifies	Limited by cloudiness Short period of records	Kogan 1995
	Standardized Vegetation Index (SVI) Combined	z-score of VI derived from remote sensing	Identifies drought impact on vegetation	Limited by cloudiness Short period of records	Peters et al. 2002; Horion et al. 2012
Combined drought index	Combined Drought Indicator	Combination of indices (SPI, pF, fAPAR) Combination of indices (SPI, pF, fAPAR)	Characterizes agricultural drought cause-effect relationship Good spatial coverage and high resolution	May not represent conditions that may carry over from season to season (i.e. uses only a single SPI value) Hard to replicate outside Europe	Sepulcre-Canto et al. 2012; Horion et al. 2012; de Jager & Vogt 2012

indices were developed on the FAO-56 concept of available water for plant and are applied for rapid monitoring of agricultural drought. Since the soil moisture based drought indices form

the core of this work they are addressed in details in chapter 4, where the new approach to develop a SMDI is covered. The other soil moisture based indices are the soil moisture deficit index (SMDI) and the evapotranspiration deficit index (EDI) developed through a distributed hydrological simulation of long term soil moisture time series (Narasimhan and Srinivasan, 2005) indices were developed on the FAO-56 concept of available water for plant and are applied for rapid monitoring of agricultural drought. Since the soil moisture based drought indices form the core of this work they are addressed in details in chapter 4, where the new approach to develop a SMDI is covered. The other soil moisture based indices are the soil moisture deficit index (SMDI) and the evapotranspiration deficit index (EDI) developed through a distributed hydrological simulation of long term soil moisture time series (Narasimhan and Srinivasan, 2005)

3.4 Remote Sensing based Indices

Regional drought monitoring through the commonly used drought indices such as the PDSI and SPI require adequate density of meteorological stations. Usually a drought index is calculated for each station over the entire region and use is made of statistical interpolation techniques to infer drought conditions over un sampled locations. The higher the density of the meteorological stations, the less the uncertainty associated with drought conditions over interpolated locations. Therefore, high uncertainty of the interpolated drought index values over un sampled location may result from climatic data obtained from a sparse network of meteorological stations. Moreover, commonly used spatial interpolation methods such as the deterministic model of inverse weighted distance and the stochastic model of ordinary kriging are affected by a number of factors. Because of these and other limitations of climatic data collected from synoptic meteorological stations, application of remote sensing for regional drought monitoring has been gaining more attention in recent times (Choi et al., 2013; Rhee et al., 2010). In areas with limited meteorological stations such as in developing countries, remote sensing may be the only reliable source of information for regional drought monitoring.

Remote sensing application in drought monitoring is based on detection of the radiometric properties of the vegetation canopies. These vegetation properties are defined by what are commonly referred to as *vegetation indices (VI)*. The most widely used vegetation index derived from the optical region of the electromagnetic spectrum is the normalized difference vegetation index (NDVI) (Choudhury, 1987). The NDVI is computed from remotely sensed

images in the near infrared (ρ_{nir}) and the red (ρ_r) spectral reflectance values as expressed in Equation (3.6):

$$NDVI = \frac{\rho_{nir} - \rho_r}{\rho_{ni_r} - \rho_r} \quad (3.6)$$

Time series of NDVI are often used for detecting anomalies in crop growth, which are supposed to be determined by the drought index.

Another widely used vegetation index for drought monitoring is the vegetation condition index (VCI) developed by Kogan (1995a). The VCI is computed by scaling NDVI between 0 and 1 for each location and VCI is calculated as:

$$VCI = \frac{NDVI - NDVI_{\min}}{NDVI_{\max} - NDVI_{\min}} \quad (3.7)$$

Kogan (1995b) similarly introduced the Temperature Condition Index (TCI). From the additive combination of the VCI and TCI, the Vegetation Health Index (VHI) was introduced. Currently many more vegetation indices exist. Their specific applications are limited by the image spatial resolution, usually the more commonly applied methods are those based on large pixel sizes and therefore appropriate for regional drought monitoring.

3.5 Conclusion

In this chapter, some of the drought indices used for agricultural drought monitoring were reviewed. The strengths and weaknesses of each of the indices highlighted as reported in the different literatures. From the reviewed literatures, some gaps in the current agricultural drought monitoring tools could be identified. One such a gap is that majority of the newly developed agricultural drought indices have not been tested in Sub-Saharan Africa. Especially the soil moisture based drought indices. One obvious reason for this could be the unavailability of soil moisture monitoring programs in Africa. Secondly, even the widely-used SPI has had very limited application in Africa especially in Uganda, one such a study was reported, moreover covering the entire east Africa (Ntale and Gan, 2003), thus focusing on large scale hydrological droughts with transboundary spatial extent.

Drought monitoring studies that have been carried out in Africa were therefore concerned mainly with the identification of extreme events, such as the monitoring of the hydrological drought. Therefore, gaps still exist in the body of the extensive literatures available on drought indices in monitoring agricultural droughts at field scale in developing countries. Matters are

complicated by limited climatic records that are always the case in developing countries especially in Africa. For instance, it is recommended that for the calculation of SPI, the commonly applied meteorological drought, requires at least 30 years of data. This requirement is seldom met by climatic records in developing countries. These challenges call for development of new indices that would circumvent the need for long term climatic data and can be applied at the field scale. The method presented in this thesis as elaborated in the next chapter 4, solves this problem by application of gridded climatic data in combination with limited observed weather data through the data propagation algorithm to create a fairly long term climatic records that can be applied for the development of the index. Moreover, the application of simulation models solves the problem of unavailability of long term records of soil moisture time series required to develop soil moisture based indices.

4 DEVELOPING A NEW APPROACH FOR THE DEFINITION OF SOIL MOISTURE DEFICIT UNDER RAIN FED CROPS

Summary

In this chapter, the core concepts developed in this thesis are presented. The chapter covers reviews of the state of the art on soil moisture based drought indices and applies the information gathered from the reviewed literature to formulate a new soil moisture deficit index (SMDI). It also covers algorithms used to derive commonly used meteorological drought indices i.e. the standardized precipitation index (SPI) and the standardized precipitation and evapotranspiration index (SPEI).

4.1 Introduction

Drought incidences are becoming more frequent with the increased climatic variability (Xinyu et al., 2017; Yu et al., 2014; Wang, 2005). Current widely applied drought indices for the detection of the onset and termination of especially agricultural droughts were developed with the aim of large scale monitoring of extreme events that are mostly common in arid and semi-arid areas. As a result, such drought indices cannot essentially be applied for monitoring agricultural droughts at field scales. This difficulty, prompted the development of soil moisture based drought indices that are suitable for field scale agricultural droughts monitoring. However, the newly developed indices rely on long term records of measured soil moisture time series that are available only in developed countries. Some of the indices apply distributed parameter hydrological models for generation of the long-term soil moisture time series (Yan et al., 2013; Narasimhan and Srinivasan, 2005). However, application of distributed parameter hydrological models requires reliable stream flow records and a host of other climatic, land use, topographic and soil parameters that are not available especially in developing countries at water shade scales (Zhang et al., 2016; Yadav et al., 2007). The aim of this chapter is to present the development of a new approach to define soil moisture deficit index (SMDI) for monitoring the onset and termination of agricultural droughts at field scales. The approach focuses on the application of freely available tools such as high resolution satellite images to estimate crop development parameters, freely available numerical codes such as Hydrus 1D, for simulation of moisture transport in to the unsaturated soil system within the root zone. The new approach also relies on a method of gap filling climatic records through application of gridded weather data in conjunction with observed weather data and evaluation of appropriate reference evapotranspiration models for specific application areas presented in chapter 5. The

schematization illustrating all the concepts applied is shown in Figure 4.1 and explained in section 4.4. These tools are all applied to generate long term records of soil moisture time series for the generation of threshold parameters of the water retention curve applied for the definition of SMDI. The chapter concludes by elaborating on algorithms for calculation of reference indices; SPI and SPE for testing the reliability of the newly developed SMDI.

4.2 Definition of The Soil Moisture Deficit Index from Soil Moisture Measurements

Early application of soil moisture information for monitoring moisture deficits in agricultural soils was done by Baier (1969) using values of field capacity and wilting point as threshold parameters for defining moisture stress condition for plants. Baier (1969) demonstrated that ET become limiting below the midpoint between field capacity and wilting point, or at 50% of total available water and developed a soil-water–ET curve which demonstrated that no reduction in ET occurred until soil water fell below 50% of field capacity. Similar elaborations were done by Purcell et al. (2003), in which he developed an atmospheric water deficit (AWD) as the difference between the 7-day running sum of precipitation and the 7-day running sum of evapotranspiration. Purcell et al. (2003) proposed to define the probability at which plants begin to experience moisture stress as 37% percent of the moisture level at field capacity. Similar approach was used by Sridhar et al. (2008) to develop a user-friendly drought index called the Soil Moisture Index (SMI) to identify a quick onset of agricultural drought. They did this, by demonstrating that the observed dryness of a soil relative to the plant's ability to extract water can be scaled over the range from field capacity to wilting point. Thus, defining SMI as a fraction of available water (F_{AW}) content between field capacity and the wilting point. The original definition of the SMI is shown in equation (4.1), (Sridhar et al., 2008). A follow up work by Hunt et al. (2009) using similar concepts to define SMI are shown in equations (4.2) and (4.3).

$$SMI = \left[\frac{5(\theta - \theta_{WP})}{(\theta_{FC} - \theta_{WP})} - 5 \right] \qquad (4.1)$$

Where θ_{FC} is the soil moisture content at field capacity and θ_{WP} is the soil moisture content at wilting point yielding values of SMI from -5 to 0.

$$SMI = -5 + 10F_{AW} \qquad (4.2)$$

SMI being scaled between -5 and +5 and F_{AW} as given by equation (4.3); defined between the Water contents at field capacity and that at the wilting point.

$$F_{AW} = \frac{\theta - \theta_{WP}}{\theta_{FC} - \theta_{WP}} \quad (4.3)$$

Using the above concepts, Sridhar et al. (2008) used soil data measured by automatic soil moisture instruments over a period of eight years and modeled soil moisture using a simple hydrological model to monitor agricultural drought using values of θ_{FC} and θ_{WP} from literatures. Whereas Hunt et al. (2009), used the same soil moisture database but defined θ_{FC} and θ_{WP} by ranking an eight year soil moisture data for the growing seasons and letting the 95th percentile to be θ_{FC} and the 5th percentile to be θ_{WP} and verified the obtained values with published values of θ_{FC} and θ_{WP} Their findings using soil data from four sites showed that the variation of SMI corresponded to rainfall variability in the two areas studied.

Recently similar concepts were applied by Martínez-Fernández et al. (2015) using REMEDHUS soil moisture database in Spain. In their case, weighted average of soil moisture values for the three profiles measurements at 5cm, 25cm and 50cm in the root zone were used to define what they termed as the soil water deficit index (SWDI) for application as a suitable agricultural drought indicator, equation (4.4). The SWDI was scaled between -10 and 10, thus giving it Agricultural meaning. Use of these approaches that rely on soil moisture databases are however only possible where such soil moisture databases exist. However, most developing countries lack availability of robust soil moisture monitoring programs as such alternative techniques for estimating long term soil moisture must be developed for these methods to be applied. Alternatively, the threshold parameters for defining the availability of water for plant i.e. θ_{FC} and θ_{WP}, can be determined in the laboratory from undisturbed soil core samples using pressure plate apparatus. This is usually done by specifying θ_{FC} as being equivalent to moisture content at matric potential pressure of 300m and θ_{WP} corresponding to moisture content at the matric potential pressure of 1500m (Romano et al., 2011).

$$SWDI = \frac{\theta - \theta_{FC}}{\theta_{FC} - \theta_{WP}} \times 10 \quad (4.4)$$

However, laboratory determination of these threshold parameters for soil water retention do not provide proper representation of the actual field soil moisture conditions (Romano et al., 2011)**.** Another method of estimation of these threshold parameters is by use of *Pedo-Transfer Functions* (PTFs); (Wegehekel and Gerke, 2015; Botula et al., 2012; Minasny, 2009; Pidgeoni, 1972). However, development of PTFs, rely on extensive databases of soil physical

characteristics that are unavailable in many developing countries. Most of the currently available PTFs, were developed based on temperate and Mediterranean soil databases that cannot be applied with confidence to other soil types such as the tropical soils (Botula et al., 2012; Romano and Palladino, 2002; van den Berg et al., 1997)

4.3 A New Approach to define The SMDI for Application in Developing Countries

Recent development in instrumentations for measurement of soil moisture has allowed increased soil moisture databases worldwide (Engda and Kelleners, 2015). Availability of low cost soil moisture monitoring sensors equipped with data loggers that allow remote transmission of soil moisture content in real time, freely available remote sensing soil moisture products such as the SMOS (Soil Moisture and Ocean Salinity) and SMAP (Soil Moisture Active and Passive); add to the growing soil moisture databases worldwide (Martínez-Fernández et al., 2016; 2015; Wagner et al., 2011). Despite the availability of these methods and tools, soil moisture databases in majority of developing countries are still lacking, as such research efforts in agricultural water management have lagged behind in areas where they are much needed (Dobriyal et al., 2012). The need to increase food production on limited land areas with declining fresh water resources requires that the limited water and soil resources are managed sustainably. This requires methods to identify and quantify shocks so as to enable formulation of strategies for their mitigation ensuring improved land and water productivity.

In this thesis, a new approach to define the soil Moisture deficit index (SMDI) is developed using soil moisture as a drought indicator. The new index is calculated using simulated root zone soil moisture time series from an agricultural field in Northern Uganda as presented in case studies of chapters 7 and 8 of this thesis. The index is verified using water deficit indicators such as AWD, SPEI and SPI (with monthly temporal resolution) as reference indices and yield data from the study area. The novelty in this approach is in the application of a physically based Agro-hydrological model for the simulation of the soil moisture content. Since such simulation models capture the actual physics of the moisture movement in the SPAC, it can be very useful in areas where reliable networks of soil moisture measuring instruments are lacking such as in developing countries. This method is very flexible and particularly applicable in areas with limited studies on impact of climatic variability on agricultural production. The steps involved rely on freely available tools such: high resolution satellite images to estimate crop/vegetation canopy parameters, freely available numerical codes for Agro-hydrological modeling, reanalysis data for filling gaps in weather data that are very common in developing countries,

testing of appropriate reference evapotranspiration models suitable for specific application areas and utilization of low cost commercial soil moisture sensors for calibration of Agro-hydrological models, as illustrated in the schematization in Figure 4.1.

4.4 Conceptual Frame Work Illustrating the New Approach to Define SMDI

The conceptual diagram in Figure 4.1, illustrates the interactions between various concepts applied in the new approach presented in this chapter for the definition of the SMDI. The development of the new approach focuses on overcoming challenges in calculation of soil moisture based drought indices for application in developing countries, especially in the humid equatorial and tropical climates. In such climates, agricultural drought is thought to set in after the onset of a meteorological drought triggered by sustained precipitation deficits. As crops continue to extract soil moisture, water storage in the soil depletes since there is no precipitation to replenish the soil moisture loss. When this reaches a critical threshold, termed wilting point (θ_{WP}), the crops dry up. However, before crops reach this critical point, when soil moisture content falls below 75% of its value at field capacity (θ_{FC}), as has been assumed here (Equation 4.5), crops begin to experience moisture deficit. When this condition persists, it is no longer possible to reverse the effects on crop yields especially if it occurs during tasseling for the case of Maize (Zea mays). This is the point that SMDI is developed to detect such that mitigation strategies can be planned.

Therefore, the conceptual diagram illustrates the different concepts applied to address moisture movement through the soil-plant-atmosphere continuum (SPAC), for the purpose of developing the new approach to define SMDI. Accounting for moisture movement in the soil requires estimation of soil hydraulic characteristics which is achieved in this schematization through the inversion of a water flow model (Hydrus 1D). Whereas accounting for water movement in the plant requires estimation of the plant development characteristics, achieved here through application of satellite remote sensing. And lastly accounting for water movement into the atmosphere requires collection of reliable climatic data which is best achieved through the concept of data propagation, for a developing country such as Uganda. Definition of the boundary conditions for the water flow model requires specification of infiltration rates and evaporation fluxes between the soil-plant-atmosphere boundary. The infiltration rates can be specified through knowledge of daily precipitation totals, since simulation was carried out at daily time steps. The evaporation fluxes are accounted for in two ways: for the calibration of the water flow model, for a short time period, usually one or two seasons of weather records

can be obtained from digital weather station from which FAO-56 is applied to calculate evaporation fluxes. Once the model is calibrated, the long-term simulation requires a less data intensive ET_o model in combination with published crop coefficient values for estimation of actual evaporation fluxes. Selection of the less data intensive ET_o requires evaluation of the various evapotranspiration models in the study area. Since the evaluation requires sophisticated methods that involve equipment that are usually not available in developing countries, it is recommended here to apply the FAO-56 PM model for the assessment of the other ET_o models. This is done in chapter 5, where 13 reference evapotranspiration models are evaluated using a 4-year datasets obtained near the study site. Once the less data intensive reference model is selected, the evaporative fluxes can be calculated throughout the simulation period to generate long term records of soil moisture time series. The long-term soil moisture records are thereafter used to calculate θ_{FC} and θ_{WP} from which SMDI can be computed. Verification of SMDI is achieved through reference indices such as SPI and SPEI whose conceptual diagrams are separately shown in Figures 4.3 and 4.4 respectively. Further verification of SMDI is also achieved through application of AWD whose calculation is similar to that of SPEI variable D. Except that the calculation of D as applied in AWD is done according to Purcell et al. (2003) as the difference between the 7-day running sum of precipitation and the 7-day running sum of ET_0.

Therefore, the development of the new approach as presented in this chapter is based on the original definition of the SMI and later elaboration by Martínez-Fernández et al. (2015). The difference from these approaches is in the way soil moisture is generated and in defining the threshold parameters (θ_{FC} and θ_{WP}) of the soil moisture retention curve. In the steps involved in this approach, there is an inherent assumption that continuous meteorological records for at least three years of especially rainfall, and air-temperature can be found in most weather stations in developing countries for which the approach is developed. If the other meteorological variables such as solar radiation, wind speed and relative humidity are available in a given weather station, they become added advantages. Secondly, it is assumed that the weather variability exhibited by meteorological data in a given location is the same everywhere in that Agro-ecological zone within which the weather station is located (Wart et al., 2013). The second assumption is particularly applicable for Northern Uganda districts, that are grouped in to one Agro-ecological zone. The steps involved are as follows:

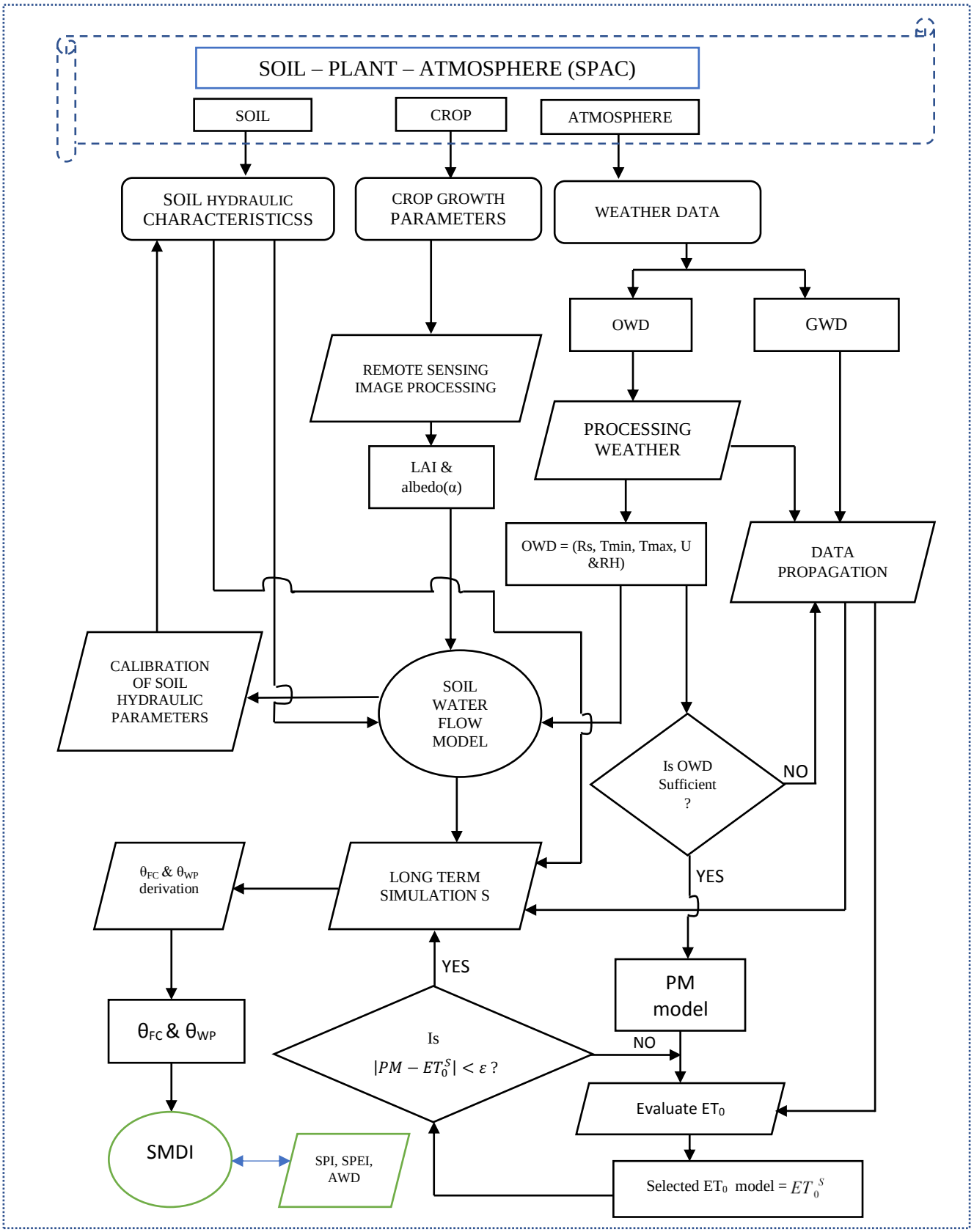

Figure 4.1 Flow chart showing conceptualization of the new methodology for development of SMDI: OWD = Observed weather data, GWD = Gridded weather data, ET_0^S = Selected ET_0 model. PM=FAO-56 ET_0 Model, ε=some value determined by RMSE, MAE, NSE, d or r^2

- Long term simulation of the one-dimensional daily soil moisture times series at a representative location for a given Agro-ecological zone.
- Statistical analysis of the simulated soil moisture times series
- Definition of the threshold parameters from the model generated soil moisture times series
- Computation of the daily SMDI using the method of Martínez-Fernández et al. (2015)
- Aggregation of the SMDI over weekly or monthly time scales for agricultural drought monitoring
- Computation of the other drought indicators such as a SPEI, AWD, CMI or monthly SPI to act as reference agricultural drought indicators
- Comparison of the developed SMDI with the reference agricultural drought indicators

The long-term simulation of the soil moisture times series can be done in a distributed way using a distributed parameter hydrological model (Narasimhan and Srinivasan, 2005). The difficulty with distributed parameter modeling in developing countries are however, the limitation of data for model calibration (Wi et al., 2015). In most cases, one basin outlet stream records exist for calibration of model parameters. Thus, whereas there are tools such as Geographical Information Systems (GIS) and Digital Elevation Models to aid spatial and topographical analysis, application of such models in developing countries are still wrought with lots of uncertainty (Andersen et al., 2001). Therefore, it is considered that application of distributed parameter models for generation of soil moisture time series for the definition of SMDI parameters would introduce serious errors when it is to be applied for operational drought monitoring at field scales. Such distributed parameter models can best be applied for the detection and analysis of extreme events that have basin and/or transboundary dimensions such as in monitoring hydrological drought. The steps in this new approach is therefore to use a one dimensional Agro-hydrological model such as Hydrus 1D for generation of soil moisture time series. It is much easier to generate data for the calibration of such a physically based model using the available tools, than when they are to be implemented in a distributed mode.

Considering the steps above; once the model is calibrated for a given location, what remains is to generate input data for the long-term simulation of the soil moisture times series. since a model such as Hydrus 1D once calibrated requires definition of the initial and the boundary conditions, for simulation of the soil moisture times series. As long as the boundary condition is defined, the calibrated model can be used for a long-term generation of the state variable such as soil moisture and pressure heads. The initial condition is defined by the initial

soil moisture or pressure heads within the soil profile during the start of the simulation which can easily be obtained by measuring the soil moisture content or the pressure heads at the beginning of the simulation using any of the low-cost soil moisture sensors. The boundary conditions have to be defined for the entire simulation periods.

The challenge with the specification of the boundary conditions throughout the simulation period is in estimation of the soil evaporation and the transpiration, treated for this study in combination as Evapotranspiration (ET). For short term period, such as two seasons it can be possible to apply data from automatic weather stations which are nowadays commercially available at reasonable prices. The automatic weather station can therefore be installed in any location to generate meteorological data say for a year or two for the calculation of the ET using the FAO-56 PM model, recommended by the Food and Agricultural Organization of the United Nations as a sole method for calculation of reference ET over diverse climates. Since such a station can generate all the data required for input in to the FAO-56 PM model.

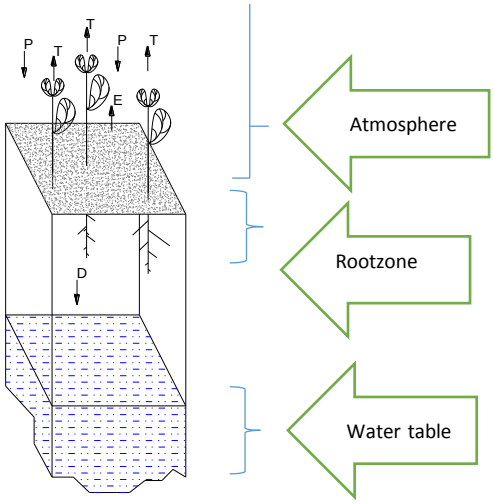

Figure 4.2 A schematic diagram showing boundary conditions in one dimensional simulation of moisture movement in the soil system: P is precipitation, T is transpiration from plants, D is deep percolation below the root zone into the water table. Some other components such as surface runoff, and interception by vegetation are not indicated.

However, for longer term simulation of soil moisture time series, some way of estimating the reference ET has to be devised other than the FAO-56 PM model, due to the limitation in the data records in developing countries. Usually the Hargreaves method has been proposed as an alternative for application over diverse climatic regions (Allen, 1998). However, the validity of using the Hargreaves (HG) method has to be assessed per specific application areas and if

possible other reference ET models with less data requirements just like the HG be tested for comparison. As a requirement for this approach, assessment of the reference ET models is done in chapter 5.

Since the application focus of this method is in areas where rain-fed farming is predominant, equation (4.4) can be modified into equation (4.5). In this case; just as Baier (1969), suggested that plants begin to respond to moisture deficit in the soil when soil moisture content is depleted to 50% of its value at field capacity. Here it is taken that below 75% of the moisture content at field capacity, plants will begin to experience moisture stress. The factor of 4 is used in the SMDI for easy comparison with the other commonly used drought indices which use similar range of values for drought indices.

$$SMDI = \left(\frac{\theta - 0.75\theta_{FC}}{\theta_{FC} - \theta_{WP}} \right) \times 4 \qquad (4.5)$$

4.5 Procedures for Deriving Reference Indices for Evaluation of the SMDI

The SPI, developed by McKee et al. (1993) is a meteorological drought index recommended by the WMO for the assessment of meteorological droughts in any part of the globe because of its comparability over different regions and requiring only precipitation data for its calculation (WMO, 2009; Ntale and Gan, 2003). Therefore, SPI was chosen for the assessment of SMDI over Northern Uganda together with SPEI and AWD which are temperature based drought indices. SPEI was developed by Vicenete-Serano et al. (2010) and has been applied over diverse climatic regions. Atmospheric Water Deficit (AWD) was developed in the United states by Purcell et al. (2003). Its calculation is based on difference between the reference evapotranspiration and precipitation just like the SPEI. However, unlike the SPEI that transforms the evapotranspiration deficit in a normalized distribution basing on a log-logistic probability distribution, the AWD directly applies the evapotranspiration directly for drought assessment (Torres et al., 2013; Purcell et al., 2003). Therefore, it has simple steps to implement compared to SPEI and SPI that require fitting distributions.

4.5.1 The SPI Algorithm

Computing SPI involves fitting a gamma probability density function to a given monthly rainfall distribution. The gamma distribution function is given by its probability density

function g(P), $g(P)=\frac{1}{\beta^{\alpha}\Gamma(\alpha)}P^{\alpha-1}e^{-x/\beta}$

(4.6)

Where parameters α and β can be estimated by the maximum likelihood method

$$\alpha=\frac{1}{4A}\left(1+\sqrt{\frac{1+4A}{3}}\right) \quad (4.7)$$

$$\beta=\frac{\alpha}{\overline{P}} \quad (4.8)$$

$$A=\ln(\overline{P})-\frac{\sum(P)}{N} \quad (4.9)$$

N is the number of the observation months. the cumulative probability can be given by

$$G(P)=\int_0^P g(P)dP=\frac{1}{\beta^{\alpha}\Gamma(\alpha)}\int_0^P x^{\alpha-1}e^{-P/\beta}dP \quad (4.10)$$

Letting $t=P/\beta$, (4.10) becomes an incomplete gamma function

$$G(P)=\frac{1}{\Gamma(\alpha)}\int_0^t x^{\alpha-1}e^{-t}dt \quad (4.11)$$

As the gamma function is undefined for $P=0$, the cumulative probability becomes

$$H(P)=q+(1-q)G(P) \quad (4.12)$$

Where q is the probability of zero precipitation. $q=\frac{m}{n}$(between the number of zeros in a precipitation time series m, and the sample size n) and G(P) is the cumulative probability distribution for gamma probability density function, calculated in equation (4.10). The cumulative probability H(P) can be transformed into the standard normal random variable with mean zero and Varian of one. This yields the monthly value of SPI viz:-

$$SPI=\begin{cases}+\left(t-\frac{c_0+c_1t+c_2t^2}{1+d_1+d_2t^2+d_3t^3}\right), 0.5<\mathrm{H(P)}<1.0\\ -\left(t-\frac{c_0+c_1t+c_2t^2}{1+d_1+d_2t^2+d_3t^3}\right),, 0<\mathrm{H(P)}<0.5\end{cases} \quad (4.13)$$

4.5.2 The SPEI Algorithm

The SPEI calculation steps is based on the original SPI algorithm. Unlike the calculation of SPI that requires only precipitation values from given station(s), SPEI is calculated from the

difference between precipitation P and Potential evapotranspiration PET. This presents the water surplus or deficit (D_n) for the for the analyzed month.

$$D_n = P_n - PET_n \tag{4.14}$$

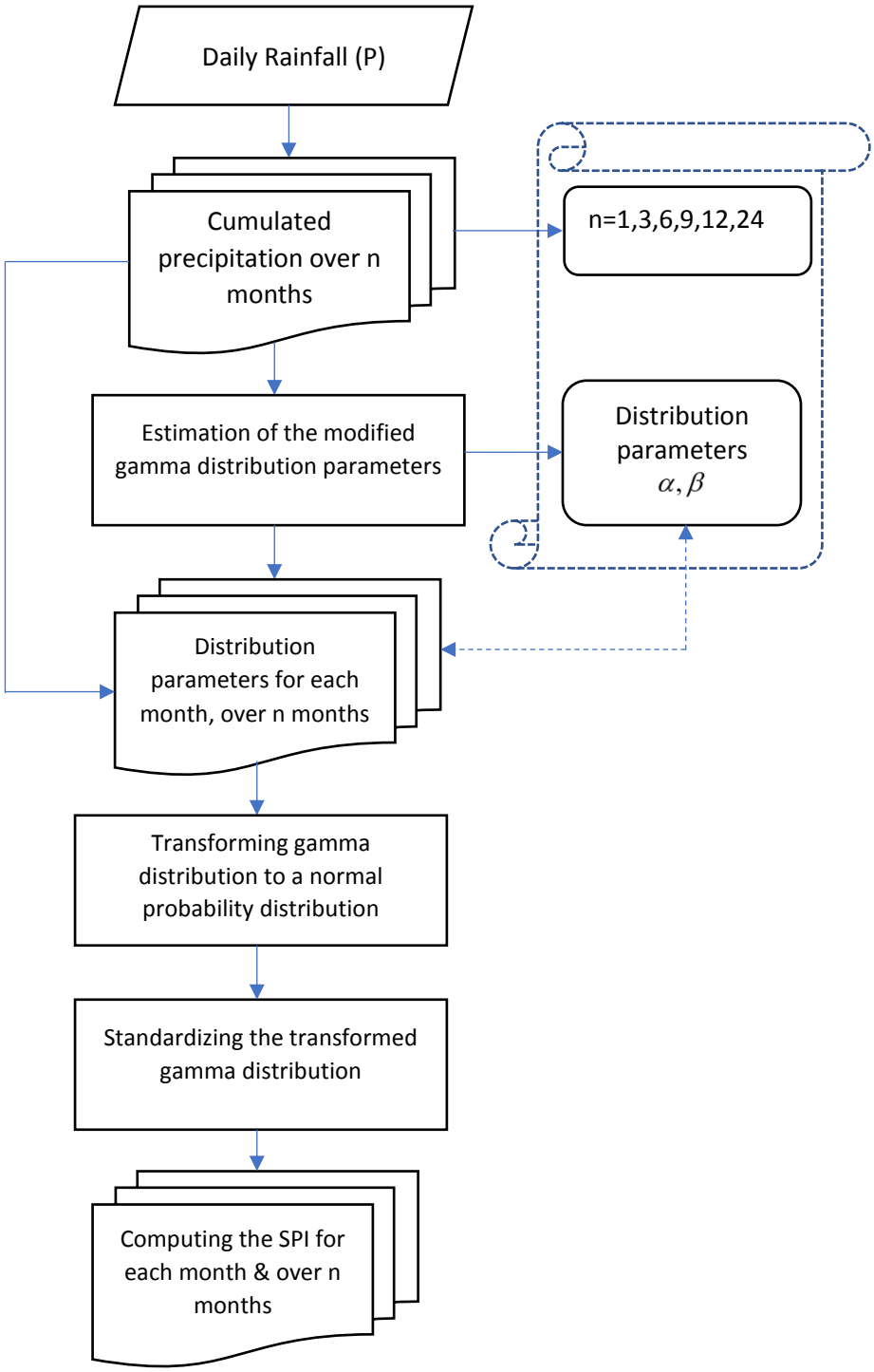

Figure 4.3 Flow chart providing the description of the SPI algorithm

The calculated D_n values are then aggregated over different time scales, following the same procedure as that of the SPI. Whereas for the SPI, the cumulated precipitation is fitted to a gamma distribution, in SPEI calculation steps the cumulated deficit is fitted on a 3-parameter log-logistic distribution function (Vicentet-Serano, et al., 2010): Thus, $D^k_{n,m}$ in a given month n and year m depends on a given time scale *t*, (Vicente-Serano, 2010)

$$x^t{}_{n,m} = \sum_{l=13-k+m}^{12} D_{n-1,l} + \sum_{n=1}^{m} D_{n,l} \quad \text{if } m < t \text{ and}$$
$$x^t{}_{n,m} = \sum_{n=1}^{m} D_{n,l} \quad \text{if } m \geq t \tag{4.15}$$

Then the cumulative deficit x is fitted to a 3-parameter log-logistic probability distribution as

$$f\left(x^t{}_{n,m}\right) = \frac{\frac{\beta}{\alpha}\left(\frac{x^t{}_{n,m}-\gamma}{\alpha}\right)^{\beta-\alpha}}{\left[1+\left(\frac{x^t{}_{n,m}-\gamma}{\alpha}\right)^{\beta}\right]^2} \tag{4.16}$$

The three parameters of the log-logistic probability distribution can be estimated following different procedures. Vicente-Serano (2010), proposed the method of L-moments following Sing et al., (1993)

$$\alpha = \frac{(w_0 - 2w_1)\beta}{\Gamma\left(1+\frac{1}{\beta}\right)\Gamma\left(1-\frac{1}{\beta}\right)} \tag{4.17}$$

$$\beta = \frac{2w_1 - w_0}{6w_1 - w_0 - 6w_2} \tag{4.18}$$

$$\gamma = w_0 - \alpha\Gamma\left(1+\frac{1}{\beta}\right)\Gamma\left(1-\frac{1}{\beta}\right) \tag{4.19}$$

Where $\Gamma(\beta)$ is the gamma function of β, and w_s is the probability weighted moments (PWMs)of order s, calculated as:

$$w_s = \frac{1}{N}\sum_{i=1}^{N}(1-F_i)^s D_i \tag{4.20}$$

and $F_i = \frac{i-0.35}{N}$, is the frequency estimator calculated following Hosking (1990), i is the range of observations arranged in increasing order and N is the number of data points. The 3-parameter log-logistic distribution was chosen as the fitting probability distribution unlike the 2-parameter gamma distribution as applied in SPI because in a 2-parameter distribution the

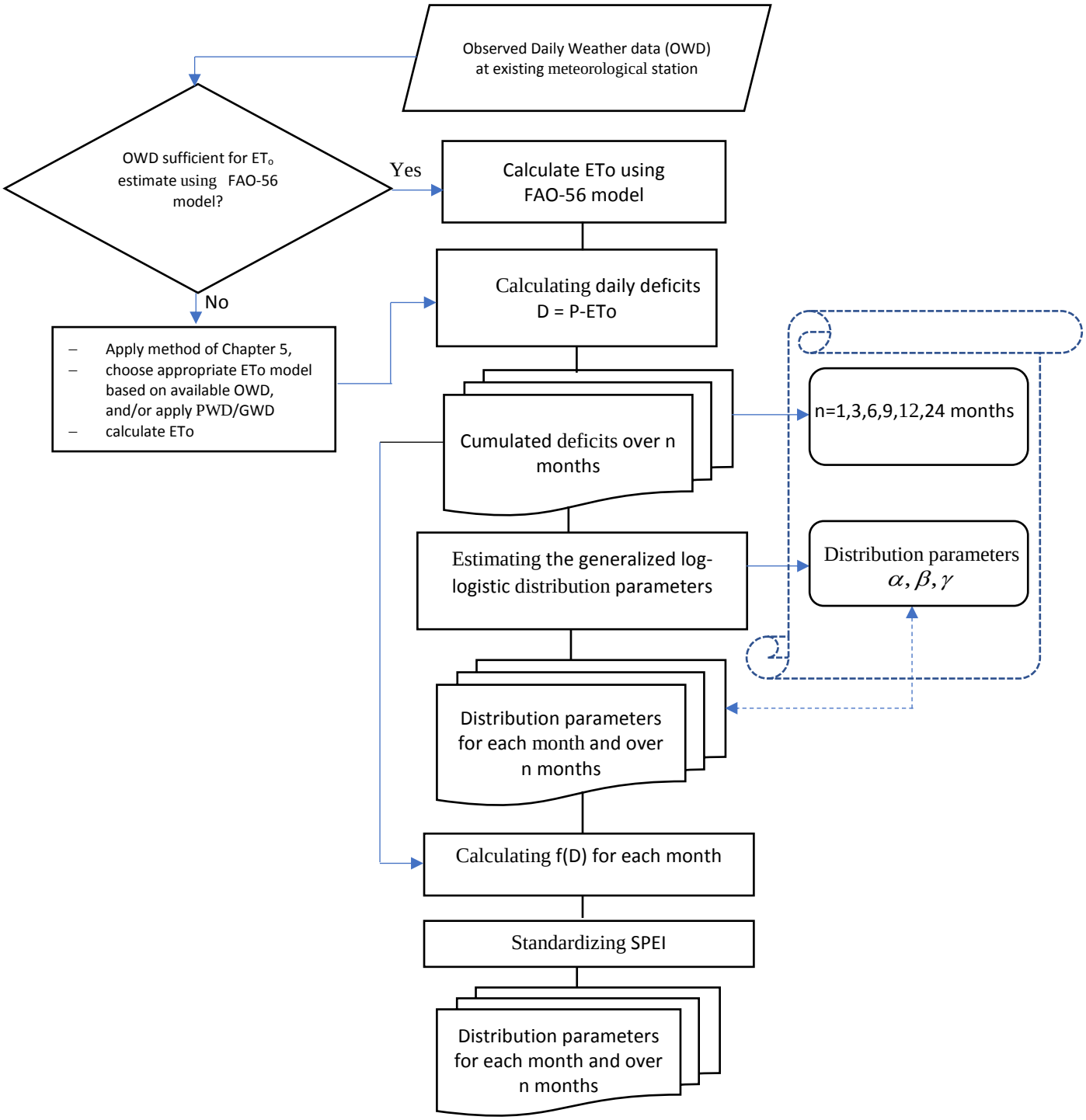

Figure 4.4 Flow chart providing the description of the SPEI algorithm as implemented to evaluate SMDI calculated using the new approach described in this chapter. OWD = Observed weather data, PWD = Propagated weather data, GWD = Gridded weather data variable x has a lower boundary of 0 $(0 < x < \infty)$, whereas in a 3-parameter distribution x takes the values $(\gamma > x < \infty)$ thus allowing for negative values which are very common in D series (Vicente-Serano, 2010).

4.6 Conclusion

In this chapter, the development of a new approach for the definition of SMDI was presented. To achieve this task, earlier works that applied SMDI for agricultural drought monitoring were reviewed in section 4.2, (Equations 4.1 to 4.4). These approaches largely relied on availability of long term records of soil moisture time series that are mostly available in developed counties. The difference in the new approach from the earlier soil moisture based indices is in the way soil moisture is generated since the method is developed for application in developing countries. As explained in section 4.3, the approach relies on a 1-dimensional agro-hydrological model for the generation of soil moisture time series from which SMDI is defined. However, since the new approach focuses on developing countries, it has to overcome the challenge of unavailability of reliable weather and crop growth data for the calibration of agro-hydrological model. These are overcome by application of gridded weather data for gap filling climatic records which often times lack continuity in developing countries as presented in chapter 5. The problem of monitoring crop growth is overcome by application of freely available high resolution satellite remote sensing images to estimate crop development parameters such as albedo and LAI as presented in chapter 6. The chapter concludes by elaborating on the algorithms for the calculation of SPI (Equations 4.6 to 4.13 & Figure 4.3) and SPEI (Equations 4.14 to 4.20 & Figure 4.4) used as reference drought indices for testing the reliability of SMDI. The overall schematization of the new approach is illustrated in Figure 4.1 and explained in section 4.4. The calculation of SMDI following the new approach is illustrated by Equation 4.5 which is based on the assumption that plants begin to experience moisture stress when soil moisture fall below 75% of its value at field capacity.

5 EVALUATING EMPIRICAL MODELS FOR ESTIMATING REFERENCE EVAPOTRANSPIRATION: *A CASE OF NORTHERN UGANDA*

Summary

The concept of reference evapotranspiration (ET_0) is important in accounting for water movement in the SPAC since it relies only on the climatic data. However, calculation of ET_0 through the recommended FAO-56 PM model is not possible in most developing countries that lack consistent and reliable records of climatic variables such as solar radiation (Ra), Temperature (T), Relative Humidity (RH) and wind speed (U); which are its input requirements. This difficulty has prompted development of various less data intensive ET_0 models for application in areas that lack these climatic records. However, application of such ET_0 models in areas for which they were not developed require testing for their validity and if possible their calibrations are always recommended. In this chapter, 13 reference ET_0 models were evaluated using the FAO-56 PM model based on a 4-year weather data near a study site in Northern Uganda. The models are grouped into 3 categories: i.e. temperature based category (T), mass transfer(MT) based category and the radiation based category (R). Results of the evaluation showed that the R-based category performed best followed by the MT category and the T-based category consistently overestimated ET_0. The best performing ET_0 model was Makkink which is R-based with RMSE = 0.6mm, MAE = 0.4mm, NSE = 0.1, d = 0.9, and r^2 = 0.7 and the worst performing ET_0 model is Thornthwaite which is T-based with RMSE = 3.5mm, MAE = 3.2mm, NSE = -10.4, d = 0.3, and r^2 = 0.2.

Evaluation of two gridded climatic data sources (ECMWF and NASA-Power Agro-climatic) were also conducted, using similar statistics as applied in ET_0 evaluations. Results showed that NASA-Power Agro-climatic source gave better comparisons with observations for the Ra (RMSE = 45.6 Wm^{-2}, MAE =40.3 Wm^{-2}, NSE=-0.2, d = 0.7, & r^2 =0.7); RH (RMSE =8.5%, MAE = 6.8%, NSE = 0.7, d = 0.9, & r^2 = 0.7) and precipitation [P] (RMSE = 8 mm, MAE = 4.1mm, NSE = -0.9, d = 0.6, & r^2 = 0.2). Whereas ECMWF gave better comparisons with observations for T_{min} (RMSE =1.61^oC, MAE =1.25 ^oC, NSE= 0.6, d = 0.67, & r^2 = 0.35), T_{max} (RMSE = 0.96 ^oC, MAE = 0.73 ^oC, NSE= 0.31, d = 0.86, & r^2 = 0.67), and U (RMSE =0.52, MAE =0.42, NSE=-1.1, d = 0.67, & r^2 = 0.2). Following the data propagation algorithm presented in this chapter Ra and RH obtained from NASA-Power can be applied without calibration whereas only the T_{max} obtained from ECMWF can be applied without calibration.

5.1 Introduction

Reference evapotranspiration is an important parameter in Agricultural water management and hydrological studies (Djaman et al., 2015). Accurate estimation of evapotranspiration is essential for understanding land-atmosphere interactions needed in applications such as hydrological modeling and in agricultural water management; for instance in improving water use efficiency in irrigated agriculture (Kwon & Choi, 2011). The FAO56-PM model has been recommended as the standard method for calculating reference evapotranspiration (ET_o) over diverse climates because it is based on fundamental physical principles that guarantee its universal validity (Bautista et al., 2009). However, use of FAO56-PM model is limited by availability of; air temperature (T), relative humidity (RH), solar radiation and wind speed (U) data. This is because most weather stations especially in developing countries have incomplete records of these data and those that have them, are of questionable accuracy. For this reason, a number of empirical models for estimating reference evapotranspiration with limited data requirements have been developed over the years. These empirical models require calibration especially in areas with different weather patterns than those in which they were developed. Usually the calibration of such ET_o models are done with flux tower, weighing lysimetric or class A Pan evaporation measuring instruments. However, these instruments are very expensive and based on sophisticated methods that are rarely applicable in developing countries. For that reason, in such circumstances, it is recommended that calibration of other ET_o models in a given area can be achieved through application of FAO-56 model, if sufficient records of Solar radiation, wind speed, RH and air temperature can be found or estimated in an area.

A number of studies have used FAO-56PM model to calibrate different empirical models for estimating reference evapotranspiration over diverse climatic regions: for instance; Berti et al., (2014) used FAO-56PM to calibrate the Hargreaves model in the Veneto region in North-Eastern Italy, Lee (2010) used the FAO-56PM to recalibrate the Hargreaves equation for the Korean Peninsula, Tabari and Talaee (2011) used FAO-56PM to calibrate the Hargreaves and the Priestley-Taylor models in arid and cold climates of Iran, Sahoo et al. (2012) used FAO-56PM model to evaluate the performance of 16 empirical models for estimation of reference evapotranspiration using both the continuous daily time series and average time series in a humid valley of cultivated range land in eastern Indian Himalayas, etc. The objective of this chapter is to evaluate the performance of 13 reference evapotranspiration models in Northern Uganda based on existing meteorological data. The second objective is to assess the

applicability of gridded climatic data for gap filling climatic data records in the study area through a data propagation algorithm proposed by Wart et al., (2015). The two objectives are required in the proposed general procedure in chapter 3 for development of SMDI for agricultural drought monitoring in the study area.

5.2 Study site and Methodology

5.2.1 Study Area

A general description of the study area is given in chapter 2, section 2.5, where brief details of Uganda's climatic condition including factors that drive the weather variables at regional scale affecting the entire country are discussed. This section focuses on Northern Uganda where the case study was conducted. Average monthly variations of weather parameters are shown in Figure 5.2, based on the last four-year data obtained from an automatic weather station at Gulu University (GU) for the period: 2012 - 2016. The administrative boundaries of Northern Uganda have considerably changed. However, what is covered here and indicated on the map in Figure 5.1 is based on a 2006 district maps for Uganda.

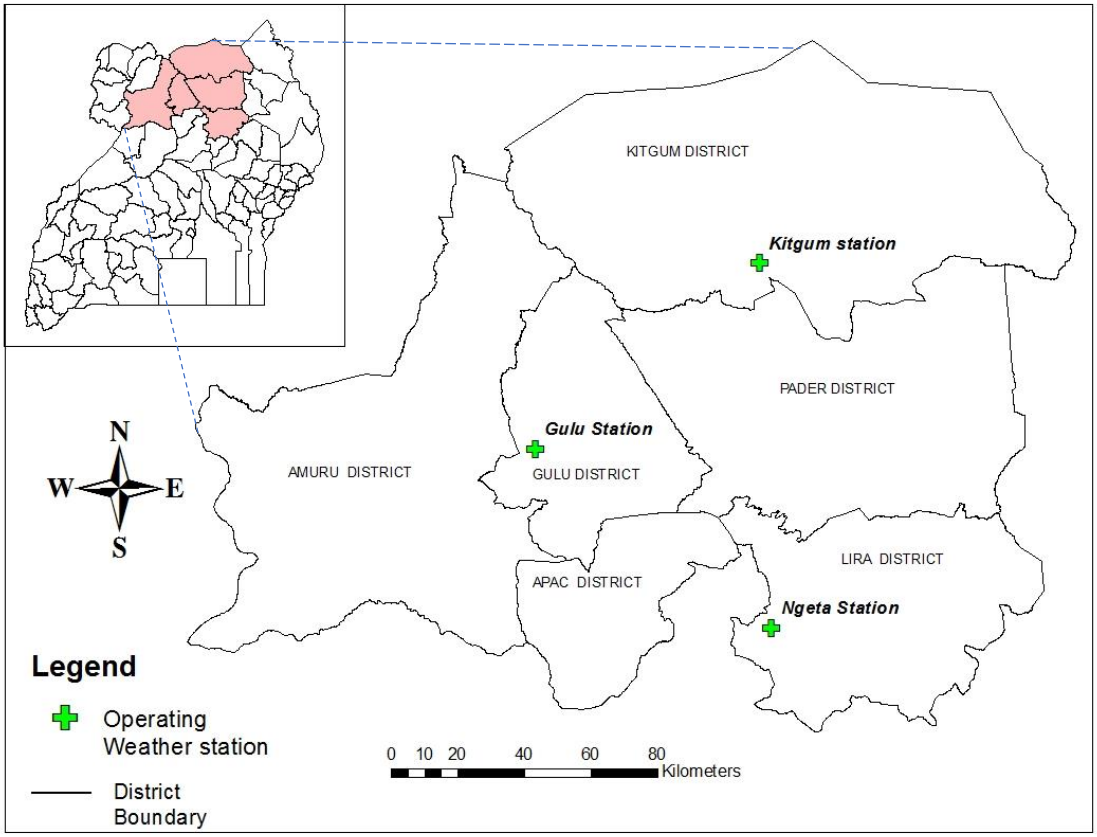

Figure 5.1 Map of Northern Uganda showing three of the operating meteorological stations. Two automatic stations one at *Gulu University* (GU) and another at *Gulu Uganda Country Dairy* (GUCD) being 2 km and 4 km respectively from the Gulu station are not shown on the map

Northern Uganda lies within the Aswa River basin and a detailed description of the study area is given by Nyeko (2010). The monthly average patterns for four of the main climatic variables of solar radiation, air temperature, relative humidity and wind speed are shown in Figure 5.2. There exists a number of meteorological stations that were established during the colonial era. However, majority of them are no longer operational except for those shown in Figure 5.1 and Table 5.1. The operations of these stations were interrupted by a number of insurgencies that took place in the area, including the 20-year insurgency of the Lord's Resistance Army (LRA).

Meteorological data were obtained from all the stations listed in Table 5.1 and data quality checks were performed to test for consistencies and assess the magnitude of gaps in each available data set. Figure 5.2 is based on only four-year complete datasets collected from the automatic station at GU. therefore, it may not capture the actual variation of the monthly climatic conditions in Northern Uganda. It is however consistent with local experience of the long term climatic pattern of the region supported by descriptions of Basaliriwa (1995) and Ogalo (1985).

Average monthly temperature varies from 22^{o}C to 27^{o}C, although temperatures as high as 37^{o}C are reported in Kitgum and Lira districts. Average monthly solar radiation varies between 150 Wm^{-2} to 240 Wm^{-2} . Average monthly relative humidity varies between 30% and 80% with low relative humidity registered between January and May of each year. Average wind speed varies between 1 m/s and 2.5m/s, although wind speed data obtained from Global Yield Gap Atlas (GYGA) shows average wind speed of 2m/s (Wart et al., 2015). However, the figures from GYGA's data are based on calibration of gridded climatic data from NASA-Power Agro-Climatic. It was not possible to find any reports on calibration of gridded climatic data over Northern Uganda using observed climatic data.

5.2.2 Reference Evapotranspiration and the concept of crop coefficient

Reference evapotranspiration, ET_o is defined as a evapotranspiration from an extensive surface of green grass of uniform height (0.12m), with an albedo of 0.23 and a fixed canopy resistance of 70s/m, actively growing, shading the ground and not short of water (Allen et al. 1998). As such reference evapotranspiration is a function of climatic variables only; such as the solar radiation (R_s), air temperature (T), relative humidity (RH) and wind speed (U). It is therefore independent of crop factors such as crop type, management practice, crop density, etc. and soil factors such as soil fertility, soil salinity and tillage type (Allen et al., 1998).

Whereas crop evapotranspiration ET_c refers to evapotranspiration rate from a particular crop under standard conditions of no water stress, free from crop disease, no incidence of crop pests and growing under best possible soil fertility (Muniandy et al., 2016; Allen et al., 1998).

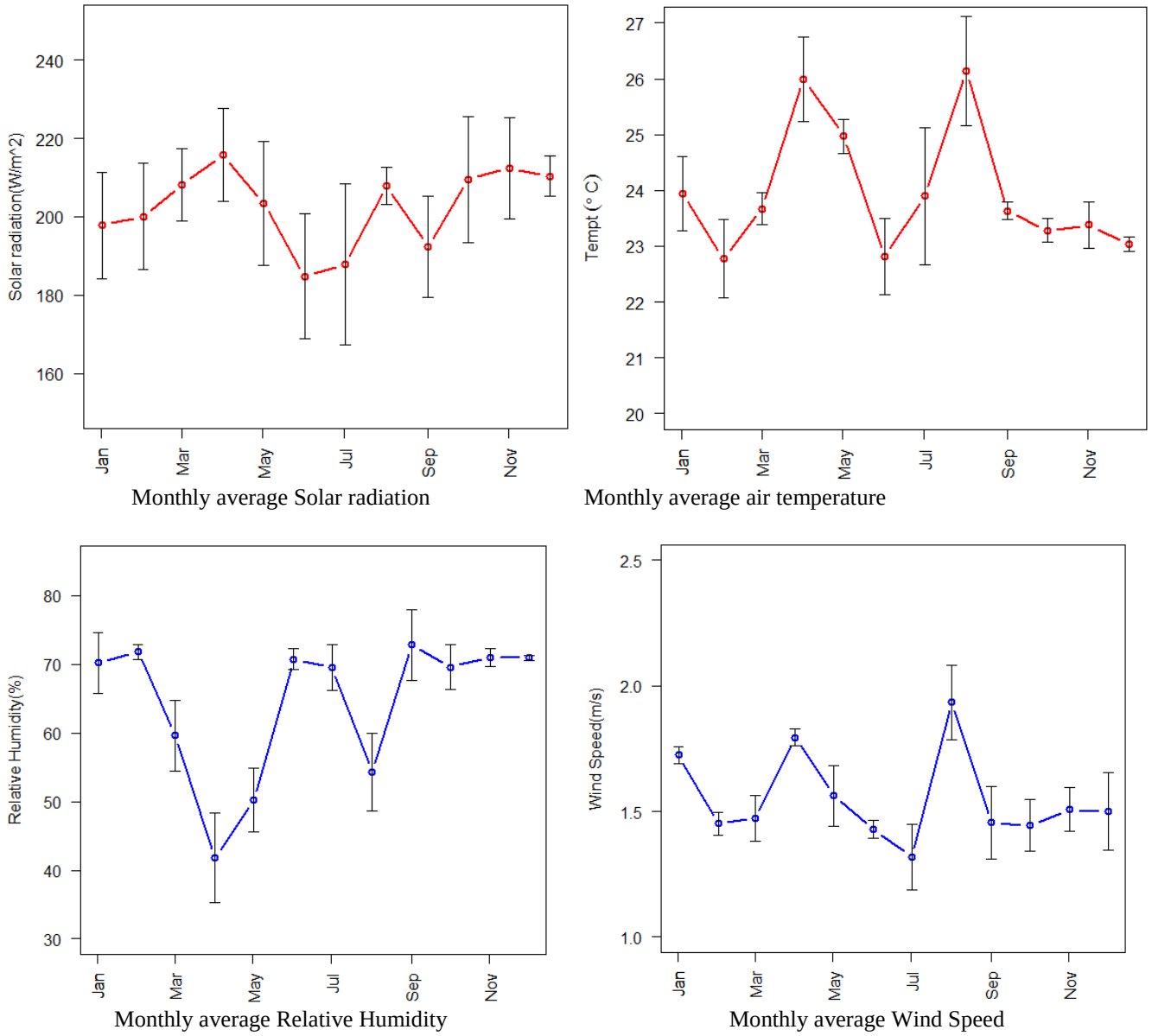

Figure 5.2 Monthly mean weather variation at the Gulu station for (2012-2016) data

Crop evapotranspiration (ET_c) is required in order to determine crop water requirements under standard conditions. ET_c has to be adjusted accordingly for crops growing under nonstandard conditions. Determination of ET_c is complicated and quite often, the required input parameters for their calculations through the recommended FAO-56, are seldom available. This difficulty has partly been solved by defining unique relationship between the ET_o (which is based purely on climatic factors) and the ET_c that requires consideration of all the other factors (i.e. crop

factors, soil factors, tillage practices and other management factors) in terms of crop coefficients (K_c). Crop coefficient is defined according to Allen et al., (1998); equation (5.1).

$$K_c = \frac{ET_c}{ET_o} \qquad (5.1)$$

Table 5.1 Location coordinates and data availability for Northern Uganda stations used in this study

Station's Location					weather variables					Status
S/N	Station's Name	Lat(°N)	Long(°E)	Z(m)	U	T	Rad	RH	P	length
1	Gulu	2.783	32.283	1100		√			√	1995-2015 a*
2	Ngetta	2.297	32.921	1080		√			√	1995-2014 a*
3	GUCD	2.805	32.285	1085	√	√	√	√	√	2015(Apr-Oct)
4	GU	2.784	32.283	1100	√	√	√	√	√	2012-2016
5	Kitgum	3.287	32.889	760		√			√	1995-2008 a**

U=wind speed(m/s), T=air temperature (°C), Rad=Solar radiation (W/m^2), P=Precipitation or rainfall (mm)
[Status i.e. length of the data collection period: a* = minor inconsistencies detected with largest gaps less than six months; a**= very large gaps, more than six months, and major inconsistencies detected such as repeated entries for some years.

Values of K_c has been published for various crops under various climatic conditions, soil types and crop management practices, (FAO, 1998). Crop coefficient has also been shown to be a function of crop development stages defined by parameters such as; the leaf area index (LAI), crop height (h_c) and albedo (Allen et al., 1998). These crop development stages can alternatively be obtained through application of remote sensing methods (D'Urso, 2001). Therefore, through the recommended FAO-56 method for calculating evapotranspiration, K_c can be defined according to D'Urso (2001), equation (5.2).

$$K_c = f\left(K^{\downarrow},\ T_a,\ RH,\ U;\ r,\ LAI,\ h_c\right) \qquad (5.2)$$

Where $K^{\downarrow}$ is the incoming short wave radiation (Wm^{-2}), r(-) albedo, *LAI* being the leaf area index, h_c is crop/vegetation canopy height and *T*, *RH* and *U* as defined in section 5.2. Equations (5.1) and (5.2) can be used to estimate the actual crop evapotranspiration once the climatic parameters can be obtained. Many times, however, climatic parameters are not available especially in developing countries and even if available, they are incomplete and of questionable quality. In such circumstances, there are other ET_o models that have been developed that do not necessarily require all the climatic variables. Once such ET_o can be calibrated and verified for the specific application areas, they can be used in combination with equation (5.1) and the published values of K_c to estimate ET_c for those areas.

5.2.3 Reference Evapotranspiration Models

Development of simplified ET_o models is driven in part by the difficulty in obtaining reliable weather variables for application of FAO-56 model. Secondly, the other accurate methods of calculating ET such as the weighing lysimetric methods, the Bowen ratio and other flux tower methods are often very sophisticated and expensive to implement. These and other factors have encouraged development of many empirical ET_o models in application today. In this section, 13 of these simplified ET_o models are evaluated using the recommended FAO-56 Penman-Monteith combination model. The evaluated models are grouped into three categories: i.e.: The *Mass Transfer based* models, the *Temperature based* models and the *Radiation based* models.

The Mass Transfer ET_o models are based on Dalton's gas law (Muniandy et al., 2016). The models under this group apply the aerodynamic concept of vapour movement from evaporating surfaces into the atmosphere. The mass transfer ET_o models considered for evaluation include: Penman (1948), Dalton (1802) and Trabert (1896); (Tabari et al., 2013; Bormann, 2011). The equations describing each ET_o model are shown in table 5.2.

The Temperature based ET_o models considered in the evaluation include: the Hargreaves (Hargreaves and Samani, 1985); the Thorn-Thwaite (Thornthwaite, 1948); Linacre (1977), Romenenko (1961) and Blaney Criddle (1962). The Temperatures based empirical ET_o models employ easy approaches in general, requiring mainly: daily mean and/or minimum and maximum air temperatures. Temperature based ET_o models have been applied over diverse climatic conditions. The main reason for their wide-spread use is because air temperature records are available in most meteorological stations worldwide. Besides, air temperature measurements do not suffer from measurement inaccuracies such as the other meteorological parameters like wind speed, RH and solar radiation (Lorite et al., 2006).

The Radiation based models evaluated in this study include: Abtew (1996), Jensen Haise (1963), Makkink (1957), Priestley Taylor (1972), Romenenko (1961), Schendel (1967) and Turc (1962). The energy source that drives the evapotranspiration process is the solar energy from the sun. The net solar energy from the sun in combination with air temperature, wind speed control the evapotranspiration processes (Priestley Taylor, 1972). The relationships among these variables have been used to develop the radiation based ET_o models.

Table 5.2, ET_o model Equations and the definition of the variables used in each case

No	Author	Model	Parameters/variables
1	Abtew (1996)	$ETo^{Abt} = 0.53\frac{R_s}{\lambda}$	R_s: solar radiation (MJm^{-2} day^{-1}); λ : latent heat of evaporation (MJ/kg)
2	Blaney Criddle (1962)	$ET_o^{BC} = p(0.46T_{mean} + 8)$	Tmean: mean temperature (◦C) and p: constant (0.274)
3	Dalton (1802)	$ETo^{Dtn} = (0.3648 + 0.07223(u))(e_s - e_a)$	e_a: actual vapor pressure (hPa); e_s: saturation vapor pressure (hPa); u: wind speed (m/s)
4	FAO56-PM (1998)	$ET_o^{PM} = \frac{0.408\Delta(R_n - G) + \gamma\frac{900}{T+273}u_2(e_s - e_a)}{\Delta + \gamma(1 + 0.34u_2)}$	Rn: net radiation (MJ/m^2); G: soil heat flux density (MJ/m2.day); T: mean temperature (◦C); u_2: wind speed at 2 m height (m/s); γ : psychrometric constant (kPa/◦C) Δ : slope vapor pressure curve (kPa/◦C); e_a: actual vapor pressure (kPa) and e_s: saturation vapor pressure (kPa)
5	Hargreaves (1985)	$ET_o^{HG} = 0.0023R_a(T_{mean} + 17.6) \times T_D^{0.5}$	R_a: extraterrestrial radiation (MJ/m^2.day); T_D: maximum and minimum temperature difference(◦C) and Tmean: mean temperature (◦C)
6	Jensen Haise (1963)	$ET_o^{JH} = \left(\frac{R_s}{\lambda}\right)(0.025T_{mean} + 0.008)$	T_{mean}: mean temperature (◦C); Rs: solar radiation (MJ m−2 day−1); _: latent heat of evaporation (MJ/kg)
7	Linacre (1977)	$ET_o^{L} = \frac{\frac{700(T_{mean} \pm 0.0006Z)}{100 - L} + 15(T_{mean} - T_d)}{80 - T_{mean}}$	Z: local altitude (m); L: local latitude (degrees) and T_d: dew point temperature (◦C); T_{mean}: mean temperature (◦C)
8	Makkink (1957)	$ET_o^{Mkk} = 0.61\left(\frac{\Delta}{\Delta + \gamma}\right)\frac{R_s}{\lambda} - 0.12$	R_s: solar radiation (MJ/m2); Δ : slope of vapor pressure curve (KPa ◦C^{-1}); γ : psychrometric constant (kPa ◦C^{-1}), λ : Latent heat of evaporation (MJ/kg)
9	Priestley Taylor (1972)	$ET_o^{PT} = \frac{\alpha}{\lambda}\left(\frac{\Delta}{\Delta + \gamma}\right)(R_n - G)$	Δ : slope of vapor pressure curve (kPa ◦C−1); R_n: net radiation (MJ/m2); G: soil heat flux density (MJ/m2 day), λ : latent heat of evaporation (MJ/kg), α: constant (1.26)
10	Penman (1948)	$ET_o^{Pnm} = 0.35\left(1 + \frac{0.98}{100u}\right)(e_s - e_a)$	e_a: actual vapor pressure (mmHg); e_s: saturation vapor pressure (mmHg); u: wind speed (miles/day)
11	Romanenko (1961)	$ET_o^{Rko} = 4.5\left(1 + \left(\frac{T_{mean}}{25}\right)\right)^2\left(1 - \frac{e_a}{e_s}\right)$	Tmean: mean temperature (◦C); ea: actual vapor pressure (hPa), es: saturation vapor pressure (hPa)
12	Schendel (1967)	$ET_o^{Sch} = 16\left(\frac{T_{mean}}{RH}\right)$	Tmean: mean temperature (◦C); RH: relative humidity (%)
	Thornthwaite (1948)	$ET_o^{Thw} = 16\left(\frac{N}{12}\right)\left(\frac{d_m}{30}\right)\left(\frac{10T_{mean}}{I}\right)^a$, where: $I = \sum_{i=1}^{12}\left(\frac{(T_{mean})_i}{5}\right)1.514$ $a = 0.49239 + 1792\times10^{-5}I - 771\times10^{-7}I^2 + 675\times10^{-9}I^3$	Tmean: mean monthly temperature (◦C)
13	Trabert (1896)	$ET_o^{Trbt} = (0.3075)\sqrt{u}(e_s - e_a)$	e_a: actual vapor pressure (hPa); e_s: saturation vapor pressure (hPa); u: wind speed (m/s)
14	Turc (1962)	$ET_o^{Tur} = 0.13\left(\frac{T_{mean}}{T_{mean} + 15}\right)(R_s + 50)$	Tmean: mean temperature (◦C); Rs: solar radiation (Cal/m^2 day); Rs: solar radiation (Cal/m^2 day)

Table 5.3 ET_0 Models and the required weather parameters for their input

No	Model	Category	Weather Data			
			R	T	U	RH
1	Abtew	R	√			
2	Blaney Criddle	T		√	√	√
3	Dalton	MT	√	√		
4	FAO56-PM	C	√	√	√	√
5	Hargreaves	T		√		
6	Jensen Haise	R	√	√		
7	Linacre	T	√	√		
8	Makkink	R	√	√		
9	Prestley Taylor	R	√	√		
10	Penman	MT		√		√
11	Romenenko	T		√		
12	Schendel	R		√		√
13	Trabert	MT		√		
14	Turc	R	√	√		√

(Note: MT=Mass transfer, R=radiation, T=temperature, C=combination)

In general, Allen et al. (1998) recommended the Hargreaves model as an alternative for the FAO-56 since it requires only the measured mean air temperature and the air temperature range and calculated extraterrestrial solar radiation (Hargreaves and Samani, 1985). However, according to Hargreaves and Samani (2003), the Hargreaves method is not recommended for daily calculation of reference evapotranspiration and furthermore, the method does not perform well over regions with extensive cloud cover. For such regions, they recommend local calibration of the Hargreaves formula. The difficulty with local calibration is that it has to be applied more than once for similar regions that may even have slight difference in atmospheric conditions. And the calibration requires sophisticated methods such as the lysimetric measurements or at least availability of data for calculation of reference evapotranspiration by the FAO-56 method, each time the calibration is undertaken. However daily estimates of ET_o is required for many hydrological and agricultural applications (Martí et al., 2015). This is the main reason why other empirical models with similar less data requirements are evaluated over Northern Uganda to verify their validity in that region. There is still no indication to date that evaluation of Empirical ET_o models such as the widely-used Hargreaves method has been done over Northern Uganda.

5.3 Evaluation Procedure of the Reference Evapotranspiration Models

Various statistics for efficiency tests between simulation (S_i) and Observations (O_i) were applied to assess the prediction accuracies of each of the 12 evapotranspiration models based on ETo values calculated by FAO-56. The test statistics used include the Coefficient of

determination (r^2), the root mean square error (RMSE), the mean absolute error (MAE), the Nash-Sutcliffe Efficiency test and the index of agreement (d) test, equations (5.3) to (5.7). In each case a given simplified ET_o model is taken as S_i and the FOA-56 is taken as O_i. the results of the statistical tests for each of the 12 evaluated models are given in the section 5.4.

5.3.1 Coefficient of determination (r^2)

$$r^2 = \left(\frac{\sum_{1=1}^{n} (O_i - \overline{O})(P_i - \overline{P})}{\sqrt{\sum_{i=1}^{n} (O_i - \overline{O})} \sqrt{\sum_{i=1}^{n} (P_i - \overline{P})}} \right)^2 \qquad (5.3)$$

With O_i being observations; $\overline{O}$ is the average of the observations; P_i is the predicted values and $\overline{P}$ being the average of the predicted values.

5.3.2 Root Mean Squared Error (RMSE)

$$RMSE = \sqrt{\frac{1}{N} \sum_{i=1}^{N} (S_i - O_i)} \qquad (5.4)$$

5.3.3 Mean Absolute Error (MAE)

$$MAE = \frac{1}{N} \sum_{i=1}^{N} |S_i - O_i| \qquad (5.5)$$

5.3.4 The index of agreement (d)

$$d = 1 - \frac{\sum_{i=1}^{N} (S_i - O_i)^2}{\sum_{i=1}^{N} \left(|S_i - \overline{O}| + |O_i - \overline{O}| \right)^2} \qquad (5.6)$$

5.3.5 The Nash-Sutcliffe Efficiency (NSE)

$$NSE = 1 - \frac{\sum_{i=1}^{N} (S_i - O_i)^2}{\sum_{i=1}^{N} (S_i - \overline{O})^2} \qquad (5.7)$$

Values of r^2 ranges from 0 to 1 with 0 indicating worst model prediction and 1 indicating the best model prediction. A RMSE value of 0 indicates, best model prediction and the higher the value the worse the prediction so is the case with MAE. The values of NSE ranges from 1.0 to -∞, with NSE=1.0, showing the best prediction and any value lower than 1.0 indicating the worst prediction. And lastly the values of d ranges from 0 to 1, with 0 indicating worst prediction and 1 indicating the best prediction (Krause et al., 2005). It was developed by Nash and Sutcliffe (1970).

5.4 Gap Filling Weather Station Data

Application of the method to calculate the SMDI, presented in chapter 4 requires assessment of simplified empirical reference evapotranspiration models. This is because the method is tailored to rain fed agricultural production areas in developing countries, where meteorological data have many gaps that require gap-filling. In many weather stations in developing countries, the first challenge is that not all the required climatic data are available for calculation of ET_o using the recommended FAO-56. For this challenge, it is recommended in the new methodology, to apply simplified models to estimate ET_o. However, in many instances the available climatic data that can facilitate application of simplified ET_o models have quality problems such as inconsistencies and data gaps. Therefore, application of the simplified empirical models for the estimation ET_o can still be hindered by such problems in in the climatic records. Dealing with those problems in available climatic records are covered in this sub-section.

5.4.1 Dealing with Gaps in Climatic Data in Developing Countries

Working with weather data in developing countries has three major challenges:

- Data quality
- Gaps in the data record
- Sparse network of operating weather stations

Each of these challenges can be addressed through statistical methods. Data quality issues are addressed through consistency and homogeneity checks. This is done for example by application of double mass curves and other statistical methods. The problem of data gaps can be handled through a number of gap filling methods proposed in published literatures. Methods such as those proposed by Allen (1998) using data from neighboring stations can be applied for gap filling. The problem of sparse network of weather stations can be addressed through interpolation algorithms such as*; least squares weighted distance method* or a geo-statistics method such as *kriging*. However, these methods are associated with lots of uncertainty in the generated climatic records at un-sampled locations. Major sources of such uncertainty arise from few number of weather stations used for interpolation and the underlying assumptions involved.

The past three decades has seen a number of advancement in satellite remote sensing technology that has revolutionized the way observations of the earth environment is conducted. This revolution has enabled generation of a number of biophysical variables at a regional to global scales. There exist gridded meteorological variables such as the reanalysis datasets from

the European Center for Medium Range Weather Forecast (ECMWF) and the NASA Power Agro-climatic, that are freely available for most locations of the globe. These data sources can be calibrated through observations from local stations to produce longer term data for locations having limited data records. This is done through the concept of data propagation that was applied to generate meteorological data for global yield gap assessment (Wart et al., 2015).

5.4.2 The Concept of Data Propagation

Stochastic weather generators can be applied to generate long term climatic data at locations that do not have them. A stochastic weather generator can generate synthetic time series of daily weather data for as many years as specified for a location based on the statistical characteristics of observed historical records. Whereas, gridded weather data are generated from interpolation of meteorological observations over space using point based weather observations. They may also be generated by climate models to estimate daily or monthly weather data over each grid cell. These are the main methods for generating climatic data for climate based studies at remote locations where weather stations are either unavailable or nonfunctional.

The needs for climatic data especially in locations that do not have weather stations is the main driver of research efforts to develop weather generators. And much progress has been made in developing new methodologies for weather data generators. Despite these efforts however, there are still considerable deviations of synthetic weather records from observations. While gridded weather records are hampered by insufficient records and poor density of weather stations that form the basis for their interpolations. These problems can partly be overcome by the concept of weather data propagation. Propagated weather data are generated by regression analysis between at least three years of observed weather records and either gridded weather data or synthetic weather data (Wart et al., 2015). The procedure proposed by Wart et al. (2015) and adopted for this study is illustrated in Figure 5.3. Evaluation of each of the variables against observations are based on efficiency statistics that are described in sub-section 5.2.3.

5.5 Results and Discussions of Evaluation of the 12 ET_o Models

The performance of each of the 12 ET_o models was evaluated by comparing their predicted values versus the FAO-56 calculated values. For evaluation of complex models such as reference evapotranspiration, it is recommended that various statistics be applied rather than relying on application of only the r^2 as has always been the case. For that reason, four statistics

were used for the comparison, i.e: the Root Mean Squared Error (RMSE), Mean Absolute Error (MAE), Nash Sutcliffe Efficiency (NSE), Index of agreement (d) and the coefficient of determination (r^2). Besides these test statistics, scatter plots were produced and lines of best fits added in each case together with the 1:1 lines to aid visual assessment of how best each ET_o model compares with FAO-56 model. The presentation of results and discussions are done under each model category: namely: Mass transfer based category, the Temperature based Category and the Radiation based Category.

5.5.1 The Mass Balance ET_o models

The mean monthly variation of ET_o values calculated by ET_o models falling under the mass transfer based category and that calculated by the FAO-56 reference model are shown in Figure 5.4. A visual inspection of the mass transfer ET_o model category i.e.: Dalton, Penman and Trabert, Figure 5.4(a), shows that Dalton is the closest to FAO-56 for the months of April to November and it is Farthest from FAO-56 for the months of January to March. Whereas Trabert and Penman's monthly variation compared to FAO-56 are very similar except for the months of January to March when Penman is closer to FAO-56 than Trabert. On the other hand, Trabert Appears closer to FAO-56 than Penman between the months of October to December, although the difference is not as pronounced as for the months of January to March. The observed difference in the monthly trend of the Mass Transfer ETo models compared FAO-56 model is due in part to the wind speed factor which is differently applied in each case, Table 5.2. The marked seasonal variation in climatic pattern over Northern Uganda with the months of December to March being dry and windy and the Months of April to November being particularly wet and less windy seem to explain the difference in performance among the Mass Transfer models basing on the way wind speed is applied in each case.

Comparisons of the mass transfer based models with FAO-56PM model basing on the test statistics, reveal that the Penman model performs best overall; Figure 5.5(a), in terms of RMSE, MAE and NSE, and Dalton perform worst in terms of RMSE. Whereas the performance of both Trabert and Dalton equal in all the other test statistics, both of them being better in their values of the coefficient of determination than Dalton, Table 5.4 ($r^2 = 0.8$ for both Penman and Trabert and ($r^2 = 0.7$ for Dalton).

5.5.2 The Temperature based ET_o Models

The ET_o models evaluated under the temperature based category include: the Hargreaves, Romenenko, Blaney Criddle and the Thornthwaite. The visual inspection of the mean monthly

plots (Figure 5.4b) show that all the temperature based ET_o models over estimate ET_o as compared to FAO-56PM model, with Romenenko model providing worst over estimate between the months of January and April. However, the Romenenko model performs better than the rest of the temperature best models between the months of April and December. Thornthwaite model performs worst overall, especially between the month of April to December being negatively correlated to FAO-56 values. Considering the test statistics in the temperature based category, Thornthwaite performs worst in all cases, Figure 5.5b. whereas Romenenko performs worst in terms of the RMSE and the MAE. Blaney Criddle performs best in terms of RSME and MAE followed closely by Hargreaves. With the respective values being RMSE = 1.8mm, MAE = 1.6mm for Blaney Criddle and RMSE = 2mm, MAE = 2mm for the Hargreaves model. Whereas Hargreaves performs best overall in this category in terms of the r^2 value being 0.7. considering the index of agreement d, Romenenko performs best followed closely by Hargreaves. Whereas considering the NSE, Thornthwaite performs worst followed by Blaney Criddle model. Whereas Romenenko performs best in terms of NSE, followed by Hargreaves. Overall in the Temperature based category, Hargreaves appears to be the best compromise followed by Romenenko then Blaney Criddle and Thornthwaite is the worst performing.

5.5.3 The Radiation Based ET_o Models

The ET_o models evaluated under the radiation based category include: Makkink, Priestley Taylor, Abtew, Turc, Schendel, Jensen Haise and the Linacre. Considering Figure 5.4(c), visual inspection of the mean monthly plots, show that Jensen Haise and Schendel over estimate ET_o compared to the rest of the models in the radiation based category. And Priestley Taylor model consistently under estimates ET_o in this category. Visual inspection of the plots also shows that Makkink model provides the best prediction except for the months from January to March. Considering the values of the test statistics, Abtew, Makkink and Turc have similar performance with respect to RMSE and MAE in each case being less than 1mm, compared to the rest of the other models in this category Figure 5.5(c). These are followed by Jensen Haise which gives equal values of RMSE and MAE of 1.3mm in each case. The worst performing model in this category in terms of RMSE is Schendel with values of 3.5mm for RMSE and 2.9 for MAE. This is followed by Linacre and Priestly Taylor with values of RMSE = 1.9mm, MAE = 1.8mm for Linacre and RMSE = 1.4mm, MAE = 1.2mm for Priestley Taylor. In terms of d and r^2, Makkink and Abtew performs best in terms of d (in both cases d = 0.9) and they both perform moderately well in terms of r^2 (Makkink = 0.7, Abtew = 0.6). The best model in

terms of r^2 in this category is Jensen Haise with r^2 = 0.8. and the worse in terms of r^2 in this category is Priestley Taylor with r^2 = 0.4.

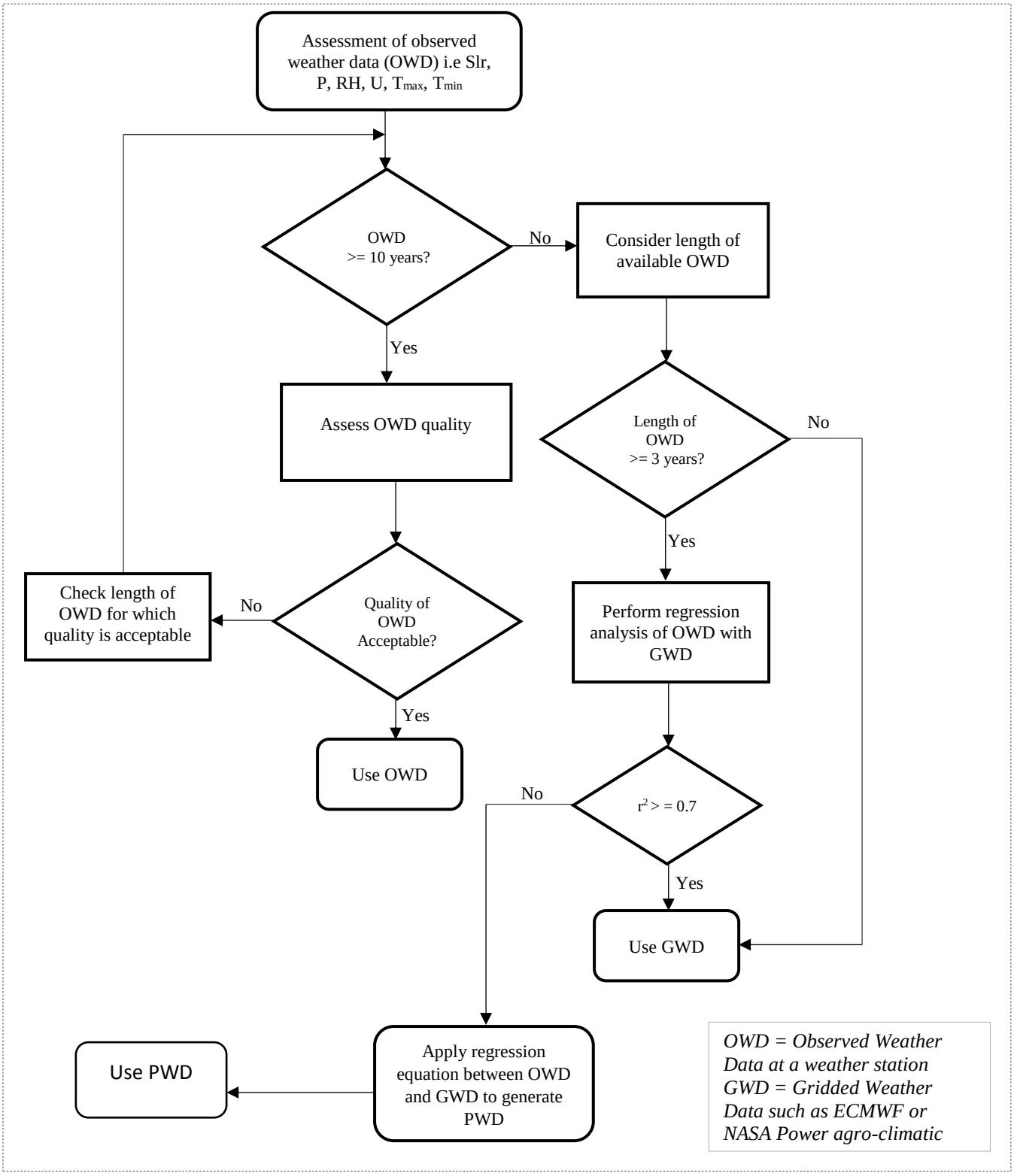

Figure 5.3 Flow chart showing the data propagation algorithm

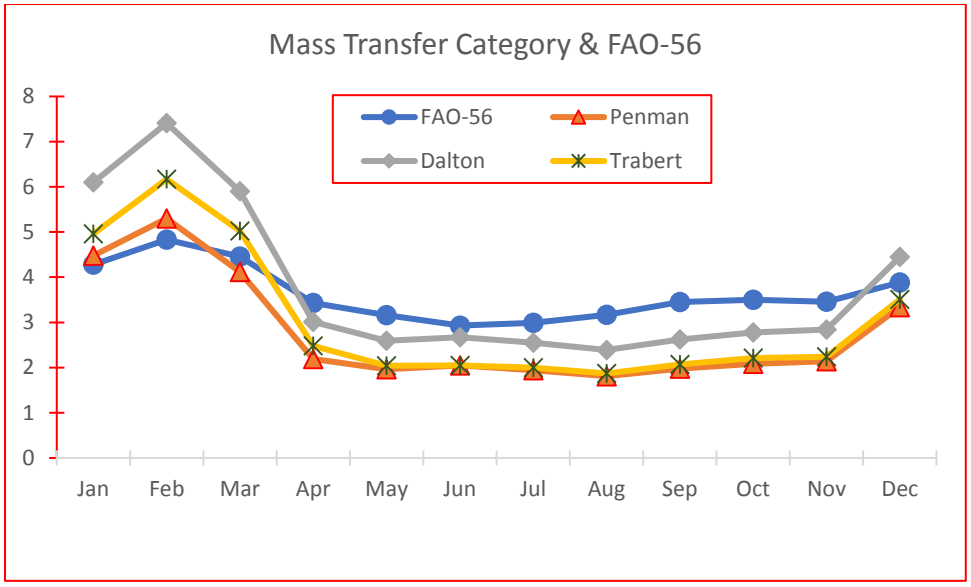

Figure 5.4(a) Monthly ET_o estimated by the different models for the period 2012-2016

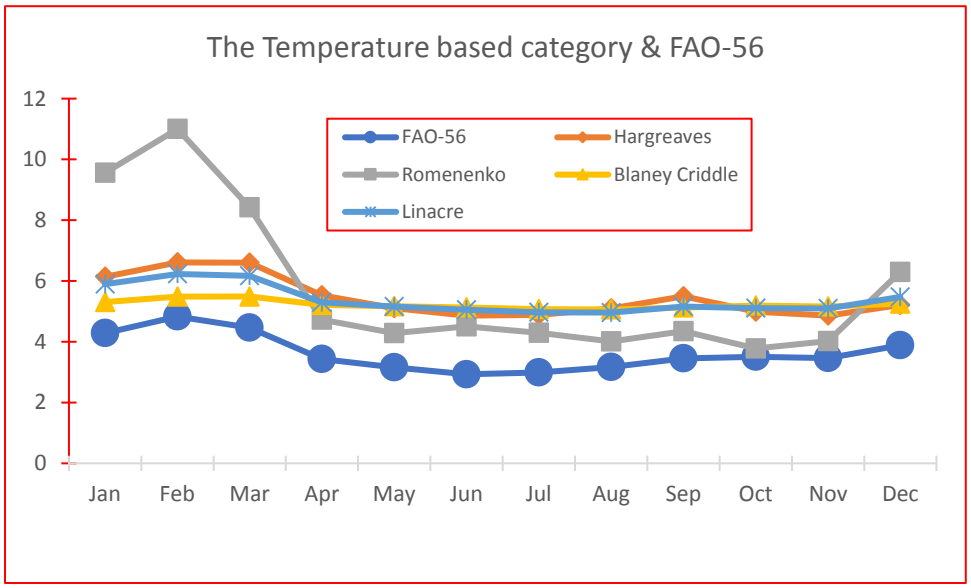

Figure 5.4(b) Monthly ET_o estimated by the different models (shown on the graph) for the period 2012-2016

Overall, the best performing models in this Category are Makkink, Abtew and Turc in that order, considering a compromise among all the statistical test indicators. And the worst performing are; Schendel, Linacre and Priestley Taylor in that order considering a compromise among all the test indicators. Considering all the three model categories, radiation based models predicts ET_o best in the study area, followed by Mass Transfer models and Temperature based models give the worst prediction after comparing all the performance of all the models in each category.

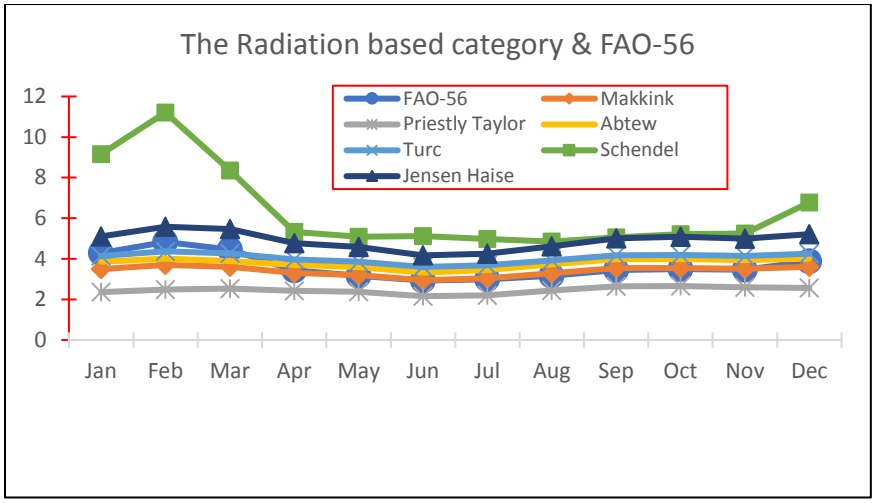

Figure 5.4(c) Monthly ET_o estimated by the different models (shown on the graph) for the period 2012-2016

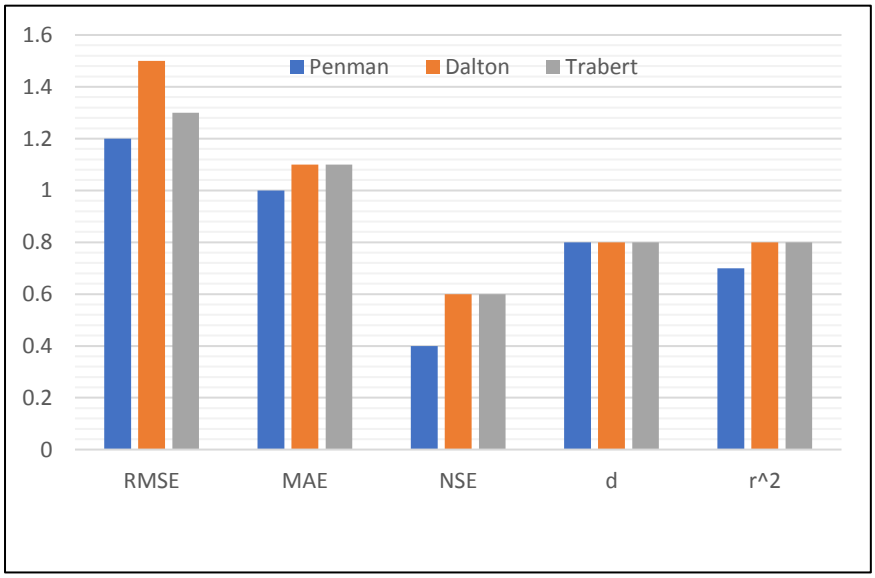

Figure 5.5 (a) Comparison of the test statistics in the Mass Transfer based Category of ET_0 models

The Hargreaves model, the best performing in the temperature based category is known for poor performance in cloudy regions (Hargreaves and Samani, 1985) and it is recommended that Hargreaves be used for monthly estimate of ET_o. This appears to be the case with all the Temperature based models because Northern Uganda is known for cloudy conditions for two third of the year, starting from the beginning of the rainy season in late March, and lasting up to early November. The scatter plots between each of the evaluated empirical model and FAO-56 are shown in Figure 5.6

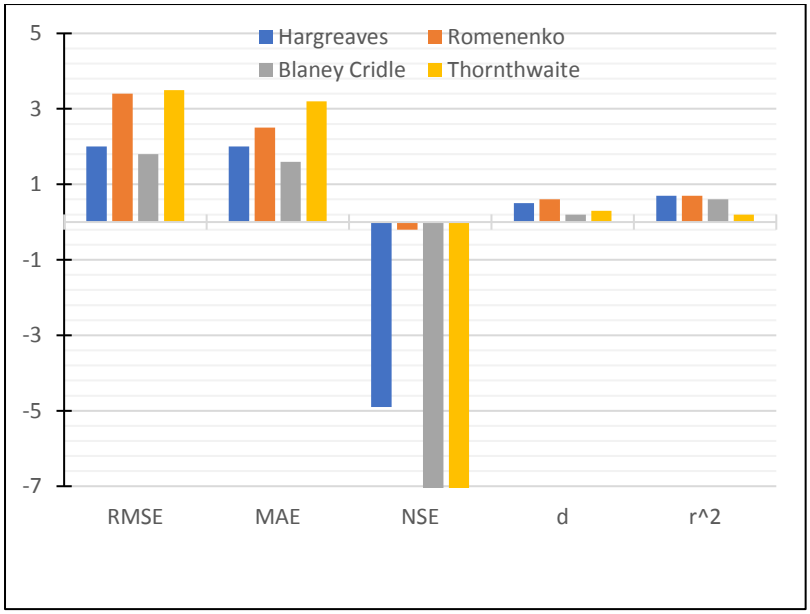

Figure 5.5 (b) Comparison of the test statistics in the Temperature based Category

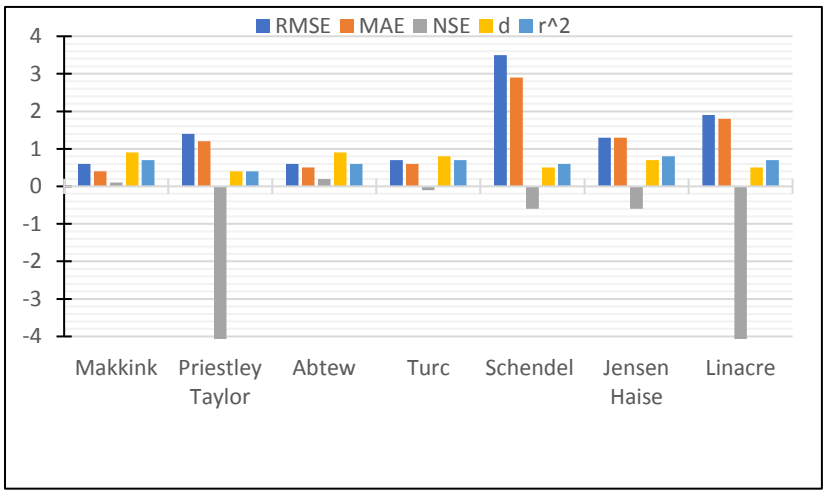

Figure 5.5 (c) Comparison of the test statistics in the Radiation based Category

The box plots in Figure 5.7 provide the descrptive statistics of each of the 13 evaluated ETo models together with values calculated by the referecnce model, i.e. the FAO-56. Whereas Figure 5.8 provides the barchart plot of daily average values of all the 13 ETo models together with the FAO-56 model used to evaluate them. The red horizontal line drawn in Figure 4.8, gives the average daily value of ETo calculated by the FAO-56 model which is considered as standard. This plots confirm the radiation based models of Makkink, Abtew, Turc and the Mass transfer model Dalton as provinding th best prediction of the ET_o when compared to FAO-56 combination model. In Table 5.4, the summary of the test statistics for the different ETo models are presented.

5.6 Results and Discussion of the Weather Data Propagation in Northern Uganda

Uganda does not have reliable climatic records, (as is always the case in many developing countries); more so in Northern Uganda where this study is conducted. Data collected from the three main stations shown in Figure 5.1 and whose details are provided in Table 5.1, were subjected to quality checks. The climatic data obtained from the three-traditional meteorological stations had records of daily precipitation, maximum and minimum air temperatures. All the other climatic parameters i.e. RH, solar radiation and wind speed were missing. However, there were two automatic stations that were installed in Gulu University and at a nearby Dairy farm, where soil moisture monitoring for this research were conducted. The details of the data length of these two stations are provided in Table 5.1. Following the procedure for assessing the reliability of local climatic data and applying the gridded data for updating them to cover longer period in a process termed; data propagation as indicated in Figure 5.3. Only data from Gulu University automatic meteorological station passed the test for being used for data propagation. The maximum temperature, minimum temperature and precipitation data at the two traditional stations in Gulu and Lira could also be used for calibration of Gridded climatic data because of their lengths; i.e. being 20 years. However, because they had a number of gaps, the process was applied mainly to fill those gaps since the two stations are located within the same agro-climatic zone as shown in Figure 2.3 (Chapter 2). The climatic data of minimum temperature, maximum temperature at the Kitgum station did not pass the consistency test and was excluded for the purpose of this study.

This section presents results of the data propagation procedure performed using the four-year data from the automatic station at Gulu University and two sources of Gridded climatic data; i.e. the reanalysis data from European Centre for Medium Range Weather Forecast (ECMWF) and NASA-Power Agro-climatic. In both cases, the gridded climatic data are obtained by applying the two-stage procedure: i.e. the analysis data and then finally the reanalysis data. The analysis data are obtained from assimilation method in combination with forecasting models to generate a continuous gridded dataset at the resolution of 0.25^0. There after reanalysis data is obtained by resampling the gridded data at 0.125^0 resolution. The data obtained from ECMWF reanalysis include solar radiation, air temperature, wind speed and rainfall for the period 1979 – 2015. While those obtained from NASA-POWER agro-climatic include solar radiation, maximum and minimum air temperatures, relative humidity and precipitation for the periods 1983-2015.

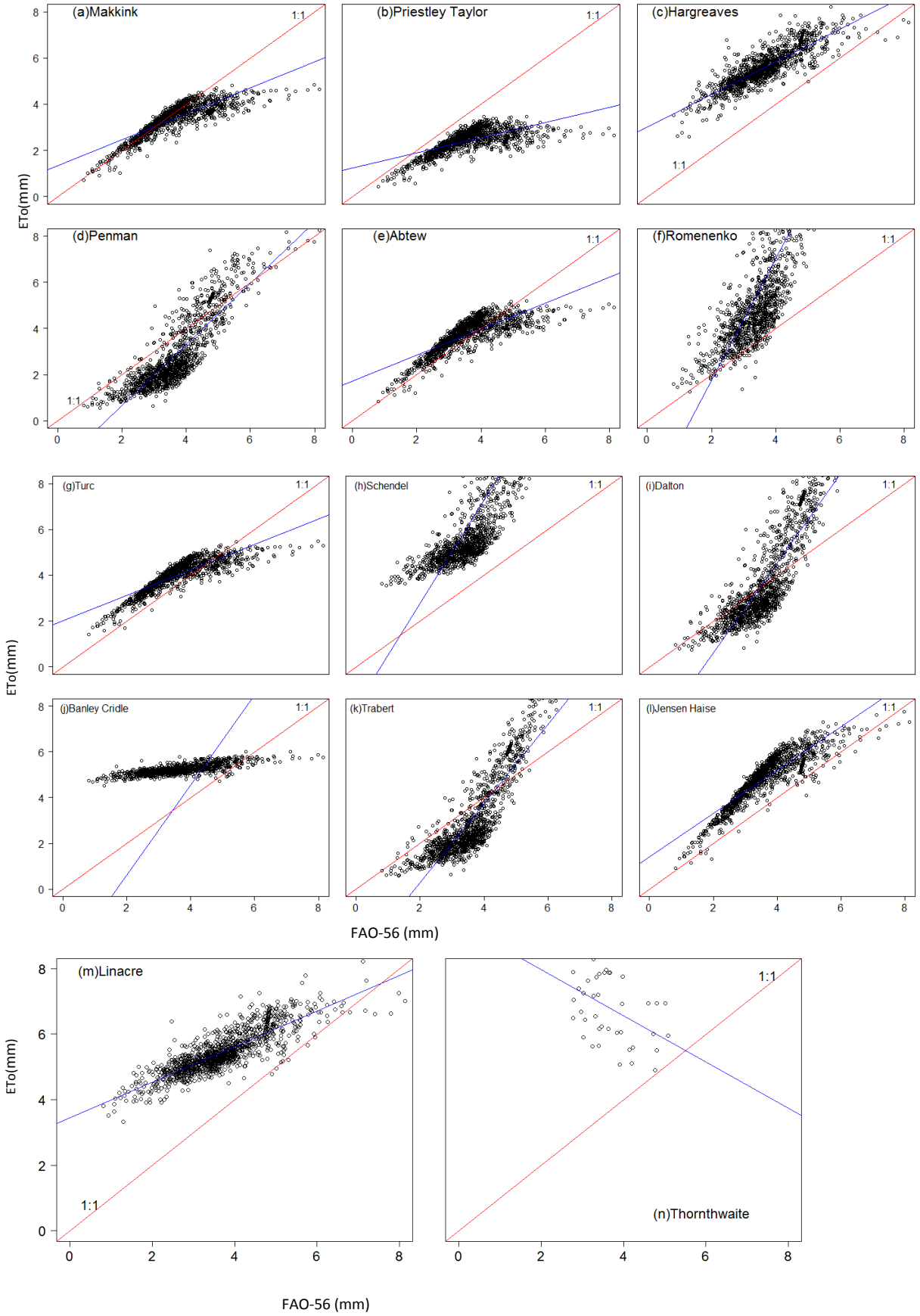

Figure 5.6 Scatter plots of the 13 different ET_o models evaluated by comparing each with FAO-56

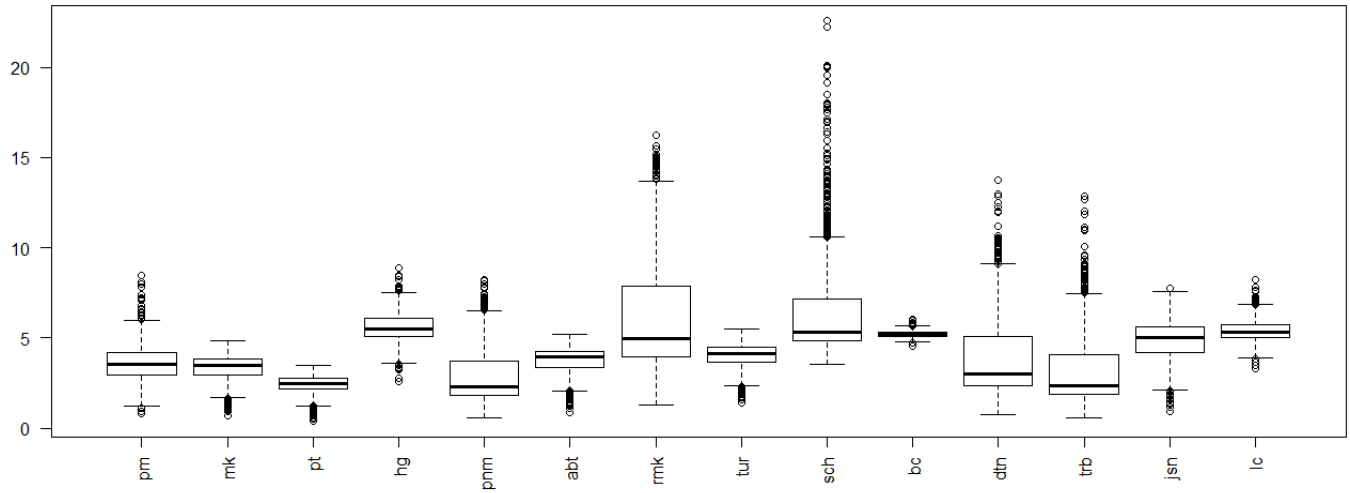

Figure 5.7 Box plots of the different reference evapotrasnpiration models for station A. In the x-axis, ET_0 is calculated in mm in each case. Each of the different ET_0 models is evaluated using the FA-O56PM combination model indicated as pm; mk = Makkink (radiation model), pt = Priestley Taylor (radiation model), hg = hargreaves (temperature model), pnm = Penman (mass transfer model), abt = Abtew (radiation model), rmk= Romenenko (temperature model), tur=Turc (radiation model), sch=Schendel (radiation model), bc = Banley Cridle (temperature model), dtn= Dalton (mass transfer model), trb = Trabert (mass transfer model), jsn = Jensen Baise (radiation model) and lc = Linacre (temperature model)

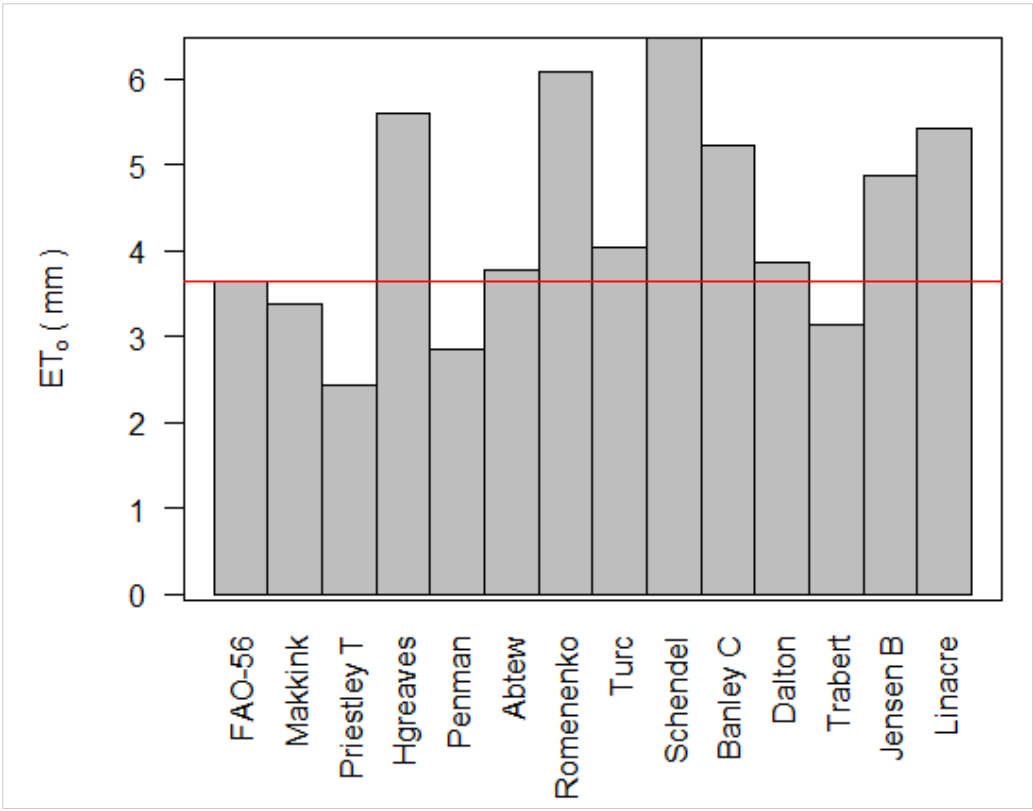

Figure 5.8 Bar plot showing average values of ETo estimatimated by the different models as compared to FAO-56PM over the period (1998 – 2012). The red line indicates the average value calculated by the FAO-56 model

Table 5.4 Statistical test results between each of the empirical ET_o model and FAO-56

ET_o MODEL	RMSE	MAE	NSE	d	r^2	a(Intercept)	b(slope)
Makkink	0.6	0.4	0.1	0.9	0.7	1.3	0.6
Priestley Taylor	1.4	1.2	-7.5	0.4	0.4	1.2	0.3
Hargreaves	2.0	2.0	-4.9	0.5	0.7	3.0	0.7
Penman	1.2	1.0	0.4	0.8	0.7	-2.0	1.3
Abtew	0.6	0.5	0.2	0.9	0.6	1.7	0.6
Romenenko	3.4	2.5	-0.2	0.6	0.7	-3.5	2.6
Turc	0.7	0.6	-0.1	0.8	0.7	2.0	0.6
Schendel	3.5	2.9	-0.6	0.5	0.6	-1.7	2.3
Blaney Cridle	1.8	1.6	-73.6	0.2	0.6	4.6	0.2
Dalton	1.5	1.1	0.6	0.8	0.8	-3.3	2.0
Trabert	1.3	1.1	0.6	0.8	0.8	-3.1	1.7
Jensen Haise	1.3	1.3	-0.6	0.7	0.8	1.4	0.9
Linacre	1.9	1.8	-7.6	0.5	0.7	3.4	0.5
Thornthwaite	3.5	3.2	-10.4	0.3	0.2	9.4	-0.7

*RMSE=Roor Means Squared Error, MAE=Mean Absolute Error, NSE=Nash Sutcliffe Efficiency, d=Index of agreement and r^2 = coefficient of determination

The test statistics used for testing the prediction accuracy of the gridded data sets from the two sources i.e. NASA-P and ECMWF are the same as those used for the evaluation of the reference evapotranspiration models. These are the RMSE, MAE, NSE, d and r^2 with the slopes and intercepts of the regression line shown for each climatic variable. The prediction of the minimum and maximum temperatures in the study area is better achieved through the reanalysis data from ECMWF than using data from NASA-P, considering all the test statistics. Whereas solar radiation and rainfall in the study area are better predicted by the NASA-P data sets except for NSE for rain in which the value for ECMWF = 0.0937 and that of NASA-P = -0.9, but overall, solar radiation and rainfall are better predicted by the NASA-P gridded climatic data in the study area considering all the test statistics except for NSE. Lastly, wind speed was better predicted by ECMWF considering RMSE, MAE, d and r^2. The RH data was only obtained from the NASA-P and the prediction seems fair, considering the different values of the test statistics. Therefore, following the procedure for data propagation proposed by Wart et al. (2015), minimum and maximum temperature values for the study area can be obtained from ECMWF reanalysis data with r^2 = 0.9, for maximum temperature and 0.7, for minimum temperature. Applying the procedure demonstrated in the flow chart; Figure 5.3, the values of the maximum and minimum temperatures can be directly used in simulation studies in the study area without calibration. Whereas solar radiation data for the study area needs to be obtained from the NASA-P agro-climatic data sets. While wind speed and rainfall data requires

calibration and readjustments using regression equations for the NASA-P agro-climatic and observed climatic data.

Table 5.5 Test statistics for the data propagation comparing the observed meteorological variable to reanalysis data obtained from NASA-Power and ECMWF-gridded datasets

	RMSE		MAE		NSE		d		r^2		b(slope)		a(intercept)	
	NASA-P	ECMWF	NASA-P	ECMWF	NASA-P	ECMWF	NASA-P	ECMWF	NASA-P	ECMWF	NASA-P	ECMWF	NASA-P	ECMWF
T_{min}	1.8	0.96	1.4	0.73	-0.4	0.31	0.6	0.67	0.2	0.35	0.4	0.3	11.5	13.13
T_{max}	2.2	1.61	1.8	1.25	0.6	0.6	0.9	0.86	0.6	0.67	0.6	0.6	13	12.58
Slr	45.6	68.67	40.3	58.34	-0.2	-2.29	0.7	0.55	0.7	0.31	0.7	0.74	22.9	106.5
U	1.4	0.52	1.1	0.42	-0.8	-1.1	0.5	0.67	0.2	0.27	0.2	0.83	1.1	0.27
RH	8.5		6.8		0.7		0.9		0.7		0.7		15.9	
Rain	8	8.06	4.1	4.21	-0.9	0.0937	0.6	0.472	0.2	0.113	0.7	0.16	1.3	2.74

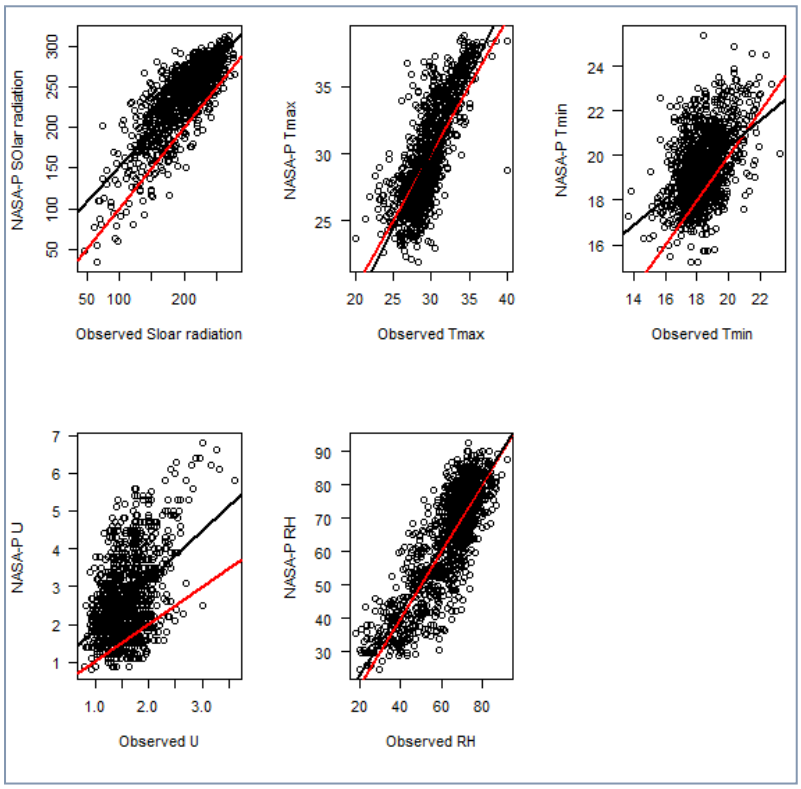

Figure 5.9 Scatter plots of NASA-P data vs Observations, showing the 1:1 line (red-line) and the line of best fit (black line)

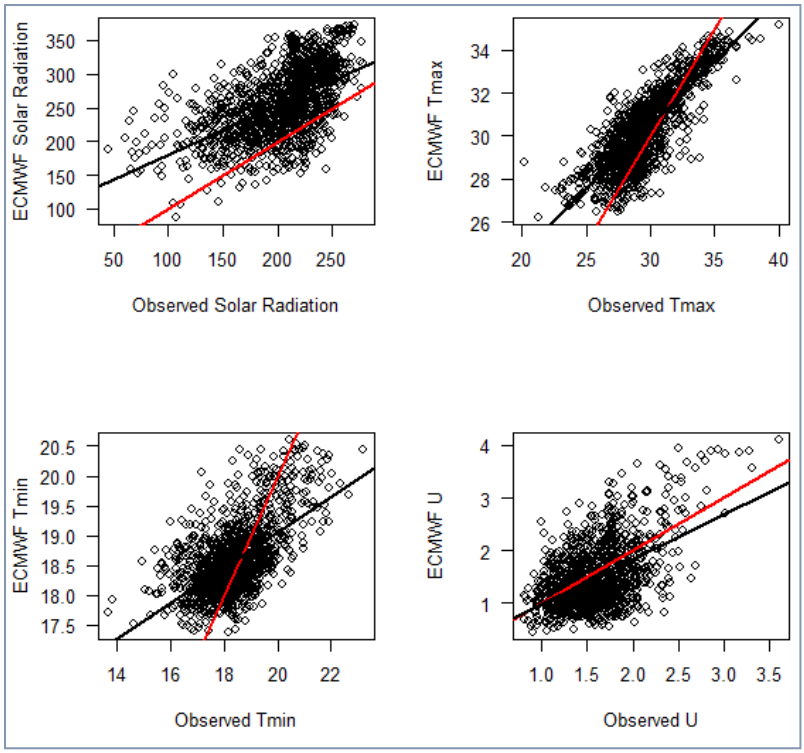

Figure 5.10 Scatter plots of the ECMWF reanalysis data vs observations showing the 1:1 (red line) line and the line of best fit (black line).

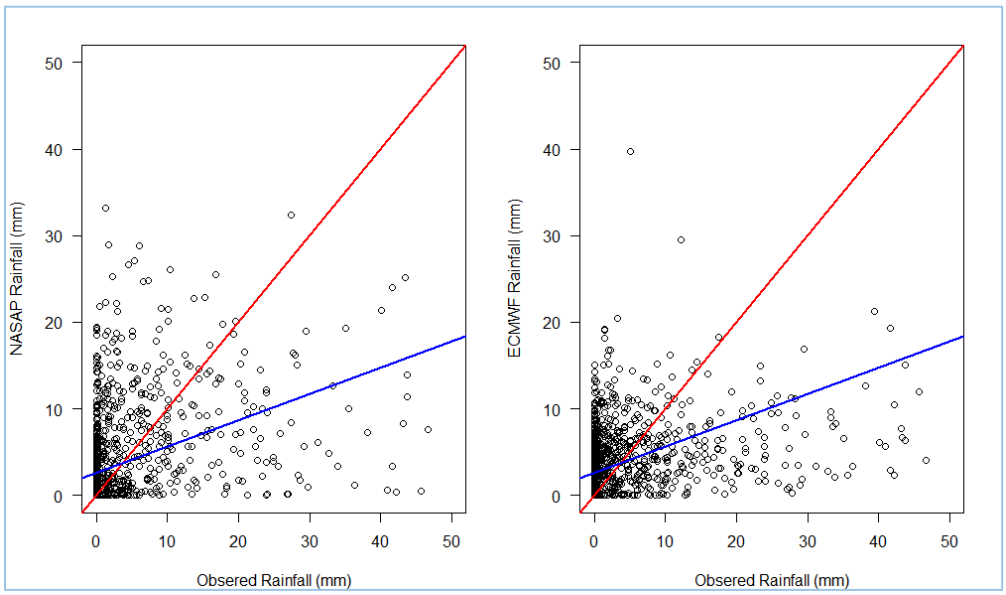

Figure 5.11 Scatter plots of the observed rainfall vs reanalysis rainfall data from NASA-P and ECMWF. Showing 1:1 line (red) and the line of best fit (blue)

5.7 Conclusion

This chapter had two main objectives namely: to evaluate 12 reference evapotranspiration models in Northern Uganda using FAO-56 model and to apply data propagation algorithm for the assessment and adjustment of gridded climatic data for gap filling observed climatic data

in Northern Uganda. The gridded climatic data were obtained from NASA-POWER agro-climatic and ECMWF websites. Observed climatic data were collected from the study area for the periods between 1995 and 2016 from 5 meteorological stations. Three of the meteorological stations are the traditional weather stations in Northern Uganda and they contained only the daily rainfall and air temperature records between 1995 and 2015, albeit with large gaps. Climatic data obtained from the two automatic stations at Gulu University include continous data for four complete years i.e from 2012 – 2016, whereas the automatic meteorological station installed at the experimental site at the Dairy farm provided data records only for one year and 8 months i.e. from April 2015 to October 2016. Subjecting the records of temperature and rainfall data from the three traditional meteorological stations made all the data to be disqualified for this analysis. For that reason the climatic records used in this analysis are only those from the two automatic stations, especially records from the Gulu University station that has been in existance since October 2012. The automatic weather instrument at the GU is a standard Campbell Scientific automatic weather station equiped with CR1000 measurement and control data logger and wind speed monitor sensor, relative humidity and temperature probes and a silicon pyranometer with fix daylight calibration for solar radiation meaurements. Whereas the automnatic station at the dairy farm is an integrated sensor suite system from DAVIS Inc. equiped with an infrared console that can receive data within a 300m radius.

Evaluation of the 12 ET_o models showed that the radiation based models had the best ETo predictions when compared to FAO-56 followed by the mass transfer based models and worst predictions were obtained from the temperature based models. Over all, Makkink, Abtew and Turc radiation models had the best predictions in that order when considering the four test statistics used. Whereas Dalton model in the mass transfer category had the best ETo prediction. Among the temperature based category Hargreaves had the best prediction overall followed by Blaney Criddle and Thornthwaite had the worst prediction. Generally, the temperature based models consistently overestimated the reference evapotranspiration in the study area. Whereas Priestley Taylor Model consistently underestimated the ET_o among the radiation based category.

The climatic data propagation algorithm proposed by Wart et al. (2015) was applied to assess the applicability of gridded climatic data in Northern Uganda. The assessment showed that the two data sources of NASA-P agro-climatic and ECMWF can be used concurrently in the study area. This is because application of regression analysis and test statistics showed that

Ra, RH and P are better predicted by NASA-P, whereas T and U are better predicted by the reanalysis data from ECMWF.

The development of a new methodology to define the soil moisture deficit index (SMDI) for the study area, proposed in chapter 4, require evaluation of simplified reference evapotranspiration models in a given study area. It also requires assessment of gridded reanalysis climatic data for gap filling climatic records. This is because the proposed method is tailored for application under rain-fed conditions in developing countries which have scarce records of climatic data with poor quality data. The two objectives were achieved in this chapter through the evaluation of different ET_o models in the study area and application of data propagation algorithm for gap filling climatic records in the study area.

6 CALIBRATION OF AGRO-HYDROLOGICAL MODEL FOR PREDICTION OF SOIL MOISTURE DYAMICS: *THEORETICAL DEVELOPMENT*

Summary

In this chapter, the main theoretical background governing water movement in the soil-plant- atmosphere continuum (SPAC) is covered. Concepts that govern application of water flow models for agro-hydrological simulation are explored. In particular, use of the Richard's equation (RE) for the prediction of water movement in the unsaturated soil system is elaborated including steps involved in the calibration of a 1-dimensional RE based model. Brief description of water flow model, Hydrus 1D is provided since it is the model that has been calibrated and applied in this study to generate long term soil moisture through agro-hydrological simulation. Furthermore, usually application of RE based models for agro-hydrological simulation requires for input crop growth parameters. In this research, remote sensing based methods have been applied to estimate crop development parameters. Therefore, this chapter concludes by covering some concepts governing application of satellite remote sensing to estimate crop growth parameters.

6.1 Introduction

It has long been recognized that monitoring agricultural drought is better done by soil moisture based drought indices (Padhee et al., 2014; Todisco et al., 2008; Mannocchi et al., 2004; McKee and Doesken, 1995). Development of such indices has depended on soil moisture monitoring programs where networks of soil sensors are deployed to obtain long term records of soil moisture time series from which the indices are formulated (Martínez-Fernández et al., 2015; Hao and Aghakouchak, 2014; Zargar et al., 2011). Alternatively, applications of water flow models that provide simplified description of water movement through the soil system without accounting for vegetation growth factors have been applied. This has been done especially in areas where extensive records of soil moisture time series are lacking. For instance, in the early development of PSDI and CMI, a simple two-layer lumped parameter model was applied to account for water storage in the upper and lower soil profiles (Ryu et al., 2014; Alley, 1984; Palmer, 1968, 1965). However, operational monitoring of agricultural drought requires indices that are developed based on long term records of soil moisture time series (Narasimhan and Srinivasan, 2005). Application of water flow models can only be valid if such models provide explicit description of water movement through the Soil-Plant-

Atmosphere Continuum (SPAC) in order to generate soil moisture times series through *agro-hydrological* simulations. Therefore, application of water flow models for the formulation of soil moisture based drought indices would require knowledge of soil hydraulic characteristics and methods for estimating dynamic vegetation growth parameters.

The first step in developing the new approach to formulate SMDI (introduced in chapter 4) therefore involves calibration of a 1-dimensional water flow model for agro-hydrological simulations to create an extended record of soil moisture time series. This is done so as to fill the gap created by lack of long term soil monitoring programs that are common in majority of developing countries. Once such extended records of soil moisture is created, they can be applied to obtain θ_{FC} *and* θ_{WP} through a method developed by Sridhar et al. (2008) and Hunt et al. (2009) to calculate SMDI. However, calibration of a water flow model such as Hydrus 1D for agro-hydrological simulation as applied in this research also require a method for estimation of the crop development parameters. As mentioned in chapter 4, this is achieved through processing of satellite remote sensing images. The aim of this chapter is to develop theoretical backgrounds including elaboration of the concepts applied to calibrate Hydrus 1D for agro-hydrological simulations in order to obtain the threshold parameters for the formulation of SMDI. The first objective deals with reviews of the concepts governing water movement in the SPAC, including description of the 1-dimensional water flow model Hydrus 1D. The second part deals with the reviews of the concepts and description of the methods applied in the estimation of crop development parameters through processing of satellite remote sensing images.

6.2 Prediction of Moisture Dynamics Through Agro-Hydrological Simulation

6.2.1 Water dynamics in the Soil Plant Atmosphere Continuum (SPAC)

In a hydrological cycle, (Figure 6.1), part of the water that is taken up from the soil by plant roots, lost through transpiration into the atmosphere and returned again to soil through precipitation; goes through what is commonly known as; Soil–Plant–Atmosphere Continuum (SPAC). This aspect of the hydrological cycle which was first given detail treatment by Cowan (1965), emphasizes the connectedness of soil, plant and atmospheric water. Phenomena involving water movement within this continuum include root and whole-plant hydraulic conductance, xylem embolism and hydraulic lift by roots (Slayter, 1967). Although the intricacies in the detailed pathways are quite complex and encompass a number of disciplines, such as: atmospheric physics, soil physics, plant physiology, root and whole plant hydraulics

(Sperry and Love, 2015), etc., the general conceptualization can be simplified through application of water balance models that integrate soil moisture characteristics, root water uptake mechanisms, evaporation from the soil, transpiration and precipitation (Levis, 2010). Proper treatment of moisture movement in the SPAC helps us to understand factors that control plant adaptation to moisture stress when soil moisture becomes limiting in the root zone (Manoli et al. 2015). A number of models have been developed over the years for simulation of moisture dynamics in the SPAC. Many of which are based on the water balance others are based on partitioning of the energy balance model (Norman and Anderson, 2003). Water balance based models have been extensively applied because they are based on concepts that require simplified treatments. Whereas the energy balance models mainly deal with application of remote sensing based algorithms that require sophisticated equipment for their verifications (Hildebrandt et al., 2016; Ting et al., 2012; Jime et al., 2009). For this reason, water balance based models have been applied in this study, because of their simplified treatment of the water movement in the SPAC and possibility of simple equipment for their verification (Brillante et al. 2014; Skaggs, 2008; Mhiza and Chibulu, 2007; Norman and Anderson, 2003; Li & Islam, 1999).

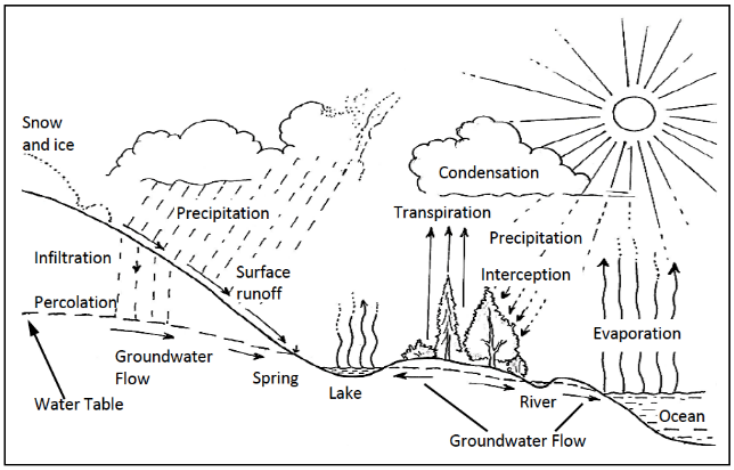

Figure 6.1, The hydrological cycle

6.2.2 Water Balance modeling in the SPAC

The water contained in the soil system is in a constant state of dynamism due to various forces acting on it. Over a given time, interval δt, the rate of change in soil water storage δs, is given by

$$\delta s = \left(P - E_s - T_p + q\right)\delta t \qquad (6.1)$$

Where P, E_s, T_p are: precipitation, soil evaporation, transpiration rates respectively and q is the water flux density through the soil defined as the rate of discharge per unit cross sectional area

perpendicular to the direction of flow (Kutilek and Nielsen, 1994). In the simplest form, the water balance model can be expressed as a bucket filling model (Figure 6.2). The bucket filling model has been widely used in many water balance studies, however its validity is being questioned due to its over simplification of some of the important terms of the water balance such as evapotranspiration (Romano et al., 2011).

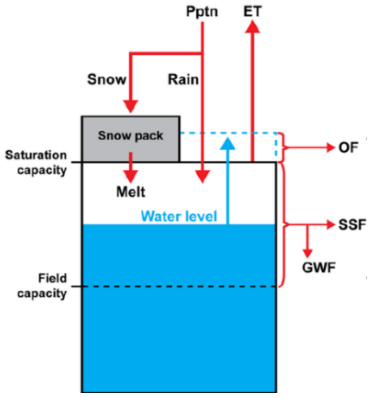

Figure 6.2 A schematic diagram for the bucket filing model

Significant progress has been made in developing modeling techniques for monitoring moisture movement in the SPAC (Ojha et al., 2014; D'Urso, 2001). This has been possible through proper understanding of the physics that govern water dynamics in the SPAC over the years. Water movement in the SPAC is best described by the famous Richard's Equation (RE), Equation (6.2); which was formulated through a combination of Darcy's law and continuity equations (Hillel, 1998; Kutilek and Nielsen, 1994; Feddes, 1997; Richard, 1931). Solution of RE is only possible through numerical methods as the soil hydraulic functions; i.e. *K(h)* and *θ(h)* that describe the input parameters are strongly non-linear (Romano et al., 2011).

$$\frac{\partial \theta}{\partial t} = \frac{\partial}{\partial z}\left[K(h)\left(\frac{\partial h}{\partial z} + 1\right) - S(h)\right] \qquad (6.2)$$

Where; θ(cm^3/cm^3) is the volumetric soil moisture content, t (days) is time, h (cm) the soil metric potential, z (cm) is vertical coordinate taken positive upwards, *K(h)* [cm/day] is hydraulic conductivity and *S(h)* [day^{-1}] denotes water uptake by plant roots estimated according to Feddes and Raats (2004), equation (6.3)

$$S(h) = \alpha(h)\frac{T_p}{|z_r|} \qquad (6.3)$$

Where T_p (cm/day) is potential transpiration, z_r (cm) is rooting depth and α(h) [dimensionless] is a reduction factor as a function of h and accounts for water deficit and oxygen deficit

(Droogers, 2000). Most numerical codes developed for the solution of equation (6.2) use close form formulations for the description of soil retention and hydraulic conductivity characteristics. Equations (6.4) to (6.6) are based on van Genuchten-Mualem formulations (Van Genuchten,1980). Other formulations for characterizing soil moisture retention are shown in Table 6.1.

$$\theta(h) = \theta_{res} + \frac{\theta_{sat} - \theta_{res}}{\left(1 + |\alpha h|^{n}\right)^{m}} \tag{6.4}$$

$$K(S_e) = K_{sat} S_e^{\lambda} \left[1 + \left(1 - S_e^{\frac{1}{m}}\right)^{m}\right]^2 \tag{6.5}$$

$$S_e = \frac{\theta - \theta_{res}}{\theta_{sat} - \theta_{res}} \tag{6.6}$$

Where θ_{sat} is the saturated water content, K_{sat} is the saturated hydraulic conductivity, θ_{res} is the residual water content, α(cm^{-1}), n (dimensionless), λ(dimensionless) are the fitting parameters and m is defined as; $m = 1 - 1/n$.

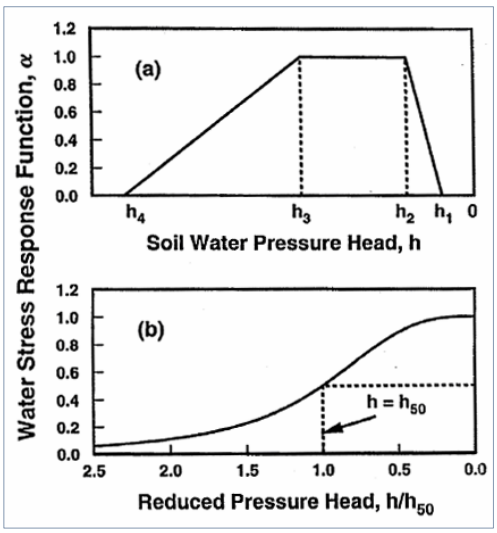

Figure 6.3. Graphs showing root water uptake stress response functions α(h) as used by (a) Feddes et al. (1978) and (b) Van Genuchten (1987)

A number of soil water retention models have been developed over the years (Ginn, 2007), a summary made by Too et al. (2014) are shown in Table 6.1. Soil Water Retention Models (SWRM) in common use are the Van Genuchten, Brooks-Corey and that due to Kosugi (Simunek et al., 2008; Chertkov, 2004; Kosugi, 1999). An evaluation of the soil water retention

models by Too et al. (2014), indicates that; Gardener and Biexponential models gave the best predictions using the statistical indicator of the RMSE, whereas the five parameter models performed best in prediction of the soil moisture retention. He further found that the Van Genuchten model performed best in the five-parameter category whereas the Kosugi model performed best in the four-parameter category. Unsaturated soil hydraulic conductivity has for the most part been estimated basing on the van Genuchten-Mualem formulation of equations (6.4 and 6.6).

Table 6.1 Summary of Soil Water Retention Curve (SWRC) models developed over the years. Source: Too et al., (2014)

Reference	**SWRC**	**Parameters**
Campbell (1974)	$\theta(h) = \theta_s(\alpha h)^{\lambda}$	$\alpha, \theta_s, \lambda$
Tani (1982); as quoted by Sillers et al., 2001	$\theta(h) = \theta_r + (\theta_s - \theta_r)[1 + (\alpha h)e^{-\alpha h}]$	$\alpha, \theta_r, \theta_s$
Exponential (Omuto, 2007)	$\theta(h) = (\theta_r + \theta_s)e^{\alpha h}$	$\alpha, \theta_r, \theta_s$
Van Genuchten (1980)	$\theta(h) = \theta_r + (\theta_s - \theta_r)[1 + (\alpha h)^n]^{-(1-\frac{1}{n})}$	$n, \alpha, \theta_r, \theta_s$
Gardner (1958)	$\theta(h) = \theta_r + [\theta_s - \theta_r](\alpha h)^{-\lambda}$	$n, \alpha, \theta_r, \theta_s$
Ruso (1988)	$\theta(h) = \theta_r + (\theta_s - \theta_r)[(1 + 0.5\alpha h)e^{-0.5\alpha h}]^{\frac{2}{n}+2}$	$n, \alpha, \theta_r, \theta_s$
Brooks-Corey (1964)	$\theta(h) = \theta_r + [\theta_s - \theta_r](\alpha h)^{-\lambda}$	$\alpha, \theta_r, \theta_s, \lambda$
Kosugi (1999)	$\theta(h) = \theta_r + \frac{1}{2}(\theta_s - \theta_r)\mathrm{erfc}\left[\frac{\ln(h/h_m)}{\sigma\sqrt{2}}\right]$	$h_m, \theta_r, \theta_s, \sigma$
Fredlung-Xing (1994)	$\theta(h) = \theta_r + \frac{\theta_s - \theta_r}{[ln\{2.7183 + (\alpha h)^n\}]^m}$	$n, m, \alpha, \theta_r, \theta_s$
Biexponential (Omuto, 2009)	$\theta(h) = \theta_r + \theta_{s1}e^{\alpha_1 h} + \theta_{s2}e^{\alpha_2 h}$	$\alpha_1, \alpha_2, \theta_r, \theta_{s1}, \theta_{s2}$

6.2.3 Estimation of Soil hydraulic parameters through direct methods

As emphasized in the section 6.2.1, numerical solution of the RE requires explicit description of soil hydraulic functions, i.e. *K(h)* and *θ(h)*. Different formulations of these functions for characterizing soil hydraulic parameters in the unsaturated zone have been advanced over the years (Table 6.2). Various numerical codes have been developed for the solution of equation (6.2), many of which rely on the van Genuchten-Mualem formulation of the soil hydraulic characteristics requiring estimation of the six parameters; Viz: water content at saturation (θ_{sat}), the residual water content (θ_{res}), soil pore connectivity parameter (n), the shape parameter of the soil water retention curve (α), the tortuosity factor (λ) and the saturated hydraulic conductivity (K_s). Estimation of these parameters are possible through laboratory

experiments based on soil core samples though it has been shown that the soil core samples usually employed in the laboratory do not represent actual flow conditions at the scale of applications (Vereecken et al., 2014). Besides, the laboratory methods are time consuming and involve tedious processes possible only in advanced laboratories that are non-existent in developing countries. As such research activities employing applications of advance modeling techniques based on RE for monitoring soil moisture movement in the SPAC are very rare in developing countries where their applications are much needed (Makurira, 2010). Because of these complexities, inverse modeling techniques have been developed for estimation of soil hydraulic characteristics.

6.2.4 Estimation of soil hydraulic Parameters through Inverse Modeling

A comprehensive review of the inverse methods for estimation of soil hydraulic characteristics have been given by Hopman et al. (2002). Generally, inverse modeling techniques involve numerical inversion of the RE. It combines forward RE based water flow models with appropriate parameter optimization techniques to find the best parameter sets that minimize a predefined objective function (Ritter et al., 2003). This is achieved through measured values of state variables such as soil moisture content θ and matric potential h. The measured values of the state variables are obtained through transient evapotranspiration experiments in the laboratory or through infiltration experiments in the field (Suhada et al., 2015; Minasny and Field, 2006). In each case, the hydraulic parameters are estimated through an inversion process using the measured values of the state variables. The inversion process is implemented either through a trial and error methodology, or through an automatic method by employing parameter optimization algorithms (Ritter et al., 2003). A number of parameter estimation algorithms have been developed. Most of the newly developed algorithms are based on global optimization techniques that are implemented by solving multiple objective functions. Whereas, the optimization techniques that are based on single objective functions are used when initial estimates of the parameters are provided and when the parameter boundaries are known.

6.3 Description of the Unsaturated Porous Media Transport Model - Hydrus 1D

A number of advanced process models based on numerical solution of the Richard's equation have been developed and freely available in the scientific domain. Their strengths and limitations vary depending on the purpose for which they were developed. However, when

considering a one-dimensional moisture transport dynamics in the root zone, the performances of these models are largely similar since they are based on similar concepts. However, the main limitation of applying these RE based models in developing countries have been input requirements for the estimation of their parameters. A comprehensive review of the development stages of the different generations of these hydrological models was given by Chen et al. (2014). In this study, Hydrus 1D was chosen because of its wide applications especially in developing countries (Simunek et al., 2016). It is freely available and has features such as the graphical user interface (GUI) making it easy to apply, unlike many other similar freely available codes which are provided without the GUI. For instance Makurira (2011) applied Hydrus 2D (a commercial version) for spatiotemporal water productivity analysis under rain fed conditions in Tanzania.

Hydrus 1D is a software package for simulating water, heat and solute transport in one dimensional variably saturated porous media. Hydrus 1D numerically solves the RE for variably saturated water flow and the advection-dispersion type equations for heat and solute transport. The flow equation incorporates a sink term to account for the root water uptake by plants; equation (6.2). The detailed description of Hydrus 1D can be found in Šimůnek et al. (2009). Use of the model for simulation of the moisture dynamics in the unsaturated soil system requires specification of the upper and the lower conditions and availability of a method to characterize the soil hydraulic parameters. Evapotranspiration is computed by the Penman Monteith combination equation and there are options to apply the Hargreaves equation as well.

6.3.1 Specification of The Initial and Boundary Conditions in Hydrus 1D

Simulation of moisture movement in unsaturated soil system using Hydrus 1D model requires specification of the initial and the boundary conditions. Usually the initial conditions are the moisture content or the matric potential values within the flow domain at the start of the simulation process. This can be achieved through initial measurements of these state variables in the soil system before the start of the simulation process. Basically, the initial conditions are the values of θ and h for all z at $t < 0$ where, z is the vertical 1-dimensional coordinates down ward within the soil system and, $t < 0;$ implies the time before the start of simulation, Kutilek and (Hillel, 1998; Nielsen, 1994). The boundary conditions in Hydrus 1D have to be specified throughout the whole simulation process. One such boundary condition for the case of field experiments as applied in this study is the topographic surface. This is usually referred to as the upper boundary condition. In a natural Agricultural field condition, the upper boundary

condition is defined by a combined action of Evapotranspiration process, precipitation and surface run off. The evapotranspiration is a very complex process involving a number of weather and crop parameters. In this study, the Evapotranspiration calculation and precipitation measurements are handled in chapter 5, whereas the crop parameters are obtained through remote sensing applications and these are covered section 6.4 of this chapter. The other boundary condition can either be a finite or an infinite length of the 1-dimensional soil column. In a field condition one such finite length is the ground water table (h = 0). Many times, the water table is very deep such that its influence on the few centimeters of the soil column from the soil surface is negligible, in such conditions the column is considered to extend to an infinite length. In such a case, Hydrus 1D imposes free drainage as the lower boundary condition, where the rate of change of moisture flux into the soil is considered constant, i.e., dq/dt = 0.

6.3.2 Preparation of soil and meteorological data for input into Hydrus 1D

Soil water retention and hydraulic conductivity parameters have to be defined for input into Hydrus 1D. A number of close form equations are available for the definition of the water retention curve and the soil hydraulic functions that are used in Hydrus are those of the Van Genuchten-Mualem equation, the Brooks-Coreys and the Kasogi formulations Table 6.1. Soil water retention curve can be determined in the laboratory through tension experiments on undisturbed soil samples or through the application of pedotransfer functions on to the soil physical characteristics. Soil hydraulic characteristics for input into Hydrus 1d can also be estimated through the single objective parameter optimization module using the *Levenberg-Marquardt* method, if feasible ranges within which the parameters lie can be estimated (Šimůnek et al., 2009). Details of the laboratory determination of the soil physical characteristics such as the soil textural properties are provided under case study in chapter 7. Analysis of the meteorological data is handled in the previous chapter 5.

6.4 Use of Satellite Remote Sensing to Estimate Crop Development Parameters for Input into Agro-Hydrological Model

Crop growth characteristics such as the leaf area index *(LAI),* albedo, here symbolized (*r)* and crop height *(h_c)* are important parameters for simulation of water movement in the SPAC. These crop characteristics vary throughout the crop development stages and as such are critical input for the calculation of evapotranspiration, an important term of the water balance (D'Urso, 2001). Although a model such as Hydrus 1D that has been implemented in this research has inbuilt modules for their estimation, actual monitoring of the canopy variables can greatly

improve the validity of the simulation results (Oguntunde & Van De Giesen, 2004). It is therefore paramount that there be a method for monitoring the crop development stages. In-situ methods for the determination of these variables have been developed (Wang and Trishchenko, 2007; Weiss et al., 2004). However, the methods are usually time consuming and difficult for operational application over large agricultural fields (Jonckheere et al., 2004). Because of these difficulties, remote sensing methods offer attractive alternatives for monitoring of canopy characteristics, such as albedo, LAI and Fraction of Absorbed Photosynthetically active radiation (FAPAR), (Tao et al. 2016; Qu et al., 2015; Zheng and Moskal, 2009; Weiss et al. 1999; Walthall et al., 1985).

6.4.1 Estimation of Surface Albedo

Albedo is defined as the amount of radiant solar energy reflected by a given surface. It is a primary variable required for the estimation of energy exchanges between the earth surface and the atmosphere (Peng et al., 2015). It provides information on the radiation budget of the surface as such, it also provides information on the water balance. Instantaneous albedo is a dimensionless biophysical characteristic of the canopy. It is expressed as the ratio of the radiant energy scattered by a surface upward in all directions to that the surface receives from all directions integrated over the wave lengths of the solar spectrum (Weiss et al., 1999). Estimation of a bidirectional hemispherical reflectance (albedo) of a surface is not possible through a single bidirectional measurement in selected wavebands (He et al., 2012). As such its estimation requires observation of a surface over all directions and overall solar spectral bands (300 – 3000 μm). This requires combination of models for the definition of the bidirectional reflectance distribution function (BRDF) (Qi et al., 2000). Due to the number of parameters required to specify the BRDF, the inversion of the physical models with the current high resolution satellite sensors is still not possible. Simplified methods for the estimation of the canopy characteristics from satellite remote sensing images is made possible through introduction of some assumptions (D'Urso, 2001). In many applications, the canopy is assumed to behave as a Lambertian surface, meaning that the canopy reflectance is taken to be constant with the angle of observation (Qu et al., 2015). The surface albedo which is obtained from the solar spectral integration of hemispherical reflectance is expressed as:

$$r = \int_{300}^{2500} \frac{\left[\int_0^{2\pi}\int_0^{\pi/2} K^{\uparrow}(\vartheta,\varphi,\lambda)\cos\vartheta\sin\vartheta\,d\vartheta\,d\varphi\right]}{K^{\downarrow}(\lambda)} d\lambda \qquad (6.7)$$

Where $K^{\downarrow}$ is the reflected solar radiance ($Wm^{-2}sr^{-1}$), λ(μm) is the wave length, ϑ being the zenith angle and φ being the azimuthal angle. As demonstrated by Tasumi et al. (2008), the albedo calculation for specifically Landsat satellite images requires the following steps:

- Calculation of at-satellite bidirectional reflectance from at-satellite radiance values assuming the absence of an atmosphere
- Calculation of at-surface reflectance from at-satellite BD reflectance values (i.e., application of atmospheric correction). The calculated at-surface reflectance is not entirely, but is predominately, BD reflectance, since it is calculated using information measured by the satellite sensor, which is a "directional" sensor. Whereas, at-surface solar radiation is a mixture of beam (i.e., directional) and diffuse (i.e., hemispherical) components, where the directional component is predominant under clear sky conditions
- Estimation of broadband surface albedo by integrating the at-surface band reflectance

Smith et al. (2015) has shown that the importance of the errors associated by the Lambertian assumption when applied to Landsat sensors can be greatly reduced, if suitable restrictions are imposed on the range of incidence and reflectance angles. In this case, any dependence of $K^{\uparrow}$ on the view angles (ϑ and φ) can be neglected when estimating *r* from Landsat sensors.

6.4.2 Estimation of surface albedo from Landsat 5TM and 7ETM+

The method for estimation of surface albedo from Landsat 5TM and Landsat 7ETM+, as elaborated by D'Urso (2001), is usually applied. Whereby the spectral integration is approximated in discrete form as expressed by the following relationship:

$$\alpha = \pi \int_{0}^{\infty} \frac{K^{\uparrow}(\lambda)}{K^{\downarrow}(\lambda)} d\lambda \approx \pi \sum_{\lambda 1}^{\lambda n} \frac{K_{\lambda}^{\uparrow}\left(d^{0}\right)^{2}}{E_{\lambda}^{0} \cos \vartheta^{0}} \qquad (6.8)$$

Where $K^{\uparrow}$(Wm^{-2}) is the reflected spectral radiance and E_{λ}^{0}(Wm^{-2}) is the extraterrestrial solar radiation, λ_i, ϑ^0 and d^0 are the wavelength, the solar zenith angle and sun-earth distance in astronomical units respectively. The $K^{\uparrow}$(Wm^{-2}) and the E_{λ}^{0}(Wm^{-2}) are integrated values over the width of each spectral band λ_i. When using Landsat 5 TM and Landsat 7 ETM+, the planetary albedo is calculated as:

$$\alpha_p = \sum\nolimits_{\lambda} w_{\lambda} \rho_{\lambda} \qquad \lambda = (wave\ lengths\ for\ bands: 1,2,\ldots,5,7) \qquad (6.9)$$

Where the weighting factors w_λ are given by:

$$w_\lambda = \frac{E_\lambda^0}{\sum_\lambda E_\lambda^0} \quad (6.10)$$

6.4.3 Estimation of surface albedo from Landsat 8 OLI

Operational algorithms for the computation of Landsat 8 OLI broadband albedo has not yet been developed (Ke et al.,2016). Unlike its predecessors, Landsat TM and ETM+ sensors, the Landsat 8 OLI has two additional spectral bands; namely: the deep blue band (0.43 – 0.54 μm) and a shortwave infrared band (1.36 – 1.39μm). The reflective bands of Landsat 8 OLI corresponding to the Landsat ETM+ bands have narrower wave band widths. This means that the algorithms that were developed for the calculation of the broadband albedo for the previous Landsat sensors (TM and ETM+) cannot be directly applied to the Landsat 8 OLI sensors. In this study the albedo calculation procedure developed by Tasumi et al. (2008) was applied as employed by Ke et al. (2016). In this method, the surface broad band albedo is computed by integrating the at-surface reflectance over the shortwave spectrum are shown in Equation (6.11).

Table 6.2 Spectral characteristics of Landsat 5 TM bands.

Landsat 5TM				
Band number	Centre wavelength (μm)	Band-width	E_λ^0 (Wm^{-2})	w_λ (-)
TM-1	485	66	129.16	0.2212
TM-2	560	82	149.98	0.2569
TM-3	660	67	104.32	0.1787
TM-4	830	128	134.02	0.2295
TM-5	1650	217	47.59	0.0815
TM-7	2215	252	18.78	0.0322

$$r = \sum_1^7 r_b \times w_b \quad (6.11)$$

Where α is the broadband albedo, r_b surface reflectance for a given band *b*, and w_b is the weighting coefficient for the individual solar radiation fraction within the spectral range for band *b* calculated according to Tasumi et al. (2008)

$$w_b = \frac{\int_{LO_b}^{UP_b} R_{s\lambda} d\lambda}{\int_{0.3}^{4} R_{s\lambda} d\lambda} \quad (6.12)$$

Where $R_{s\lambda}$ is at surface hemispherical solar radiation for wave length λ(μm), UP_b and LO_b are upper and lower wave length bounds respectively for a given Landsat 8 OLI band b. Table 6.4 gives the weights for the corresponding bands for both Landsat 8 OLI and Landsat 7 ETM+ sensors calculated using SMART2 radiative transfer model. The weighting coefficients are calculated according to Tasumi et al. (2008) as applied by Ke et al. (2016) using the SMARTS radiatiative transfer model which is freely available (Gueymard, 2006). Table 6.3 Spectral characteristics of Landsat 8 OLI and Landsat 7 ETM+.

Table 6.3 Spectral characteristics of Landsat 8 OLI and Landsat 7 ETM+

Landsat 8 OLI			Landsat 7 ETM+		
Band number	Band Limits (μm)	UP_b - LO_b	Band number	Band Limits (μm)	UP_b - LO_b
1	0.43 – 0.45	0.300 – 0.450	1	0.45– 0.52	0.300 – 0.520
2	0.45 – 0.51	0.450 – 0.520	2	0.52 – 0.60	0.520 – 0.615
3	0.53 – 0.59	0.520 – 0.615	3	0.63 – 0.69	0.615 – 0.725
4	0.64 – 0.67	0.615 – 0.760	4	0.77 – 0.90	0.725 – 1.225
5	0.85 – 0.88	0.760 – 1.225	5	1.55 – 1.75	1.225 – 1.915
6	1.57 – 1.65	1.225 – 1.880	6	10.40 – 12.50	Thermal
7	2.11 – 2.29	1.880 – 4.000	7	2.09 – 2.35	1.915 – 4.000

Table 6.4 Weighting coefficients based on at surface solar radiation derived from SMARTS model (Ke et al. 2016)

sensor	Band Number							Total
	1	2	3	4	5	6	7	
Landsat 8 OLI	0.130	0.155	0.143	0.180	0.281	0.108	0.041	1
Landsat 7 ETM+	0.254	0.149	0.147	0.311	0.103	–	0.036	1

6.4.4 Estimation of Leaf Area Index

The *LAI* is a biophysical variable that is required for input into hydrological models, crop growth models and soil-vegetation-transfer (SVAT) models. This is because LAI affects the rate of photosynthesis and transpiration by plants (Ishihara and Hiura 2011). Leaf area index is defined as one half of the total leaf area per unit ground area (Xiaohua et al., 2013). There are a number of methods for the estimation of LAI that have been developed over the years (Su et al., 2015). These include the direct and the indirect methods. The direct method are usually destructive methods that require harvesting of the leaves and physically measuring leaf dimensions and computing the leaf areas. the direct method has the disadvantage of being destructive and time consuming. For this reason, a number of indirect methods have been

developed. One of these method is the remote sensing method that include photogrammetry and satellite remote sensing. Vegetation indices are related to LAI as follows:

$$VI = VI_{\infty} - (VI_{\infty} - VI_s)e^{-\beta' LAI} \quad (6.13)$$

Equation (6.13) describes the variation of absorption and reflection in a canopy partially covering the soil. The parameter VI_s depends on the soil reflectance and corresponds to the value of the vegetation index for bare soil, while VI_{∞} corresponds to full cover. The parameter β is an extinction coefficient corresponding to the increase of *VI* for a unit increase of *LAI*. The simplified model CLAIR is based on the weighted difference vegetation index (*WDVI*) defined as follows:

$$WDVI = \rho - \rho \frac{\rho_{si}}{\rho_{sr}} \quad (6.14)$$

Where ρ_r and ρ_i indicates the reflectance of observed canopy in the red and infrared bands respectively, while ρ_{si} and ρ_{sr} are the corresponding values for bare soil conditions. The *LAI* is related to *WDVI* of the observed surface through the expression:

$$LAI = -\frac{1}{\alpha^*} \ln\left(1 - \frac{WDVI}{WDVI_{\infty}}\right) \quad (6.15)$$

In the equation (6.15), α^* is an extinction coefficient similar to β' usually determined from the simultaneous measurements of *LAI* and *WDVI*; $WDVI_{\infty}$ is the asymptotic value of *WDVI* for $LAI \to \infty$

6.4.5 Estimation of Canopy Aerodynamic Property

The aerodynamic properties of uniform vegetation canopies are strictly linked to crop height h_c and the LAI. Estimation of canopy heights through remote sensing applications is associated with a number of difficulties. According to D'Urso (2001), a preliminary sensitivity analysis associated with changes in the evapotranspiration calculations resulting from minute changes in h_c based on actual meteorological data of the study area be carried out. Such sensitivity analysis is important because it provides the precision required for the estimation of h_c corresponding to a predefined model performance accuracy. Considering the limitation of estimation of h_c, usually the mean crop height is associated with each land use class derived from the satellite data. This may provide satisfactory compromise in situations where the roughness length is of minor importance in the calculation of evapotranspiration (D'Urso, 2001).

6.5 Conclusion

In this chapter, theoretical background governing water movement in the SPAC was presented (Section 6.2, Equations 6.1 – 6.6). Brief descriptions of a 1-dimensional water flow model; i.e. Hydrus 1D, as applied for agro-hydrological simulations were provided (Section 6.3). The descriptions covered: specification of the initial and boundary conditions and preparation of soil and meteorological data input for calibration of soil hydraulic parameters through model inversion.

Calibration of Hydrus 1D also requires for input crop development parameters such as albedo and LAI. Therefore a brief theoretical background governing application of satellite remote sensing images for estimation of vegetation canopy variables was covered (Sub-section 6.4). The approaches applied for the estimation of the canopy variables are described (Sub-sections 6.4.1 – 6.4.4). Finally, the actual calculation steps for the estimation of each of the crop development parameters ; namely: Surface albedo (r) and LAI were presented.

From the reviewed literatures, derivation of r from satellite remote sensing images require a multitude of functions to define the BRDF. The inversion of the BRDF from such large number of models are not currently possible with single angle viewing satellite sensors. As such simplification is introduced through the Lambertian assumption of the canopy surfaces. This allows r to be estimated from simplified algebraic equations by considering reflectance in each satellite band with the associated band weights. Equations (6.8 – 6.10) can be applied for Landsat 5TM and Landsat 7 ETM+ images. However, for the purpose of this study, Landsat 8 OLI images were acquired, therefore, Equations (6.11 and 6.12) were applied for the actual calculation of r and derivation of band specific weights respectively. Calculation steps for estimation of LAI based on satellite remote sensing as implemented in this study are achieved through the model CLAIR: Equations (6.13) – (6.15). Finally, it was shown that currently, remote sensing based method for the estimation of crop heights *(h_c)* in a developing country such as Uganda, cannot be practically implemented.

7 CASE STUDY FOR THE AGRO-HYDROLOGICAL MODEL CALIBRATION AT THE STUDY SITE IN NORTHERN UGANDA

Summary

Derivation of drought indices for agricultural drought monitoring are best achieved through long term records of measured soil moisture time series that can only be obtained through dedicated soil moisture monitoring programs. However, reliable soil moisture monitoring programs presently are lacking in most developing countries. This challenge can be overcome through agro-hydrological simulation of soil moisture time series, taking into consideration the effects of crop growth on the simulation outputs. This chapter presents the methodology and the results of a case study conducted in a small agricultural farm of 10ha in Northern Uganda, to calibrate and validate an agro-hydrological model, Hydrus 1D. The calibration was achieved through an inversion module in Hydrus 1D that utilizes *Marquardt-Levenberg* parameter optimization algorithm. Sensitivity analyses of the van Genuchten parameters (vGPs) were first conducted to determine the set parameters that needed the most attention during calibration process. Crop growth parameters were estimated through analysis of Landsat 8 OLI images. Soil moisture and matric potential data for numerical inversion of agro-hydrological model were obtained through installation of soil sensors equipped with data loggers between February and March, 2015. However, only the soil moisture data were used, matric potential data were only applied to specify the initial condition at the start of the simulation. Meteorological data were obtained from an automatic weather station installed at the experimental site in early April 2015.

The results of the sensitivity analyses showed that model outputs were most sensitive to α and n compared to the rest of the vGPs; with the model outputs being more sensitive to n by two orders of magnitude than to α. Calibration results showed good agreements between model predictions and observations, with coefficients of determination ($r^2 = 0.73$) during calibration and ($r^2 = 0.70$) during validation. A sensitivity analysis of model outputs to changes in LAI, showed that the model is more sensitive to LAI values at the start of the crop growth stages than at the peak and later growth stages. The satellite remote sensing estimated LAI values were more comparable to published values than albedo values that were rather very low. The calibrated soil hydraulic parameters were used for long term simulation of soil moisture time-series for the development of SMDI as presented in chapter 8.

7.1 Introduction

Operational monitoring of short term agricultural droughts requires application of soil moisture based drought indices (Martinez-Fernandez et al., 2016; 2015). Accuracy of such drought indices depends on the availability of reliable records of measured soil moisture time series that can only be obtained through dedicated soil moisture monitoring programs. However, there exists very few deliberate programs for monitoring soil moisture variations presently (Dobriyal et al., 2012; Dorigo et al., 2011). As a result, most relevant information on agricultural droughts especially in developing countries are lacking. Moreover, the need to sustainably increase food production to feed the growing global population requires that more food be produced on limited agricultural land with diminishing fresh water resources (Nijbrock and Andelman, 2016; Godfray et al., 2010). Increased climatic variability and soil exhaustion compounds these challenges by putting constraints on attempts to increase agricultural productivity (Makurira 2010; Jewitt, 2006; Breman et al., 2003). There are therefore urgent needs more than ever before to devise coping strategies to multitudes of challenges facing the agricultural sector, especially in developing countries that rely solely on rain fed farming systems.

Developing coping strategies to deal with agricultural droughts in areas with the least of information on soil and climatic variables such as in Uganda has been the main aim of this research. This chapters presents two objectives; namely: - description of the of methodologies that were applied in a case study in a small agricultural farm in Northern Uganda to calibrate an agro-hydrological simulation model Hydrus 1D. the second objective was to present the calibration and validation results obtained. Calibration of agro-hydrological model is important in areas such as Northern Uganda that lack reliable soil moisture information. Because such calibrated model can be applied with some of the now freely available tools to simulate soil moisture time series thereby replacing the need to expensive soil moisture monitoring programs that are not affordable in many of the developing countries.

Calibration of Hydrus 1D was carried out in Northern Uganda, to enable the model to generate a long-term soil moisture series to develop SMDI. This was achieved through an inversion process that required: soil moisture data for at least two seasons to aid the inversion procedure, specification of the initial and the boundary conditions and derivation of crop development parameters such as LAI and albedo. The soil moisture data was obtained through installation of a frequency domain soil sensors equipped with data loggers for data transmission. The initial measurements of pressure heads provided the initial conditions.

Whereas a 4-year weather data collected within the vicinity of the study site provided weather variables for the calculation of ETo through the FAO56-PM model.

7.2 Case study site, soil moisture content measurements and meteorological data collection

This case study was conducted in a dairy farm of area: 10 ha, where maize, cowpea and alfalfa are grown under rain fed conditions for making silage for cow feeds. The soil water content was monitored with frequency domain reflectometry probes equipped with data loggers (ECH2O sensors and data loggers, EM-50, Decagon Devices Inc. PULLMAN) at four locations in the dairy farm fields. Soil sensor probes were installed at 20 cm, 40 cm and 60cm below the surface within the soil profile at each of the four locations. Figure 7.1 shows a topographic map of the 10ha land area in which the soil sensors were installed. The installation of the soil sensors took place between February 12, 2015 and March 6, 2015. Monitoring of soil moisture content (at the three profile positions), soil moisture matric potential and soil temperature (at 20cm and 60cm) was conducted between April 10, 2015 and May 23, 2016. However, only the soil moisture content measurements were used for model calibration, although monitoring of soil temperature and matric potential were concurrently done during the same period. Consistent Soil moisture content observations were downloaded from each of the data loggers for a period covering two growing seasons for Maize (Zea mays) crops (April 2, 2015 to November 22, 2015).

The manufacturer of the Decagon soil sensors recommends site specific calibration to achieve the highest possible accuracy and especially if the required accuracy is less than 3% (Cobos and Chambers, 2005; Czarnomski et al., 2005; Starr and Paltneau, 2002). In this experiment, calibration of the sensor probes was not possible and therefore not done. However, we assumed that the reported accuracy of 3% can be tolerated within the experimental limitations and for the purposes of this research. Meteorological data were obtained from an automatic weather station installed at dairy farm on 2nd April, 2015. The meteorological data consistency was cross checked using data from another automatic Meteorological station 4km from the dairy farm at Gulu University. This automatic station had been in operation since 2012. The details of both stations are provided in chapter 5. The details of the climatic condition and soil type in the study area are provided in section 2.3 (chapter 2) and section 5.2 of chapter 5.

7.3 Calibration of The Agro-Hydrological Model at The Study Site

The one-dimensional water flow model described in equation (6.2) Chapter 6, according to Richard (1931) is solved numerically in Hydrus 1D by employing Gerlakin finite element method with an implicit scheme for time discretization (Šimůnek et al., 1998). For the solution of Richard's equation, the water retention $\theta(h)$ and the hydraulic conductivity $K(h)$ functions,

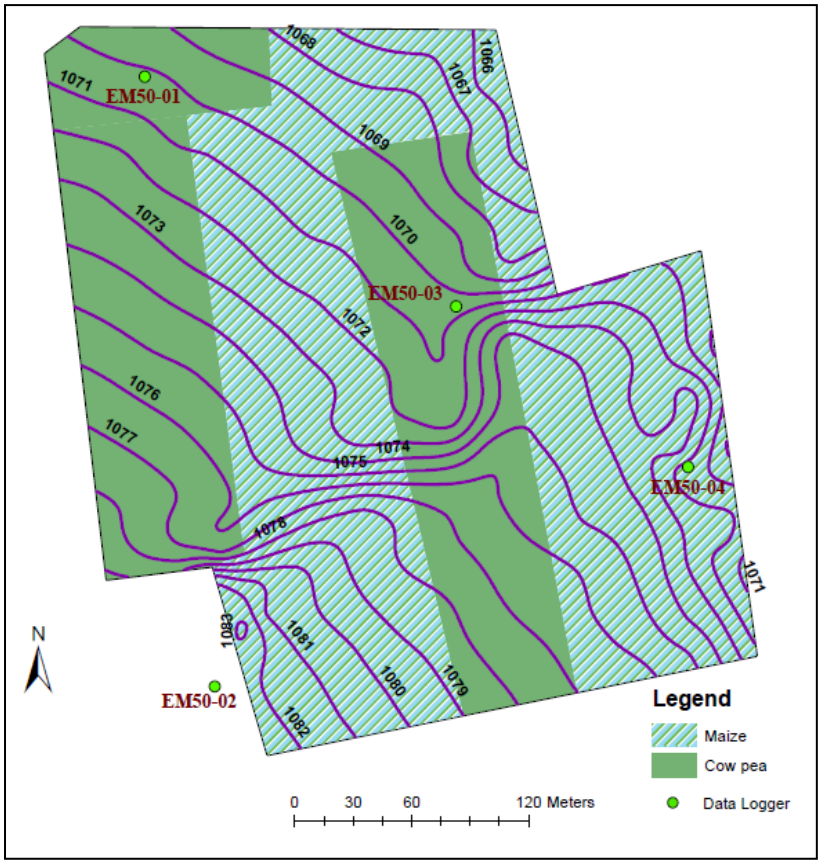

Figure 7.1 Topographic map of the study site showing positions of each of the four data loggers. Data logger EM50-01 malfunctioned, therefore soil sensor data from that location was not included for model calibration.

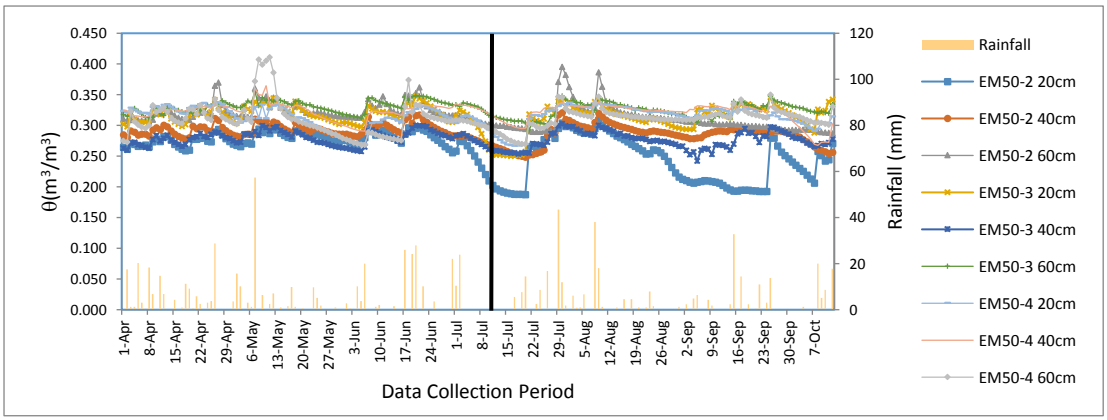

Figure 7.2. Time series of Soil moisture measurements using theta probes at three locations in the dairy farm. Locations of each of the data loggers is shown in Figure 7.1. Daily rainfall totals during the soil moisture measurement period is plotted on the same graphs

must be defined. In Hydrus 1D; *θ(h)* and *K(h)* are defined by the Van Genuchten-Mualem models, Table 6.1 (chapter 6), and equations (6.4) to (6.6). A one-dimensional vertical domain of 80-cm length was defined. The length of the domain was so determined to cover the soil rooting depth. Equal element size of 0.8 cm throughout the domain depth comprising of 101 nodes was specified. Three observation points corresponding to the three soil sensors were specified at 20cm, 40cm and 60cm within the soil profile. Because use was made of van Genuchten-Mualem model and soil properties being considered homogeneous, the hydraulic parameters were expressed with a parameter vector of six elements, i.e., $p = (K_s, \theta_s, \theta_r, \alpha, n, \lambda)$ from Equations: (6.4) and (6.5). The simulation runs in inverse mode covered a time period of 85 days beginning from April 15, 2015 running to July 1, 2015. Although actual trial simulation runs began much earlier on March 25, 2015, but those data points were not considered in the calibration results (Sub-Section 7.5.2). It is recommended that after a long dry period before rain, numerical simulation should start at least 30 days after installation of the soil sensors in to the soil profile (Seki et al., 2015). This serves to allow the sensors to equilibrate with the soil system, especially in this particular case where water from outside was used to facilitate digging of the hole for installing the sensors. The time variable *t* (T) was defined as t = 0 at mid-night of April 15, 2015. Soil moisture observations for the 85-day for each data logger positions shown in Figure 7.1, were used as input data for the inversion process.

7.3.1 The Initial and the Boundary Conditions

Simulation of moisture movement into the unsaturated soil profile requires specification of the initial and the boundary conditions as briefly explained in chapter 6, section 6.3. According to Šimůnek et al. (2009), the initial conditions are described by the initial pressure heads at the start of the simulation period given by Equation 7.1.

$$h(z,t) = h_i(t_0) \qquad (7.1)$$

Where h_i *(L)* is the prescribed function of *z* and t_0 is the time when simulation begins. One of the boundary conditions must be specified at the soil surface, *z = L* or at the bottom of the soil profile (z = 0)

$$
\begin{aligned}
&h(z,t) = h_0(t) && at\ z = 0\ or\ z = L \\
&-K\left(\frac{\partial h}{\partial z} + 1\right) = q_0(t) && at\ z = 0\ or\ z = L \\
&\frac{\partial h}{\partial z} = 0 && at\ z = 0
\end{aligned}
\qquad (7.2)
$$

Where $h_0(L)$ and $q_0(TL^{-1})$ are the prescribed values of the pressure heads and soil water flux at the boundary respectively. Equation (7.2) is what is referred to as the system independent boundary condition (Šimůnek et al., 2009). Whereas systems dependent boundary conditions can also be considered which involves the soil air interface exposed to the atmosphere. The potential fluid flux at this soil-atmosphere interface is controlled by both the external conditions such as evapotranspiration and infiltration through precipitation process and the prevailing transient soil moisture condition near the soil surface (Šimůnek et al., 2009). In such as circumstance the numerical solution is governed by the two conditions following Neuman et al. (1974)

$$
\begin{aligned}
&\left|-K\frac{\partial h}{\partial z} - K\right| \le \mathrm{E} && \text{at z = L (a)} \\
&\text{and} \\
&h_A \le h \le h_S && \text{at z = } L \quad \text{(b)}
\end{aligned}
\qquad (7.3)
$$

Where E is the maximum potential rate of infiltration or evaporation under the current atmospheric condition (LT^{-1}), h_A and h_S are the maximum pressure head and minimum pressure head respectively at the soil surface allowed under the prevailing soil conditions *(L)*. The system dependent boundary condition defined by Equation 7.3 is what was specified in this study.

In this case study, dry planting of maize and alfalfa had been done between February 25, 2015 and March 3, 2015. There were no rains for the previous two months and the soil was very dry as is always the case in the study area during this period. Therefore, digging the holes through the soil profile was facilitated by pouring water and allowing the water to drain through the hardened soil overnight, as this was a dry period. The last soil sensor was installed on March 6, 2015 and datasets for the inversion was considered from April 15, 2015 in order to allow the effects of the water used to facilitate digging the hole to equilibrate. This is a period of more than one month and it is considered that after such a period the soil sensors were recording the actual moisture dynamics in the soil resulting from prevailing soil conditions. The first sign of

a rain shower was registered on April 2, 2015, the day the automatic weather station was installed. And intermittent precipitation continued up to the time simulations and collection of soil moisture data for the inversion started.

The initial boundary conditions were specified by the pressure head readings on the start of the simulation period. The pressure heads sensors were installed only at two profile positions i.e. at 20 cm and at 60 cm below the soil surface. Therefore, the vertical distribution of the pressure head into the soil profile at the start of the simulation process was interpolated using the two recorded values of the pressure heads. The upper boundary condition for the entire calibration period was specified by values of precipitation registered during the simulation period and Evapotranspiration calculated through the Penman-Monteith module in Hydrus 1D. For the calculation of evapotranspiration; daily average values of solar radiation (Rs), wind speed (U), relative humidity (RH), minimum and maximum temperature records were prepared and added as meteorological data input into Hydrus 1D, covering the entire simulation period.

Crop growth parameters such as the LAI, and albedo (r) were obtained through analysis of remote sensing images obtained during the simulation periods. Details of the procedures for the estimation of the LAI and *r* are covered in chapter 6, section 6.4. Crop heights (h_c) were obtained by sampling maize crops in the entire field and computing the average height for each measurement day. This was done after every three weeks had elapsed, and the values were interpolated throughout the simulation process. Root development was not monitored, and root growth process was estimated from Hydrus root development module. This was done by specifying 50% of root growth in mid-season (Hoffman and van Genuchten,1983). The lower boundary condition was considered as free drainage since water table in the area is deeper than 15m according to information obtained from a contractor who drilled a nearby well in 2012.

7.3.2 Estimation of the Soil Hydraulic Parameters through Inverse Simulation

According to Šimůnek et al. (1998), the objective function Φ to be minimized during the parameter estimation process may be defined as follows:

$$\Phi(b,q,p)=\sum_{j-1}^{m_q} v_j \sum_{i-1}^{n_{qj}} w_{i,j}\left[q^*{}_j(x,t_i)-q_j(x,t_i,b)\right]^2 + \sum_{j-1}^{m_p} \overline{v}_j \sum_{i-1}^{n_{pj}} \overline{w}_{i,j}\left[p^*{}_j(\theta_i)-p_j(\theta_i,b)\right]^2 + \sum_{j-1}^{n_b} \hat{v}_j\left[b^*{}_j-b_j\right]^2 \quad (7.4)$$

where the first term on the right-hand side represents deviations between measured and calculated space-time variables, such as pressure heads, water contents in the flow domain, or

actual/cumulative moisture fluxes versus time across a certain boundary for the case of the soil moisture inverse simulation. Various options for defining the first term of Equation (7.4) for the different equilibrium and nonequilibrium water flow and solute transport models are listed in (Šimůnek et al., 1998). In the first term of Equation (7.4), m_q is the number of different sets of measurements, $n_{q\,j}$ is the number of measurements in a particular measurement set, $q^*{}_j(x,t_i)$ represents specific measurements at time t_i for the j^{th} measurement set at location *x(r,z)* and $q_j(x,t_i\ ,b)$ are the corresponding model predictions for the vector of optimized parameters $p = b(K_s\,,\theta_s\,,\theta_r\,,\alpha,n,\lambda)$ and v_j and $w_{i,j}$ are weights associated with a particular measurement set or points, respectively. The second term of Equation (7.4) represents differences between independently measured and predicted soil hydraulic properties (e.g., retention, $\theta(h)$ and/or hydraulic conductivity, $K(\theta)$ or $K(h)$ data), while the terms m_q, $n_{q\,j}$, $p^*{}_j(\theta_i) - p_j(\theta_i,b)$, v_j and , $\overline{w}_{ij}$ have similar meanings as for the first term but now for the soil hydraulic properties. The last term of (7.4) represents a penalty function for deviations between prior knowledge of the soil hydraulic parameters, b_j^*, and their final estimates, b_j, with n_b being the number of parameters with prior knowledge and $\mathbf{j_v}$ representing pre-assigned weights. Estimates, which make use of prior information (such as those used in the third term of Equation (7.4)) are known as Bayesian estimates. The weighting coefficients v_j, which minimize differences in weighting between different data types because of different absolute values and numbers of data involved, are given by (Clausnitzer and Hopmans, 1995):

$$vj = \frac{1}{n_j \sigma_j{}^2} \qquad (7.5)$$

which causes the objective function to become the average weighted squared deviation normalized by the measurement variances σ_j^2.

7.3.3 Marquardt-Levenberg Optimization Algorithm

Minimization of the objective function Φ is accomplished by using the Levenberg-Marquardt nonlinear minimization method (a weighted least-squares approach based on Marquardt's maximum neighborhood method) (Marquardt, 1963). This method combines the Newton and steepest descend methods, and generates confidence intervals for the optimized parameters. The method was found to be very effective and has become a standard in nonlinear least-squares fitting among soil scientists and hydrologists (Seki et al. 2015; Kool et al., 1985; van Genuchten, 1981).

7.3.4 Statistics of the Inverse Solution

As part of the inverse solution, Hydrus 1D produces a correlation matrix, which specifies degree of correlation between the fitted coefficients. The correlation matrix quantifies changes in model predictions caused by small changes in the final estimate of a particular parameter, relative to similar changes as a result of changes in the other parameters. The correlation matrix reflects the nonorthogonality between two parameter values. A value of ±1 suggests a perfect linear correlation whereas 0 indicates no correlation at all. The correlation matrix may be used to select which parameters, if any, are best kept constant in the parameter estimation process because of high correlation. An important measure of the goodness of fit is through the coefficient of determination (r^2) defined in equation (5.3). The r^2 value is a measure of the relative magnitude of the total sum of squares associated with the fitted equation; a value of 1 indicates a perfect correlation between the fitted and observed values. Whereas a value of 0 shows no correlation between the fitted and observed values.

Hydrus provides additional statistical information about the fitted parameters such as the mean, standard error, T-value, and the lower and upper confidence limits (given in output file FIT.OUT). The standard error, $s(b_j)$, is estimated from knowledge of the objective function, the number of observations, the number of unknown parameters to be fitted, and an inverse matrix (Daniel and Wood, 1971). The T-value is obtained from the mean and standard error using the equation (7.6).

$$T = \frac{b_j}{s(b_j)} \qquad (7.6)$$

The values for T and $s(b_j)$ provide absolute and relative measures of the deviations around the mean. Hydrus 1D also specifies the upper and lower bounds of the 95% confidence level around each fitted parameter b_j. It is desirable that the real value of the target parameter always be located in a narrow interval around the estimated mean as obtained with the optimization program. Large confidence limits indicate that the results are not very sensitive to the value of a particular parameter. There are sometimes problems related to convergence and parameter uniqueness. In such circumstances, Šimůnek et al. (2009) recommends to routinely rerun the program with different initial parameter estimates to verify that the program indeed converges to the same global minimum in the objective function. This is especially important for field data sets, which often exhibit considerable scatter in the measurements, or may cover only a narrow range of soil water contents, pressure heads, and/or concentrations.

7.4 Derivation of the crop development parameters in the study area

Agro-hydrological simulations require for input, the crop development parameters such as the leaf area index *(LAI),* albedo *(r)* and crop height *(h_c).* These crop parameters are required input to estimate the roughness length *(r_h)* in the Penman Monteith equation, for the calculation of crop evapotranspiration ET_c (Allen, 1998). There are methods for estimation of these parameters during the crop phenological development. However, many of the methods require sophisticated equipment and especially field based estimation of LAI rely on destructive methods that are best carried out in dedicated experimental plots. In this research, the PM based method of FAO-56 was applied as implemented in Hydrus 1D for the calibration of model parameters. This required estimation of: *LAI*, *r* and h_c; during the inversion process in the first season from April 15th to July, 2nd, 2015. The crop development parameters were also applied in the direct mode implementation of Hydrus 1D simulation during the validation period from July 28th to October 10th, 2015. In this section description of the procedures applied to derive LAI and albedo from Landsat 8 OLI satellite images during the model calibration and validation between March and October 2015 at the study site are presented.

7.4.1 Steps for The Derivation of Albedo and LAI from Landsat 8 OLI Images as Implemented in The Study Site

The albedo *(r)* and the *LAI* for the study area were estimated based on the steps presented in chapter 7. It is usually recommended that cloud free images be processed for the derivation of the crop development parameters such as *r* and *LAI* by applying appropriate atmospheric correction algorithms (Mattar et al., 2014) and (Tasumi et al.,2008). The advantages with Landsat 8 OLI, level 1 satellite products obtained from USGS archives (https://earthexplorer.usgs.gov), are already atmospherically and geometrically corrected, besides being radiometrically calibrated for direct application. The derivation of albedo at the study site involved the following steps:

- Calculation of the reflectance (r_b) for each band of the Landsat 8OLI satellite image based on scaling parameters provided for each band in the image metadata to convert the pixel digital numbers(DN) to actual surface reflectance
- Computation of the weighting coefficients for each band according to equation (6.10), chapter 6. For this study, the band specific weights provided in Table 6.3 computed by SMARTS2 radiative transfer model was used (Gueymard, 2006).
- Calculation of the surface albedo by applying equation (6.9), chapter 6

Whereas LAI is calculated by application of equations (6.13) to (6.15) according to the following steps:

- Generation of the soil line graphs to derive the slope of the regression line between ρ_{nir} and ρ_r for application into equation (6.14). This is done by application of NDVI map generated by Equation (3.6), chapter 3. The regions within the image having values of NDVI > 0.2 were considered bare soil and DN values of these images for bands 4 and 5 are corresponding to ρ_r and ρ_{nir} reflectances, used to plot the soil line graphs
- Application of Equation 6.15 to generate the WDVI maps.
- Analysis of the frequency distribution values of the albedo and the WVDI maps to estimate the values of α^* and $WDVI_\infty$. According to these frequency distributions of the pixel values of albedo and WDVI for the cloud free images analyzed, the values were $\alpha^* = 0.42$ and $WDVI_\infty = 0.45$, so that the equation (6.15) becomes:

$$LAI = -\frac{1}{0.42}\ln\left(1-\frac{WDVI}{0.45}\right) \qquad (7.7)$$

Equation (7.7) was used to generate the LAI map for each analyzed Landsat 8 OLI image. The values of the crop heights h_c were measured from the field as yet there are no operational methods based on satellite remote sensing for field based estimation of crop heights that can be implemented with confidence in a location such as the study area (D'Urso, 2001).

7.4.2 Sensitivity of Agro-hydrological simulation outputs to crop development parameters

Crops in the study area are grown during the rainy seasons beginning from end of March to end of October of each year. This is one of the cloudiest period in Northern Uganda, therefore only three relatively cloud free Landsat 8 OLI images that were acquired on March 6th, April 23rd and June 10th, 2015 were used to estimate the *r* and *LAI* for the first season. Whereas images acquired on July 12th, August 13th, September 14th and September 30th were applied for *r* and *LAI* derivation in the second season. The second season images were rather cloudy, so that the values of the *LAI* estimated from them contained some uncertainties. Besides, there was no independent verification method for the values of *r* and *LAI* estimated. Because of these difficulties, sensitivity analysis was carried out specially to assess the model sensitivity to perturbations in *LAI* values. This was done by assessing the changes in Evapotranspiration calculated by Hydrus 1D caused by small changes in values of *r* and *LAI*. A sensitivity in some dependent variables ξ due to generic parameters $P_i(i = 1,2,3...)$ can be estimated according to Mattar et al. (2014)

$$\xi = \frac{\partial P_i}{\partial O_i} \qquad (7.8)$$

Where ξ indicates the model sensitivity and ∂P_i indicates changes in model parameter such as LAI and finally, $\partial O_i (i = 1,2,3...)$ indicates changes in model output such as evapotranspiration calculated by Hydrus 1D in our case.

7.5 Results and discussions of the Calibration process undertaken in the case study

In this sub-section, the results of all the procedures that were undertaken to facilitate calibration of Hydrus 1D are presented. The results presented here include:

- results obtained from the satellite remote sensing based derivation of the crop development parameters such as the albedo *(r)* and *LAI* for the study area
- results obtained from laboratory analyses of disturbed and undisturbed soil samples that were brought in Italy in February 2015 and done from the soil hydrological laboratory of the department of Agriculture University of Naples
- results of the calibration process which include: preliminary sensitivity analyses of change in simulation outputs due to perturbations in each of the soil hydraulic parameters; range of values of the calibrated soil hydraulic parameters; comparison between simulated soil water storage and observations obtained from the data loggers during both the calibration and validation periods.

7.5.1 Results and Discussions of The Remote Sensing Based Derivation of The Crop Development Parameters

The results obtained from satellite remote sensing based derivation of crop development parameters include: Regression plots of the soil line for each image analyzed during the calibration and the validation periods between March and September of 2015. These plots are shown in Figure 7.2 for four of the images. The values of the Pearson's correlation between the bare soil reflectance at near infra-red and the corresponding values for the red bands for each of the analyzed images are shown in Table 7.1. Tabular values of the descriptive statistics of crop development parameters extracted from the *LAI* and albedo *(r)* maps are shown in Table 7.3 and 7.4.

The *LAI* and the albedo maps from which the presented values are shown are instantaneous values for each satellite over pass time. These values are affected by a number of factors such

as horizontal visibility whose values were not obtained; they are also affected by the cloud covers. The values presented are obtained from a number of pixels covering the study site. The albedo values obtained are rather low compared to similar values reported for Maize and cowpea in a comparable agrometeorological condition in Ghana (Oguntunde and Giensen, 2004), Table 7.3 and Figure 7.3. Whereas the *LAI* values are fairly comparable to those reported by the same Authors.

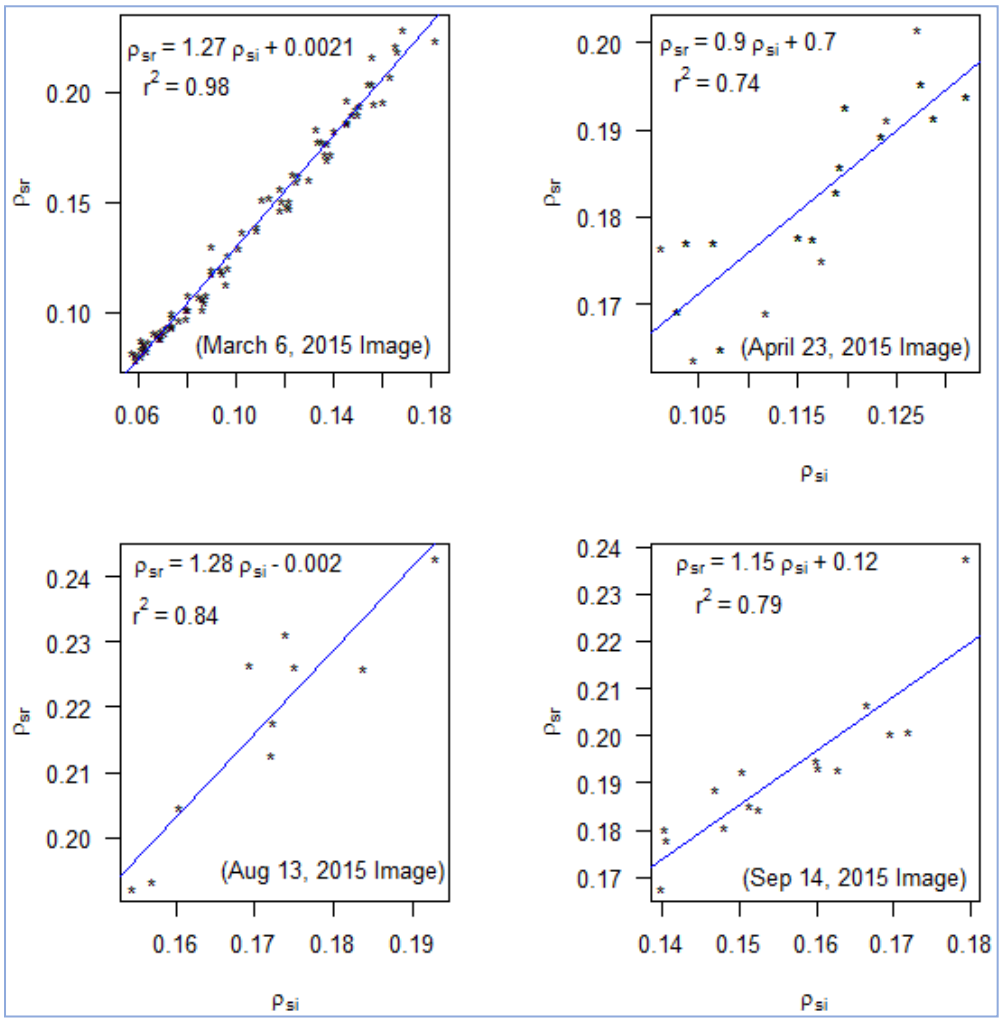

Figure 7.3 The soil line plots for Landsat 8 OLI Images with indicated overpass dates

Table 7.1 Correlation coefficients defining the soil lines

Date	Correlation coefficients
6-Mar	0.99
23-Apr	0.86
10-Jun	0.93
12-Jul	0.91
13-Aug	0.92
14-Sep	0.89
30-Sep	0.97

Table 7.2 Summary of the Landsat Image acquisition for Northern Uganda used to estimate crop growth canopy variables for the Agro-hydrological calibration

Image date	(UTC)	Sun Zenith Angle (degrees)	Sun Azimuth (degrees)
Mar 06,2015	8.06	30.60	106.36
Apr 23,2015	8:06	27.38	80.85
Jun 10, 2015	8:06	32.61	49.71
Jul 12, 2015	8:06	33.23	52.62
Aug 13, 2015	8:06	29.85	64.96
Sep 14, 2015	8:06	25.50	87.96
Sep 30, 2015	8:06	24.66	102.94

Table 7.3 Mean of five r values, LAI and hc for maize and cowpea fields during two planting dates in Ghana 2002. (Oguntunde and Giensen, 2004)

Crop	Phenological stage	Mean α		LAI		CH (m)	
		First planting	Second planting	First planting	Second planting	First planting	Second planting
Maize	Emergence	0.179	0.196	0.48	0.42	0.11	0.09
	Vegetative	0.232	0.242	2.77	2.55	1.00	1.10
	Flowering	0.270	0.254	4.02	3.70	1.81	1.76
	Maturity	0.276	0.256	4.47	4.21	1.82	1.76
Cowpea	Emergence	0.204	0.195	0.57	0.45	0.05	0.05
	Vegetative	0.252	0.242	4.13	3.92	0.51	0.49
	Flowering	0.260	0.261	5.38	5.02	0.63	0.58
	Maturity	0.253	0.245	4.05	4.02	0.71	0.66

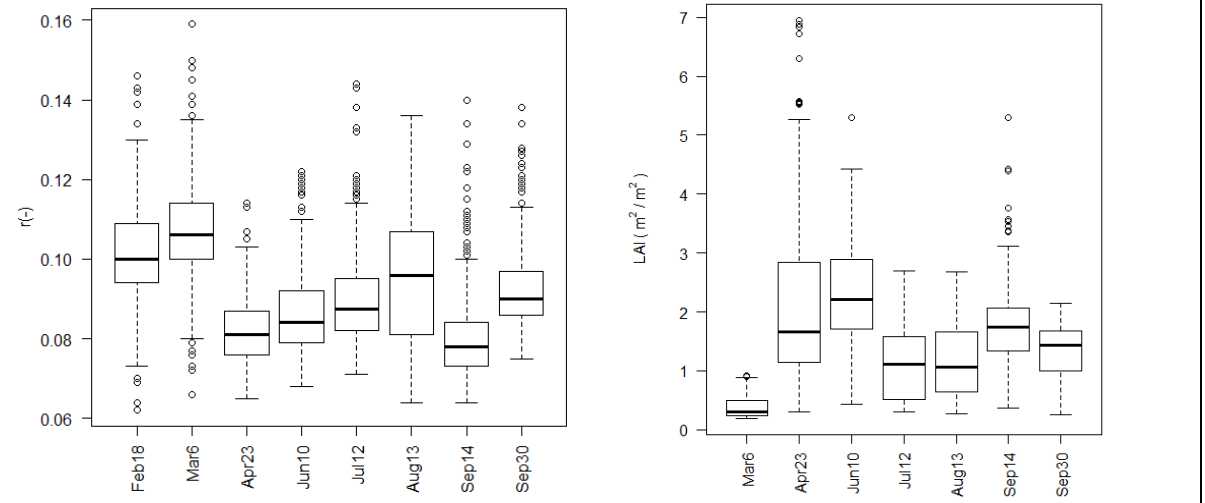

(a) Albedo plots

(b) LAI Box plots

Figure 7.4 Box plots of the derived albedo and LAI values from Landsat 8 satellite images during the following overpass dates: March 6, 2015; April 23, 2015, June 10, 2015, July 12, 2015 and August 13, 2015

Table 7.4 Descriptive statistics of the derived albedo values for the given Landsat 8 OLI overpass dates. Considering pixel values of the Albedo maps over the experimental field

Dates	1stQ	Min	Median	Mean	3rdQ	Max
18-Feb	0.0620	0.0940	0.1000	0.1013	0.1090	0.1460
6-Mar	0.0660	0.1000	0.1060	0.1060	0.1138	0.1590
23-Apr	0.0650	0.0760	0.0810	0.0820	0.0868	0.1140
10-Jun	0.0680	0.0790	0.0840	0.0867	0.0920	0.1220
12-Jul	0.0710	0.0820	0.0875	0.0899	0.0950	0.1440
13-Aug	0.0640	0.0810	0.0960	0.0958	0.1070	0.1360
14-Sep	0.0640	0.0730	0.0780	0.0814	0.0840	0.1400
30-Sep	0.0750	0.0860	0.0900	0.0937	0.0970	0.1380

Table 7.5 Descriptive statistics of the derived LAI values for the given Landsat 8 OLI overpass dates.

Date	Min.	1stQ	Median	Mean	3rdQ	Max.
6-Mar	0.19	0.23	0.30	0.37	0.49	0.91
23-Apr	0.30	1.15	1.67	2.10	2.84	6.95
10-Jun	0.44	1.71	2.21	2.24	2.88	5.30
12-Jul	0.31	0.51	1.12	1.12	1.58	2.70
13-Aug	0.27	0.65	1.07	1.19	1.66	2.68
14-Sep	0.37	1.34	1.74	1.76	2.06	5.30
30-Sep	0.25	1.01	1.43	1.33	1.68	2.15

From the study site, maize emergence date was between 31st March, 2015 and 4th April 2015. Maize in this particular dairy farm are planted with a row spacing of 0.91m and 0.2m between subsequent plants in a single row. Considering the emergence dates, the derived *LAI* values increased with crop growth as shown in Figure 7.3(b), between March 6th and July 12th 2015 and between, July and September 2015 during the second growing season. A similar but a weaker increment can be noticed in the values of the albedo in Figure 7.3(a) and Table 7.4. Similar trends were reported by Oguntunde and Giensen (2004). The lower values of albedo obtained from the albedo map for February 18, 2015 are comparable to values reported for bare lands by (Beg et al., 2016). February is a dry period in Northern Uganda, and most areas are burnt leaving out exposed bare ground, hence the low albedo values. Although there were no independent measurements for albedo and *LAI*, the values obtained here are comparable to reported values in literatures in terms of the increasing trends with crop development.

Because of the uncertainty in the obtained values of the *LAI* and *r*, *LAI* particularly, was subjected to uncertainty analysis. This was achieved by carrying out the sensitivity analysis of the changes in simulated evapotranspiration output due to small perturbations in *LAI* values. Of the crop development parameters usually monitored, LAI has the greatest impact in the

evapotranspiration process (Peng et al., 2015). The crop albedo also depends on *LAI*, for this reason only the sensitivity of *LAI* was carried out for this study.

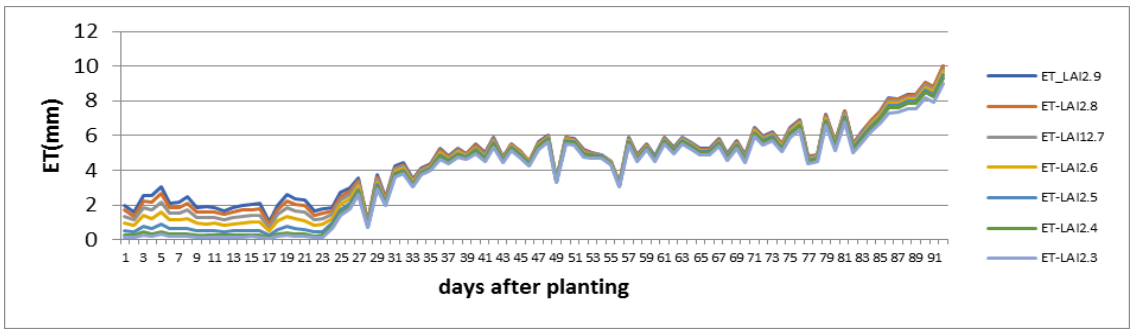

Figure 7.5 Sensitivity of the ET simulation outputs due to a stepwise increase of LAI values by 0.1

Figure 7.4, shows that the changes in values of *LAI* has the greatest impact at the beginning of plant development as at this stage Evapotranspiration is dominated by Soil evaporation. As the plant grows, the model become less sensitive to changes in the values of *LAI*. For instance, a 4% increment in *LAI* at the beginning of the crop development resulted in a 14% increase in the value of evapotranspiration simulated. Whereas a similar increase in the *LAI* value in mid-season resulted in a 9.6% change in the value of evapotranspiration.

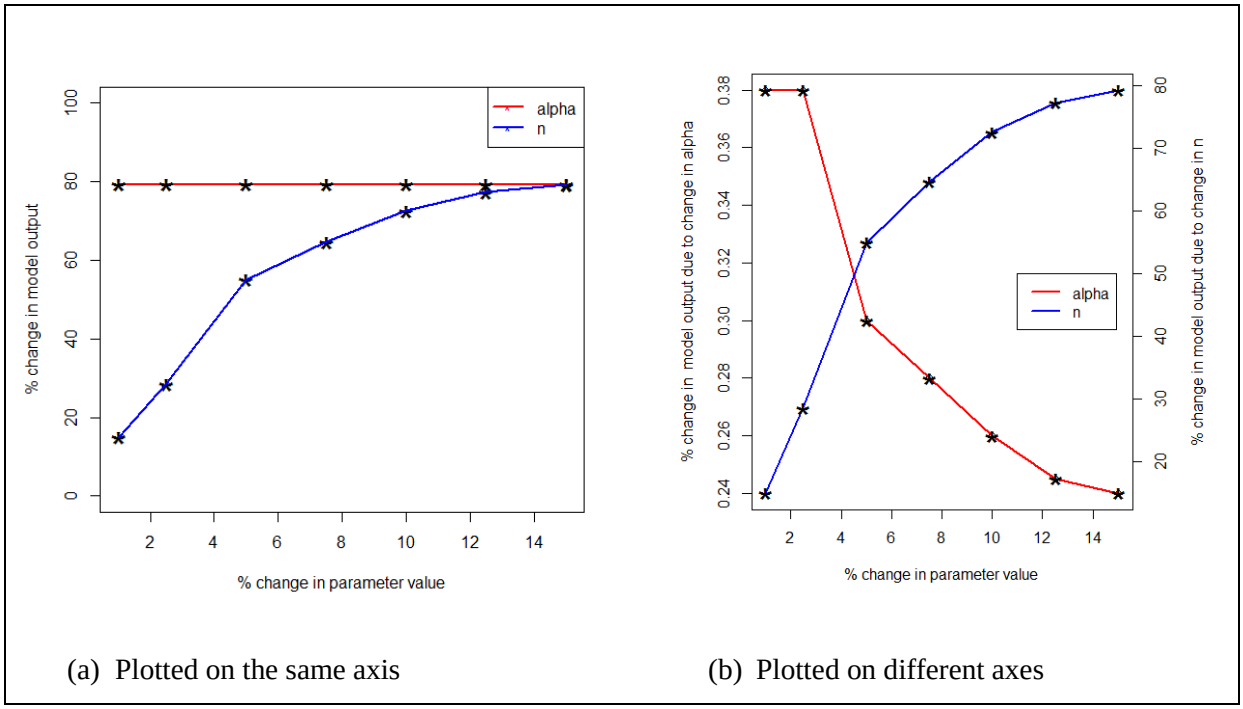

(a) Plotted on the same axis (b) Plotted on different axes

Figure 7.6 Sensitivity of the model simulation outputs due to a stepwise increase in the values of α and n by 2.5%. Preliminary simulation runs performed before the inversion showed that perturbations of the other soil hydraulic parameters (i.e. θ_r, θ_s, K_s, l) did not result in significant changes in simulation outputs as compared to α and n. Therefore, only the sensitivities of α and n were analyzed and plotted on the same graph as shown.

7.5.2 Results and Discussions of The Calibration and validation of Hydrus 1D at the study site

The calibration and the validation accuracy of estimated parameters were assessed through visual inspection of the time series plots of soil moisture storage as compared to those for simulations as shown in Figures 7.6 (a) for the calibration period and Figure 7.6(b) for the validation period. Another assessment procedure was through calculations of coefficients of determination (r^2) between simulations and observations during both calibration and validation periods. Calibration and validation were restricted to the soil sensor installed in the maize fields. This was because of the difficulty encountered in monitoring crop development of cowpeas as they were harvested more frequently and the transition between the previous crop to the next was not clear cut unlike for maize crop.

It can be observed that the calibrated parameters enabled reasonably fair modal prediction of the soil water storage as indicated by the r^2 value of 0.73 during the calibration process within the limitations of the experimentation, Figure 7.7(a). Whereas the validation period resulted in the r^2 value of 0.7 considering the soil water storage between the z = -15cm and z = -65cm, Figure 7.7(b). Soil data for the model inversion were obtained from April 15, 2015 to Jul 1, 2015. And Soil moisture observations applied for the model validation period were those obtained from July 28, 2015 to October 10, 2015.

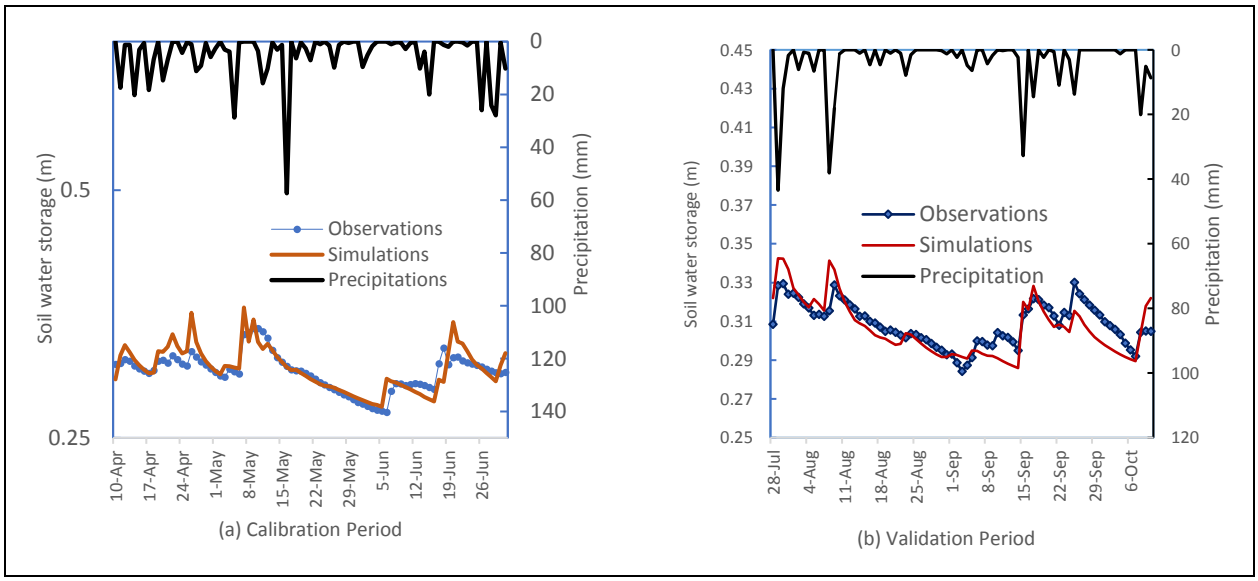

Figure 7.7 Calibration and Validation results showing evolution of Soil moisture storage between the depths of -15cm and -65cm using calibrated soil hydraulic parameters during (a) Calibration and (b) Validation. Figure shown is for a sensor that had been under Maize crop only for both periods.

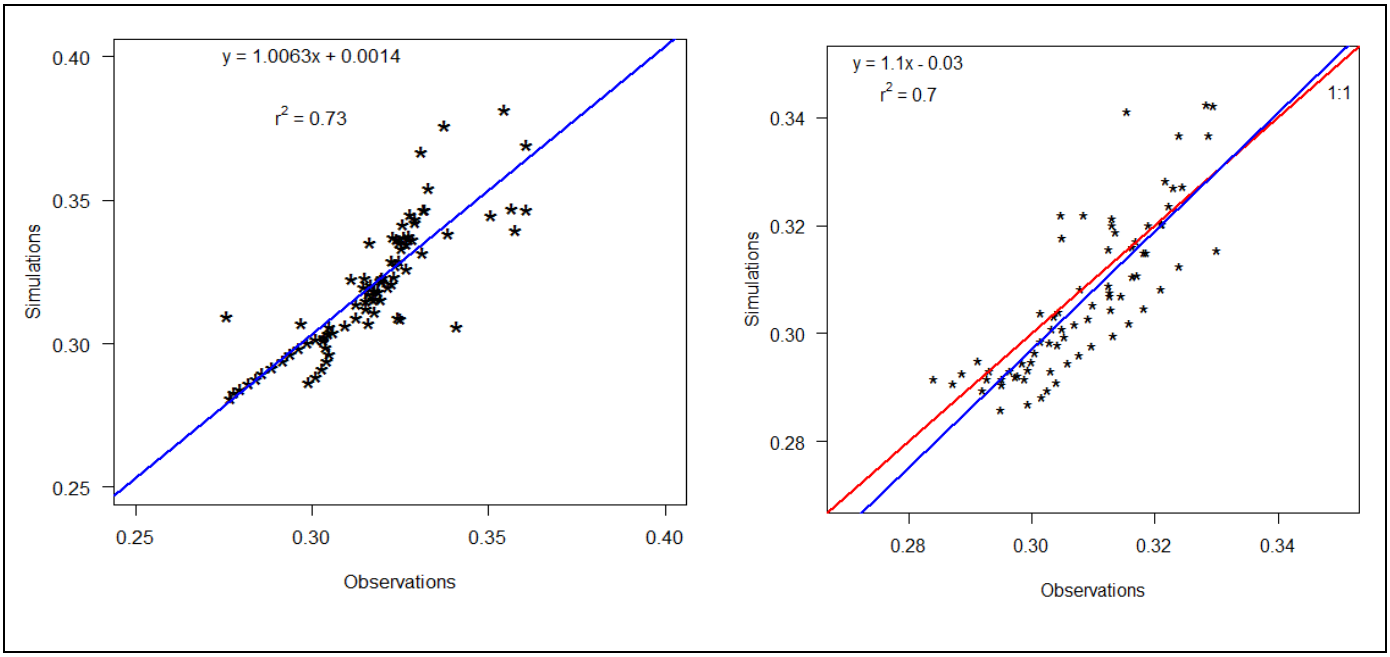

Figure 7.8 Full profile scatter plots of Simulations versus observations during (a) Calibration Period and (b) validation periods showing respective r^2 values and the regression equations

Model calibration was achieved through the inbuilt inversion module within Hydrus 1D. In this inverse parameter estimation process, the Marquardt-Levenberg parameter optimization algorithm is applied. This is a single objective optimization algorithm that has the possibility of being trapped in local minima during the optimization process (Hopman et al., 2002). However, whenever the initial values of the parameter vectors can be estimated, a single objective parameter optimization can be implemented with satisfactory results (Chen et al., 2012). Since crop development parameters were very critical factors for the inversion, only a short simulation period for both model calibration and validation were accessed during which period crop development could be accurately accounted for. Besides, only Maize was considered because of the purpose of the calibration being to generate the parameters for the derivation of SMDI. Since maize yields could be accessed for the validation of SMDI.

The range of values of the calibrated parameters as shown in table 7.6. It is recommended that before the inversion process, a sensitivity of the model parameters to the simulation outputs be analyzed to "know" model parameters that need the most focus during the parameter estimation process. For this reason, sensitivity of each model parameter was analyzed at the beginning of the parameter estimation process. Results of the sensitivity analyses are shown in Figure 7.5 for α and n. Preliminary simulation runs had revealed that perturbations in the values of α and n have the greatest percentage change in model outputs compared to the other

parameter vectors. From the figure, it can be seen that the changes in the values of n are most sensitive to model output than the changes in the values of α. Therefore, during the calibration process, greater calibration efforts were directed to the values of n in each of the soil profile dephs.

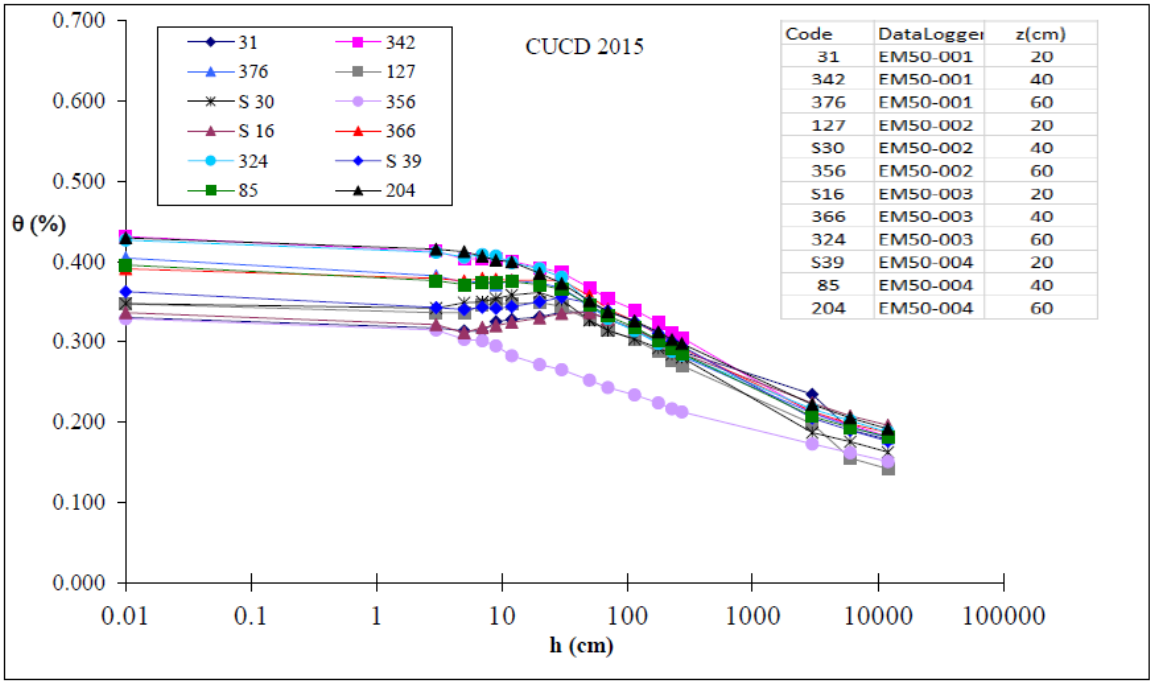

Figure 7.9 Laboratory determined water retention curve for different soil profile positions. Codes for the data loggers and steel samplers are shown including the profile depths corresponding to each steel sampler. Steel soil samples were used to collect undisturbed soil core samples

Table 7.6 Calibrated parameter values for the different soil profiles and sensors

EM50-002	θs	θr	α	n	Ks	l
20cm	0.045	0.31	0.004	1.1	12	0.4
40cm	0.035	0.33	0.003	1.2	120	0.4
60cm	0.054	0.34	0.02	1.12	15	0.4
EM50-003						
20cm	0.0728	0.34	0.0064	1.125	3.8	0.5
40cm	0.0282	0.3	0.015	1.091	15	0.5
60cm	0.075	0.39	0.011	1.229	18.84	0.5
EM50-004						
20cm	0.045	0.37	0.0132	1.055	151	0.4
40cm	0.056	0.33	0.0002	1.2	112	0.4
60cm	0.081	0.4	0.0004	1.35	15	0.4

7.6 Conclusion

In this chapter, a report of the case study for the calibration of the agro-hydrological model, Hydrus 1D was presented. The calibration was conducted through the inbuilt inversion module in Hydrus 1D. Crop development parameters were estimated through analyses of cloud free satellite remote sensing images of Landsat 8 OLI bands. Since there were no independent measurements for the verification of the estimated albedo and LAI values, a sensitvity analysis of particularly LAI was conducted before actual inversion process using Equation (7.8). Likewise, sensitivity analysis of each of the vanGenuchten parameters (vGp) was conducted before calibration to determine which model parameters needed the most attention during calibration based on the same Equation (7.8). Finally, after calibration process, the model simulation outputs were compared to observations through time series plots and calculation of coefficients of determination (r^2) during both calibration and validation periods.

Table 7.7 Laboratory determined Soil Textural characteristics and the van Genuchten hydraulic parameters predicted by the Rosetta PTF as initial estimates for the inversion process

Instrument	Depth (cm)	Sand (%)	Silt(%)	Clay(%)	BD[gm-3]	USDA textural Class	θr (cm3/cm3)	θs (cm^3/cm^3)	α(cm^{-1})	n	Ks [est] (cmh^{-1})	Ks[expt] (cmh^{-1})	Porosity [expt]	θs (cm^3/cm^3) [expt]
EM50-001	20	60	23	17	1.608	Sandy loam	0.0498	0.3636	0.0264	1.3536	15.65	15.13	0.393	0.331
	40	46	18	36	1.491	Sandy clay	0.0803	0.4231	0.0195	1.3021	10.77	0.23	0.437	0.431
	60	45	17	38	1.473	Sandy clay	0.0832	0.4307	0.0198	1.2961	12.08	0.2	0.444	0.405
EM50-002	20	56	21	23	1.644	Sandy clay loam	0.0569	0.3629	0.0243	1.291	8.85	13.29	0.380	0.347
	40	52	20	28	1.588	Sandy clay loam	0.0662	0.3851	0.0209	1.2987	8.66	0.76	0.401	0.348
	60	56	23	21	1.666	Sandy clay loam	0.0529	0.3535	0.0255	1.2904	8.6	45.89	0.371	0.329
EM50-003	20	54	17	29	1.619	Sandy clay loam	0.0656	0.3784	0.0231	1.2634	8.26	0.12	0.389	0.336
	40	47	18	35	1.543	Sandy clay	0.0766	0.407	0.0202	1.2813	8.53	0.2	0.418	0.391
	60	42	17	41	1.386	Clay	0.0899	0.4591	0.0195	1.3137	17.58	0.31	0.477	0.427
EM50-004	20	54	14	32	1.627	Sandy clay loam	0.0685	0.38	0.0244	1.235	8.16	0.83	0.386	0.363
	40	48	19	33	1.568	Sandy clay loam	0.0731	0.3973	0.0202	1.2816	7.71	14.14	0.408	0.396
	60	43	21	37	1.511	Clay loam	0.0802	0.4163	0.0182	1.3123	8.49	0.11	0.430	0.430

The results obtained show that the variation of both the albedo and LAI values esimated show similar variations during crop development when compared to publised values. However, the values of albedo estiamted were rather low compared to punlished values. Whereas the estimated values of LAI were more comparable to published values than the albedo estimates. The results of the senitivity analysis of LAI showed that LAI is more sensitve to the model output at the beginning of the growing season. The LAI sensitivities decrease during the crop development with the lowest sensitivities registered during the peak growing period. Whereas

of the six vG parameters, α and n were found to be more sensitive to the model output compared to the rest of the parameters and therefore more calibration efforts were directed on them. Between the more sensitive parameters (i.e. α and n), n was found to be more sensitive to model output by up to two orders of magnitude compared to α as shown in Figures 7.5(a) and (b).

Comparions between simulations and observations based on calibrated parameters showed good agreement with the coefficient of determination ($r^2 = 0.73$), during calibration and $r^2 = 0.7$, during validation. The manufacturer of the soil sensors used to obtain soil water content data applied in the inversion of Hydrus 1D, recommends calibration of the sensors to local soil conditions to ensure maximum accuracy of the soil water content measurements. Otherwise the expected accuracy of the sensors is at least 3% based on the factory calibration. Due to technical difficulties it was not possible to calibrate the sensors for the study site, therefore, the results obtained are based on the factory allowed accuracy of at least 3%. For the purposes of this research and within the experimental limitations of this study, the factory calibration accurcy was considered acceptible.

8 AGRO-HYDROLOGICAL SIMULATION TO DERIVE THE *SMDI* FOR THE STUDY SITE AND ITS UPSCALING THROUGH ENERGY BALANCE MODELING

Summary

This chapter concludes the development of the SMDI as presented in this thesis by applying all the concepts developed in chapters 4, and 6 and the case study results of chapters 5 and 7 to calculate threshold parameters for the definition of SMDI in Northern Uganda. This is achieved through applying all the results obtained to simulate a 21-year time series of soil moisture using the calibrated agro-hydrological model, Hydrus 1D. The simulated soil moisture time series were used to derive the SMDI for the study site. Reference indices i.e. SPI, SPEI and AWD were calculated using algorithms elaborated in chapter 4, for testing SMDI through correlation analyses. And finally, in order to apply the SMDI to the entire agro-hydrological zone, a regression equation was developed between SMDI and an evaporative fraction (Λ) derived from an energy balance model, S-SEBI. Results showed that the threshold parameters; i.e. water content at field capacity (θ_{FC}) and water retention at wilting point (θ_{WP}), derived from the agro-hydrological simulations compared well with the laboratory determined values, with the coefficient of determination ($r^2 = 0.95$). Secondly, SMDI correlated negatively with the yield records at the study site with the coefficient of determination ($r^2 = 0.64$).

Precipitation (P) and Precipitation deficit (D = P-ETo) were fitted on a gamma and log-logistic probability distributions, to calculate SPI and SPEI respectively, for the study site. Both theoretical distributions fitted the empirical distributions with acceptable Kolmogorov-Smirnov goodness of fit test at 95% level of confidence. Positive correlation coefficients were obtained between each of the reference indices with SMDI, further demonstrating the robustness of the SMDI. Lastly, the SMDI could be predicted with the evaporative fraction (Λ) obtained from the energy balance model, S-SEBI with the coefficient of determination ($r^2 = 0.84$), based on cloud free images. A regression equation developed between SMDI and Λ was cross validated using different set of satellite images. The derived SMDI–Λ regression equation predicted the SMDI obtained from agro-hydrological simulation with ($r^2 = 0.85$) based on images obtained between January and March, 2014. Application of SMDI to delineate the study site into wet and dry seasons showed that dry season starts between November 25 to December 10 of each year and wet season starts between March 26 and April 5 of each year. The results of this chapter were used to formulate a soil water management decision support scheme that can be applied in the study area to mitigate the impacts of agricultural drought.

8.1 Introduction

Most universally applied drought indices such as the SPI and PDSI do not either entirely account for actual soil moisture and crop dynamics (Martínez-Fernández et al., 2015; Niemeyer, 2008), or apply an overly simplified representation of moisture movement in the SPAC (Wells, 2004; Alley, 1984) respectively. These factors motivated development of soil moisture based drought indices such as the Soil water index (SWI) by Hunt et al. (2009); the Soil Water Deficit Index (SWDI) by Martínez-Fernández et al. (2015) and the Soil Moisture Deficit Index (SMDI) and Evapotranspiration Deficit Index (ETDI) by Narasimhan and Srinivasan (2005) for monitoring agricultural droughts. All these indices except those developed by Narasimhan and Srinivasan (2005) use actual measurements of soil moisture through comprehensive soil moisture monitoring programs such as REMEDHUS (Soil Moisture Measurements Stations Networks) in Spain, (Sánchez et al., 2012) and large soil moisture monitoring networks and databases in European countries and the USA. However, such approaches are not practical in developing countries where soil moisture monitoring networks are unavailable (Dobriyal et al., 2012). For this reason, an approach was presented in Chapter 4, to apply a one-dimensional Agro-hydrological model to generate soil moisture time series from which threshold parameters of the soil moisture retention curve i.e.; θ_{FC} and θ_{WP} can be calculated. These parameters are then applied to define SMDI for operational monitoring of agricultural drought in developing countries that do not have soil moisture monitoring programs such as in Uganda.

This case study was conducted in Northern Uganda, where many small, medium scale to large agricultural farms are being opened in large numbers. However, the farmers who rely entirely on rainfall for agricultural production, hardly have any access to climatic information because of scarcity of climatic data in Northern Uganda. Relatively high rainfall received over Northern Uganda lasts only for about six months effectively between March and November (Nsubuga et al., 2014; Basaliriwa, 1995; 1991; Ogalo, 1981). Moreover, the rains exhibit high spatiotemporal variability and the abundant rainfall received during the wet season is easily lost during dry spells. The aim of this research (as has been elaborated throughout the previous chapters) is to transform the scanty climatic and soil information in Northern Uganda into a tool for operational monitoring of agricultural droughts. Such a tool once availed to farmers would enable them plan ahead of time to counter frequent risks posed to rain fed farming by increasing unpredictability in weather patterns. It could further help in guiding farmers to plan best soil water management strategies based on information of common drought characteristics

that the developed index would provide that is currently lacking. Lastly the index can be used as a proxy for soil moisture status thereby guiding farmers on the best time for field operations such as first and second ploughing and on the best planting dates especially for maize (Zea mays) in the Northern Uganda.

The aim of this chapter is to apply the methodologies discussed in chapter 4 in a case study conducted in Northern Uganda through implementation of five key objectives, namely:

- To apply the calibrated soil hydraulic parameters obtained in chapter 7 together with the published crop coefficients in FAO-56 manual and the best performing evaluated reference ET_o (ET_o^{Mkk}) model in chapter 5 to simulate time series of soil moisture for; 1995 – 2015, at the study site;
- To use the simulated soil moisture time series to generate the threshold parameters of the soil water retention curve i.e. θ_{FC} and θ_{WP} for the computation of SMDI as elaborated in chapter 4, and to validate SMDI at the study site through a correlation analysis with the reference indices (i.e. SPI and SPEI) and yield data obtained from the study site.
- To upscale the derived SMDI for application to the entire agro-ecological zone of the study site through development of a SMDI-Λ regression equation
- To present the results obtained and their discussions.
- To apply the results obtained to formulate a soil water management decision support scheme for mitigation of agricultural droughts in the study site

8.2 Generation of Long Term Soil Moisture Time Series at the Study site

The method presented in chapter 4 assumes that it is possible to calibrate a one dimensional agro-hydrological model in the area of application. The theoretical background for the calibration of such a model is covered in chapter 6. The methods applied for the calibration of Hydrus 1D and the results obtained are presented in chapter 7. This section is concerned with application of a calibrated model to generate long term soil moisture times series.

8.2.1 Steps taken to generate long term records of soil moisture time series

the steps involved include:

- Specification of the initial condition at the start of the simulation period
- Specification of the boundary condition throughout the simulation period

- Setting up the agro-hydrological model for the long-term simulation of the soil moisture for the considered locality. A period of 5 years' simulation or longer is preferable based on available literatures on the subject.
- Generation of the thresh hold parameters i.e. the θ_{FC} and θ_{WP}, following the statistical method proposed by Hunt et al. (2009). i.e. arranging the daily soil moisture time series in ascending order and calculating 5^{th} and the 95^{th} percentiles to represent water content at θ_{WP} and θ_{FC} respectively
- Assessment of the validity of the generated threshold parameters either through laboratory experiment or through the published values

The uniqueness of this particular work is in the fact that it overcomes two kinds of challenges experienced in developing countries: i.e.

- the inadequacy or complete lack of soil moisture monitoring networks
- the insufficiency of the meteorological variables (both in terms of quantity and quality) that are very critical in defining the initial and the boundary conditions (Wart et al., 2015).

The first challenge is compounded by the second challenge. However, the approach developed here, overcomes both of the challenges through:

- Utilization of low cost commercially available soil sensors to calibrate an agro-hydrological model as presented in chapter 7.
- application of data propagation methodologies discussed in chapter 5 for the generation of reference evapotranspiration models applied in combination with published crop coefficients for the specification of the boundary conditions for the long-term soil moisture simulation.
- Evaluation of appropriate less data intensive ETo model for application specific areas as discussed in chapter 5

8.2.2 Model set up: specification of the initial and the boundary conditions

Hydrus 1D model was set in a direct simulation mode, and simulation started in January 1, 1995 with initial conditions estimated at a pressure head of 10,000m. this is the critical pressure head provided for in Hydrus 1D. such a pressure head represents dry soil system as revealed by no rainfall recorded right from the beginning of December 1994 in Northern Uganda. Simulations were run for a period of 21 years i.e. from January 1, 1995 to December 31, 2015. The calibrated soil hydraulic parameters were adjusted slightly whenever simulations

failed to run in each case. this step was repeated for all the four profile locations in Figure 7.1, chapter 7.

The soil moisture values generated for the four locations were used to generate pairs of values of (θ_{WP}, θ_{FC}), following the procedures proposed by Hun et al. (2009). A regression analysis was thereafter performed by comparing these model generated values to those generated from the soil hydrological laboratory in the University of Naples Federico II, on undisturbed soil core samples that were brought to Italy for analysis. The laboratory determination of the threshold parameters was achieved for each undisturbed soil core samples using pressure plate apparatus. The pairs of values, i.e. (θ_{WP}, θ_{FC}) were determined corresponding to suction pressure at 10,000m and 300m for θ_{WP} and θ_{FC}, respectively. These suction pressures were selected for the threshold parameters based on soil survey report for the study area classifying the soils as mainly low activity Ferrallisols (Pidgeoni, 1972; Chenery, 1960). These types of soils have suction pressure heads corresponding to field capacity of 30kPa and 10kPa corresponding to wilting point instead of the recommended pressure heads of 33kPa and 15kPa for these threshold water content values respectively (van den Berg et al., 1997).

For the long-term simulation of the soil moisture time series, the reference ET_o model, Makkink, was used together with crop coefficient values for maize obtained from FAO-56 manual (Allen, 1998). Makkink ET_o model provided the best prediction of the ET_o among the 13 models evaluated in chapter 5. The Makkink ET_o model requires solar radiation and mean air temperature values. Both of these climatic parameters can be obtained from the gridded climatic data through the data propagation algorithm described in chapter 5. Application of the data propagation methodology in chapter 5 showed that; both solar radiation and average temperatures can be derived from limited meteorological observations together with the gridded climatic data with acceptable level of confidence.

The K_c values cover a wide range of agro-climatic regions and it is assumed here that maize crops are grown under best management practices such that the only limitation is rainfall during dry periods. This is because the agro-hydrological simulation for the generation of the threshold parameters as implemented in this research applies to rain fed cropping system. Therefore, the K_c values together with ET_o calculations obtained through Makkink model in conjunction of gap-filled precipitation data obtained from the study site, provided the boundary conditions throughout the entire 21-year period, for the daily simulations.

8.3 Computation of Reference Drought Indices for Assessment Of SMDI

The reference drought indices computed in these sections are the SPI, SPEI and the AWD. The algorithms for the SPI and the SPEI are presented in chapter 4. These reference indices especially the SPI are the standard meteorological indices applied usually to assess the performance of the newly developed indices (Xinyu et al., 2017; Yu et al., 2014; Torres et al., 2013; WMO, 2009; Purcell et al., 2003). Meteorological drought is the primary trigger of all the other drought types. Therefore, a positive correlation between newly developed indices with the standard meteorological drought indices confirms the applicability of the developed indices (Martinez-Fernandez et al., 2015).

8.3.1 Fitting the Empirical Probability Distributions on to Theoretical Distributions for The Study Area Data

In order to compute SPI and SPEI for a given location, it is required that in both cases the empirical cumulative probability distributions of Precipitation P, (for the calculation of SPI) and the precipitation deficit D, (for the calculation of SPEI) are fitted on to the respective theoretical distributions (Makee et al., 1994; Vicente-Serrano et al., 2010). For the study area, cumulative frequency distributions of P and D were fitted on the 2-parameter gamma distribution and the 3-parameter log-logistics distribution respectively. In each case, the goodness of fit test was conducted based on the Kolmogorov-Smirnov goodness of test fit statistics. For computation of the empirical commutative probability distributions for generating SPI, a 32-year precipitation data was applied. Consistency checks and gap filling were done by applying the data propagation algorithm described in chapter 5 and the 21-year precipitation data was extended to 32-year for computation of SPI (1983 – 2015). Whereas the corresponding empirical distribution for D was calculated based on computation of ET_0 using Makkink ET_o model for the same period. However, verification of SMDI was based on 21-year portions of both SPI and SPEI, i.e. from 1995 to 2015 corresponding to the simulation periods.

$$D = P - ET_0^{Mkk} \tag{8.1}$$

Where D is the precipitation deficit for the calculation of SPEI, and P is precipitation and ET_0^{Mkk}, is the reference evapotranspiration calculated using the Makkink ETo Model. Then the goodness of fit test for each case was conducted based on Equation (8.2).

$$D_n = \max_n \left[F_n(x) - F(x) \right] \tag{8.2}$$

Where $F_n(x)$ is the empirical cumulative distribution for the Precipitation P and precipitation deficit D. F(x) is the theoretical distribution function evaluated at x. Under a null hypothesis that D_n does not exceed a critical value at a given level of significance (for the data drawn from the theoretical distribution). According to Lloyd-Hughes and Saunders (2002), If D_n exceeds the critical value, the null hypothesis is rejected at the given level of significance.

8.3.2 Correlation Analysis Between SMDI and The Reference Drought Indices

Correlation analysis was carried out to evaluate the suitability of SMDI for operational drought monitoring in the study area. A positive correlation between SMDI with reference indices: i.e. SPI, SPEI and AWD would indicate that SMDI can be applied in the study area for agricultural drought monitoring. The reference indices chosen are widely used meteorological indices. Since a meteorological drought precedes agricultural drought, a good agricultural index would exhibit a positive correlation with a meteorological drought index. Pearson's correlation coefficient is defined as the degree of linear association/relationship between two variables. It is a measure that determines the degree to which the moments of two variables are associated. The range of values for the correlation coefficient is -1.0 to +1.0. A correlation of -1.0 indicates a perfect negative association or negative relationship between the two variables. While a correlation of +1.0 indicates a perfect positive relationship. Calculation of a correlation coefficient between two variables x and y is given by:

$$r = \left(\frac{\sum_{1=1}^{n} (x_i - \bar{x})(y_i - \bar{y})}{\sqrt{\sum_{i=1}^{n} (x_i - \bar{x})} \sqrt{\sum_{i=1}^{n} (y_i - \bar{y})}} \right) \qquad (8.3)$$

Correlation coefficients were calculated between SMDI and the reference indices. In order to check the applicability of the reference indices to evaluate SMDI, correlation coefficients were also calculated to assess, how each reference index relates with the rest of each other.

8.4 Upscaling the SMDI Through Cross Validation with An Energy Balance Model

8.4.1 Energy Balance Modeling

Recent developments in satellite remote sensing have made it possible to acquire crucial variables for characterizing land surface interactions (Loveland and Irons, 2016; Ke et al., 2016; Jiménez-Muñoz et al., 2009; Tasumi et al., 2008; Moran et al., 1992). Over the last two decades, the requirement for quantifying ET at regional scale, together with the recent advances

in satellite remote sensing technology, has led to many studies on mapping large scale ET (Ali et al., 2016; Bhattarai et al., 2016; Kilic et al., 2016; Kosa, 2011; Waters et al., 2002; Roerink et al., 2000; Bastiaanssen et al., 1998). The surface energy balance algorithms based on the energy balance equation is one of the most widely used approaches for obtaining large scale (regional) estimates of remotely sensed ET at multi temporal and spatial scales (Bala et al., 2013;). Energy and mass are exchanged between the land and the atmosphere. When the heat fluxes that are transported by the horizontal advection and the photosynthetic vegetation are assumed negligible, the one-dimensional form of the energy balance equation on an instantaneous time scale can be expressed as

$$R_n = G_o + H + \lambda E \qquad (8.4)$$

Where, R_n is net radiation, H is sensible heat flux, G_o is soil heat flux and λE is latent heat flux; each of which having the unit of W/m^2. Many of the SEB models rely on equation 8.4 to estimate large scale ET. There are four SEB models that are in common use namely: Surface Energy Balance for Land (SEBAL), ALEXI, Simplified Surface energy Index (S-SEBI) and Surface Energy Balance Systems (SEBS) (Liou and Kar, 2014; Bala et al., 2013). Among these commonly used SEB models, it is ALEXI that is based on two source ET calculation, i.e. ET is calculated separately as soil evaporation and transpiration from vegetation, then E and T are added after computation. The rest combines calculation of soil evaporation and transpiration in combination as Evapotranspiration (ET). The rest of the mentioned SEB models require field measurements of parts of the variables for the estimation of the ET except S-SEBI. In application of the S-SEBI algorithm, only a satellite image is required as long as sufficient dry and wet condition can be identified in an image. For this reason, S-SEBI model was used in this research.

8.4.2 The Simplified Energy Balance Index S-SEBI

The simplified surface energy balance index (S-SEBI) was developed to solve the energy balance with remote sensing method on a pixel by pixel basis. S-SEBI requires scanned spectral radiances under cloud free conditions in the visible, near infrared and thermal infrared range to estimate its different parameters which are: the reflectance, surface temperature and the vegetation index. With these input the energy budget at the surface can be partitioned. First the net radiation is determined as the rest term of all the incoming and outgoing shortwave and long wave radiations, some of which can be detected directly by the remote sensing techniques. Secondly, the soil heat flux is derived from an empirical relationship of the surface and

vegetation characteristics. The sensible and the latent heat flux are not partitioned as separate parameters, but as the evaporative fraction Λ ; equation (8.5).

$$\Lambda = \frac{T_H - T_o}{T_H - T_{\lambda E}} \qquad (8.5)$$

When the assumption of constant atmospheric condition over the image is fulfilled and sufficient dry and wet pixels can be identified throughout the reflectance spectrum within the image; T_H and $T_{\lambda E}$ can be determined from the image itself (Roerink et al., 2000).

8.4.3 Deriving the Parameters for the Implementation of the S-SEBI Algorithm

Calculation of the parameters of Equation (8.5) involves the following steps according to; (Roerink et al., 2000):

- Identification of hot and cold pixels from each Landsat 8 TIR image,
- Extraction of the reflectance and land surface temperatures from the different pixel sets of both cold and hot regions
- Plotting the feature space on a graph similar to Figure 8.1, with values of the extracted reflectance on the x-axis and values of land surface temperature on the y-axis
- Calculating the averages of the cold and hot pixel sets and plotting them on the same graph, in order to guide the delineation of the evaporation controlled and the radiation controlled regions within the feature space plot.
- Determining the regression coefficients for the evaporation controlled and the radiation controlled lines on the plots

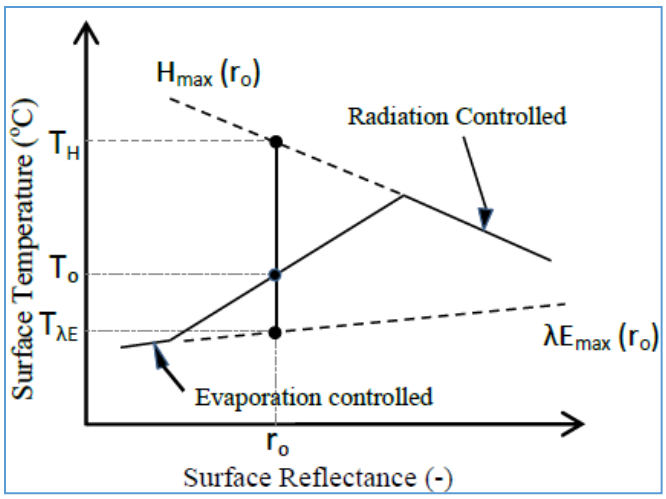

Fig. 8.1 A scheme showing the relationship between surface reflectance and temperature as applied in S-SEBI algorithm; (Roerink et al. 2000).

$$T_H = a_H + b_H \alpha_o \quad (8.6)$$

$$T_{\lambda E} = a_{\lambda E} + b_{\lambda E} \alpha_o \quad (8.7)$$

Where; a_H, b_H are the regression coefficients for the radiation controlled line and $a_{\lambda E}$, $b_{\lambda E}$ are the corresponding regression coefficients for the evaporation controlled line.
Substituting equations (8.6) and (8.7) in to (8.5) gives:

$$\Lambda = \frac{a_H + b_H \alpha_o - T_o}{a_H + b_H \alpha_o - \left(a_{\lambda E} + b_{\lambda E} \alpha_o\right)} \quad (8.8)$$

8.4.4 Estimation of the Land Surface Temperature from Satellite Data

Land surface temperature is an important variable in land surface remote sensing (Yu et al., 2014). Its estimation requires calculation of several parameters and the steps involved are as follows:

The spectral radiance L_λ ($Wm^{-2}sr^{-2}\mu m^{-1}$), given by:

$$L_\lambda = ML \times Q_{cal} + AL \quad (8.9)$$

Were *ML* and *AL* being the band specific multiplicative factor and additive rescaling factors respectively both of which can be obtained from Landsat metadata. Q_{cal} is the *digital number* (DN).

The spectral radiance L_λ ; is applied in the radiative transfer model to estimate the surface emitting radiance L_T through the inversion of the equation (8.10)

$$L_\lambda = \tau\varepsilon L_T + L_u + \tau(1-\varepsilon)L_d \quad (8.10)$$

In Equation (8.10); τ (-) is the atmospheric transmission; ε (-) is the emissivity of the surface, specific to the target type; L_u ($Wm^{-2}sr^{-2}\mu m^{-1}$) is the upwelling or the atmospheric path radiance; L_d ($Wm^{-2}sr^{-2}\mu m^{-1}$) is the down-welling or the sky radiance. Estimation of the land surface temperature (LST) from Equation (8.11) helps accounts for the atmospheric correction if the following can be estimated i.e. the emissivity ε, the upwelling or the atmospheric path radiance L_u and the down welling or the sky radiance L_d, and the atmospheric transmission τ. The land surface emissivity can be estimated from the NDVI (Momeni and Saradjian, 2007; Valor and Caselles, 1996; Van de Griend and Owe, 1993). Whereas, the three parameters L_u, L_d and τ are obtained from the web based calculator (Barsi et al., 2003). Radiance to temperature conversions can be achieved by the application of the plank equation or the Landsat specific estimate of the plank curve: Equation (8.11)

$$T_{lst} = \frac{k_2}{ln\left(\frac{k_1}{L_T}+1\right)} \quad (8.11)$$

Where T_{lst} is the land surface temperature in Kelvin; L_T ($Wm^{-2}sr^{-2}\mu m^{-1}$) being, surface specific spectral radiance obtained by the inversion of Equation (8.10), k_1 and k_2 are calibration constants that can be obtained from the that Landsat8 TIR metadata.

$$L_T = \frac{L_{TOA} - L_u - \tau(1-\varepsilon)L_d}{\tau\varepsilon} \quad (8.12)$$

8.4.5 Estimation of Surface Emissivity from Normalized Difference Vegetation Index

The emissivity of a given a vegetated surface can be estimated from the normalized difference vegetation index (NDVI); the NDVI is obtained from the near infrared and the red bands of the Landsat 8 satellite as in Equation (3.6), in chapter 3. It is then used to calculate the surface cover factor F_r which is in turn used to calculate ε as shown in the Equations: (8.13) to (8.15).

$$F_r = \frac{\rho_{nir} - \rho_r}{\rho_{nir} + \rho_r} \quad (8.13)$$

$$F_r = \left(\frac{NDVI - NDVI_0}{NDVI_{\max} - NDVI_0}\right)^2 \quad (8.14)$$

$$\varepsilon = F_r\varepsilon_v + (1-F_r)\varepsilon_s \quad (8.15)$$

Where F_r is the cover factor with values ranging from 0 to 1, 0 being the value for bare soil and 1 corresponding to full vegetation cover; $NDVI_0$ is the NDVI value corresponding to bare soil and $NDVI_{max}$ is the NDVI value corresponding to the full vegetation cover (Jiménez-Muñoz *et al.*, 2009); ε is the surface emissivity required for the calculation of the surface temperature, ε_v is the emissivity of full vegetation cover, ε_s is the emissivity of bare soil. Calculations for the purpose of this case study were based on values of $\varepsilon_v = 0.99$, and $\varepsilon_s = 0.97$, according to Yu et al. (2014)

Table 8.1 Calibration parameters for the estimation of the surface radiances

Sensor	Band	k_1 $(Wm^{-2}sr^{-1}\mu m^{-1})$	k_2 (K)
Landsat-8	10	774.89	1321.08
Landsat-8	11	480.89	1201.14
Landsat-7 ETM+	6	666.09	1282.71
Landsat-5 TM	6	607.76	1260.56

Table 8.2 Landsat bands information

Sensor	Wave length (μm)	Resolution (m)	Band
Landsat 5	10.4 – 12.50	120	6
Landsat 7	10.40 – 12.50	60	6
Landsat 8	10.60 – 11.19	100(30*)	10
Landsat 8	11.50 – 12.51	100(30*)	11

8.5 Presentation of the results of long-term agro-hydrological simulations and discussions

In this study, a new methodology to define water deficits to agricultural crops grown under rain fed conditions was presented in chapter 4. The method relies on detailed calibration of a one dimensional agro-hydrological model in areas that do not have reliable information on crop development and weather parameters. A 1-dimensional agro-hydrological model, Hydrus 1D was calibrated in the study area (i.e. Northern Uganda) and the calibration and validation results presented in chapter 7 (section 7.4). In the new methodology, development of a soil moisture deficit index (SMDI) is achieved through long term simulation of soil moisture time series to generate threshold parameters that Agronomists use to characterize water availability to plants i.e: soil water retention between field capacity (θ_{FC}) and wilting points (θ_{WP}) (Martínez-Fernández et al., 2015; Allen, 1998; Pidgeoni, 1972). Usually, these threshold parameters are determined in laboratory through pressure plate apparatuses. Sometimes the values are estimated through application of empirical relations between the threshold parameters and soil physical characteristics such as the bulk density, percent of sand, clay and silt using pedotransfer functions (Tomasella et al., 1988). However, these methods are not feasible in developing countries such as Uganda. Therefore, Hydrus 1D was calibrated and validated in a small agricultural field in Northern Uganda to facilitate computation of these threshold parameters. The long-term simulation results to calculate these threshold parameters for the study site is presented and discussed in this sub-section.

8.5.1 Results of the simulated threshold parameters

The threshold parameters for the definition of SMDI were derived through the method developed by Hunt et al. *(*2009). Daily soil moisture time series for the four locations where disturbed and undisturbed soil samples were taken and analyzed were simulated for 21 years (1995 – 2015). The soil moisture time series were arranged in ascending order and the 5th and the 95th Percentiles were computed to represent θ_{WP} and θ_{FC} respectively for each location.

Because, the soil hydraulic parameters were not calibrated at location of the data logger EM50-001, the values estimated by the Rosetta Pedotransfer functions were used for the long-term simulations for this location. The obtained values for the four data logger positions, Figure 7.1, were compared with the Laboratory estimated values by means of scatter plots and r^2 between simulated and laboratory determined threshold parameters. The scatter plots between the simulated threshold parameters (i.e. θ_{FC} and θ_{WP}) and Laboratory determined values are shown in Figure 8.3. Coefficient of determination (r^2 = 0.95) was obtained between the laboratory determined threshold parameters and those obtained through long term agro-hydrological simulations.

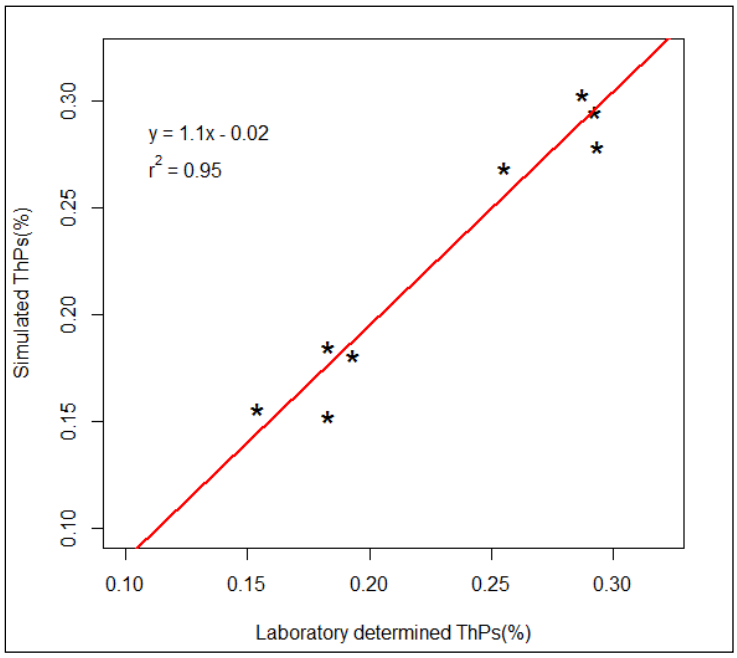

Figure 8.3 Scatter plots between the Threshold parameters for the definition of SMDI. ThP = Threshold Parameters i.e. water content at wilting point (θ_{WP}) and that at field capacity (θ_{FC}), estimated from the long-term simulations vs those estimated from the laboratory

Determination of the threshold parameters through the 5th percentile and the 95th percentile to represent θ_{FC} and θ_{WP} respectively was reported by Martínez-Fernández et al. (2015). They obtained r^2 value of 0.81 using separate scatter plots for θ_{FC} and θ_{WP} partly because they had more data points from the many stations from which soil moisture sensors were located. However, in their case they applied actual soil moisture observations for a period of 8 years, this could explain why the results presented here are better due to application of 21 years of soil moisture data to derive SMDI and combination of both the threshold parameters in the same plot. Although it seems more appropriate to plot these values on separate graphs as these

authors did which can be possible with many data points not possible in our study. This results further demonstrated a superior estimation of the threshold parameters compared to similar other reported results that have been reported (Hogg et al., 2013; Hunt et al, 2009; Lagergren and Lindroth, 2002). The result (i.e. $r^2 = 0.95$) was nevertheless obtained without calibration of the soil sensors used, therefore the comparison is based on relative accuracy of 3% or more of the soil moisture sensors used for calibration of the agro-hydrological model as reported by the manufacturer of DECAGON soil sensors. If calibration of soil sensors were carried out for the study site perhaps high values of the coefficient of determination would have been obtained. Use of long term simulated soil moisture time series may also have contributed to the relatively high value of the coefficient of determination obtained in this study. Availability of long-term soil moisture time series captures all the possible values of the soil moisture content that can be obtained in different climatic periods. This is particularly the strength of applying the calibrated simulation model to obtain time series of soil moisture for any length of time depending on the length of the climatic parameters obtainable.

8.5.2 Results and Discussions of the goodness of fit test for the fitting distributions applied for the implementation of the SPI and the SPEI algorithms in the study area.

The algorithms to calculate two of the reference indices (i.e. SPI and SPEI) applied for the evaluation of the SMDI in the study area require fitting of their main variables onto the theoretical probability distributions that best describe these variables in the study site. The fitted variables are precipitation (P) applied in the algorithms for the calculation of SPI and precipitation deficit (D) applied for the calculation of the SPEI. Therefore a 32-year precipitation data were fitted on to a gamma probability distribution function using the method of maximum likelihood, implemented in R environment using *fitdistrplus* package (Delignette-muller and Dutang, 2015). A similar procedure was repeated for fitting D on to a 3-parameter log-logistics distribution for the calculation of SPEI. In both cases, both P and D were fitted on to the theoretical distributions with acceptable Kolmogorov-Smirnov goodness of fit test statistic at 95% level of significance.

8.5.3 Results and discussions of the correlation analyses between the SMDI with the reference indices: SPI, SPEI and AWD

Suitability of the derived SMDI for operational drought monitoring was tested against known drought indices such as SPI (Mckee et al., 1993); SPEI (Vicente-Serano, 2010), and AWD (Purcell et al, 2003) through correlation analyses. The results of the correlation

coefficients between SMDI and the reference indices for both the growing and the dry seasons are presented in Table 8.3. The growing season in Northern Uganda starts from the beginning of April and lasts through October of each year. The dry season starts in December and last through March of the next year (Basaliriwa, 1995). There was positive correlation between SMDI with each of the reference indices as shown in Table 8.3. The growing season highest correlation coefficient was obtained between SMDI and SPI (r = 0.49), and the lowest correlation was obtained between SMDI and SPEI (r = 0.37). The range of correlation coefficients are comparable to the values reported by Martínez-Fernández et al. (2015) between SWDI and AWD. Higher correlation coefficients between SMDI with each of the reference indices were obtained during the dry period from December to March. This demonstrates that SMDI is more sensitive to dry periods than AWD when compared with the SPI and SPEI which are widely used drought indices.

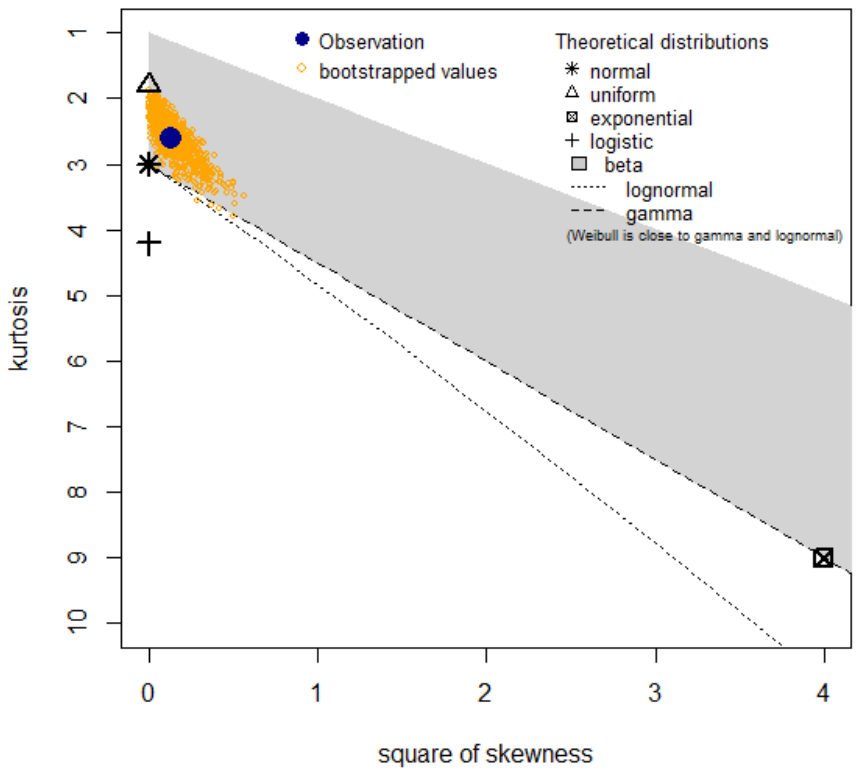

Goodness-of-fit statistics (1-mle-gamma)	Value of the test statistic
Kolmogorov-Smirnov statistic	0.137038
Cramer-von Mises statistic	1.475928
Anderson-Darling statistic	8.008295

Goodness-of-fit criteria (1-mle-gamma)	Value of the fit criteria
Akaike's Information Criterion (AIC)	2861.521
Bayesian Information Criterion (BIC)	2868.532

Figure 8.4 Cullen and Frey Graph, showing skewness-Kurtosis plot for selection of candidate theoretical probability distributions for observed average monthly precipitation (1995 – 2015), based on 1000 bootstrapped values. The right goodness of fit statistic for 2-parameter gamma distribution function is shown the right-hand side. Parameters estimated by maximum likelihood method. Graphs for D that were fitted on a 3-parameter log-logistic distribution function are not shown. Those of P are shown in Figure 8.4 using two candidate distribution functions.

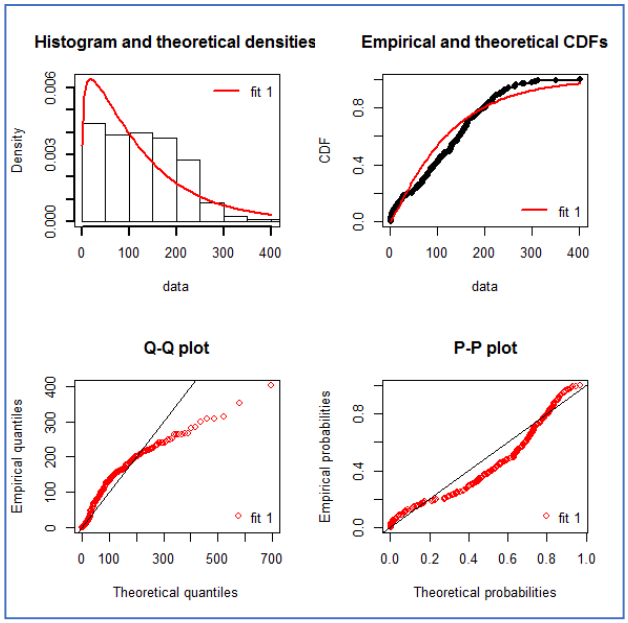

(a) Gamma Distribution

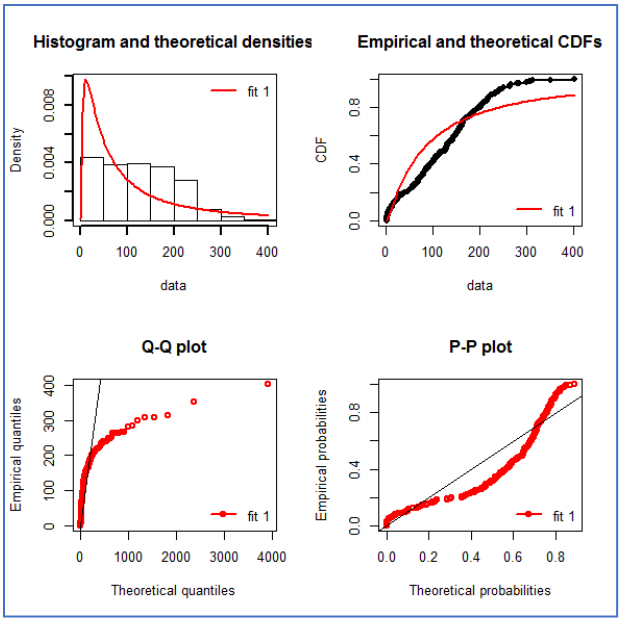

(b) Lognormal Distribution

Figure 8.5 Distribution plots for fitting observed Precipitation on theoretical (a) gamma probability distribution and (b) Lognormal Probability distributions

Monthly evolution of SMDI was plotted with AWD, as shown in Figure 8.6, and it can be seen that SMDI responds to dry period better than AWD. Whereas, AWD responds to wet period better than SMDI. Since the dry season in Northern Uganda under normal dry conditions register no precipitation, the only factor determining the values of AWD is evapotranspiration controlled by soil moisture. This explains the reason why SMDI responds to dry season better than AWD, since it is based on soil moisture. Testing newly developed agricultural drought indices using meteorological drought indices are a common practice, since meteorological drought indices are more comparable across space and time in almost all climatic regions (WMO, 2009). Time series plots both SPI and SPEI shown in Figures 8.7 (a) and (b) show similar response of the meteorological drought indices compared SMDI, i.e. that in both cases SMDI responds better to dry conditions.

8.5.4 The correlation between SMDI with observed yield within the same agro-ecological zone

Yield data for evaluation of SMDI was obtained from an agricultural research station approximately 75 km from the experimental site. The experimental site and the research station are considered to be in the same agro-ecological zone. Yield data for maize (Zea mays), was obtained for six years (2007 – 2010, 2014 and 2015), with yield data only for the first growing seasons for 2007 – 2010, 2015 and data for both seasons only in 2014. A regression analysis

was done between the number of days for which SMDI < 0 during the growing season and the yield data. The result of this assessment showed a negative correlation between the number of days for which SMDI < 0 and yields, with the value of the coefficient of determination (r^2 = 0.64), as shown in Figure 8.8. Yield data obtained from the experimental site could not be used, as maize biomass is harvested instead of grains and it was not clear how the records available were estimated. Likewise, the simulated yield records obtained from GYGA database were also not used because they appeared to be overly generalized since they were simulated by WOFOST model whose calibrations were based on very coarse global scale parameterizations of soil hydraulic characteristics (Wart et al., 2013).

Table 8.3 Growing season and dry Season Correlation Coefficients

		SMDI	SPI	AWD	SPEI
GROWING SEASON	SMDI	1	0.49	0.40	0.37
	SPI	0.49	1	0.79	0.96
	AWD	0.40	0.79	1	0.79
	SPEI	0.37	0.96	0.79	1
		SMDI	SPI	AWD	SPEI
DRY SEASON	SMDI	1	0.54	0.46	0.56
	SPI	0.54	1	0.53	0.90
	AWD	0.46	0.53	1	0.48
	SPEI	0.56	0.90	0.48	1

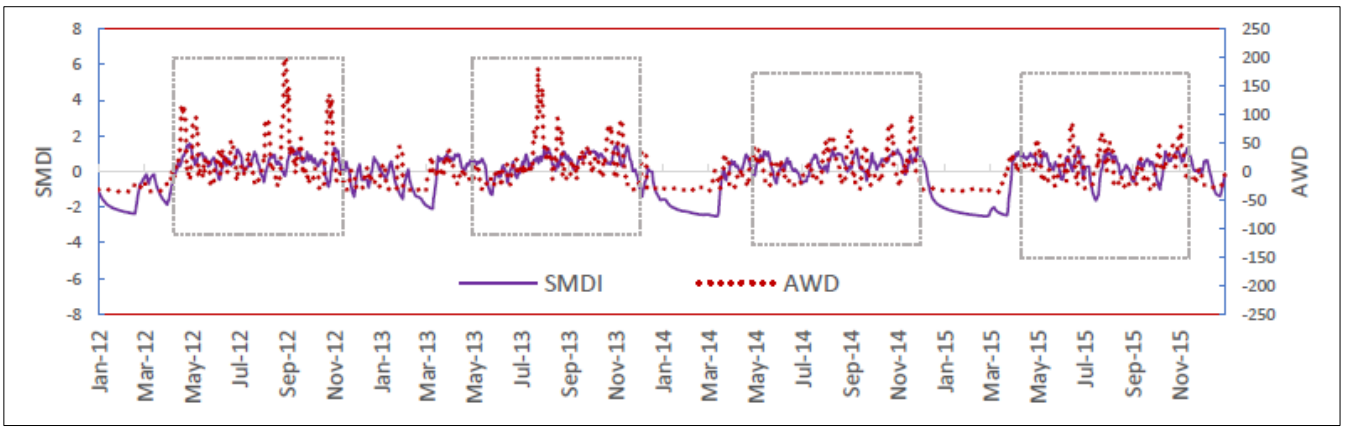

Figure 8.6 Time series plots of weekly SMDI and AWD from 2012 – 2015 showing seasonal variability.

8.6 Results of the Energy Balance Modeling and Discussions

The results for the implementation of the energy balance model S-SEBI in the study area are presented in this section. Relatively cloud free Landsat 8 TIRS images obtained between

April and October, 2015 were analyzed and parameters for the implementation of S-SEBI to derive Λ were extracted as elaborated in section 8.4. Table 8.4 shows the atmospheric correction parameters for thermal band 10 of Landsat 8 as calculated by the NASA web calculator. Whereas the scatter plot between the SMDI and Λ for two of the analyzed thermal images that had best triangular feature space plots are shown in Figure 8.9. Only two images obtained on April 23, 2015 and June 10, 2015 had reasonable values of r and T_{lst} as shown in Figure 8.10. By reasonable it means that the values of albedo (r) were close to published values for vegetated canopies that are normally common in study area during the growing seasons and the values of Land surface temperatures (T_{lst}) are not negative due to the fact that the study area is located at latitudes of between 1.5°N and 3.3°N, where the aerodynamic temperatures that are approximated by the land surface temperatures never reach negative values. Therefore, images that had more unreasonable values of r and T_{lst} determined according to these criteria were not used for this analysis.

8.6.1 Results of the regression equation developed between SMDI and Λ

The regression equation obtained from the scatter plots between SMDI and Λ shown in Figure 8.9(a) due to cloud free images having "reasonable" values of r and T_{lst} for the pixels corresponding to three sensor locations (i.e., EM50-002, 003 and 004, shown in Figure 7.1, chapter 7) showed good agreement with the coefficient of determination ($r^2 = 0.84$) between SMDI and Λ. This is expected for cloud free images since Λ is a proxy for soil moisture condition representing ratio of actual ET (ET_a) to reference ET (ET_0).

8.6.2 Validation results of applying the SMDI-Λ regression equation to calculate SMDI

In order to validate the developed regression equation between SMDI and Λ, SMDI was calculated through input of Λ values estimated by the S-SEBI algorithm using different sets of cloud free images obtained in 2014 into the SMDI-Λ regression equation developed on the basis of images obtained in 2015. The scatter plots using three cloud free images between the SMDI obtained through the regression equation and SMDI derived through agro-hydrological simulations as shown in Figure 8.9(b) demonstrated good agreement with the coefficient of determination ($r^2 = 0.85$). The good agreement through the high value of the coefficient of determination shows that SMDI can be calculated for the study area through the developed regression equation. This can be done by analysis of images from Landsat 8 thermal bands through application of S-SEBI algorithm to generate Λ, and applying the developed SMDI-Λ

regression equation to calculate the SMDI that can be used for drought monitoring in similar areas.

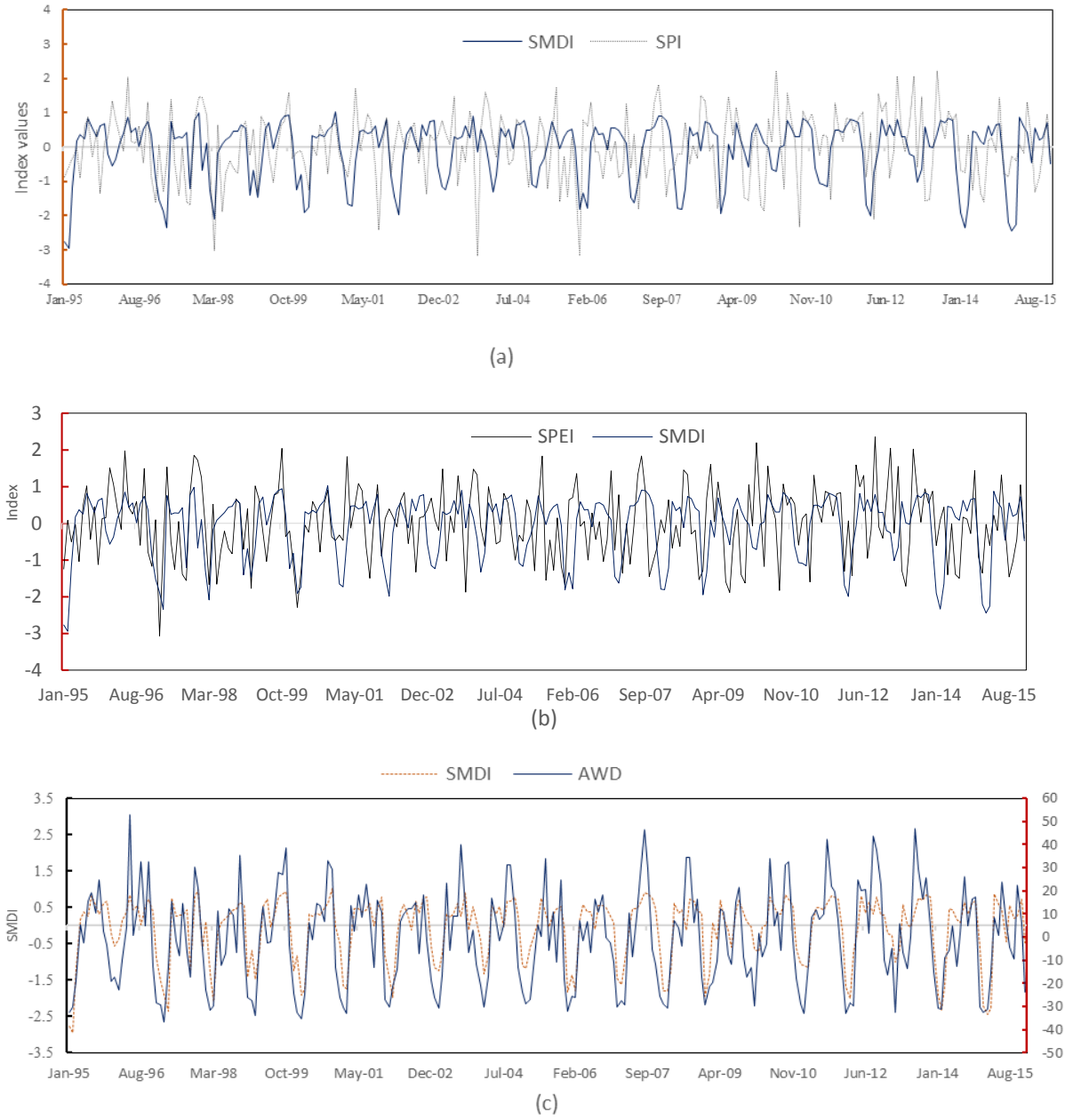

Figure 8.7 Monthly Evolution of the SMDI with (a) SPI-1, (b) SPEI-1 and weekly evolution of SMDI with(c) AWD for the period1995 – 2015

8.7 Applying SMDI for on farm decisions support

Proper farm management involves a set of decisions that the farmer makes in order to achieve the desired productivity. The risks involved in the alternative sets of options that provide the basis for the decision depends on a number of factors used to guide the decision-making process. Usually a farmer is faced with alternative course of actions that require timely decision making (Singh et al., 2008). Traditionally, tools such as multicriteria optimization

have been widely applied in decision support involving environmental, socio-economic and political constraints (Pettit and Puller, 2002). Their applicability in irrigation management and large scale management of water resources are more wide spread (Navarro-hellin et al., 2016). In a multi-criteria decision framework, a set of management options and associated constraints form input data in to an optimization algorithm (Larsson et al., 2014; Peng et al, 2011). In soil water management decision making process, applying a multi-criteria decision support system would require conceptual or physical simulation of different management options under various management constraints and considering their results based on social, political economic and environmental impacts. This makes the process tedious and computationally very demanding especially for small-scale farmers, thus rendering the decision process expensive in terms of time and resources (Kuarathna, 1992). However, currently better understanding of the physical processes that drive water dynamics in the SPAC has enabled development of better tools that can facilitate formulation of simplified deterministic approaches for soil water management (Aguilera et al., 2016; D'Urso, 2001).

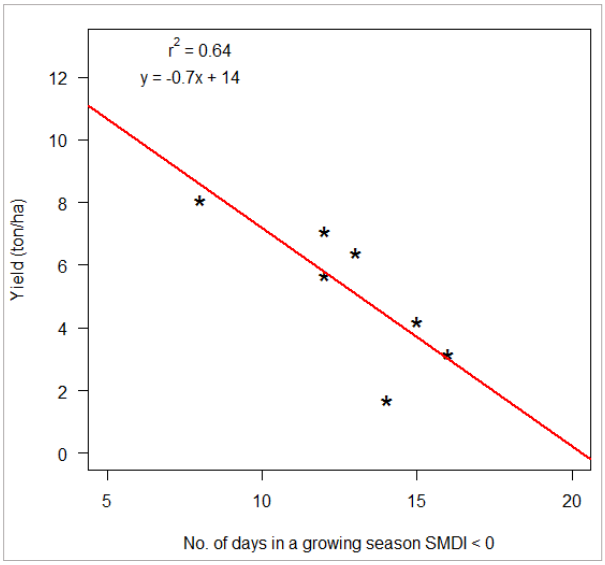

Figure 8.8 Scatter Plots of Yield versus the number of days SMDI < 0 within a growing season.

Table 8.4 Landsat 8TIRS Band 10 Atmospheric Correction parameters for indicated image dates

Image date	τ (band average)	L_u (effective band pass Upwelling radiance) $\left(Wm^{-2}sr^{-1}\mu m^{-1}\right)$	L_d(effective band pass downwelling radiance) $\left(Wm^{-2}sr^{-1}\mu m^{-1}\right)$
April 23,2015	0.71	2.05	3.37
June 10, 2015	0.54	3.37	5.03
July 12, 2015	0.61	3.03	4.64
Aug 13, 2015	0.65	2.80	4.34
Sep 14, 2015	0.57	3.32	5.02
Sep 30, 2015	0.61	3.06	4.69

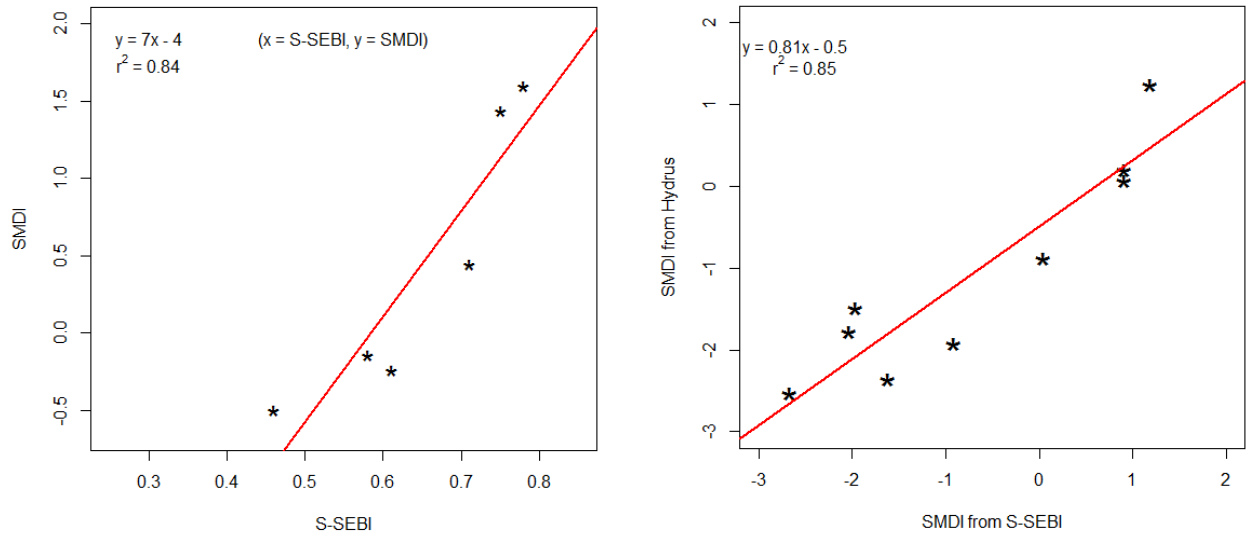

(a) (b)

Figure 8.9 Scatter plot of SMDI vs Evaporative Fraction (Λ) derived through the energy balance model S-SEBI for (a) 2015 calibration Landsat 8 TIRS images and (b) 2014 validation Landsat TIRS images

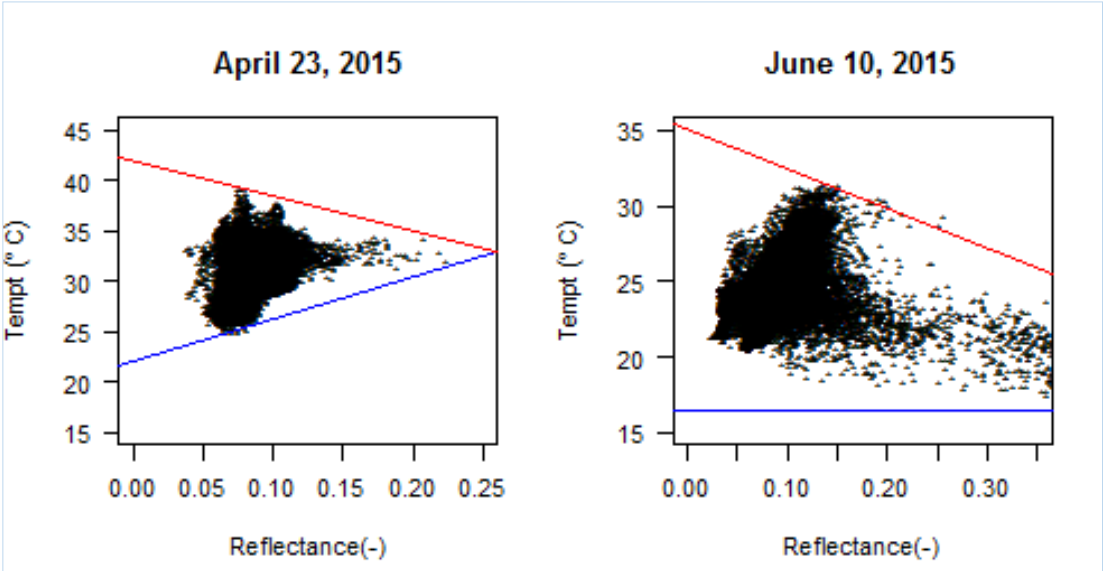

Figure 8.10 LST-Albedo feature plots for the derivation of Λ

Through application of modeling tools, different sets of management options can be assessed a priori before committing huge amount of resources to "know" the best course of actions. In agricultural water management, major constraints to decision making are availability of reliable climatic records that form the major input data in an optimization algorithm to generate different management scenarios based on alternative input data (Gadgil et al., 2002). Uncertainty on climatic information and soil factors account for major production risks in rain fed farming and therefore limit technology uptake among rural communities (Juma

et al., 2009). The methodology developed in this thesis partly solves the problem of uncertainty in climatic records in developing countries.

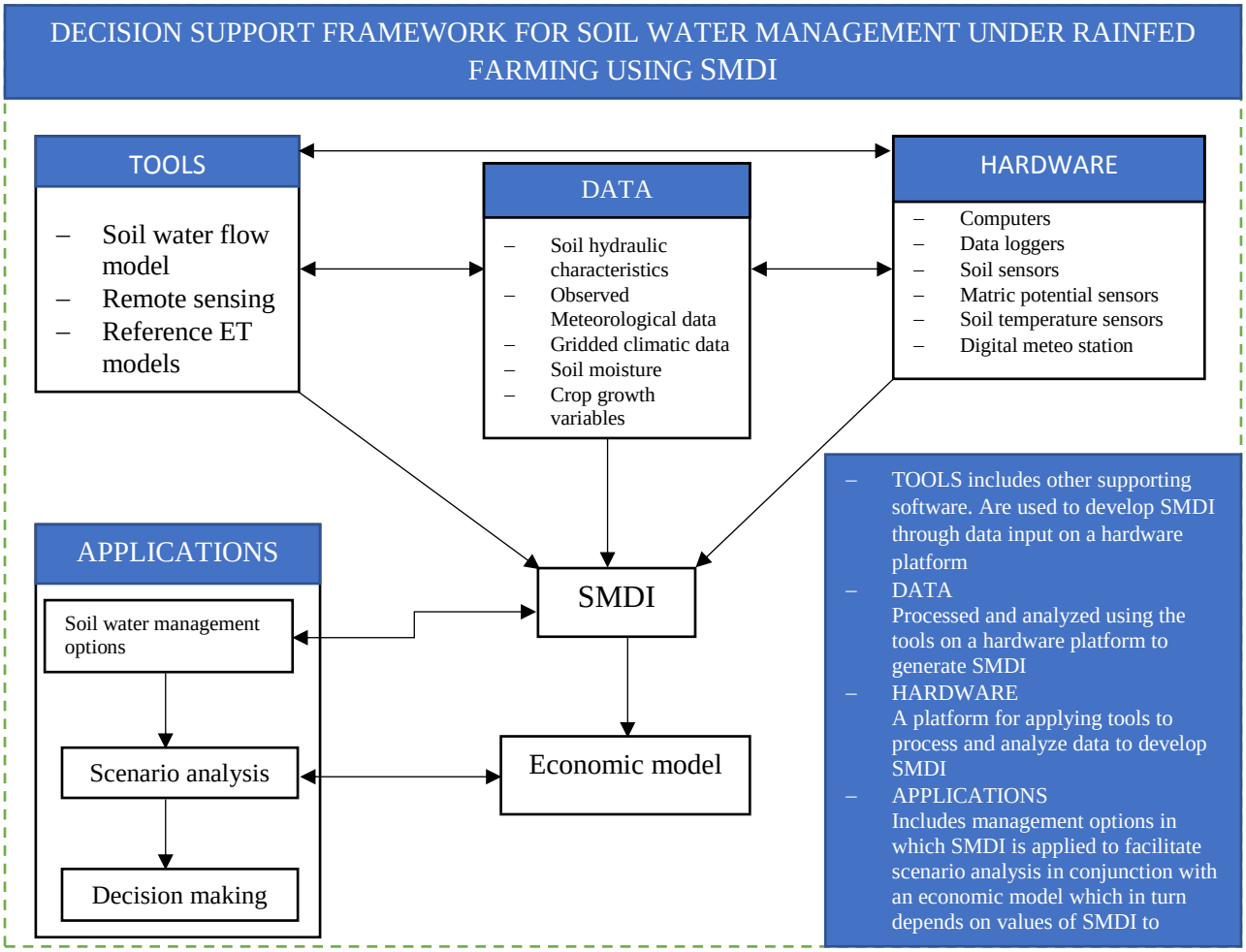

Figure 8.11 SMDI decision support Framework

Long term monitoring of soil moisture has traditionally been used to provide knowledge of the relationship between water use efficiency and crop yields (Qin and Oenema, 2013). Measured records of soil moisture in the root zone can be applied as indicators for adopting appropriate soil water management methods. Such records have been used to assess fire risks, wetland degradations and thereby help in planning environmental protection strategies (Aguilera et al., 2016). Since, soil moisture monitoring programs are lacking in most developing countries, application of simulation models offer attractive alternatives. Calibration of such models is possible nowadays in any remote location. Thus, enabling prediction of long term soil moisture times series with a great deal of flexibility. This progress has motivated and enabled development of SMDI as implemented and reported in this thesis. In this sub-section, a framework for utilizing the developed SMDI in decision support for soil water management

is proposed as shown in Figure 8.11. The proposed framework however requires additional data from experimental trials involving different soil water methodologies to test its effectiveness.

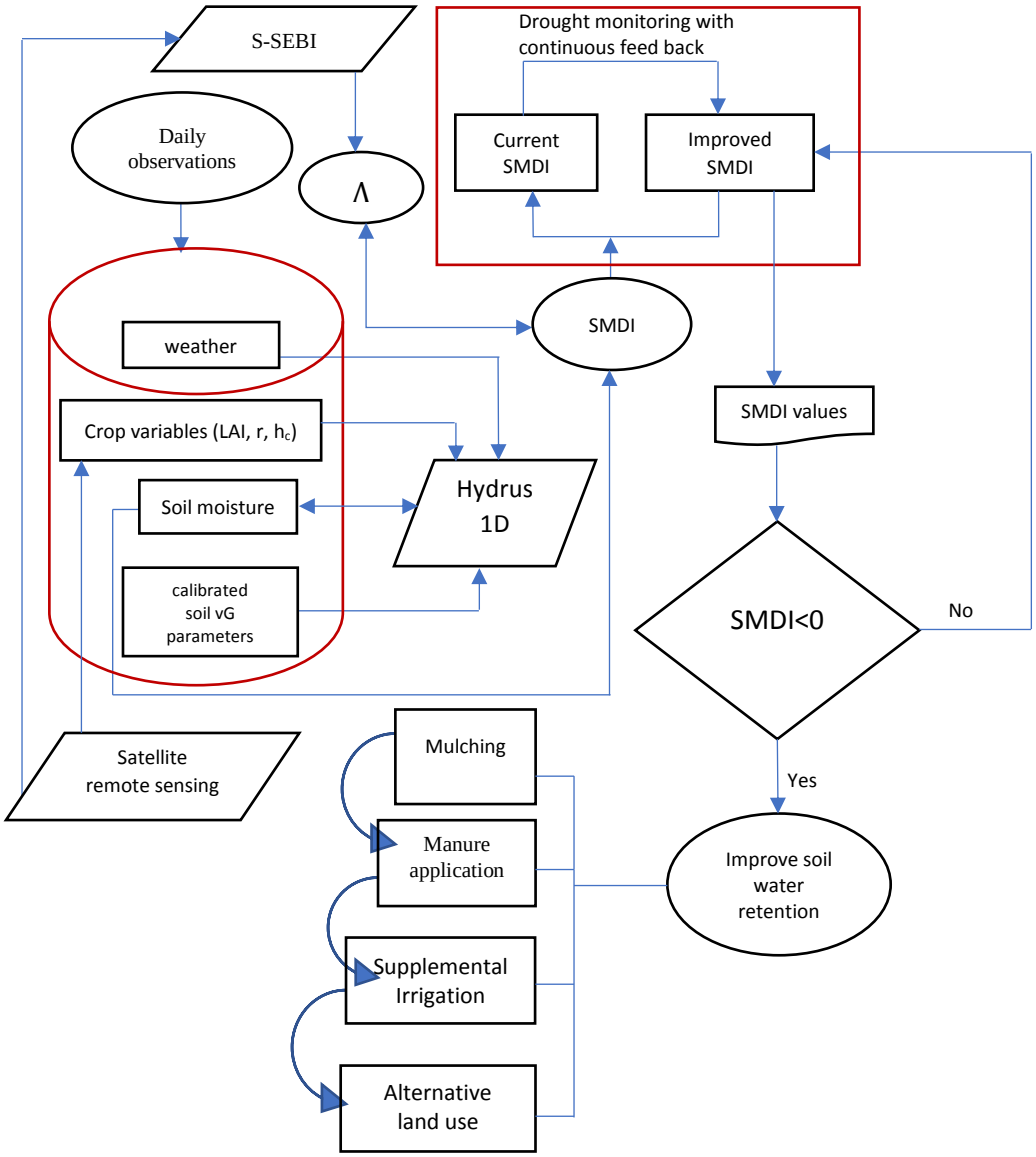

Figure 8.12 Conceptual Diagram for the application of SMDI in on farm decision making. Adopted with modifications from a decision support scheme for management of semi-arid wetland drying episodes using Soil Water Atmosphere (SWAP) numerical model developed by Aguilera et al. (2016)

It is hoped that application of SMDI in this framework will facilitate informed technological uptake/adoption of appropriate soil water management techniques rainfed farming system thereby ensuring soil and water productivity.

8.7.1 Formulating a decision support framework based on SMDI for soil water management under rain fed farming system

A decision support system refers to application of computerized tools (i.e. hardware and software) for monitoring a set of variables that determine the behavior of a complex system and for evaluating a system's response due to changes in its variables (Singh et al 2008; D'Urso 2001). In a soil water management framework, there are tools that are designed to monitor crops response to perturbations in climatic, soil factors and different farm management options. Such tools have been successfully applied in irrigation management, wetlands management and in land use planning (Aguilera et al., 2016; Navarro-Hellín et al., 2011; Pettit and Pullar, 2002). Computer based simulation models can be used to recreate past information in areas with limited historical climatic and soil productivity indicators. Such indicators are valuable parameters that can inform timely on farm decision making.

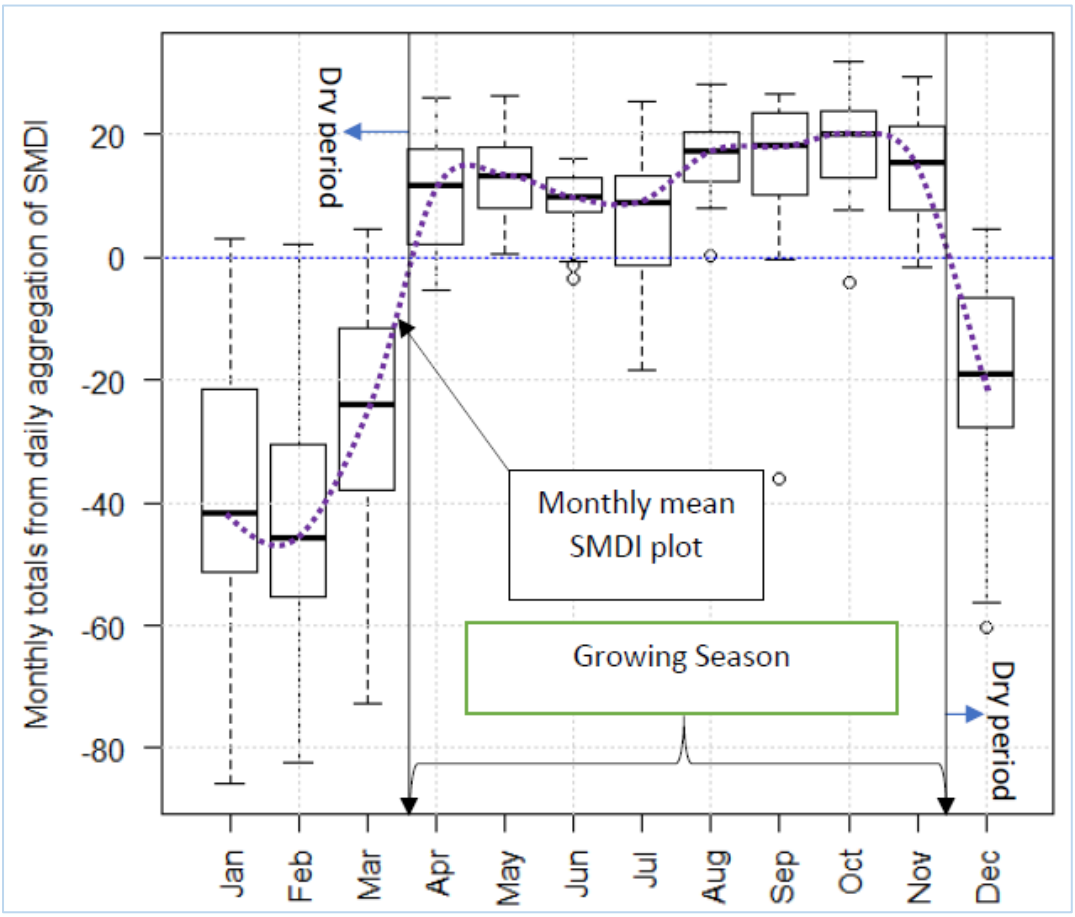

Figure 8.13 Delineation of the dry and raining season in Northern Uganda through application of SMDI

Significance of drought indices in providing decision support on insurable risks especially in dry land farming is gaining popularity in recent times (Villarroya, 2016; Kost et al., 2013;

Burke et al., 2010). For instance, NDVI derived from MODIS satellite data values have recently been used to support formulation of insurance policy for livestock keepers in semi-arid Kenya (Klisch and Atzberger, 2016; Mude et al., 2009). Similar such other application was reported in Burkina Faso (Berg et al., 2009). In this thesis SMDI has been developed for monitoring agricultural drought under rain fed farming areas. The framework under which SMDI may be used in decision support for soil water management, is in operational monitoring of agricultural drought. Through the simplified approach developed in this research, different soil water management options can be implemented and values of SMDI calculated in each case. Then, through scenario analysis based on the values of SMDI in conjunction with an economic model, best soil water management option can be selected for specific locality based on expert information obtained through the framework. This would save time and cost in choosing appropriate soil water management methods whose performance would have been analyzed a head of time before actual implementation.

8.7.2 Description of the conceptual decision scheme as applied to on farm decision support framework using SMDI

The schematization in Figure 8.11, illustrates how SMDI can be applied to support an on-farm management decision. This is done through operational drought monitoring using SMDI with continuous feedback. After a water flow model such as Hydrus 1D is calibrated and possible values of the soil hydraulic parameters are known, agro-hydrological simulations following the steps presented in section 8.2, can be carried out to update SMDI. Alternatively, an energy balance model can be used to derive the evaporative fraction Λ and apply the SMDI-Λ regression equation developed to calculate values of SMDI for deciding possible the course of action. Throughout the drought monitoring, values of SMDI computed using either method can be used to check whether there is need to improve soil moisture retention through the available methods such as mulching, manure application or to even think of implementing supplemental irrigation. The last resort can be to change the land use altogether if the options provided are not possible to implement; either because of the costs involved or some other reason such that the values of SMDI remains below zero. In a nutshell, the conceptual diagram of Figure 8.10 provides a framework under which the schematization in Figure 8.11, may be implemented.

8.7.3 Applying SMDI for analysis of monthly drought scenarios

Knowledge of monthly evolution of agricultural drought episodes can be obtained through soil moisture observations when networks of soil sensors for soil moisture monitoring exists. Alternatively values of soil moisture time series can continuously be obtained through agro-hydrological simulations as presented early on in this chapter. However, applying soil moisture directly for monitoring agricultural drought is not very realistic. Therefore, soil moisture availability to plants is considered for the calculation of the SMDI. When soil moisture content falls below 75% of field capacity plants begin to experience moisture stress, this corresponds to the value of SMDI = 0. Therefore, the average monthly values of SMDI<0 can be calculated throughout the long-term simulation period. This is done by averaging the values of SMDI<0 in each of the 12 months for the entire simulation period, and these monthly averages can be used to assess actual monthly drought episodes.

8.7.4 Seasonal delineation through application of the SMDI in the Northern cattle and millet agro-ecological zone

Northern Uganda has some very distinct dry periods always taken to start in December of the previous year extending to the end of March of the following year. This has been based on local experience and some reported studies that have been carried out in the region over the years (Nsubuga et al., 2014; Basaliriwa. 1990; Ogalo, 1981). However, these studies were conducted based on some general analysis of rainfall distribution in the area. Application of such results to distinctly delineate seasonal time boundaries for supporting farm planning decisions cannot be very reliable since it is known that meteorological droughts always precedes agricultural droughts. Such seasonal delineation requires knowledge of soil moisture over long periods of time to calculate some probabilities of expecting soil moisture of a certain threshold to be consistently exceeded either negatively or positively to decide the setting in of a new season (Torres et al., 2013). This can best be achieved through analyzing daily values of SMDI and computing the number of times it is below zero to decide the setting in for example of a dry season and vice versa for deciding the setting in of a wet season.

8.7.5 Applying the SMDI-Λ regression equation to map out drought prune areas in Northern Uganda

Northern Uganda is fairly homogenous in terms of agro-meteorological conditions. However, there are subtle variations that can best be decided by specialization of the drought

indices over the entire region to map out areas that are exposed to frequent droughts. This can be achieved through application of the SMDI- Λ regression equation developed in section 8.6. Routine availability of cloud free satellite remote sensing images in the dry seasons offer promising possibility to apply the energy balance model, S-SEBI to derive Λ from which SMDI can be computed through the regression modeling. Spatial variability in the values of SMDI can help in deciding drought prune areas, since areas that have received more rainfall during the rainy season should have more positive values of SMDI than those that have received less rainfall. As shown in Figures 8.14 – 8.17, drought prune areas can be marked out on each of the map layers. The different maps can then be overlaid on one another to identify persistent drought prune areas.

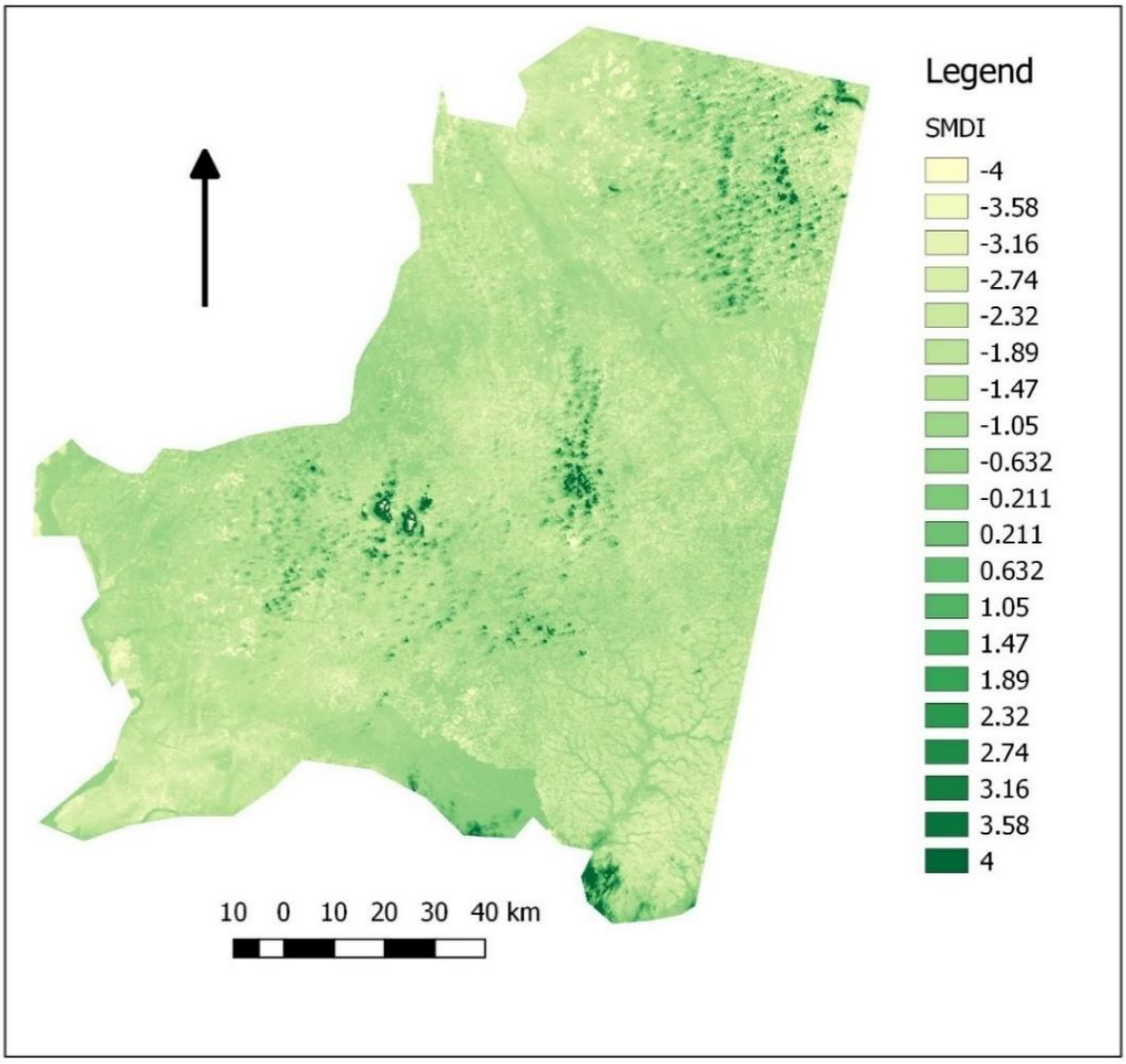

Figure 8.14 SMDI map generated from SMDI-Λ regression Equation for August 13, 2015. Image (path =172, row = 58)

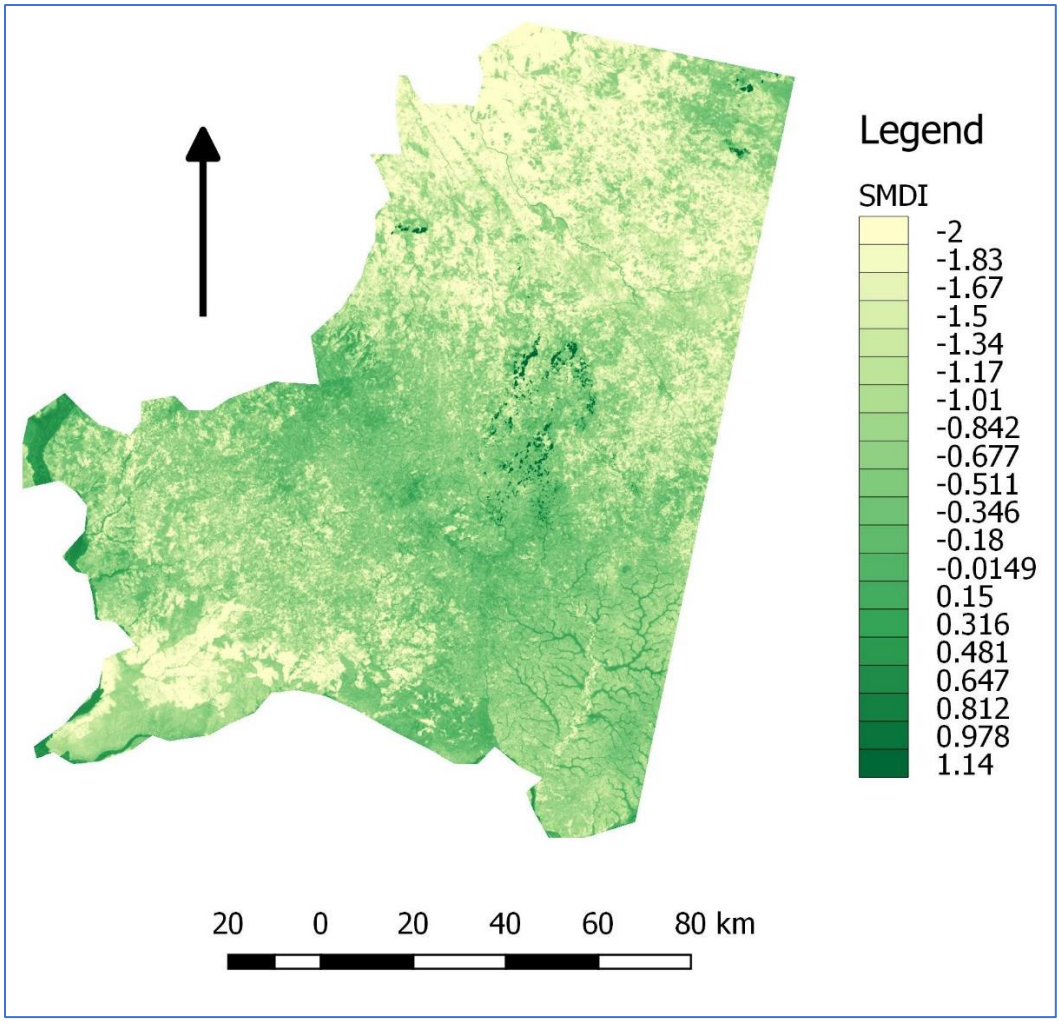

Figure 8.15 SMDI map generated from SMDI-Λ regression Equation for Jan 14, 2015. Image (path =172, row = 58)

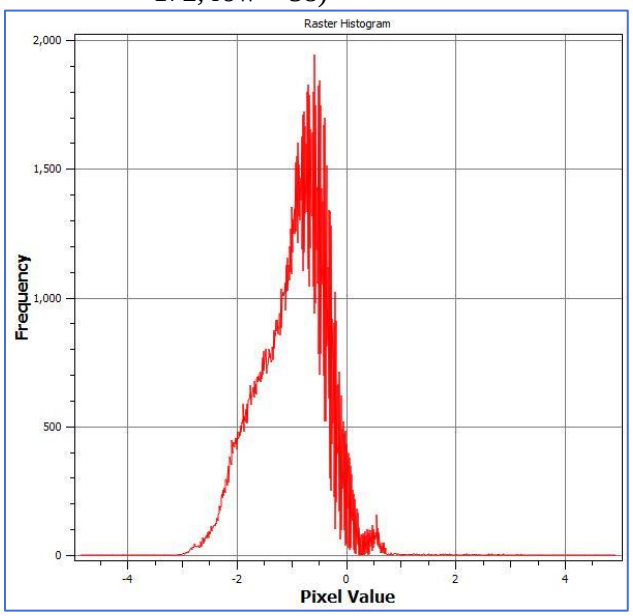

Figure 8.16 Pixel Histogram of SMDI values for January 14, 2014 Image showing values of SMDI concentrating between -2 and 1.5 thus, clearly showing the dry periods usually experienced in January. Image (path =172, row = 58)

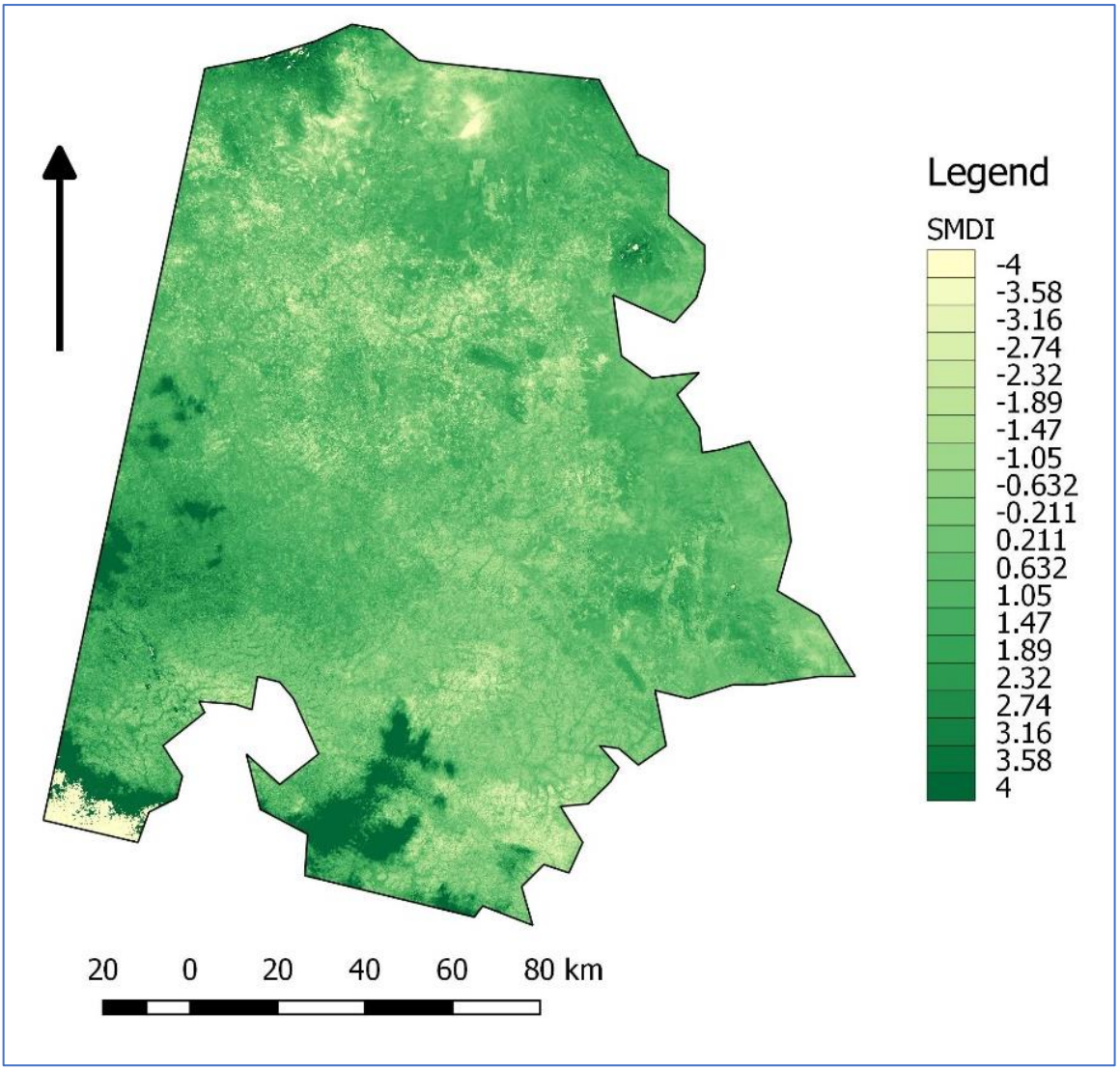

Figure 8.17 SMDI map generated from SMDI-Λ regression Equation for May 18, 2015. Image (path =171, row = 58)

8.8 Conclusion

In this chapter SMDI development was achieved through a case study in Northern Uganda by carrying out a long-term agro-hydrological simulation for 21 years to generate soil moisture time series from which the threshold parameters for the calculation of SMDI are estimated. Results obtained demonstrated good agreement between the threshold parameters generated from the long-term simulations. Verification of SMDI through application of three reference indices showed positive linear relationship with SMDI in each case. Values of SMDI<0 equivalent to drought periods correlated negatively with yield data obtained for seven seasons between 2007 and 2015 in the study area. This further illustrates the appropriateness of SMDI

for agricultural drought monitoring in the study area. Since a negative correlation is expected between values of a good drought indicator and yields.

A regression equation was further established between SMDI and Λ and later verified with a different set of images in the study area. this regression equation can be used to upscale SMDI to the entire agro-ecological zone. Finally, the SMDI was used to develop a soil water management decision support scheme that can be applied in the study area to select appropriate soil water conservation options in the study area based on values of SMDI generated continuously through application of the agro-hydrological model or through the energy balance model based on the established regression equation.

9. GENERAL CONCLUSIONS AND FUTURE OUTLOOK

9.1 General Conclusions

The primary goal of most soil water management programs in agricultural production systems is to provide mitigation measures against the impacts of agricultural droughts. Developing such measures to mitigate against drought impacts for developing countries where crop production is predominantly rainfed coupled with increasing climatic unpredictability is no easy task. As obstacles such as limited climatic data and lack of relevant information on soil characteristics have to be dealt with. However, currently, there are tools that can be harnessed to address these problems. Many of the tools were developed with these problems in focus and therefore are based on proper understanding of the physics that govern water movement in the SPAC. Freely available numerical codes for agro-hydrological simulations can be calibrated almost in any remote location to aid in generating soil moisture time series that are very critical in drought mitigation. Calibration of such numerical codes are very demanding especially if one hopes to apply distributed parameter models for simulating water dynamics in large spatial extents. However, for 1-dimensional agro-hydrological simulations the codes can be calibrated by applying other related tools that are either freely available or can be obtained at low costs.

The approach in this thesis has been to integrate these tools with limited climatic and soil data at a study site in Northern Uganda to develop a SMDI (Soil Moisture Deficit Index) for monitoring agricultural drought under rain fed farming system. SMDI can be used to support Soil water management decisions in developing countries to decide among alternative soil water conservation options for specific application areas under rain fed farming system.

The new approach for the definition of SMDI was developed in chapter 4. The approach takes into consideration the fact that merely availability of soil moisture time series is not enough to monitor agricultural drought. It requires explicit specification of soil water availability to plants through knowledge of the water retention threshold parameters such as water content at field capacity (θ_{FC}) and that at wilting point (θ_{WP}). SMDI as defined in this thesis is derived from these threshold parameters with the assumption that plants begin to experience water deficit when soil water content falls to 75% below its value at field capacity. Therefore, the tasks involved in this approach was to integrate all the available tools to generate these threshold parameters. It is widely recognized through the reviewed literatures that application of laboratory methods to generate these values are impractical for operational

application as the laboratory samples are always not representative of the actual field conditions. An alternative method through application of regression relations between these values and soil physical properties in what is termed pedotransfer functions (PTFs), cannot be applied in most developing countries. This is because most of the developed PTFs are based on soil physical characteristics in temperate and Mediterranean soils. Therefore, the approach developed in chapter 4 was to apply calibrated water flow model such as Hydrus 1D to generate long term soil moisture time series through which the threshold parameters can be calculated. In advanced countries where soil moisture monitoring networks exist, soil moisture observations can be directly applied. However, even in developed countries, the length of most soil moisture monitoring networks rarely exceeds 20 years, therefore the application of this method can still be appropriate for any location. Moreover, such soil moisture monitoring networks rarely exist in most developing countries, and this is the main driving motivation for application of the approach in this study.

Different methods exist for the calculation of these threshold values from long term records of soil moisture time series. The method used in this thesis apply arrangement of long term soil moisture time series from smallest to greatest and taking the 95^{th} percentile to represent θ_{FC} and the 5^{th} percentile to represent θ_{WP}. Other method that have been used in the reviewed literatures are the long-term minimum value to represent θ_{WP} and the minimum of the growing season long term maximums to represent θ_{FC} considering seasonal values of the soil moisture time series. chapter 4 concluded by elaborating on algorithms to calculate reference indices i.e. SPI and SPEI for verification of SMDI in the study area.

Generation of the long-term soil moisture time series require calibration of the agro-hydrological models. This was achieved through chapters 5, 6 and 7. Chapter 5 covered evaluations of less data intensive evapotranspiration models in the study area since data for the recommended FAO-56PM model are always lacking in developing countries. Chapter 5 also covered application of the data propagation algorithms to fill gaps in climatic records and to extend the limited records to cover as long time period as far as the gridded reanalysis data availability permits. Two sources of the gridded reanalysis data were evaluated based on a 4-year meteorological observations in the study area.

Chapter 6 covered application of satellite remote sensing principles to estimate crop growth parameters that are always needed for input for detailed calibration of agro-hydrological models. Chapter 7 covered presentation of calibration methodologies and results

using a case study in Northern Uganda. In the methodologies, soil hydraulic parameters were obtained through numerical inversion of the agro-hydrological model by application of low cost commercial soil sensors equipped with data loggers and an automatic weather station both of which were installed in the study site for two seasons to generate soil moisture data, matric potential data and meteorological data for input into the agro-hydrological model for the numerical inversion. The first season data were used for calibration and the second season data were used for validation.

The actual implementation of the calibrated agro-hydrological model for long term simulation of soil moisture time series was done in chapter 8. Through the long-term simulations, values of θ_{FC} and θ_{WP} were generated to derive the SMDI. Thereafter reference indices were calculated to verify SMDI through correlation analysis between SMDI and each of the reference indices. Yield data obtained from the study site were also used to verify the applicability of SMDI. Application of the energy balance model S-SEBI was also covered in chapter 8 to upscale SMDI through a regression equation developed between SMDI and evaporative fraction (Λ) derived from the energy balance model.

The main results of the study include calibration and validation results of the agro-hydrological simulation model Hydrus 1D. Coefficient of determination was used to compare simulated soil water storage and observations in the root zone between z = -15cm and z = -65 cm and. The results obtained are $r^2 = 0.73$ for calibration and $r^2 = 0.70$ for validation. Evaluation of the 12 reference evapotranspiration models in the study area showed that Makkink radiation model gave the best prediction of ET_0 and Thornthwaite gave the worst ET_0 prediction using FAO-56PM as a reference. The 13 ET_0 models were grouped into three categories i.e. the mass transfer category (MT-based), the Temperature category (T-based) and the radiation category (R-based). Results showed that R-based gave the best prediction of ET_0 overall followed by MT-based category and T-based category consistently overestimated ET_0 in the study area. This finding is important because many times Hargreaves method which is in a T-based category has been applied in developing countries where reliable weather data that can be found are mainly the minimum, maximum temperatures and precipitation. And many times, the Hargreaves model are not evaluated to test its suitability for the calculation of ET_0.

Values of the crop growth parameters estimated were compared to published values and the results showed that the estimated albedo values were rather low compared to published values. This is because independent measurement of r and LAI was not possible at the study

site. Whereas the LAI values were comparable to published values. A sensitivity analysis of the model output to changes in the values of LAI was conducted since LAI is considered the most important crop growth parameter. Results of the sensitivity showed that the model output is more sensitive to the values of LAI at the beginning of the growing season than in mid-season.

Verification of the developed SMDI was done using reference indices such as SPI, SPEI and AWD. Algorithms to calculate SPI and SPEI in the study area as elaborated in chapter 4 requires fitting the frequency distribution of precipitation (P) and precipitation deficit (D) on to a 2-parameter gamma probability distribution and a 3-parameter log-logistic probability distribution functions respectively. Applying Kolmogorov goodness of fit test statistic gave an acceptable goodness of fit at 95% level of significance in both cases. Pearson's correlation coefficients calculated between each of the reference indices and SMDI all showed positive linear relationship demonstrating the robustness of SMDI for agricultural drought monitoring in the study area.

SMDI was also compared to yield data for maize obtained from a research station within the same agro-ecological zone as the study site through a regression analysis. The result showed negative relationship between the values of SMDI<0 (which defines periods of drought within each season) and SMDI with $r^2 = 0.64$. a negative linear relationship is expected between the SMDI values that demonstrate occurrence of agricultural drought and yields. Thus, further demonstrating the appropriateness of SMDI for monitoring agricultural drought in the study area. Finally, a linear relationship was established between SMDI and Λ with $r^2 = 0.84$. A regression equation developed between SMDI and Λ was used to calculate SMDI using values of Λ estimated through the S-SEBI algorithm using a different set of images and the calculated SMDI values were compared with those generated through the agro-hydrological simulations. The result of the comparison obtained was $r^2 = 0.85$. This shows that energy balance can be used to spatialize SMDI in the study area.

A decision support scheme developed to manage soil moisture in the study area showed SMDI is able to delineate between the wet season and the dry season in line with local experience in the study area. Further, there is need to carry out another study to demonstrate the effectiveness of the decision support scheme for the selection of appropriate soil water conservation options for the study area basing on cost implications.

9.2 Highlights of innovative aspect of the study

The section highlights some of the innovative aspects of this research. In this study, a SMDI has been developed as a drought monitoring tool for supporting soil water management decisions under rain fed farming systems in developing countries. Some of the innovative aspects of these study are as follows:

Application of the threshold parameters i.e.: soil water content at field capacity (θ_{FC}) and that at wilting (θ_{WP}) point to define SMDI for detection of agricultural droughts when the soil moisture content fall below 75% of its value at field capacity. Early indices developed used 50% of θ_{FC} as the starting point below which crops begin to experience moisture stress, this value is considered rather low for soil types in Northern Uganda that is dominated by low activity Ferrallisols. Such soils drain so easily with the high equatorial climatic temperature experienced in Northern Uganda therefore a higher value of 75% of θ_{FC} was considered appropriate value at which plants would begin to experience moisture deficit. When soil moisture content reaches this point, for those considering implementing supplemental Irrigation, this would be the point to trigger irrigation application. This value of the soil moisture content corresponds to the value of SMDI = 0. Therefore, agricultural drought is considered to set in when the value of SMDI drops to below zero. Other studies have used the actual value of field capacity to be the value below which plants begin to experience moisture deficit. However, this is considered a more alarmist consideration since most equatorial/tropical crops varieties that are being developed through plant breeding programs have drought tolerant traits that would survive perfectly by the time soil moisture content drops to 75% of θ_{FC}.

The second innovative aspect of this study is the application of low cost commercial soil sensors and digital meteorological stations to facilitate calibration of agro-hydrological simulation model through numerical inversion. This will make it possible to conduct such a study almost in any remote location of the globe since low costs commercial soil moisture sensors are becoming more available. Moreover, application of satellite remote sensing to estimate crop growth parameters enable detailed calibration of the agro-hydrological model that can be used to generate soil moisture time series with high level of reliability that can be comparable to existence of soil moisture monitoring networks with very high level of flexibility for agricultural soil water management especially in rain fed farming system.

Application of evaluation procedure to select appropriate less data intensive evapotranspiration models in specific application areas. Many such studies for evaluation of less data intensive empirical ET_0 models have been done but not directly linked to operational application especially for agricultural drought monitoring as has been applied in this study. Besides most of those studies have attempted to calibrate for instance Hargreaves models without exploring the possibilities of using the other models that could be more appropriate than Hargreaves model.

Application of weather data propagation algorithms for gap filling limited climatic records with gridded climatic data that are becoming more available solves the ever-nagging problem of limited climatic data in developing countries. Moreover, no evaluation studies on the application of the gridded weather data have been done before in the study area as has been implemented in this study.

Lastly, a soil moisture management decision support scheme as formulated in this study can aid selection of various soil water management options in the study area using application of SMDI in a feedback mechanism. This scheme can be very useful to decide whether to apply supplemental irrigation or choose the other less costly soil water enhancement techniques. Such alternatives can be simulated ahead of time through the developed decision support scheme in conjunction with some economic models for instance thus making farming in rain fed system more predictable. And this scheme can be taken up by insurance companies to advise farmers on the possible insurable risks through evaluation of different soil water management scenarios.

9.3 Future Outlook

A research of this nature has not been done before in the study area. This makes it a bit difficult to evaluate its exact importance. However, farming in Uganda is becoming more commercially oriented with many large farms being opened especially in Northern Uganda because of the vast expanse of fertile land, some of which have never been cultivated before. Some farmers have been coming to Gulu University to seek local climatic data to understand seasonal variations based on raw facts other than relying only on local experience. This study will become more relevant to such farmers that are engaging in commercial farming with profit making as the driving motive. They will therefore need application of the decision support scheme as formulated in this study to evaluate the different soil water management options ahead of time before actual implementation.

Additionally, the involvement of many professional farmers some of whom coming from overseas is creating more interest in involving scientific knowledge for realizing improved crop productivity unlike in the past when subsistence farmers depended more on local traditional knowledge. This study therefore remains very strategic for such farmers that would wish for instance to engage in all year-round farming in an area that has distinct dry and wet seasons to know the timing and when to apply supplemental irrigation through the tools developed in this study.

The costs involved in the implementation of the tools developed in this study should therefore make it more attractive in the near future in the study area and similar other areas as more and more low cost commercial sensors become available and accessible since the world has become a global village. Through the use of internet connectivity, knowledge about low cost commercial soil sensors can be gained in any location and professional advice given in real time. Moreover, development of remote sensing technology for earth observation is becoming more advanced with higher resolution satellite images in the optical region of the electromagnetic spectrum seem to being made more available in the near future. This will make application of this methodology more accurate for agricultural drought monitoring in the coming years.

REFERENCES

Aghakouchak, A., Farahmand, A., Melton, F. S., Teixeira, J., Anderson, M. C., Wardlow, B. D., and Hain, C. R., 2015. Remote sensing of drought : Progress , challenges and opportunities. NASA Publications. Paper 151.

Aguilera, H., Aguilera, H., Moreno L., Wesseling, J G., E. Jiménez-Hernández, M E., Castaño, S., 2016. Catena Soil moisture prediction to support management in semiarid wetlands during drying episodes. *Catena*, 147: 709–724.

Allen, R.G., Pereira, L. S., Raes. D., Smith, M.,1998. Crop evapotranspiration - Guidelines for computing crop water requirements - FAO Irrigation and drainage paper 56.

Ali, A., Beg1, F., Ahmed, H. Al-Sulttani, A. H., Ochtyra, A., Jarocińska, A., Marcinkowska, A., 2016. Estimation of Evapotranspiration Using SEBAL Algorithm and Landsat-8 Data—A Case Study: Tatra Mountains Region. Journal of Geological Resource and Engineering, 6: 257–270.

Alley, W.M., 1984. The Palmer Drought Severity Index: Limitations and Assumptions. Journal of Climate and Applied Meteorology, 23(7): 1100–1109.

Amin, M., Zarch, A., Sivakumar, B., Sharma, A., 2015. Droughts in a warming climate : A global assessment of Standardized precipitation index (SPI) and Reconnaissance drought index (RDI). Journal of Hydrology, 526: 183–195.

Andersen, J., Refsgaard, J.C., Jensen, K.H., 2001. Distributed hydrological modelling of the Senegal River Basin - Model construction and validation. Journal of Hydrology, 247(3–4): 200–214.

Anderson, M.C., Kustas, W.P. & Norman, J.M., 2003. Upscaling and Downscaling - A Regional View of the Soil-Plant-Atmosphere Continuum. Agronomy Journal, 95(6): 1408–1423.

Asadi-Zarch, M.A., Sivakumar, B., Sharma, A., 2015. Droughts in a warming climate: A global assessment of Standardized precipitation index (SPI) and Reconnaissance drought index (RDI). Journal of Hydrology, 526: 183–195.

Baier, W. 1969. Concepts of soil moisture availability and their effect on soil moisture estimates from a meteorological budget. Agricultural Meteorology 6: 165–178.

Bala, E.A., Singh R.K., Gayathri, V., 2013. Review on different Surface Energy Balance algorithms for Estimation of Evapotranspiration through Remote Sensing. International Journal of Emerging Technology and Advanced Engineering, 3(7): 582–588.

Barsi, J.A., Barker,, J.L., Schott, J.R., 2003. An Atmospheric Correction Parameter Calculator for a single thermal band earth-sensing instrument. IEEE International Geoscience and Remote Sensing Symposium 2003, 0(C): 2–4.

Basalirwa, C.P.K., 1995. Delineation of Uganda into climatological rainfall zones using the method of principal component analysis. International Journal of Climatology, 15(10): 1161–1177.

Basalirwa, C.P.K., 1995. Rain gauge network dsign for Uganda. PhD Thesis, University of Nairobi.

Bastiaanssen, W.G.M. et al., 1998. A remote sensing surface energy balance algorithm for land (SEBAL), 213: 198–212.

Bautista F., Bautista, D., Delgado-Carranza, C., 2009. Calibration of the equations of Hargreaves and Thornthwaite to estimate the potential evapotranspiration in semi-arid and subhumid tropical climates for regional applications. Atmósfera, 22(4): 331-348.

Beguería, S., Vicente-Serrano, S. M., Reig, F., Latorre, B., 2014. Standardized precipitation evapotranspiration index (SPEI) revisited: Parameter fitting, evapotranspiration models, tools, datasets and drought monitoring. International Journal of Climatology, 34(10): 3001–3023.

Berg, A., Quirion, P., Sultan, B., 2009. Can weather index drought insurance benefit to Least Developed Countries' farmers? A case study on Burkina Faso. Weather, Climate and Society, 1(1): 71–84.

Berti, A., Tardivoa, G., Chiaudanib, A., Rechc, F., Borina, M., 2014. Assessing reference evapotranspiration by the Hargreaves method in. Agricultural Water Management, 140: 20–25.

Bhattarai, N., Shaw, S. B., Quackenbush, L. J., Im, J., Niraula, R., 2016. Evaluating five remote sensing based single-source surface energy balance models for estimating daily evapotranspiration in a humid subtropical climate. International Journal of Applied Earth Observation and Geoinformation, 49(July 2016): 75–86.

Biggs, T.W., Mishra, P.K., Turral, H., 2008. Evapotranspiration and regional probabilities of soil moisture stress in rainfed crops, southern India. Agric For Meteorol. 148:1585–1597

Bigirimana, P., 2012. Impacts, Rainfall Variability Risk, Drought Strategy, Management. 4–80.

Botulaa, Y.D., Cornelisa, W.M., Baertb, G., Van Ranstc, E., 2012. Evaluation of pedotransfer functions for predicting water retention of soils in Lower Congo (D.R. Congo). Agricultural Water Management, 111:1–10.

Breman, H., Debrah, K., 2003. Imporving African food Security. SAIS Review, 23: 153 – 170.

Brillante, L., Bois, B., Mathie, O., Bichet, V., Michot, D., Lévêque, J., 2014. Monitoring soil volume wetness in heterogeneous soils by electrical resistivity . A field-based pedotransfer function. Journal of Hydrology, 516: 56 – 66.

Brooks, R.H. and Corey, A.T. (1964) Hydraulic Properties of Porous Media. Hydrology Paper, Vol. 3, Colorado State University, Fort Collins.

Bulcock, L.M., Jewitt, G.P.W., 2013. Key physical characteristics used to assess water harvesting suitability. Physics and Chemistry of the Earth, 66: 89–100.

Burke, M., De Janvry, A., Quintero, J., 2010. Providing index -based agricultural insurance to smallholders : Recent progress and future promise. , pp.1–38.

Chávez, P.S.J., 1996. Image-Based Atmospheric Corrections - Revisited and Improved. Photogrammetric Engineering and Remote Sensing, 62(9): 1025–1036.

Chen M., Willgoose G.R., Saco P.M., 2014. Spatial prediction of temporal soil moisture dynamics using HYDRUS 1D. Hydrol. Process, 28: 171–185, 185.

Chertkov, V.Y., 2004. A physically based model for the water retention curve of clay pastes. Journal of Hydrology, 286(1–4): 203–226.

Choi, M. Jacobs, J. M., Anderson, M. C., Bosch, D. D., 2013. Evaluation of drought indices via remotely sensed data with hydrological variables. Journal of Hydrology, 476: 265–273.

Clausnitzer, V., Hopmans, J. W. 1995. Non-linear parameter estimation: LM_OPT. General purpose optimization code based on the Levenberg-Marquardt algorithm, *Land, Air and Water* Resources Paper No. 100032, University of California, Davis, CA.

Cobos, D.R., Chambers, C., 2005. Application Note Calibrating ECH 2 O Soil Moisture Sensors

Cowan, I.R. 1965. Transport of water in the soil-plant-atmosphere system, J. Appl. Ecol. 2:221-239.

Czarnomski, N. G. Moore, T. Pypker, J. Licata, and B. Bond. 2005. Precision and accuracy of three alternative instruments for measuring soil water content in two forest soils of the Pacific Northwest Can. J. For. Res. 35(8): 1867-1876.

Dai A., 2011. Drought under global warming: A review. Wiley Interdisciplinary Reviews: Climate Change. 2(1): 45–6 5.

Daniel, C., Wood, F.S., 1971. Fitting Equations to Data. Wiley-Inter-science, New York.

Das, P.K., Dutta, D., J. R. Sharma, J.R., Dadhwal.V.K., 2016. Trends and behaviour of meteorological drought (1901-2008) over Indian region using standardized precipitation-evapotranspiration index. International Journal of Climatology. 36(2): 909–916.

Delignette-muller, M.L. Dutang, C., 2015. fitdistrplus : An R Package for Fitting Distributions. Journal of Statistical Software. 64(4): 1–34.

Dirmeyer, P.A. Gao, X., Zhao,M., Guo,Z., Oki,T., Hanasaki, N.,., 2006. GSWP-2: Multimodel analysis and implications for our perception of the land surface. Bulletin of the American Meteorological Society, 87(10): 1381–1397.

Djaman, K., Balde, A. B., Show, A., Muller, B., Irmak, S., N'Diaye, M.K., Manneh, B., Moukoumbi, Y.D., Futakuchi, K, Saito, K., 2015. Evaluation of sixteen reference evapotranspiration methods under sahelian conditions in the Senegal River Valley. Journal of Hydrology, 3: 139–159.

Dobriyal, P., Qureshi, A., Badola, R., Hussain, S.A., 2012. A review of the methods available for estimating soil moisture and its implications for water resource management. Journal of Hydrology.458–459: 110–117.

Dorigo, W. A., Wagner, W., Hohensinn, R., Hahn, S., Paulik, C., Xaver, A., Gruber, A., Drusch, M., Mecklenburg, S. van Oevelen, P. Robock, A.,Jackson, T., 2011. The International Soil Moisture Network: A data hosting facility for global in situ soil moisture measurements. Hydrology and Earth System Sciences. 15(5): 1675–1698.

Droogers, P., 2000. Estimating actual evapotranspiration using a detailed agro-hydrological model. Journal of Hydrology, 229(1–2): 50–58.

D'Urso, G., 2001. Simulation and Management of On-Demand Irrigation Systems: A combined agro-hydrological and remote sensing approach. PhD Thesis, Wageningen University, Wageningen, The Nertherlands, 174p.

Engda, T.A., Kelleners, T.J., 2015. Soil moisture-based drought monitoring at different time scales: a case study for the U.S. Great Plains. JAWRA Journal of the American Water Resources Association. 52(1): 77–88

Espino, A., Mallants, D., Vanclooster, M., Feyen., 1996. Cautionary notes on the use of pedotransfer functions for estimating soil hydraulic properties. Agricultural Water Management. 29(3): 235–253.

Etienne, E. Devineni, N., Khanbilvardi, R., Lall, U., 2015. Development of a Demand Sensitive Drought Index and its Application for Agriculture over the Conterminous United States. Journal of Hydrology, 534(2016): 219–229

Everingham, Y.L., Muchow, R.C., Stone, R.C., Inman-Bamber, N. G., Singels, A., Bezuidenhout, C.N., 2002. Enhanced risk management and decision-making capability across the sugarcane industry value chain based on seasonal climate forecasts. Agricultural Systems , 74: 459–477.

Fang, B. & Lakshmi, V., 2014. Soil moisture at watershed scale : Remote sensing techniques. Journal of Hydrology, 516: 258–272.

FAO, 2015. Coutry Fact Sheet on Food and Agriculture Policy Trends. Country situation and

role of Agriculture in Uganda. 25 (September).

Feddes, R.A.,Raats, P.A.C., 2004. Parameterizing the Soil - Water - Plant root system. Wageningen Frontis Series, 6: 95–141.

Feddesb, R.A., 1997. The scaling characteristics of soil parameters : From plot scale heterogeneity to subgrid parameterization. , 190, pp.363–396.

Ford, T.W., Harris, E., Quiring, S.M., 2014. Estimating root zone soil moisture using near-surface observations from SMOS. Hydrology and Earth Systems Sciences, (1994): 139–154.

Fredlund, D.G., Xing, A., 1994. Equations for the soil–water characteristic curve. Canadian Geotechnical Journal 31, 521–532.

Friedlingstein, P., Cox, P., Betts, R., Bopp, L., Von Bloh, W., Brovkin, V., Cadule, P., Doney, S., Eby, M., Fung, I., Bala, G., John, J., Jones, C., Joos, F., Kato, T., Kawamiya, M., Knorr, W., Linsay, K., Mathews, H. D., Raddatz, T., Rayner, P., Reick, C., Roeckner, E., Schnitzler, K. G., Schnur, R. Strassmann, K., Weaver, A. J., Yoshikawa, C., Zeng, N., 2006. Climate – Carbon Cycle Feedback Analysis : Results from the C ^{4} MIP Model Intercomparison. Journal of Climate, 19:3337–3353.

Gadgil, S., Rao, P.R.S., Rao, K.N., 2002. Use of climate information for farm-level decision making : rainfed groundnut in southern India. , 74: 431–457.

Gardner, W., 1958. Some steady-state solutions of the unsaturated moisture flow equation with application to evaporation from a water table. Soil Sci. 85 (4), 228–232

Gautam, M., 2006. Managing Drought in Sub-Saharan Africa : Policy Perspectives. Invited Paper Prepared for a Panel Session on Drought: Economic Consequences and Policies for Mitigation at the IAAE Conference. August: 12–18, 2006.

Ginn, T.R., 2007. Richards Equation – Based Modeling to Estimate Flow and Nitrate Transport in a Deep Alluvial Vadose Zone.

Godfray, H.C.J., Beddington, J.R., Crute, I.R., Haddad, L., Lawrence, D., Muir, Pretty,J., Robinson, S., Thomas, S.M., Toulmin, C., 2010. Food Security: The Challenge of Feeding 9 Billion People. Science, 327(5967): 812–818.

Gueymard, C.A., 2006. SMARTS CODES For Windows USER ' S MANUAL.

Hao, Z., Aghakouchak, A., 2014. A Nonparametric Multivariate Multi-Index Drought Monitoring Framework. Journal of Hydrometeorology, 89–101.

Hargreaves, G.H., Allen, R.G., 2003. History and evaluation of Hargreaves evapotranspiration equation. Journal of Irrigation and Drainage Engineering-ASCE, 129(1): 53–63.

Hargreaves, G.H., Samani Z.A., 1985. Reference crop evapotranspiration from temperature. Transaction of ASCE 1(2):96-99.

Hayes, M.J., Svoboda, M.D., Wilhite, D.A., Vanyarkho, O.V., 1996. Monitoring the 1996 Drought Using the Standardized Precipitation Index. Bulletin of the American Meteorological Society, 80: 429–438.

He, T., Liang, S., Wang, D,. Wu, H.,Yu, Wang,J., 2012. Remote Sensing of Environment Estimation of surface albedo and directional re fl ectance from Moderate Resolution Imaging Spectroradiometer (MODIS) observations. Remote Sensing of Environment, 119: 286–300.

Hildebrandt, A., Kleidon, A., Bechmann, M., 2016. A thermodynamic formulation of root water uptake. Hydrology and Earth System Sciences. 20(8): 3441–3454.

Hillel, D., 1998. "Environmental Soil Physics." Academic Press, San Diego, CA.

Hoffman G. J., van Genuchten M. Th., 1983. Soil properties and efficient water use: Water management for salinity control. In: H. M. Taylor, W. R. Jordan, and T. R. Sinclair (eds.), Limitations and Efficient Water Use in Crop Production, Am. Soc. Of Agron., Madison, WI. 73-85, 1983.

Hogg, E.H., Barr, A.G., Black, T.A., 2013. A simple soil moisture index for representing multi-year drought impacts on aspen productivity in the western Canadian interior. Agric. For. Meteorol. 178–179: 173–182.

Hopmans, J.W., Nielsen, D.R., Bristow, K.L., 2002. How Useful are Small-Scale Soil Hydraulic Property Measurements for Large-Scale Vadose Zone Modeling?

Hopmans, J. W., Šimůnek, J., Romano, N., Durner, W., 2002. Inverse Modeling of Transient Water Flow, In: Methods of Soil Analysis, Part 1, Physical Methods, Chapter 3.6.2, Eds. J. H. Dane and G. C. Topp, Third edition, SSSA, Madison, WI, 963-1008

Horion, S. Carrão H., Singleton A., Barbosa P. and Vogt J., 2012. JRC experience on the development of Drought Information Systems. European Commission - Joint Research Centre - Institute for Environment and Sustainability.

Hunt, E.D., Hubbard, K.G., Wilhite, D.A., Arkebauer, T.J., Dutcher, A.L., 2009. The development and evaluation of a soil moisture index. Internaltional Journal of Climatology, 29: 747–759.

Ishihara, M.I. & Hiura, T., 2011. Modeling leaf area index from litter collection and tree data in a deciduous broadleaf forest. Agricultural and Forest Meteorology: 151(7): 1016–1022.

Islam, N. Wallender, W.W., Mitchell, J. P., Wicks, S., Howitt, R. E., 2006. Performance evaluation of methods for the estimation of soil hydraulic parameters and their suitability in a hydrologic model. Geoderma, 134: 135–151.

Jägermeyr, J., Gerten, D., Schaphoff, S., Heinke, J., Lucht, W., Rockström, J., 2016. Integrated crop water management might sustainably halve the global food gap. Environ. Res. Lett. 11 (2016) 025002

Jewitt, G., 2006. Integrating blue and green water flows for water resources management and planning. Physics and Chemistry of the Earth, Parts A/B/C, 31(15–16): 753–762.

Jime, C., Prigent, C., Aires, F., 2009. Toward an estimation of global land surface heat fluxes from multi-satellite observations, J. Geophys. Res., 114, D06305, doi:10.1029/2008JD011392114.

Jiménez-Muñoz, J.C. Sobrino, J.A., Plaza, A., Guanter, L., Moreno,J., Martínez, P., 2009. Comparison between fractional vegetation cover retrievals from vegetation indices and spectral mixture analysis: Case study of PROBA/CHRIS data over an agricultural area. Sensors, 9(2): 768–793.

Jonckheere, I., Fleck, S., Nackkaerts, K., Muys, B., Coppin, P., Weiss, M., Baret, F 2004. Review of methods for in situ leaf area index determination Part I . Theories , sensors and

hemispherical photography. Agricultural and Forest Meteorology, 121: 19–35.

Jhorar, R.K., Van Dam, J.C., Bastiaanssen, W.G.M., Feddes, R. A., 2004. Calibration of effective soil hydraulic parameters of heterogeneous soil profiles. , 285, pp.233–247.

Jhorar, R.K., Bastiaanssen, W.G.M., Feddes, R. A., Van Dam, J.C., 2002. Inversely estimating soil hydraulic functions using evapotranspiration ¯ uxes. , 258, pp.198–213.

Juma, M., Nyangena, W., Yesuf, M., 2009. Environment for Development Production Risk and Farm Technology Adoption in Rain-Fed , Semi-Arid Lands of Kenya. , (October).

Kazoora, C. 2002. Road map for resource mobilisation for the implementation of national action programme to combat desertification and land degradation in Uganda. Ministry of Agriculture, Animal Industry and Fisheries and Ministry of Finance, Planning and Economic Development, Kampala.

Ke, Ke, Y., Im, J., Park, S., Gong, H., 2016. Downscaling of MODIS One kilometer evapotranspiration using Landsat-8 data and machine learning approaches. Remote Sensing, 8(3): 1–26.

Khodaverdiloo, H., Homaee, M., van Genuchten, M. Th., Dashtaki, S. G., Deriving and validating pedotransfer functions for some calcareous soils. Journal of Hydrology, 55(1987): 1261–1274.

Kilic, A. Allen, R., Trezza, R., Ratcliffe, I., Kamble, B., Robison, C., Ozturk, D., 2016. Remote Sensing of Environment Sensitivity of evapotranspiration retrievals from the METRIC processing algorithm to improved radiometric resolution of Landsat 8 thermal data and to calibration bias in Landsat 7 and 8 surface temperature. Remote Sensing of Environment, 185: 198–209.

Kilimani, N., van Heerden, J., Bohlmann, H., Roos L., 2015. Impact of drought on the Ugandan economy . Economic Society of South Africa (ESSA) Biennial Conference, University of Cape Town, (2^{nd}-4^{th} September, 2015): 1–29.

Klisch, A., Atzberger, C., 2016. Operational drought monitoring in Kenya using MODIS NDVI time series. Remote Sensing, 8(4).

Kogan, F.N., 1995a. Application of vegetation index and brightness temperature for drought

detection. Advances in Space Research, 15(11): 91–100.

Kogan, F.N., 1995b. Droughts of the Late 1980s in the United States as Derived from NOAA Polar-Orbiting Satellite Data. Bulletin of the American Meteorological Society, 76(5): 655–668.

Kongo, V.M., Jewitt, G.P.W., 2006. Preliminary investigation of catchment hydrology in response to agricultural water use innovations: A case study of the Potshini catchment - South Africa. Physics and Chemistry of the Earth, 31(15–16): 976–987.

Kool, J. B., Parker, J. C., van Genuchten, M. Th., 1985. Determining soil hydraulic properties from one-step outflow experiments by parameter estimation: I. Theory and numerical studies, Soil Sci. Soc. Am. J., 49: 1348-1354.

Kosa, P., 2011. The Effect of Temperature on Actual Evapotranspiration based on Landsat 5 TM Satellite Imagery. Evapotranspiration, 56(56): 209–228.

Kost, A. Laderach, P., Fisher, M., Cook, S., Gomez, L., 2012. Improving Index-Based Drought Insurance in Varying Topography: Evaluating Basis Risk Based on Perceptions of Nicaraguan Hillside Farmers. PLoS ONE, 7(12): 1–11.

Kosugi, K., 1996. Lognormal distribution model for unsaturated soil hydraulic properties, Water Resour. Res., *32*(9): 2697-2703.

Kularathna, M.D.U.P., 1992. Application of dynamic programming for analysis of complex water resources systems. PhD Thesis, Wageningen Agricultural University, 163 pp.

Kutilek, M., and Nielsen, D. R., 1994. "Soil Hydrology." Catena Verlag, Cremlingen, Germany

Kwon, H., Choi, M., 2011. Error assessment of climate variables for FAO-56 reference evapotranspiration. Meteorol Atmos Phys, 112:81–90.

Lagergren, F., Lindroth, A., 2002. Transpiration response to soil moisture in pine and spruce trees in Sweden. Agric. For. Meteorol. 112, 67–85.

Laguardia, G., Niemeyer, S., 2008. On the comparison between the LISFLOOD modelled and the ERS/SCAT derived soil moisture estimates. Hydrology and Earth System Sciences Discussions, 5(3): 1227–1265.

Larsson, A. Ibrahim, O., Talantsev A., 2014. Towards a Decision Support Framework for public policy making. Stochlm University, department of computer and and System Science. pp.1–36.

Lee, K., 2010. Relative Comparison of the Local Recalibration of the Temperature-Based Evapotranspiration Equation for the Korea Peninsula. Journal of Irrigation and Drainage Engineering, 136(9): 585–594.

Levis, S., 2010. Modeling vegetation and land use in models of the Earth System. Advanced Reveiw, 1: 840–856.

Li, J., Islam, S., 1999. On the estimation of soil moisture profile and surface fluxes partitioning from sequential assimilation of surface layer soil moisture. Journal of Hydrology , 220: 86–103.

Liou, Y.A., Kar, S.K., 2014. Evapotranspiration estimation with remote sensing and various surface energy balance algorithms: a review. Energies, 7(5): 2821–2849.

Lloyd-Hughes, B. and Saunders, M. A., 2002. A drought climatology for Europe. International Journal of Climatology, 22(13): 1571–1592.

Lorite, I.J. Gavila, P., Tornero, S., J. Berengena, J., 2006. Regional calibration of Hargreaves equation for estimating reference ET in a semiarid environment. , 81: 257–281.

Loveland, T.R., Irons, J.R., 2016. Landsat 8: The plans, the reality, and the legacy. Remote Sensing of Environment, 185: 1–6.

Lü, H. Yua, Z., Zhua, Y., Drake, S., Haoa, Z., Sudicky, E. A., 2011. Dual state-parameter estimation of root zone soil moisture by optimal parameter estimation and extended Kalman filter data assimilation. Advances in Water Resources, 34(3): 395–406.

Makurira, H.,2010. Water Productivity In Rainfed: Redrawing the rainbow of water to achieve food security in rainfed smallholder systems. PhD Thesis, UNESCO-IHE, Delft, The Netherlands.

Mannocchi, F., Todisco, F., Vergni, L., 2004. Agricultural drought: Indices, definition and analysis. The Basis of Civilization - Water Science? (Proceedings of die UNESCO/IAHS/IWIIA symposium held in Rome. December 2003), (286), pp.246–254.

Manoli, G., Bonetti, S., Scudiero, E., Morari, F., Putti, M., Teatini, P., 2015. Modeling Soil – Plant Dynamics : Assessing Simulation Accuracy by Comparison with Spatially Distributed Crop Yield Measurements.Vadose Zone J. doi:10.2136/vzj2015.05.0069

Marletto, V., Zinoni F., Botarelli L., Alessandrini C., 2005. Studio dei fenomeni siccitosi in Emilia-Romagna con il modello di bilancio idrico CRITERIA. Rivista Agrometeorologia, 10(1): 32–33.

Marletto, V., Zinoni, F., 2004. Un indicatore di siccità agricola: applicazione alla siccità estiva del 2003 in Emilia-Romagna, pp.1–8.

Marquardt, D.W., 1963. An algorithm for least-squares estimation of nonlin- ear parameters. SIAM J. Appl. Math. 11:431–441.

Martí, P., Zarzo, M., Vanderlinden, K., Girona, J., 2015. Parametric expressions for the adjusted Hargreaves coefficient in Eastern Spain. Journal of Hydrology, 529: 1713–1724.

Martínez-Fernández, J. González-Zamora, A., Sánchez, N., Gumuzzio, A., 2015. A soil water based index as a suitable agricultural drought indicator. Journal of Hydrology, 522: 265–273.

Martínez-Fernández, J. González-Zamora, A., Sánchez, N., Gumuzzio., Herrero-Jiménez, C. M., 2016. Satellite soil moisture for agricultural drought monitoring: Assessment of the SMOS derived Soil at: Remote Sensing of Environment, 177, pp.277–286. AvailableWater Deficit Index.

Masih, I. et al., 2014. A review of droughts on the African continent: A geospatial and long-term perspective. Hydrology and Earth System Sciences, 18(9): 3635–3649.

Mattar, C., Maskey, S., Mussá, F.E.F., Trambauer, P., 2014. Impacts of the broadband albedo on actual evapotranspiration estimated by S-SEBI model over an agricultural area. Remote Sensing of Environment, 147, pp.23–42.

McKee T.B., Doesken N.J., Kiest, J., 1995. Drought monitoring with multiple time scales. Proceedings of the 9th Conference on Applied Climatology, pp.233–236.

Minasny, B. and Field, D.J., 2006. Estimating soil hydraulic properties and their uncertainty : the use of stochastic simulation in the inverse modelling of the evaporation method. ,

126(2005), pp.277–290.

Minasny, B., McBratney, A.B. 2002. The neuro-m method for fitting neural network parametric pedotransfer functions. Soil Sci. Soc. Am. J. 66(2): 352-361.

Mishra, A.K., Singh, V.P., 2010. A review of drought concepts. Journal of Hydrology, 391(1–2): 202–216.

Montzka, C., Moradkhani, H., Weihermüller, L., Franssen, H-J. H, Canty, M., Vereecken., H., 2011. Hydraulic parameter estimation by remotely-sensed top soil moisture observations with the particle filter. Journal of Hydrology, 399(3–4): 410–421.

Moran, M.S. Kerr, J.Q.Y.H., Weltz, M., Huete, A.R., Sorooshian, S., Bryant R., 1992. Evaluation of simplified procedures for retrieval of land surface reflectance factors from satellite sensor output. Remote Sensing of Environment, 41(2–3): 169–184.

Mude, A., Barrett, C.B., Carter, M.R., Chantarat, S., Ikegami, M., McPeak, J., 2009. Index Based Livestock Insurance for Northern Kenya's Arid and Semi-Arid Lands: The Marsabit Pilot. SSRN Electronic Journal.

Muniandy, J.M., Yusop, Z., Askari, M., 2016. Evaluation of reference evapotranspiration models and determination of crop coefficient for Momordica charantia and Capsicum annuum. Agricultural Water Management, 169: 77–89.

MW&E., 2011. A National Irrigation Master Plan: Republic of Uganda, A report from the Ministry of Water and Environment.

Myhill, A., Allen, J., 2002. The Extent and Nature of the Problem of Land degradationin Uganda. Home Office.

Narasimhan, B. et al., 2005. Srinivasan, R., Arnold, J. G., Di Luzio M., 48: Estimation of long-term soil moisture using a distributed parameter hydrologic model and verification using remotely sensed data. ASABE, 48(3): 1101–1113.

Narasimhan, B., Srinivasan, R., 2005. Development and evaluation of Soil Moisture Deficit Index (SMDI) and Evapotranspiration Deficit Index (ETDI) for agricultural drought monitoring. Agricultural and Forest Meteorology,133: 69–88.

Naumann, G. Barbosa, P., Garrote, L., Iglesias, A., Vogt, J., 2014. Exploring drought vulnerability in Africa: An indicator based analysis to be used in early warning systems. Hydrology and Earth System Sciences, 18(5): 1591–1604.

Navarro-hellín, H., Martínez-del-Rincon, J., Domingo-Miguel, R., Soto-Valles, F., Torres-Sánchez, R., 2016. Original papers A decision support system for managing irrigation in agriculture. , 124: 121–131.

Neuman, S. P., Feddes, R. A., Bresler, E.,1974. Finite element simulation of flow in saturated unsaturated soils considering water uptake by plants. Third Annual Report, Project No. A10-SWC-77, Hydraulic Engineering Lab., Technion, Haifa, Israel.

Nicholson, S.E., 2001. Climatic and environmental change in Africa during the last two centuries. Climate Research, 17: 123–144.

Nielsen, D. R., Luckner, M., 1992. Theoretical aspects to estimate reasonable initial parameters and range limits in indentification procedures for soil hydraulic properties. In, Proc. Intl. Workshop on Indirect Methods for Estimating the Hydraulic Properties of Unsaturated Soils, edited by M. Th van Genuchten, F. J. Leij, and L. J. Lund, University of California, Riverside, pp. 147-160.

Niemeyer, S., 2008. New drought indices. *Options Méditerranéennes*, 80(80): 267–274.

Nijbroek, R.P., Andelman, S.J., 2016. Regional suitability for agricultural intensification : a spatial analysis of the Southern Agricultural Growth Corridor of Tanzania. International Journal of Agricultural Sustainability, 14(2): 231–247

Norman, J.M., Anderson, M.C., 2003. SOIL – PLANT – ATMOSPHERE CONTINUUM. , (1982).

Nsubuga, F.N.W., Namutebi, E.N., Nsubuga-ssenfuma, M., 2014. Water Resources of Uganda : An Assessment and Review. Journal of Water Resource and Protection, 6: 1297-1315,

Ntale, H.K. & Gan, T.Y.E.W., 2003. Drought Indices And Their Application To East Africa. Int. J. Climatol. 23: 1335–1357.

Nyeko, M., 2010. Land Use Changes in Aswa Basin-Northern Uganda: Opportunities and Constrains to Water Resources Management. PhD Thesis, University Of Naples Federico II Faculty Of Agriculture.

Ogallo, L., 1981. Trend of rainfall in East Africa. Kenya Journal of Science and Technology, (A) (1981) 2: 83-90

Oguntunde, P.G., Van De Giesen, N., 2004. Crop growth and development effects on surface albedo for maize and cowpea fields in Ghana, West Africa. International Journal of Biometeorology, 49(2): 106–112.

Ojha, R. Morbidelli, R., Saltalippi,C., Flammini,A., Govindaraju, R.S., 2014. Scaling of surface soil moisture over heterogeneous fields subjected to a single rainfall event. Journal of Hydrology, 516: 21–36.

Olson, J. M. 1998. A conceptual framework of land use change in the East African Highlands. Paper read at Earth's Changing Land: Joint Global Change and Terrestrial Ecosystems and Land Use and Land Cover Change Open Science Conference on Global Change, Barcelona, Spain.

Omuto, C.T., 2009. Biexponential Model for Water Retention Characteristics. *Geoderma*, 149, 235-242.

Omuto, C.T., 2007. HydroMe: Estimation of Soil Hydraulic Parameters from Experimental data. R Comprehensive R Archive Network, USA.

Owens, T., Hoddinott, J., Kinsey, B., 2003. Ex-Ante Actions and Ex-Post Public Responses to Drought Shocks : Evidence and Simulations from Zimbabwe. World Development, 31(7): 1239–1255.

Padhee, S.K. Nikam,B.R., Aggarwal, S. P., Garg, V., 2014. Integrating effective drought index (EDI) and remote sensing derived parameters for agricultural drought assessment and prediction in Bundelkhand Region of India. International Archives of the Photogrammetry, Remote Sensing and Spatial Information Sciences - *ISPRS Archives*, 40(8): 89–100.

Palmer, W., 1965. Meteorological Drought. *Research Paper*, pp.1–65. Available at: http://www.ncdc.noaa.gov/temp-and-precip/drought/docs/palmer.pdf.

Palmer, W.C., 1968. Keeping Track of Crop Moisture Conditions, Nationwide: The New Crop

Moisture Index. Weatherwise, 21(4): 156–161.

Peng, J., Fan, W., Xu, X., Wang, L., Liu, Q., Li, J., Zhao, P., 2015. Estimating crop Albedo in the application of a physical model based on the law of energy conservation and spectral invariants. Remote Sensing, 7(11): 15536–15560.

Peng, Y., Zhang, Y., Tang, Y., Shiming, L., 2011. An incident information management framework based on data integration , data mining , and multi-criteria decision making. Decision Support Systems, 51(2): 316–327.

Peters, A.J. Walter-Shea, E. A., JI, L., Vliia, A., Hayes, M., Svoboda, M. D., 2002. Drought monitoring with NDVI-based standardized vegetation index. Photogrammetric engineering and remote sensing, 68(1): 71–75.

Pettit, C., Pullar, D., 2002. An integrated multi-scaled decision support framework used in the formulation and evaluation of land-use planning scenarios for the growth of Hervey Bay. Proceedings of the 1st Biennial Meeting of the International Environmental Modeling and Software Society, 36–41.

Pidgeoni, D., 1972. The measurement and prediction o f available water capacity of ferrallitic soils in uganda. Journal of SOU Science. 23(4): 431–441.

Purcell, L.C., Sinclair, T.R., McNew, R.W., 2003. Drought avoidance assessment for summer annual crops using long-term weather data. Agron. J. 95, 1566–1576.

Qi, J., Kerr, Y.H., Moran, M. S., Weltz, M., Huete, A.R., Sorooshian, S., Bryant, R., 2000. Leaf Area Index Estimates Using Remotely Sensed Data and BRDF Models in a Semiarid Region. Remote Sensing of Environment, 73: 18 - 30.

Qin, W., Chi, B., Oenema, O., 2013. Long-Term Monitoring of Rainfed Wheat Yield and Soil Water at the Loess Plateau Reveals Low Water Use Efficiency. PLOS ONE, 8(11), e78828: 10p

Qu, Y., Liang, S., Liu, Q., He, T., Liu, S., Li, X., 2015. Mapping Surface Broadband Albedo from Satellite Observations: A Review of Literatures on Algorithms and Products.Remote sensing, 7: 990–1020.

Rajkai, K., Kabos, S., van Genuchten, M.T., 2004. Estimating the water retention curve from

soil properties: comparison of linear, nonlinear and concomitant variable methods. Soil and Tillage Research, 79(2): 145–152.

Republic, C., Drought, N., 2017. Why Do Different Drought Indices Show Distinct Future: Drought Risk Outcomes in the U.S. Great Plains? Journal of Climate, 30: 265–278.

Rhee, J., Im, J., Carbone, G.J., 2010. Monitoring agricultural drought for arid and humid regions using multi-sensor remote sensing data. Remote Sensing of Environment, 114(12): 2875–2887.

Richards. L.A. Capillary conduction of Liquids through porous media. Physics, 1: 318 - 333

Ritter, A. Hupet, F., Mun-Carpena, R., Lambot, S., Vanclooster, M., 2003. Using inverse methods for estimating soil hydraulic properties from field data as an alternative to direct methods. Agricultural Water Management, 59: 77 - 96.

Roerink, G.J., Su, Z., Menenti, M., 2000. S-SEBI: A simple remote sensing algorithm to estimate the surface energy balance. Physics and Chemistry of the Earth, Part B: Hydrology, Oceans and Atmosphere, 25(2): 147–157.

Romano, N., 2014. Soil moisture at local scale : Measurements and simulations. Journal of Hydrology, 516: 6–20.

Romano, N., Palladino, M., Chirico, G.B., 2011. Parameterization of a bucket model for soil-vegetation-atmosphere modeling under seasonal climatic regimes. Hydrology and Earth System Sciences, 15(12): 3877–3893.

Romano, N., Palladino, M., 2002. Prediction of soil water retention using soil physical data and terrain attributes. Journal of Hydrology, 265, pp.56–75.

Russo, D., 1988. Determining soil hydraulic properties by parameter estimation: On the selection of a model for the hydraulic properties, Water Resour. Res., 24, 453-459.

Ryu, J.H., Sohrabi, M., Acharya, A., 2014. Toward Mapping Gridded Drought Indices to Evaluate Local Drought in a Rapidly Changing Global Environment. Water Resour Manage 28:3859–3869.

Sahoo, B., Walling, I., Deka, B.C., Bhatt, B. P., 2012. Standardization of Reference Evapotranspiration Models for a Subhumid Valley Rangeland in the Eastern Himalayas. Journal of Irrigation and Draingae Engineering, ASCE, (October), pp.880–896.

Sánchez, N. et al., 2012. Water balance at plot scale for soil moisture estimation using vegetation parameters. *Agricultural and Forest Meteorology*, 166–167, pp.1–9.

Savva, A.P., Frenken, K., 2002. A FAO manual of Crop Water Requirements and Irrigation Scheduling.

Seki, K., Ackerer, P. & Lehmann, F., 2015. Sequential estimation of hydraulic parameters in layered soil using limited data. Geoderma, 247–248, pp.117–128.

Settin, T. Botter, G., Rodriguez-Iturbe, I., Rinaldo A., 2007. Numerical studies on soil moisture distributions in heterogeneous catchments. Water Resources Research, 43(5): 1–13.

Shiferaw, B., Tesfaye, K., Kassie, M., Abate,T., Prasanna,B. M., Menkir, A., 2014. Managing vulnerability to drought and enhancing livelihood resilience in sub-Saharan Africa: Technological, institutional and policy options. Weather and Climate Extremes, 3: 67–79.

Shin, Y., Mohanty, B.P., 2013. Development of a deterministic downscaling algorithm for remote sensing soil moisture footprint using soil and vegetation classifications. Water Resources Research, 49: 6208–6228.

Shokoohi, A., Morovati, R., 2015. Basin wide Comparison of RDI and SPI Within an IWRM Framework. Water Resour Manage, 29: 2011–2026.

Sillers, W. S., Fredund, D. G., Zakerzadeh, N., 2001. Mathematical attributes of soil – water characteristics curve. Geotechnical and Geological engineering. Kulwer academic publishers. 19, 243 – 283.

Šimůnek, J. Šejna, M., Saito, H., Sakai, M., van Genuchten, M. Th., 2009. "The HYDRUS-1D software package for simulating the one-dimensional movement of water, heat, and multiple solutes in variably-saturated media. Version 4.08. HYDRUS Softw. Ser. 3. Dep. of Environ. Sci., Univ. of Calif., Riverside., (January), p.332.

Šimůnek, J., Šejna, M., van Genuchten, M. Th., 1998. The HYDRUS-1D software package for simulating the one-dimensional movement of water, heat, and multiple solutes in variably

saturated media, Version 2.0. IGWMC - TPS - 70, International Ground Water Modeling Center, Colorado School of Mines, Golden, Colorado, 162pp

Šimůnek, J., van Genuchten, M.Th., Šejna, M., 2008. Development and applications of the HYDRUS and STANMOD software packages, and related codes, Vadose Zone J., Special Issue "Vadose Zone Modeling", *7*(2): 587-600.

Šimůnek, J., Jacques, D., van Genuchten, M.Th., Mallants, D., 2006c. Multicomponent geochemical transport modeling using the HYDRUS computer software packages, J. Am. Water Resour. Assoc., 42(6): 1537-1547.

Singh, M., Singh, P., Singh, S.B., 2008. Decision Support System for Farm Management. International Journal of Biological, Biomolecular, Agricultural, Food and Biotechnological Engineering, 2(3): 346–349.

Slayter, R.O. 1967. Plant-water relationships. Academic Press, London

Skaggs, T.H., 2008. Determination of root-zone water storage in a desert woodland using a two-layer moisture balance model. Hydrological Research in China: Process Studies. Modelling Approaches and Applications (Proceedings of Chinese PUB International Symposium. Beijing. (September 2006): 246–251.

Smith, J.A., Lin, T.L., Ranson, K.J., 1980. The Lambertian Assumption and Landsat Data. Photogrammetric Engineering and Remote sensing. 46(9): 1180–1189

Sperry, J.S., Love, D.M., 2015. What plant hydraulics can tell us about responses to climate-change droughts. New Phytologist, 207: 14–27

Sepulcre-Canto, G. Horion, S., Singleton, A., Carrao, H., Vogt., J., 2012. Development of a Combined Drought Indicator to detect agricultural drought in Europe. Natural Hazards and Earth System Science, 12(11): 3519–531.

Spinoni, J., Naumann, G., Vogt, J., Barbosa, P., 2016. Meteorological Droughts in Europe: Events and Impacts – Past Trends and Future Projections, Luxembourg. JRC Techncal Report. The EU.

Sridhar, V. et al., 2008. Development of the Soil Moisture Index to Quantify Agricultural Drought and Its "User Friendliness" in Severity-Area-Duration Assessment. *Journal of*

Hydrometeorology, 9(4), pp.660–676.

Starr, J.L., and I.C.Paltineanu. 2002. Methods for Measurement of Soil Water Content: Capacitance Devices. p. 463-474. In J.H.Dane, and G.C.Topp (ed.) Methods of Soil Analysis:Part 4 Physical Methods. Soil Science Society of America, Inc., Soil Science Society of America, Inc

Stefanski, R., Drought Monitoring and Early Warning Systems. First Regional Workshop on NDMP – Bucharest - 9-11 July 2013

Su, L., Wang, Q., Wang, C., Shan, Y., 2015. Simulation models of leaf area index and yield for cotton grown with different soil conditioners. PLoS ONE, 10(11): 1–19.

Suhada, N. A. R., Askari, M., Tanaka, T., Simunek., vanGenuchten., M. Th., 2015. Geoderma Inverse estimation of soil hydraulic properties under oil palm trees. Geoderma, 241–242: 306–312.

Tabari H., Talaee, P.H., 2011. Local Calibration of the Hargreaves and Priestley-Taylor Equations for Estimating Reference Evapotranspiration in Arid and Cold Climates of Iran Based on the Penman-Monteith Model. Journal of Hydrologic Engineering, 16: 837–845.

Tani, M., 1982. The properties of a water table rise produced by a one-dimensional vertical unsaturated flow (in Japanese with an English Summary). Journal of Japan for Society. 64, 409 – 418

Tao, X., Liang, S., He, T., Jin, H., 2016. Remote Sensing of Environment Estimation of fraction of absorbed photosynthetically active radiation from multiple satellite data : Model development and validation. Remote Sensing of Environment, 184: 539–557.

Tasumi, M., Allen, R.G., Trezza, R., 2008. At-Surface Reflectance and Albedo from Satellite for Operational Calculation of Land Surface Energy Balance. Journal of Hydrologic Engineering, 13: 51–63.

Ting, Y.Y., Hao, S.S., HuaDe, G., 2012. Development of a soil-plant-atmosphere continuum model (HDS-SPAC) based on hybrid dual-source approach and its verification in wheat field. Science China Technological Sciences, 55(10): 2671–2685.

Todisco, F., Vergni, L., Mannocchi, F., 2008. An evaluation of some drought indices in the

monitoring and prediction of agricultural drought impact in central Italy. Irrigation in Mediterranean agriculture: challenges and innovation for the next decades. Bari : CIHEAM, 84: 203–211 (Options Méditerranéennes : Série A: Séminaires Méditerranéens),

Tomasella, J., Hodnett, M.G., Rossato, L., 1988. Pedotransfer Functions for the Estimation of Soil Water Retention in Brazilian Soils. , (1976): 327–338.

Too, V.K., Omuto, C.T., Biamah, E. K., Obiero, J . P., 2014. Review of Soil Water Retention Characteristic (SWRC) Models between Saturation and Oven Dryness. Open Journal of Modern Hydrology, 4: 173–182.

Torres, G. M., Lollato, R.P., Ochsner., T.E., 2013. Comparison of Drought Probability Assessments Based on Atmospheric Water Deficit and Soil Water Deficit. Agronomy Journal, 105(2): 428–436

Tsakiris, G. Pangalou, D., Vangelis, H., 2007. Drought characterization [Part 1. Components of drought planning. 1.3. Methodological component]. Drought management guidelines technical annex, 58(58): 85–102.

Tsakiris, G., Vangelis, H., 2005. Establishing a Drought Index Incorporating Evapotranspiration. , European Water 9/10: 3-11.

Ujeneza, E.L., Abiodun, B.J., 2015. Drought regimes in Southern Africa and how well GCMs simulate them. Climate Dynamics, 44(5–6): 1595–1609.

UNEP.,1994. Status and Trends of Global Biodiversity. Chapter 1, https://www.cbd.int/gbo1/chap-01.shtml.

U.S.G.S., 2005. Department of the interior geological survey. America, 8(1993).

Valor, E.; Caselles, V., 1996. Mapping land surface emissivity from NDVI: Application to European, African, and South American areas. *Remote Sens. Environ. 57*: 167–184.

Van den Berg, M., Klamt, E., van Reeuwijk, L.P., Sombroek, W.G., 1997. Pedotransfer functions for the estimation of moisture retention characteristics of Ferralsols and related soils. Geoderma, 78(3–4): 161–180.

Van de Griend, A.; Owe, M., 1993. On the relationship between thermal emissivity and the normalized difference vegetation index for natural surfaces. *Int. J. Remote Sens*. 14:1119–1131.

Van Der Knijff, J.M., Younis, J., De Roo, P.J., 2010. LISFLOOD: A GIS-based distributed model for river basin scale water balance and flood simulation. International Journal of Geographical Information Science, 24(2): 189–212.

Vangelis, H., Spiliotis, M., Tsakiris, G., 2011. Drought Severity Assessment Based on Bivariate Probability Analysis. Water Resour Manage, 25:357–371

van Genuchten, M. Th., 1981. Non-equilibrium transport parameters from miscible displacement experiments. Research Report No. 119, U.S. Salinity Laboratory, Riverside, CA.

van Genuchten, M. Th., 1980. A closed-form equation for predicting the hydraulic conductivity of unsaturated soils, Soil Sci. Soc. Am. J., 44: 892-898.

Van Ittersum, M.K. et al., 2013. Yield gap analysis with local to global relevance-A review. Field Crops Research, 143, pp.4–17.

Vereecken, H., Huismana, J.A., Pachepsky, Y., Montzkaa, C., van der Kruk, J., Bogena, H., Weihermüller, L., Herbst, M., Martinez, G., Vanderborght, J., 2014. On the spatio-temporal dynamics of soil moisture at the field scale. Journal of Hydrology, 516: 76–96.

Vermote, E. Justice, C., Claverie, M., Franch, B., 2016. Remote Sensing of Environment Preliminary analysis of the performance of the Landsat 8 / OLI land surface re fl ectance product. Remote Sensing of Environment, 185: 46–56.

Vicente-serrano, S.M., Beguería, S., Azorin-molina, C., 2015. Contribution of precipitation and reference evapotranspiration to drought indices under different climates. Journal of Hydrology, 526: 42–54.

Vicente-Serrano SM, Beguería S, Azorín-Molina C, López-Moreno JI.,2015. Contribution of precipitation and reference evapotranspiration to drought indices under different climates. Journal of Hydrology, 526: 42-54

Vicente-Serrano, S.M. Vicente-Serrano, S.M., Lopez-Moreno, J. I., Beguería, S., Lorenzo-Lacruz, J., Sanchez-Lorenzo, A., José M García-Ruiz, J.M., Azorin-Molina, C., Morán-

Tejeda, E., Revuelto, J., Trigo, R., 2014. Evidence of increasing drought severity caused by temperature rise in southern Europe. Environ. Res. Lett. 9 (2014) 044001

Vicente-Serrano, S.M., Beguería, S., López-Moreno, J.I., 2010. A Multiscalar Drought Index Sensitive to Global Warming: The Standardized Precipitation Evapotranspiration Index. Journal of Climate, 23(7): 1696–1718.

Villarroya T M., 2016. Hydrological Drought Index Insurance for Irrigated Agriculture. A Doctoral Thesis, Polytechnic University of Madrid

Wagner, N., Emmerich, K., Bonitz, F., Kupfer, K., 2011. Experimental Investigations on the Frequency- and Material Properties of Soil. , 49(7): 2518–2530.

Walthall, C.L. Norman, J. M., Welles, J. M., Campbell, G., Blad., B.L., 1985. Simple equation to approximate the bidirectional reflectance from vegetative canopies and bare soil surfaces. 24(3): 383–387.

Wang, G., 2005. Agricultural drought in a future climate: results from 15 global climate models participating in the IPCC 4th assessment. Climate Dynamics, 25(7–8): 739–753.

Wang, S., Trishchenko, Æ.A.P., 2007. Simulation of canopy radiation transfer and surface albedo in the EALCO model. Clim Dyn, 29:615–632.

Wart, J. V., Grassini, P., Yang, H., Claessens, L., Jarvisd, A., Cassman, K.G.,Grassini, P., Yang, H., Claessens, L., Jarvisd, A., Cassman, K.G., 2015. Agricultural and Forest Meteorology Creating long-term weather data from thin air for crop simulation modeling. Agricultural and Forest Meteorology, 209–210: 49–58.

Wart, J. V., van Bussel, L. G. J., Wolf, J., Licker,R., Grassini, P., Nelson, A., Boogaard, H., Gerber,J., Mueller, N. D., Claessens, L., van Ittersum, M. K., Cassman, K.G., 2013. Field Crops Research Use of agro-climatic zones to upscale simulated crop yield potential. Field Crops Research, 143: 44–55.

Waters, R., Allen, R., Tasumi, M., Trezza, R., Bastiaanssen, W., 2002. Surface Balance Algorithm for Land (SEBAL), Idaho Implementation. Advanced Training and Users' Manual, pp.1–98.

Wegehenkel, M. and Gerke, H.H., 2015. Water table effects on measured and simulated fluxes

in weighing lysimeters for differently-textured soils. , pp.82–92.

Weiss, M., Baret, F., Smith, G.J., Jonckheere, I., Coppin, P., 2004. Review of methods for in situ leaf area index (LAI) determination Part II . Estimation of LAI, errors and sampling. Agricultural and Forest Meteorology 121: 37–53..

Weiss, M., Baret, F., Leroy, M., Be'gue', A., Hautecoeur, O., Santer, R., 1999. Hemispherical reflectance and albedo estimates from the accumulation of across-track sun-synchronous satellite data .Journal of Geographical Research , 104(22): 221–232.

Wells, N., Goddard, S., Hayes, M. J., 2004. A Self-Calibrating Palmer Drought Severity Index. American Meteorological Society, 2335–2351.

Wi, S., Yang, Y. C. E., Steinschneider, S., Khalil, A. Brown, C. M., 2015. Calibration approaches for distributed hydrologic models in poorly gaged basins: Implication for streamflow projections under climate change. Hydrology and Earth System Sciences, 19(2), pp.857–876.

WMO, 2015. The Climate in Africa: 2013,

Xiaohua, Z.H.U., Yingshi Z., Xiaoming, F., 2013. A Methodology for Estimating Leaf Area Index by Assimilating Remote Sensing Data into Crop Model Based on Temporal and Spatial Knowledge. Chinese Geographical Science, 23(5): 550–561.

Xinyu, Z., Benlin, S., Yunchuan, H., Yanyann, Y., 2017. Drought characteristics of Henan province in 1961-2013 based on Standardized Precipitation Evapotranspiration Index. Journal of Geographical Sciences, 27(3): 311–325.

Yadav, M., Wagener, T., Gupta, H., 2007. Regionalization of constraints on expected watershed response behavior for improved predictions in ungauged basins. Advances in Water Resources, 30(8): 1756–1774.

Yan, D. Shi, X., Yang, Z., Li, Y., Zhao, K., Yuan, Y., 2013. Modified Palmer Drought Severity Index Based on Distributed Hydrological Simulation. Mathematical Problems in Engineering, Vol. 2013: 8p

Yu, M. Li, Q., Hayes, M. J., Svoboda, M. D., Heim, R.R., 2014. Are droughts becoming more frequent or severe in China based on the standardized precipitation evapotranspiration index: 1951-2010? International Journal of Climatology, 34(3): 545–558.

Yu, X., Guo, X., Wu, Z., 2014. Land surface temperature retrieval from landsat 8 TIRS-comparison between radiative transfer equation-based method, split window algorithm and single channel method. Remote Sensing, 6(10): 9829–9852.

Zake, J.S., Nkwijn, C., Magunda, M.K. 1999. Uganda. In: Nabhan, H., Mashali, A.M. & Mermut, A.R. (eds). Integrated soil management for sustainable agriculture and food security in Southern and East Africa. Proceedings of the Expert Consultation, Harare, Zimbabwe. AGL/MISC/23/99. FAO, Rome. ftp://ftp.fao.org/agl/agll/docs/misc23.pdf

Zargar, A., Sadiq, R., Naser, B., Khan, F.I,. 2011. A review of drought indices. Environmental Reviews, 19(NA): 333–349.

Zhang, H., Hendricks-Franssen, H., Han, X., Vrugt, J., Vereecken, H., 2016. Joint State and Parameter Estimation of Two Land Surface Models Using the Ensemble Kalman Filter and Particle Filter. *Hydrology and Earth System Sciences Discussions*, (February), pp.1–39.

Zhang, L., Jiao, W., Zhang, H., Huang C., Tong, Q., 2017. Studying drought phenomena in the Continental United States in 2011 and 2012 using various drought indices. Remote Sensing of Environment, 190: 96–106.

Zheng, G., Moskal, L.M., 2009. Retrieving Leaf Area Index (LAI) Using Remote Sensing: Theories, Methods and Sensors. Sensors, 9: 2719–2745.

ANNEXES

Annex 1:Steps to estimate reference evapotranspiration with the PM method

Annex 1:Steps to estimate reference evapotranspiration with the PM method

The term evapotranspiration (*ET*) is commonly used to describe two processes of water loss from land surface to atmosphere, evaporation and transpiration. Evaporation is the process where liquid water is converted to water vapor (vaporization) and removed from sources such as the soil surface, wet vegetation, pavement, water bodies, etc. Transpiration consists of the vaporization of liquid water within a plant and subsequent loss of water as vapor through leaf stomata. Evaporation and transpiration occur simultaneously and both processes depend on solar radiation, air temperature, relative humidity (i.e., vapor pressure deficit) and wind speed. Transpiration rate is also influenced by crop characteristics, environmental aspects, and cultivation practices. Different kinds of plants may have different transpiration rates. Not only the type of crop, but also the crop development, environment, and management should be considered when assessing transpiration. For example, when the crop is small, water is predominately lost by soil evaporation because little of the soil surface is covered by the plant, but once the crop is well developed and completely covers the soil, transpiration becomes the main process (Allen et al. 2005).

A large number of empirical methods have been developed over the last 50 years to estimate evapotranspiration from different climatic variables. Some of these derived from the now well-known Penman equation (Penman, 1948) to determine evaporation from open water, bare soil, and grass (now called evapotranspiration) based on a combination of an energy balance and an aerodynamic formula, given as:

$$\lambda E = \frac{\left[\Delta\left(R_n - G\right)\right] + \left(\gamma \lambda E_a\right)}{\left(\Delta + \lambda\right)} \qquad \text{(A1-1)}$$

Where; λE= evaporative latent heat flux (MJ m^{-2} day^{-1}), Δ= slope of the saturated vapor pressure curve, Rn = net radiation flux (MJ m^{-2} day^{-1}), G = Soil heat flux (MJ $m^{-2}day^{-1}$), γ = psychrometric constant (kPa $°C^{-1}$), and E_a = vapor transport of flux (mm day^{-1}).

Various derivation of the Penman equation included a bulk surface resistance term (Monteith, 1965), and the resulting equation is now called the Penman-Monteith equation, which may be expressed for daily values as:

$$\lambda ET_o = \frac{\Delta(R_n - G) + \left[86{,}400 \frac{\rho_a C_p (e_s - e_a)}{r_a}\right]}{\Delta + \gamma\left(1 + \frac{r_s}{r_a}\right)} \quad \text{(A1-2)}$$

$$r_a = \frac{\ln\left(\frac{z_m - d}{z_{om}}\right)\ln\left(\frac{z_h - d}{z_{oh}}\right)}{k^2 u_z} \quad \text{(A1-3)}$$

Where r_a is the aerodynamics resistance, z_m is the height of wind speed measurement, d is the zero-plane displacement height, z_h is the height of humidity measurement, z_{om} is the roughness length governing momentum transfer, zoh is the roughness length governing transfer of heat and vapour, k is the von Karman's constant =0.41 (-) and u_z is the wind speed.

$r_c = \frac{r_1}{LAI_{active}}$ where r_c is the (bulk) surface resistance, r_1 is the bulk stomatal resistance of a well illuminated leaf and LAI_{active} is effective fraction of the leaf area index actively taking part in the evapotranspiration process.

An updated equation was recommended by FAO (Allen et al.1998) with the FAO–56 Penman–Monteith equation, simplifying equation A1-2 by utilizing some assumed constant parameters for clipped grass reference crop. It was assumed that the definition for the reference crop was a hypothetical reference crop with crop height of 0.12m, a fixed surface resistance of 70sm^{-1} and an albedo value (i.e., portion of light reflected by the leaf surface) of 0.23 (Smith et al., 1992). The new equation is

$$ET_o = \frac{0.408\Delta(R_n - G) + \gamma \frac{900}{T + 273} u_2 (e_s - e_a)}{\Delta + \gamma(1 + 0.34u_2)} \quad \text{(A1-4)}$$

Where; ET_o = reference evapotranspiration rate (mm day^{-1}), T = mean air temperature (^{0}C) and u2 = wind speed (ms^{-1}) at 2m height above the ground. Equation 3 can be applied to an hourly data if the value "900" is divided by 24 for the hours in a day and the Rn and G terms are expressed as $MJm^{-2}h^{-1}$.

Required parameters to calculate ET_o

Reference evapotranspiration estimation method is based on the climatic data, which can be obtained from local meteorological station. The equation uses standard climatological records of solar radiation (sunshine), air temperature, humidity and wind speed. To ensure the integrity of computations, the weather measurements should be made at 2m (or converted to

that height) above an extensive surface of green grass, shading the ground and not short of water.

Required weather variables:

Solar radiation (R_s); Wind speed (U_2); Minimum and maximum air temperature (T_{max} and T_{mean}); Max and minimum relative humidity (RH_{max} and RH_{mean}); Dew point temperature (T_{dew}); Wet bulb temperature (T_{WB}); Dry bulb temperature (T_{DB}).

Calculation steps

Step 1: Mean daily temperature

The average daily maximum and minimum air temperatures in degrees Celsius (°C) are required. Where only average daily temperatures are available, the calculations can still be executed but some underestimation of ETo will probably occur due to the non-linearity of the saturation vapor pressure - temperature relationship (Allen et al. 1998). Average temperature is calculated by:

$$T_{mean} = \frac{T_{max}+T_{min}}{2} \quad \text{(A1-5)}$$

Where, T_{mean} = mean daily air temperature, °C; T_{max} = maximum daily air temperature, °C; T_{min} = minimum daily air temperature, °C

Step 2: Mean daily solar radiation (Rs)

The average daily net radiation expressed in megajoules per square meter per day (MJ m-2 day-1) is required. A simple average of solar radiation values obtained from a weather station in the period of 24h (0:00:01 am to 11:59:59 pm) is required. The conversion of units may be required when solar radiation is expressed in watts per square meter per day (W m-2 day-1).

$Rs\ (MJ\ m^{-2}\ day^{-1}) = Rs\ (W\ m^{-2}\ day^{-1}) * 0.0864$ (A1-6)

Step 3: Wind speed (u_2)

The average daily wind speed in meters per second (m s-1) measured at 2 m above the ground level is required. It is important to verify the height at which wind speed is measured, as wind speeds measured at different heights above the soil surface differ. The wind speed measured at heights other than 2 m can be adjusted according to the follow equation:

$$u_2 = u_h \frac{4.87}{\ln(67.8h-5.42)} \quad \text{(A1-7)}$$

Where, u_2 = wind speed 2 m above the ground surface, m s^{-1}; u_h = wind speed at the height h of measurement; h = height of the measurement above the ground surface, m. In case of wind speed is given in miles per hour (mi h^{-1}) the conversion to m s^{-1} is required.

Step 4: Slope of saturation vapor pressure curve (Δ)

For the calculation of evapotranspiration, the slope of the relationship between saturation vapor pressure and temperature, Δ, is required.

$$\Delta = \frac{4098\left[0.6108 exp\left(\frac{17.27 * T_{mean}}{T_{mean}+273.3}\right)\right]}{(T_{mean}+273.3)^2} \quad \text{(A1-8)}$$

T_{mean} = mean daily air temperature, ºC, [Eq. 5]; exp = 2.7183 (base of natural logarithm).

Step 5: Atmospheric Pressure (P)

The atmospheric pressure, P, is the pressure exerted by the weight of the earth's atmosphere. Evaporation at high altitudes is promoted due to low atmospheric pressure. This effect is, however, small and in the calculation procedures, the average value for a location is sufficient. A simplification of the ideal gas law, assuming 20°C for a standard atmosphere, can be employed to calculate P in kPa at a particular elevation:

$$P = 101.3\left[\frac{273-0.0065z}{293}\right]^{5.26} \quad \text{(A1-9)}$$

Where: z = elevation above sea level, m.

Step 6: Psychrometric constant (γ)

The psychrometric constant relates the partial pressure of water in air to the air temperature so that vapor pressure can be estimated using paired dry and wet thermometer bulb temperature readings. Another way to describe the psychrometric constant is the ratio of specific heat of moist air at constant pressure (Cp) to latent heat of vaporization. The specific heat at constant pressure is the amount of energy required to increase the temperature of a unit mass of air by one degree at constant pressure. Its value depends on the composition of the air, i.e., on its humidity. For average atmospheric conditions a Cp value of 1.013 10^{-3} MJ kg^{-1} $°C^{-1}$ can be used. As an average atmospheric pressure is used for each location, the psychrometric constant is kept constant for each location depending of the altitude [Eq. 10].

$$\gamma = \frac{C_p P}{\varepsilon \lambda} = 0.000665P \quad \text{(A1-10)}$$

γ = psychrometric constant, kPa °C-1; P = atmospheric pressure, kPa, [Eq. 10]; λ = latent heat of vaporization, 2.45, MJ kg^{-1}; c_p = specific heat at constant pressure, 1.013 10^{-3}, MJ kg^{-1} $°C^{-1}$; μ = ratio molecular weight of water vapour/dry air = 0.622.

Step 7: Delta Term (DT) (auxiliary calculation for Radiation Term)

In order to simplify the ETo calculation, several terms are calculated separated. The delta term is used to calculate the Radiation Term of the overall ETo equation (Eq. 33)

$$DT = \frac{\Delta}{\Delta+\gamma(1+0.34u_2)} \quad \text{(A1-11)}$$

Where, Δ = slope of saturation vapor curve [Eq.9]; γ = psychrometric constant, kPa °C^{-1}, [Eq.11]; u2 = wind speed 2 m above the ground surface, m s^{-1}, [Eq.7].

Step 8: Psi Term (PT) (auxiliary calculation for Wind Term)

The psi term is used to calculate the Wind Term of the overall ETo equation [Eq. 32]

$$PT = \frac{\gamma}{\Delta+\gamma(1+0.34u_2)} \quad \text{(A1-12)}$$

Where,

Δ = slope of saturation vapor curve [Eq. 9]; γ = psychrometric constant, kPa °C^{-1}, [Eq. 11]; u_2 = wind speed 2 m above the ground surface, m s^{-1}, [Eq. 9].

Step 9: Temperature Term (TT) (auxiliary calculation for Wind Term)

The temperature term is used to calculate the Wind Term of the overall ETo equation (Eq. 34)

$$TT = \left[\frac{900}{T_{mean}+273}\right] * u_2 \quad \text{(A1-13)}$$

Where, T_{mean} = mean daily air temperature, ºC, [Eq. 5].

Step 10: Mean saturation vapor pressure derived from air temperature(e_s)

As saturation vapor pressure is related to air temperature, it can be calculated from the air temperature. The relationship is expressed by:

$$e_{(T)} = 0.6108exp\left[\frac{17.27T}{T+237.3}\right] \quad \text{(A1-14)}$$

Where, e(T) = saturation vapor pressure at the air temperature T, kPa; T = air temperature, °C.

Therefore, the mean saturation vapor pressure is calculated as the mean between the saturation vapor pressure at both the daily maximum and minimum air temperatures.

$$e_{(T_{max})} = 0.6108exp\left[\frac{17.27T_{max}}{T_{max}+273.3}\right] \quad \text{(A1-15)}$$

$$e_{(T_{min})} = 0.6108exp\left[\frac{17.27T_{min}}{T_{min}+273.3}\right] \quad \text{(A1-16)}$$

Where, T_{max} = maximum daily air temperature, °C; T_{min} = minimum daily air temperature, °C. The mean saturation vapor pressure for a day, week, decade, or month should be computed as the mean between the saturation vapor pressure at the mean daily maximum and minimum air temperatures for that period:

$$e_s = \frac{e_{(T_{max})}+e_{(T_{min})}}{2} \quad \text{(A1-17)}$$

Step 11: Actual vapor pressure (e_a) derived from relative humidity

The actual vapor pressure can also be calculated from the relative humidity. Depending on the availability of the humidity data, different equations should be used.

$$e_a = \frac{e_{(T_{min})}\left[\frac{RH_{max}}{100}\right] + e_{(T_{max})}\left[\frac{RH_{min}}{100}\right]}{2} \quad \text{(A1-18)}$$

Where, e_a = actual vapour pressure, kPa; $e(T_{min})$ = saturation vapour pressure at daily minimum temperature, kPa, [Eq. 17]; $e(T_{max})$ = saturation vapour pressure at daily maximum temperature, kPa, [Eq. 16]; RH_{max} = maximum relative humidity, %; RH_{min} = minimum relative humidity, %.

Note I: (a) When using equipment where errors in estimating RH_{min} can be large, or when RH data integrity are in doubt, use only RH_{max}:

$$e_a = e_{(T_{min})}\left[\frac{RH_{max}}{100}\right] \quad \text{(A1-19)}$$

(b) In the absence of RH_{max} and RH_{min}

$$e_a = \frac{RH_{mean}}{100}\left[\frac{e_{(T\min)} + e_{(T_{max})}}{2}\right] \quad \text{(A1-20)}$$

Note II: For missing or questionable quality of humidity data, the ea can be obtained by assuming when the air temperature is close to T_{min}, the air is nearly saturated with water vapor and the relative humidity is near 100%, in other words, dew point temperature (T_{dew}) is near the daily minimum temperature (T_{min}). If T_{min} is used to represent T_{dew} then:

$$e_a = e_{(T\min)} = 0.6108exp\left[\frac{17.27T_{min}}{T_{min}+273.3}\right] \quad \text{(A1-21)}$$

Step 12: The inverse relative distance Earth-Sun (dr) and solar declination (d**)**

The inverse relative distance Earth-Sun, dr, and the solar declination, d, are given by:

$$d_r = 1 + 0.033cos\left[\frac{2\pi}{365}J\right] \quad \text{(A1-22)}$$

$$\delta = 0.409sin\left[\frac{2\pi}{365}J - 1.39\right] \quad \text{(A1-23)}$$

Where, J = number of the day in the year between 1 (1 January) and 365 or 366 (31 December). Note: to convert date (MM/DD/YYYY) to Julian in Microsoft Excel the following command can be used: = ((MM/DD/YYYY)-DATE (YEAR ((MM/DD/ YYYY)),1",1")+1)

Step 13: Conversion of latitude (φ) in degrees to radians

The latitude, φ, expressed in radians is positive for the northern hemisphere and negative for the southern hemisphere (see example below). The conversion from decimal degrees to radians is given by:

$$\varphi[Radians] = \frac{\pi}{10}\varphi[decimal\ degrees] \quad \text{(A1-24)}$$

Example 1: to convert 13º44N to decimal degrees = 13+44/60 = 13.73; Example 2: to convert 22º54S to decimal degrees = (-22) + (- 54/60) = -22.90

Step 14: Sunset hour angle (ω_s)

The sunset hour angle (…s) is given by:

$$\omega_s = arccos[-tan(\varphi)tan(\delta)] \quad \text{(A1-25)}$$

Where, φ = latitude expressed in radians, [Eq. 25]; d = solar declination, [Eq. 22];

Step 15: Extraterrestrial radiation (Ra)

The extraterrestrial radiation, Ra, for each day of the year and for different latitudes can be estimated from the solar constant, the solar declination and the time of the year by: Where, φ = latitude expressed in radians, [Eq. 25]; d = solar declination, [Eq. 24];

$$R_a = \frac{24(60)}{\pi} G_{sc}\, d_r[(\omega_s sin\phi sin\delta) + co\phi sin(\omega_s] \quad \text{(A1-26)}$$

Where, Ra is the extraterrestrial solar radiation in $MJm^{-2}day^{-1}$; G_{sc} = the solar constant 0.0820 $MJm^{-2}min^{-1}$; d_r = the inverse relative distance Earth-Sun, ω_s = the sunset hour angle in radians; φ = the latitude in radians; δ = the solar declination in radians.

Step 16: Clear sky solar radiation (Rso)

The calculation of the clear-sky radiation is given by:

$$R_{so} = (0.75 + 2E10 - 5z)R_a \quad \text{(A1-27)}$$

Where, z = elevation above sea level, m; Ra = extraterrestrial radiation, MJ m^{-2} day^{-1}, [Eq. 26];

Step 17: Net solar or net shortwave radiation (Rns)

The net shortwave radiation resulting from the balance between incoming and reflected solar radiation is given by:

$$R_{ns} = (1 - \alpha)R_s \quad \text{(A1-28)}$$

Where, R_{ns} = net solar or shortwave radiation, MJ m-2 day-1; α = albedo or canopy reflection coefficient, which is 0.23 for the hypothetical grass reference crop, dimensionless; R_s = the incoming solar radiation, MJ m^{-2} day^{-1}, [Step 2, Eq. 5];

Step 18: Net outgoing long wave solar radiation (Rnl)

The rate of longwave energy emission is proportional to the absolute temperature of the surface raised to the fourth power. This relation is expressed quantitatively by the Stefan-Boltzmann law. The net energy flux leaving the earth's surface is, however, less than that emitted and given by the Stefan-Boltzmann law due to the absorption and downward radiation from the

sky. Water vapor, clouds, carbon dioxide, and dust are absorbers and emitters of longwave radiation. It is thereby assumed that the concentrations of the other absorbers are constant:

$$R_{nl} = \sigma \left[\frac{(T_{max}+273.16)^4+(T_{min}+273.16)^4}{2}\right] \left(0.34 - 0.14\sqrt{e_a}\right) \left(1.35\,\frac{R_s}{R_{so}} - 0.35\right) \qquad \text{(A1-29)}$$

Where, Rnl = net outgoing longwave radiation, MJ m^{-2} day^{-1}; σ = Stefan-Boltzmann constant [4.903 10^{-9} MJ K^{-4} m^{-2} day^{-1}]; T_{max} = K maximum absolute temperature during the 24-hour period [K = °C + 273.16],; T_{min} = K minimum absolute temperature during the 24- hour period [K = °C + 273.16]; e_a = actual vapor pressure, kPa; R_s = the incoming solar radiation, MJ m-2 day-1, [Step 2, Eq.6]; R_{so} = clear sky solar radiation, MJ m-2 day-1, [Step 16, Eq. 27].

Step 19: Net radiation (Rn**)**

The net radiation (Rn) is the difference between the incoming net shortwave radiation (Rns) and the outgoing net longwave radiation (Rnl):

$$R_n = R_{ns} - R_{nl} \qquad \text{(A1-30)}$$

Where, Rns = net incoming solar or shortwave radiation, MJ m-2 day-1, [Step 17, Eq. 28]; Rnl = net outgoing longwave radiation, MJ m-2 day-1,[Step 18, Eq. 29]. To express the net radiation (Rn) in equivalent of evaporation (mm) Rng:

R_{ng} = 0.408Rn, (A1-31)

Where, Rn = net radiation, MJ m-2 day-1, [Eq. 30];

FS1. Radiation term (ETrad**)**

*ET*rad = *DT* R*ng (A1-32)

Where, ETrad = radiation term, mm d^{-1}; DT = Delta term, [Step 7, Eq. 11]; Rng = net radiation, mm, [Eq. 31]

FS2. Wind term (ETwind**)**

ETwind = PT * TT (es - ea) (A1-33)

Where, ETwind = wind term, mm d-1; PT = Psi term, [Step 8, Eq. 12]; TT = Temperature term, [Step 9, Eq. 13]; ea = actual vapor pressure, kPa, [Step 11, Eq. 18]; es = mean saturation vapor pressure derived from air temperature, kPa, [Step 10, Eq. 14];

Final Reference Evapotranspiration Value (ETo**)**

*ET*o = *ET*wind + *ET*rad (A1-34)

Other notes

What is measured at the meteorological station is the incoming shortwave solar radiation R_s, whereas what is needed for the calculation of the ET is net radiation R_n, given by [Eq. 30].

Values of albedo (α) i.e. the fraction of the solar radiation reaching a surface that is reflected, which is dimensionless vary from as high as 0.95 for snow to as low as 0.05 for wet bare soil. The values for the green vegetation is between 0.20 – 0.25. The green reference crop has a value of 0.23

Applying the Hagreave's method;

$$R_s = k_{R_s}\left(\sqrt{T_{max} - T_{min}}\right)R_a \quad \text{(A1-35)}$$

Where R_s is the incoming short wave radiation, R_a is the extraterrestrial radiation. Sometimes the ground heat flux G is also required, in which case it can be calculated using Eq. 36

$$G = C_G(-\beta LAI)R_n \quad \text{(A1-36)}$$

where the parameter C_G values between 0.3 and 0.4 representing the ratio G/R_n and β is the extinction coefficient that can be taken to be 0.5 although its value varies with canopy variable and solar zenith angle.

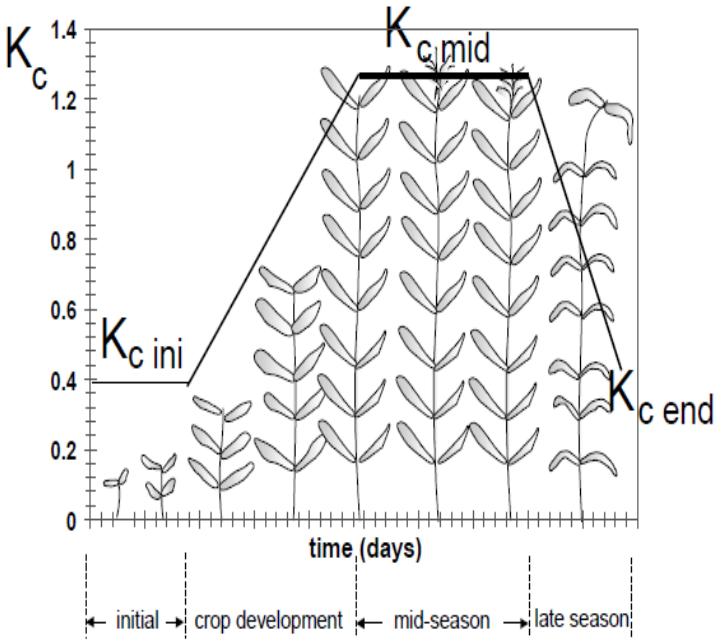

Figure A2.1 Variation of crop coefficient with crop development

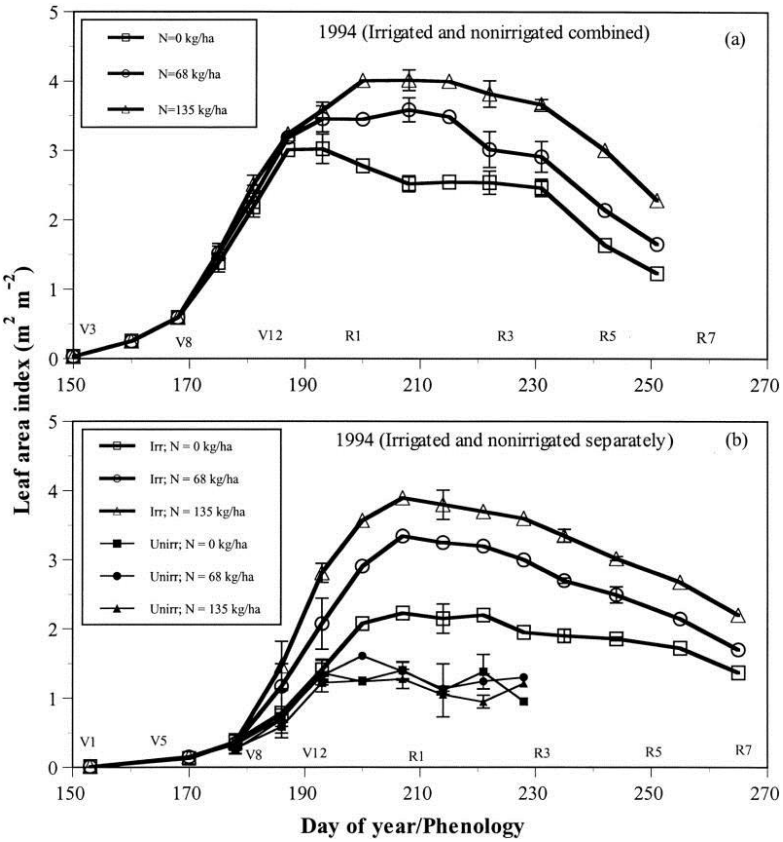

A2.1 LAI for Irrigated and non-Irrigated crops

Annex 3: Time series plots of drought evolution in the study area based on the reference indices

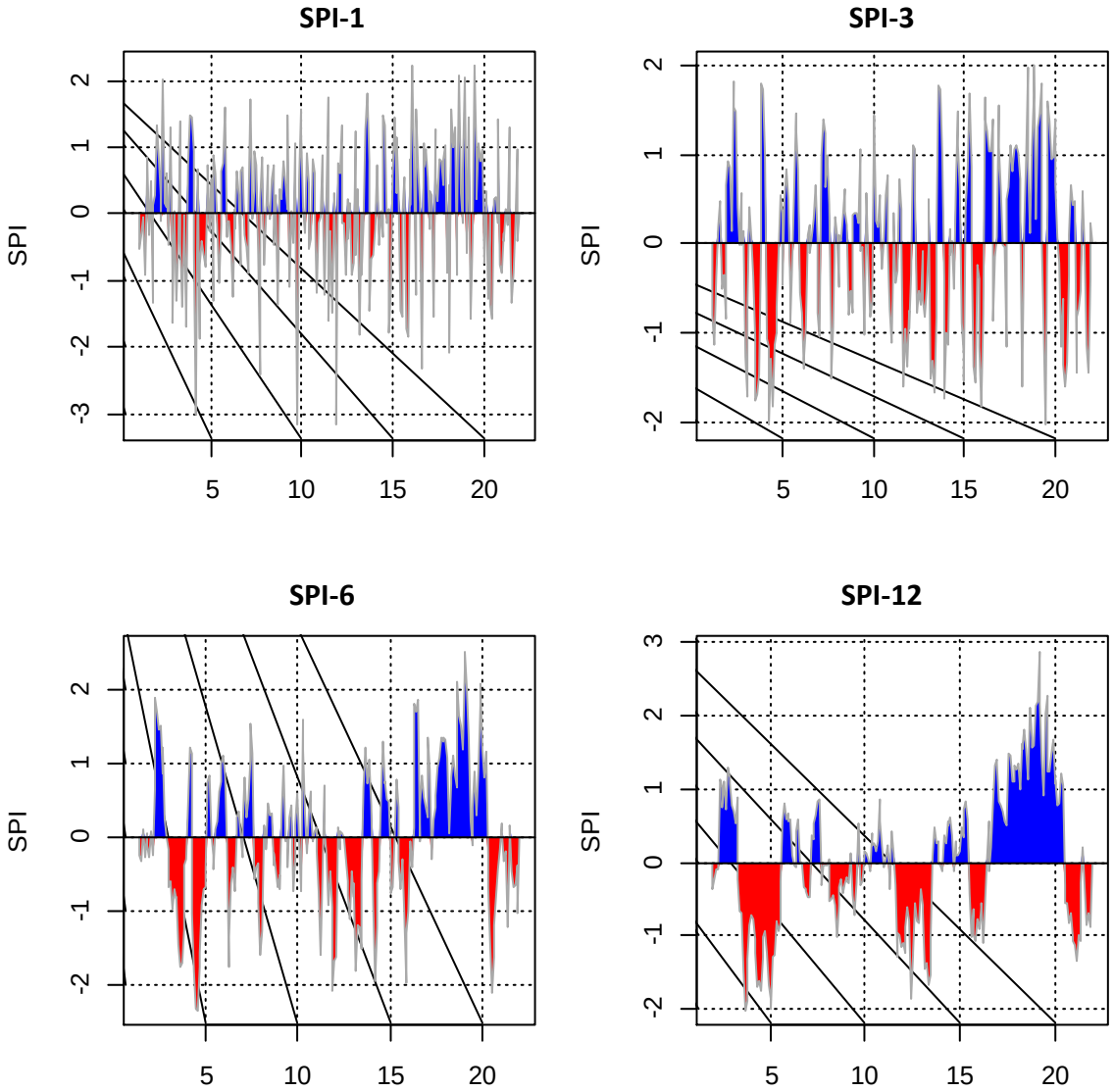

Figure A3-1. Time series of SPI for 1-, 2-, 3-, 6- and 12-monthly time scales

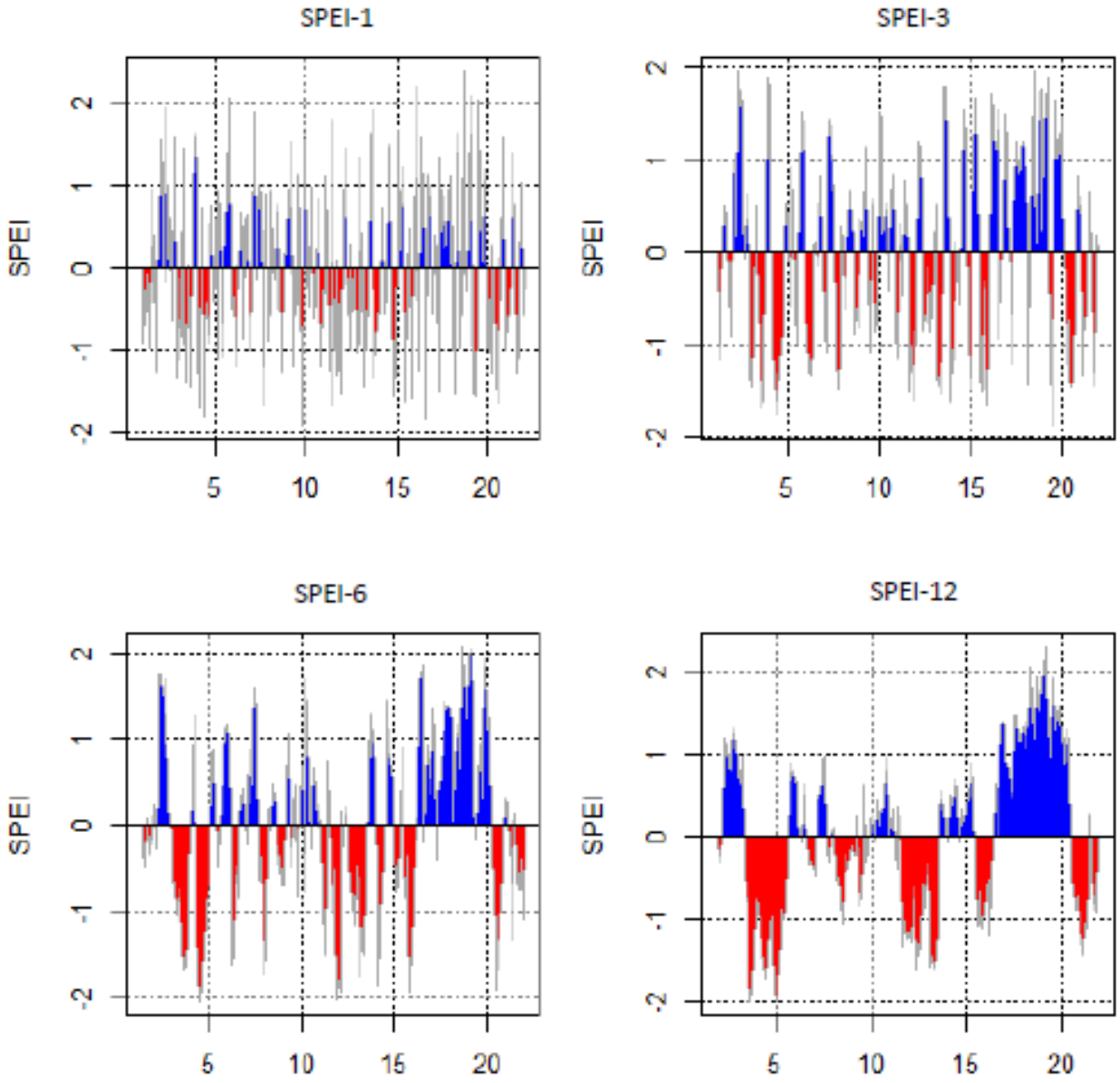

Figure A3-1. Time series of SPEI for 1-, 2-, 3-, 6- and 12-monthly time scales

Annex 4: Frequency distribution plots of the image pixel values applied to derive LST

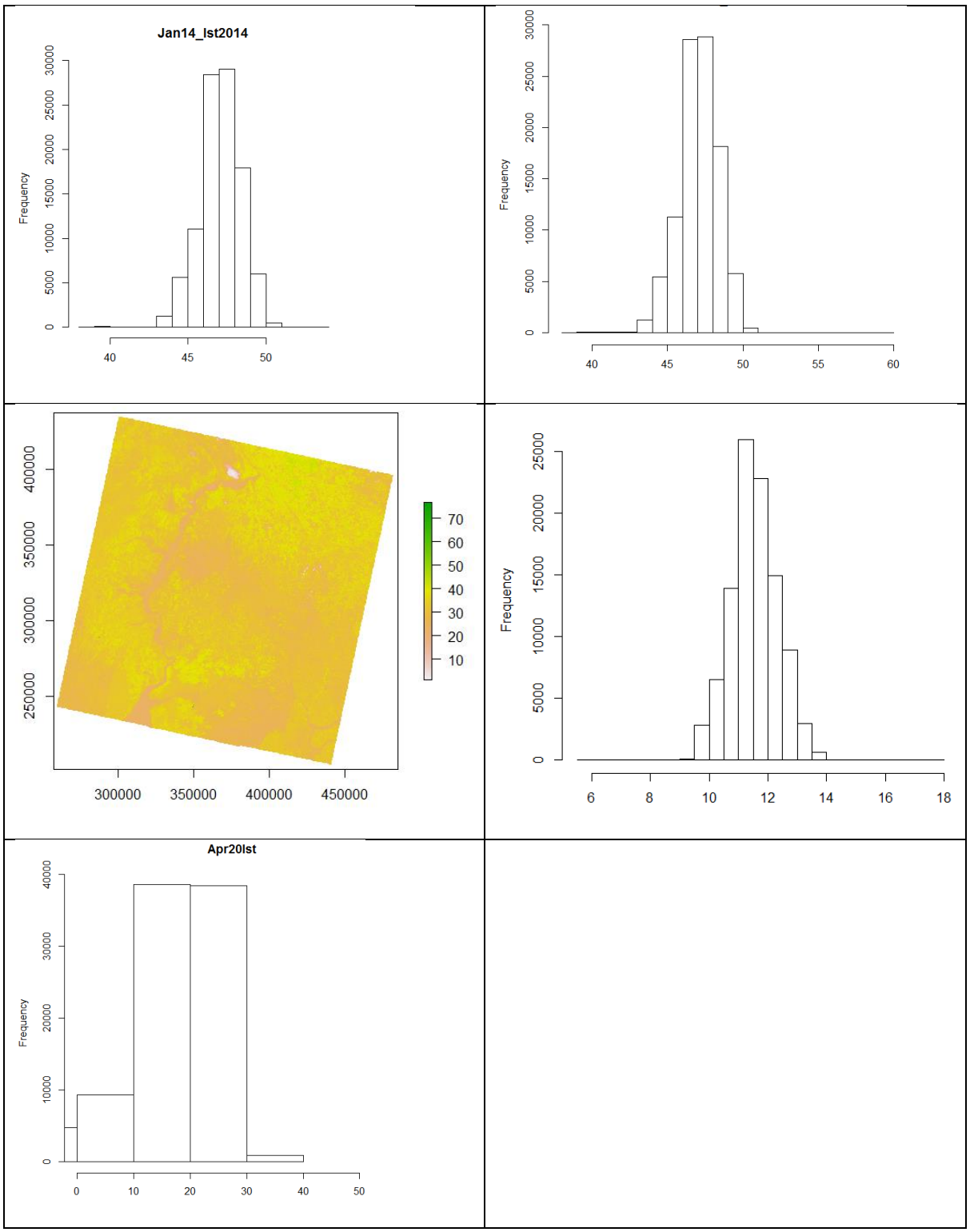

Figure A4-1. Pixel frequency distribution for LST

Annex 5: *r-LST* plots used to generate regression parameters to implement the S-SEBI algorithm

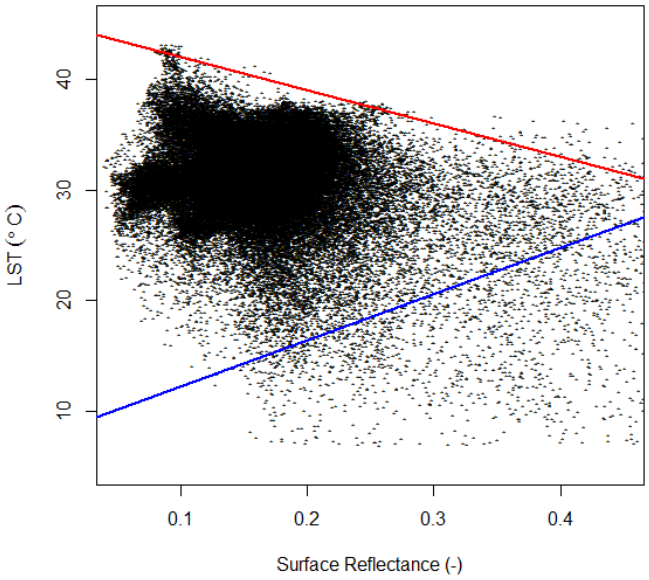

January 14, 2014

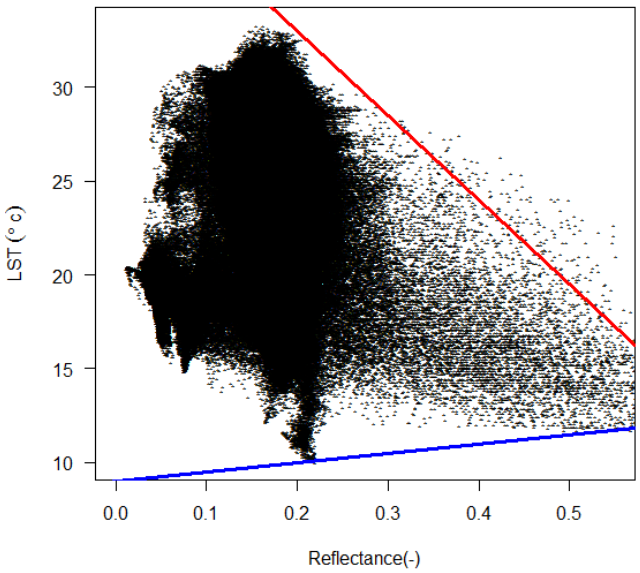

February 14, 2014

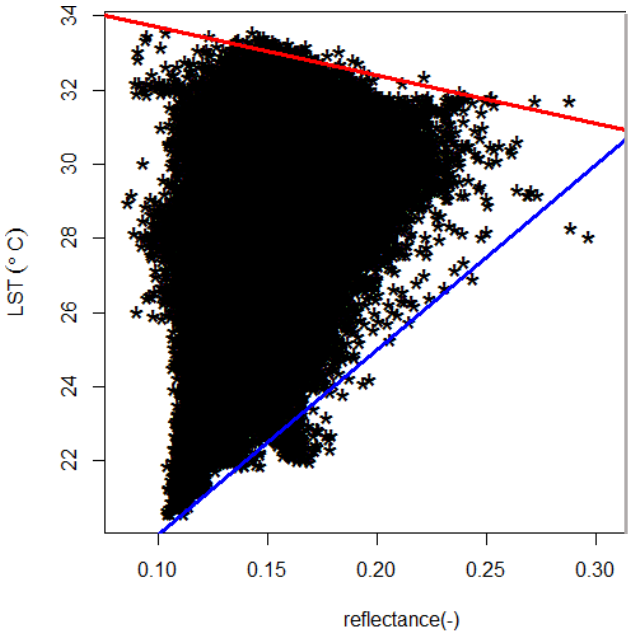

March 19, 2014

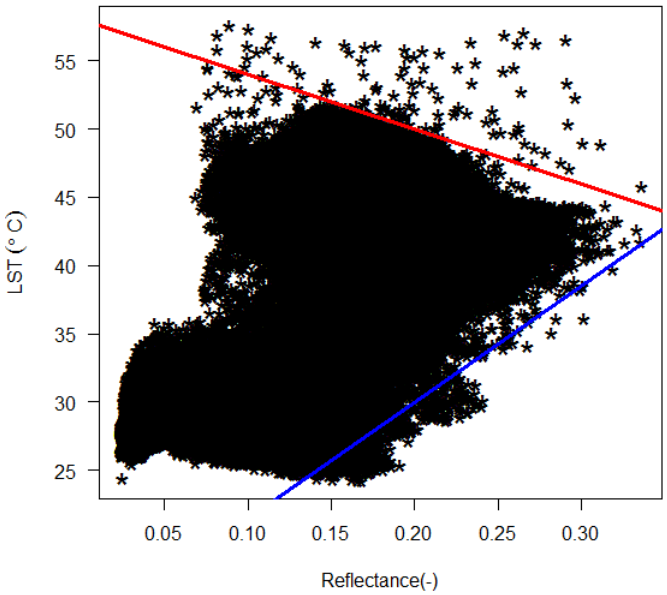

April 20, 2014

Figure A5-1 r-LST plots for 2014 Images

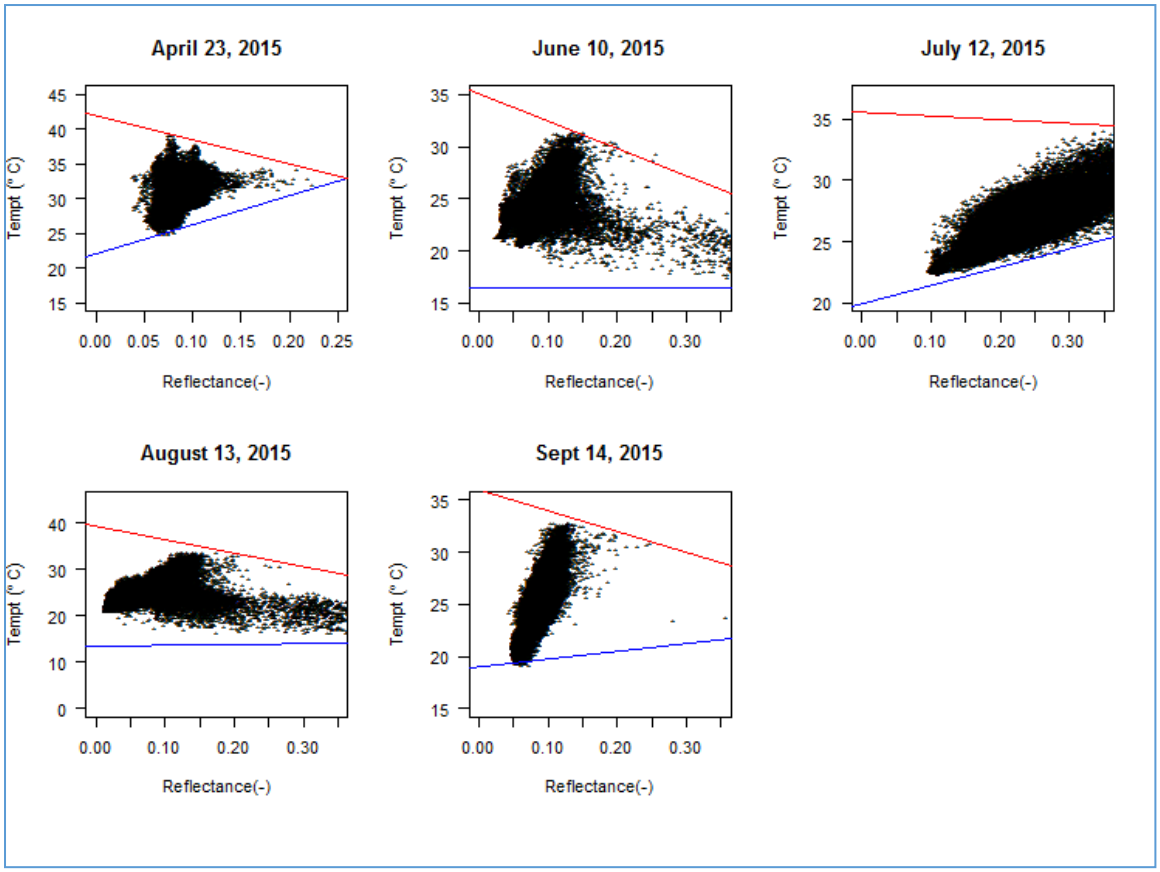

Figure A5-2. r-LST feature plots for 2015 images (Image path 172, row = 58)

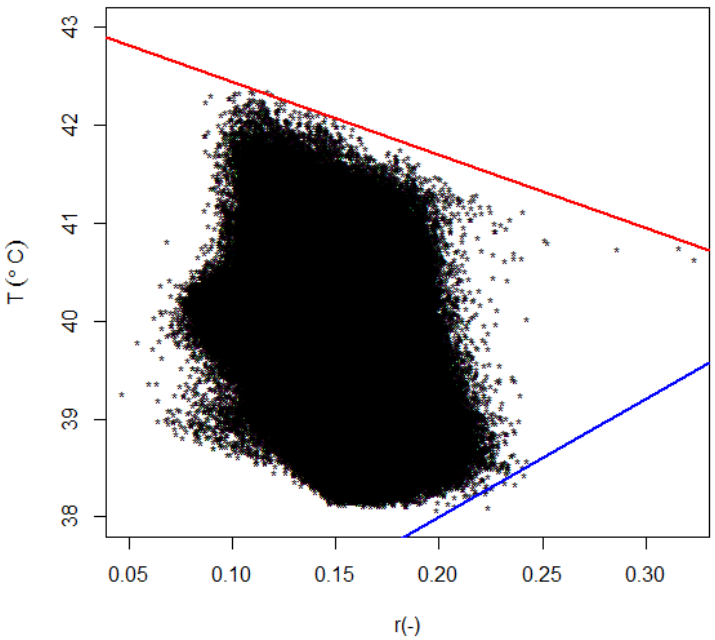

Figure A5-3. r-LST feature plots for 2015 images, Date: May 18, 2015. (Image path 172, row = 58)

S-SEBI Equations

$$\Lambda_{\text{Apr23}} = \frac{42 - 35\alpha_o - T_o}{42 - 35\alpha_o - (22 + 42\alpha_o)} \quad \text{(A6-1)}$$

$$\Lambda_{\text{Jun10}} = \frac{35 - 26\alpha_o - T_o}{35 - 26\alpha_o - (16.5 + 0.005\alpha_o)} \quad \text{(A6-2)}$$

$$\Lambda_{\text{Jul12}} = \frac{35.5 - 3\alpha_o - T_o}{35.5 - 3\alpha_o - (20 + 15\alpha_o)} \quad \text{(A6-3)}$$

$$\Lambda_{\text{Aug13}} = \frac{39.5 - 29.5\alpha_o - T_o}{39.5 - 29.5\alpha_o - (13.5 + 2\alpha_o)} \quad \text{(A6-4)}$$

$$\Lambda_{\text{Sep14}} = \frac{36 - 20\alpha_o - T_o}{36 - 20\alpha_o - (19 + 7.5\alpha_o)} \quad \text{(A6-5)}$$

Annex 6: Atmospheric profiles generated through NASA web calculator

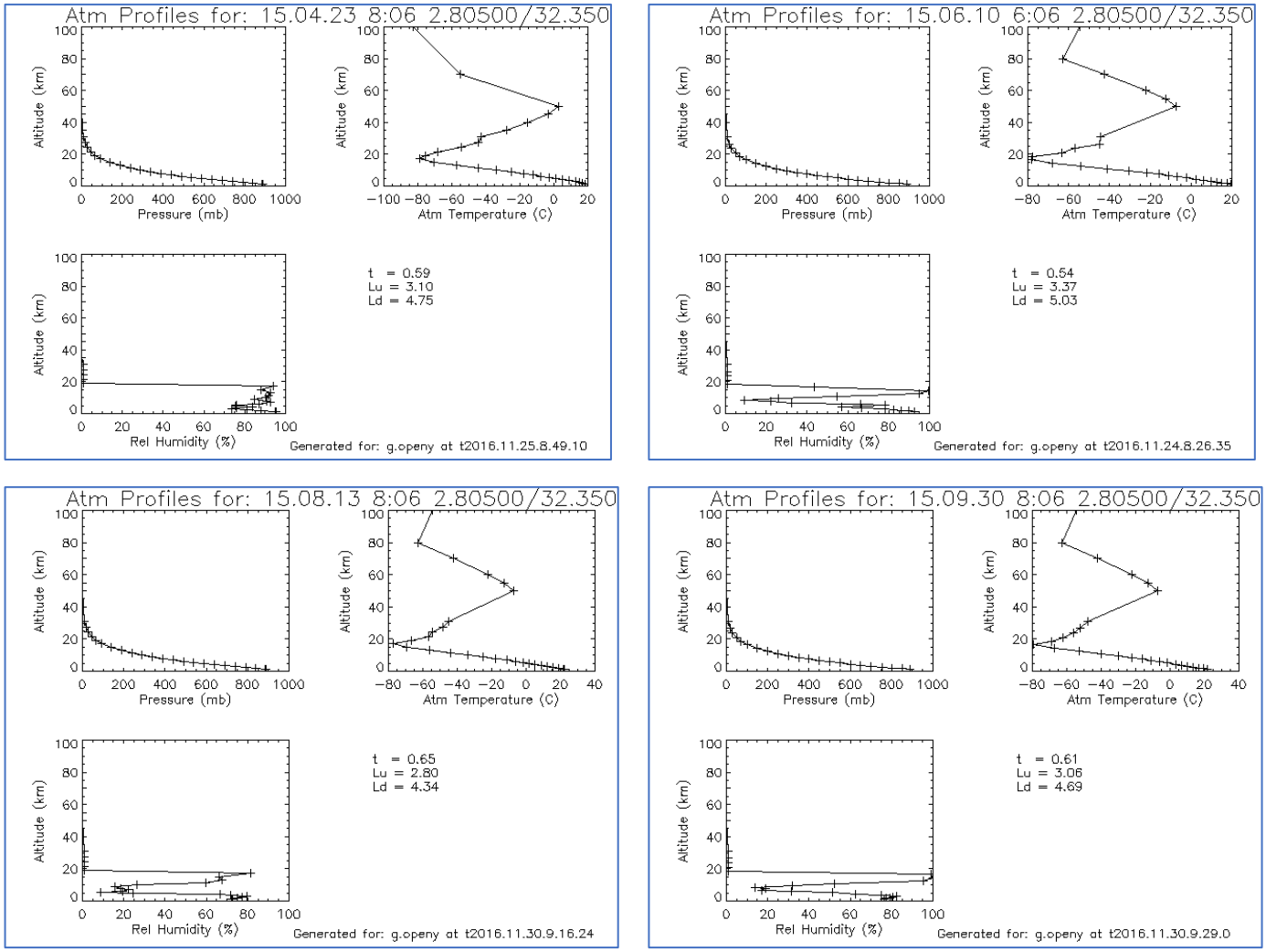

Figure A6-1 Atmospheric profiles for the indicated over pass dates: 2015 images

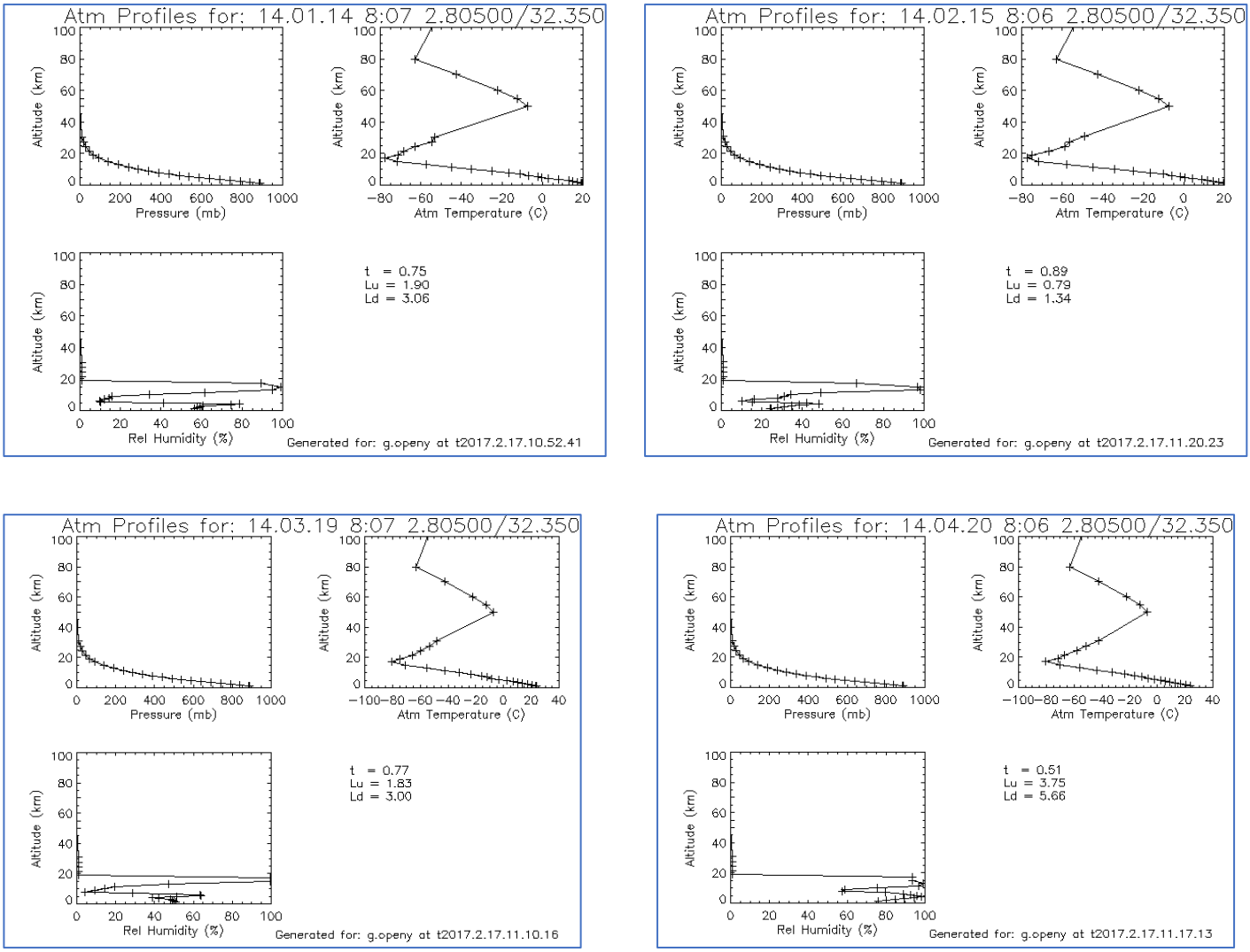

Figure A6-2 Atmospheric profiles for the indicated overpass dates: 2014 Images

Table A6-1 summary of atmospheric correction parameters for 2015 analyzed images

Input summary --- Date (yyyy-mm-dd): 2015-04-23 Lat/Long: 2.805/ 32.350 GMT Time: 8:06 L8 TIRS Band 10 Spectral Response Curve Mid-latitude summer standard atmosphere User input surface conditions Surface altitude (km): 1.08000 Surface pressure (mb): 890 Surface temperature (C): 18.6000 Surface relative humidity (%): 95.5000 Output summary --- Band average atmospheric transmission: 0.59 Effective bandpass upwelling radiance: 3.10 W/m^2/sr/um Effective bandpass downwelling radiance: 4.75 W/m^2/sr/um	Input summary --- Date (yyyy-mm-dd): 2015-06-10 Lat/Long: 2.805/ 32.350 GMT Time: 6:06 L7 Spectral Response Curve from handbook Mid-latitude winter standard atmosphere User input surface conditions Surface altitude (km): 1.08000 Surface pressure (mb): 890 Surface temperature (C): 19.5600 Surface relative humidity (%): 92.8000 Output summary --- Band average atmospheric transmission: 0.54 Effective bandpass upwelling radiance: 3.37 W/m^2/sr/um Effective bandpass downwelling radiance: 5.03 W/m^2/sr/um
Input summary --- Date (yyyy-mm-dd): 2015-08-13 Lat/Long: 2.805/ 32.350 GMT Time: 8:06 L8 TIRS Band 10 Spectral Response Curve Mid-latitude winter standard atmosphere User input surface conditions Surface altitude (km): 1.08000 Surface pressure (mb): 891 Surface temperature (C): 21.9800 Surface relative humidity (%): 72.3700 Output summary --- Band average atmospheric transmission: 0.65 Effective bandpass upwelling radiance: 2.80 W/m^2/sr/um Effective bandpass downwelling radiance: 4.34 W/m^2/sr/um	Input summary --- Date (yyyy-mm-dd): 2015-09-30 Lat/Long: 2.805/ 32.350 GMT Time: 8:06 L8 TIRS Band 10 Spectral Response Curve Mid-latitude winter standard atmosphere User input surface conditions Surface altitude (km): 1.08000 Surface pressure (mb): 888 Surface temperature (C): 21.8000 Surface relative humidity (%): 76.2800 Output summary --- Band average atmospheric transmission: 0.61 Effective bandpass upwelling radiance: 3.06 W/m^2/sr/um Effective bandpass downwelling radiance: 4.69 W/m^2/sr/um

Table A6-2 Atmospheric correction parameters for 2014 analyzed images

Date (yyyy-mm-dd): 2014-01-14 Input Lat/Long: 2.805/ 32.350 GMT Time: 8:07 L8 TIRS Band 10 Spectral Response Curve Mid-latitude winter standard atmosphere User input surface conditions Surface altitude (km): 1.080 Surface pressure (mb): 889.000 Surface temperature (C): 19.350 Surface relative humidity (%): 56.300 Band average atmospheric transmission: 0.75 Effective bandpass upwelling radiance: 1.90 W/m^2/sr/um Effective bandpass downwelling radiance: 3.06 W/m^2/sr/um	Date (yyyy-mm-dd): 2014-02-15 Input Lat/Long: 2.805/ 32.350 GMT Time: 8:07 L8 TIRS Band 10 Spectral Response Curve Mid-latitude winter standard atmosphere User input surface conditions Surface altitude (km): 1.080 Surface pressure (mb): 888.000 Surface temperature (C): 19.770 Surface relative humidity (%): 24.100 Band average atmospheric transmission: 0.89 Effective bandpass upwelling radiance: 0.79 W/m^2/sr/um Effective bandpass downwelling radiance: 1.34 W/m^2/sr/um
Date (yyyy-mm-dd): 2014-03-19 Input Lat/Long: 2.805/ 32.350 GMT Time: 8:07 L8 TIRS Band 10 Spectral Response Curve Mid-latitude winter standard atmosphere User input surface conditions Surface altitude (km): 1.080 Surface pressure (mb): 888.000 Surface temperature (C): 23.700 Surface relative humidity (%): 51.020 Band average atmospheric transmission: 0.77 Effective bandpass upwelling radiance: 1.83 W/m^2/sr/um Effective bandpass downwelling radiance: 3.00 W/m^2/sr/um	Date (yyyy-mm-dd): 2014-04-20 Input Lat/Long: 2.805/ 32.350 GMT Time: 8:06 L8 TIRS Band 10 Spectral Response Curve Mid-latitude winter standard atmosphere User input surface conditions Surface altitude (km): 1.080 Surface pressure (mb): 889.000 Surface temperature (C): 23.860 Surface relative humidity (%): 75.710 Band average atmospheric transmission: 0.51 Effective bandpass upwelling radiance: 3.75 W/m^2/sr/um Effective bandpass downwelling radiance: 5.66 W/m^2/sr/um

Table A6-3 Atmospheric profile summaries for the indicated overpass dates

2015-April-23

Atmospheric Profile Summary

User selected to use the profile generated by interpolating between the surrounding four profiles

Profile used:

Altitude (km)	Pressure (mb)	Temperature (C)	Rel Humidity (%)
1.080	890.000	18.600	95.500
1.141	884.354	18.385	94.675
1.637	838.646	16.641	87.994
2.165	789.944	14.783	80.875
2.720	738.761	12.830	73.394
3.307	688.761	9.144	75.750
3.928	638.761	5.235	83.619
4.591	588.761	1.383	75.329
5.301	538.761	-2.995	76.144
6.067	488.761	-7.842	87.054
6.901	438.761	-12.296	92.688
7.819	388.761	-17.810	90.635
8.838	338.761	-24.906	84.720
9.983	288.761	-33.647	90.350
11.294	238.761	-44.315	91.548
12.836	188.761	-57.126	92.494
14.747	138.761	-70.759	88.168
17.034	93.257	-78.616	94.074
19.045	65.505	-75.373	1.000
21.262	45.505	-68.598	1.000
24.258	27.752	-54.443	1.000
27.379	17.752	-44.655	1.000
30.980	10.000	-43.004	1.000
35.000	6.520	-27.950	0.010
40.000	3.330	-15.650	0.006
45.000	1.760	-3.250	0.003
50.000	0.951	2.550	0.002
70.000	0.067	-55.050	0.001
100.000	0.000	-82.650	0.016

Below follow the model profiles for the surrounding integer lat/longs
and for the 2 surrounding times

The following four profiles are for the integer lat/long corners
on 2015-04-23 at GMT 6:00

At 2 North 32 East

Altitude (km)	Pressure (mb)	Temperature (deg C)	Relative Humidity (%)	Zonal Wind (m/sec)	Meridional Wind (m/sec)
1.115	891.1	21.75	91.0	-999.00	-999.00
-999.000	-999.0	-999.00	-999.0	-999.00	-999.00
-999.000	-999.0	-999.00	-999.0	-999.00	-999.00
-999.000	-999.0	-999.00	-999.0	-999.00	-999.00
-999.000	-999.0	-999.00	-999.0	-999.00	-999.00
-999.000	-999.0	-999.00	-999.0	-999.00	-999.00
1.523	850.0	19.35	72.0	-4.71	6.29
2.044	800.0	17.05	69.0	-3.07	3.83
2.592	750.0	13.55	72.0	-3.04	0.93
3.171	700.0	10.05	70.0	-5.93	-4.36
3.783	650.0	6.05	84.0	-7.60	-9.11
4.436	600.0	2.35	77.0	-11.23	-10.51
5.134	550.0	-2.25	85.0	-9.04	-8.45
5.885	500.0	-6.85	91.0	-4.07	-4.26
6.701	450.0	-11.45	100.0	-2.16	1.78
7.596	400.0	-16.35	97.0	-1.50	2.70
8.588	350.0	-23.15	92.0	-0.70	3.70
9.697	300.0	-31.65	100.0	-1.80	5.30
10.960	250.0	-41.75	100.0	0.60	4.70
12.430	200.0	-54.15	100.0	1.90	0.90
14.212	150.0	-67.55	84.0	1.77	1.46
16.578	100.0	-79.75	98.0	-7.56	2.66
18.608	70.0	-75.75	-999.0	-2.78	-0.76
20.565	50.0	-72.55	-999.0	-11.33	-0.62
23.657	30.0	-56.15	-999.0	-30.65	2.02
26.344	20.0	-45.95	-999.0	15.98	-3.00
30.981	10.0	-43.25	-999.0	17.36	-5.32

Pressure Reduced to MSL (mb) 1014.7
Pressure @tropopause (mb) 98.6
Altitude @tropopause (km) 16.660
Temperature @tropopause (deg C) -80.05
Column Water (cm) 3.82
Cloud Cover 0.0%

At 2 North 33 East

Altitude (km)	Pressure (mb)	Temperature (deg C)	Relative Humidity (%)	Zonal Wind (m/sec)	Meridional Wind (m/sec)
1.059	896.9	22.75	79.0	-999.00	-999.00
-999.000	-999.0	-999.00	-999.0	-999.00	-999.00
-999.000	-999.0	-999.00	-999.0	-999.00	-999.00
-999.000	-999.0	-999.00	-999.0	-999.00	-999.00

2015-Jun-10

Atmospheric Profile Summary

User selected to use the profile generated by interpolating between the surrounding four profiles

Profile used:

Altitude (km)	Pressure (mb)	Temperature (C)	Rel Humidity (%)
1.080	890.000	19.560	92.800
1.523	849.752	17.456	89.718
2.045	802.365	14.980	86.089
2.595	752.489	12.373	82.270
3.173	699.986	9.629	78.250
3.785	649.986	6.143	66.456
4.437	599.986	2.252	56.879
5.134	549.986	-2.450	78.324
5.885	499.986	-6.771	66.226
6.701	449.986	-10.984	32.265
7.598	399.986	-15.421	22.216
8.594	349.986	-21.710	9.403
9.709	299.986	-30.328	25.710
10.977	249.986	-41.142	54.737
12.451	199.986	-53.905	94.987
14.235	149.986	-67.991	99.399
16.606	99.991	-78.315	43.429
18.632	69.994	-77.634	1.000
20.615	49.994	-63.408	1.000
23.822	29.997	-56.822	1.000
26.477	19.997	-44.874	1.000
31.084	10.000	-44.276	1.000
50.000	0.683	-7.450	0.000
55.000	0.362	-12.550	0.000
60.000	0.188	-22.350	0.000
70.000	0.047	-42.450	0.000
80.000	0.010	-63.050	0.000
100.000	0.001	-54.550	0.000

Below follow the model profiles for the surrounding integer lat/longs
and for the 2 surrounding times

The following four profiles are for the integer lat/long corners
on 2015-06-10 at GMT 6:00

At 2 North 32 East

Altitude (km)	Pressure (mb)	Temperature (deg C)	Relative Humidity (%)	Zonal Wind (m/sec)	Meridional Wind (m/sec)
1.115	891.0	21.15	82.0	-999.00	-999.00
-999.000	-999.0	-999.00	-999.0	-999.00	-999.00
-999.000	-999.0	-999.00	-999.0	-999.00	-999.00
-999.000	-999.0	-999.00	-999.0	-999.00	-999.00
-999.000	-999.0	-999.00	-999.0	-999.00	-999.00
-999.000	-999.0	-999.00	-999.0	-999.00	-999.00
1.522	850.0	20.15	57.0	0.77	4.10
2.043	800.0	17.65	57.0	-1.09	7.75
2.592	750.0	13.95	72.0	-2.43	11.24
3.171	700.0	9.75	80.0	-3.41	5.61
3.783	650.0	6.25	61.0	-8.32	-2.33
4.435	600.0	2.95	25.0	-10.80	-6.14
5.134	550.0	-2.25	79.0	-6.73	-5.01
5.885	500.0	-6.65	63.0	-2.84	-2.43
6.701	450.0	-11.05	49.0	-3.33	1.05
7.598	400.0	-15.15	16.0	-5.70	2.70
8.595	350.0	-21.45	12.0	-6.90	1.80
9.711	300.0	-30.55	30.0	-7.20	-1.00
10.977	250.0	-41.25	58.0	-12.40	-2.70
12.449	200.0	-54.05	97.0	-16.90	-5.20
14.233	150.0	-67.95	100.0	-26.60	-5.20
16.604	100.0	-78.55	48.0	-11.32	4.28
18.629	70.0	-77.65	-999.0	-17.82	4.05
20.613	50.0	-62.95	-999.0	-25.16	-4.88
23.822	30.0	-57.05	-999.0	-5.20	-0.60
26.478	20.0	-45.15	-999.0	16.40	1.20
31.085	10.0	-44.75	-999.0	6.40	-0.70

Pressure Reduced to MSL (mb) 1014.3
Pressure @tropopause (mb) 95.1
Altitude @tropopause (km) 16.890
Temperature @tropopause (deg C) -79.55
Column Water (cm) 2.99
Cloud Cover 0.0%

At 2 North 33 East

Altitude (km)	Pressure (mb)	Temperature (deg C)	Relative Humidity (%)	Zonal Wind (m/sec)	Meridional Wind (m/sec)
1.059	896.7	23.05	81.0	-999.00	-999.00
-999.000	-999.0	-999.00	-999.0	-999.00	-999.00
-999.000	-999.0	-999.00	-999.0	-999.00	-999.00

2014-January-14

Atmospheric Profile Summary

User selected to use the profile generated by interpolating between the surrounding four profiles

Profile used:

Altitude (km)	Pressure (mb)	Temperature (C)	Rel Humidity (%)
1.080	889.000	19.350	56.300
1.123	885.039	19.178	56.414
1.628	838.504	17.163	57.752
2.158	789.744	15.051	59.154
2.714	738.548	12.833	60.627
3.298	688.548	7.770	74.314
3.916	638.548	2.790	78.695
4.572	588.548	-0.370	40.995
5.280	538.548	-2.347	10.337
6.047	488.548	-6.906	9.800
6.884	438.548	-10.857	12.236
7.807	388.548	-16.773	14.148
8.826	338.548	-25.130	15.584
9.968	288.548	-35.116	34.341
11.272	238.548	-44.866	61.747
12.814	188.548	-57.529	95.102
14.724	138.548	-71.620	98.912
17.005	93.129	-77.754	89.541
19.037	65.419	-71.016	1.000
21.283	45.419	-68.405	1.000
24.279	27.710	-62.680	1.000
27.247	17.710	-54.651	1.000
30.652	10.000	-53.318	1.000
50.000	0.683	-7.450	0.000
55.000	0.362	-12.550	0.000
60.000	0.188	-22.350	0.000
70.000	0.047	-42.450	0.000
80.000	0.010	-63.050	0.000
100.000	0.001	-54.550	0.000

Below follow the model profiles for the surrounding integer lat/longs
and for the 2 surrounding times

The following four profiles are for the integer lat/long corners
on 2014-01-14 at GMT 6:00

At 2 North 32 East

Altitude (km)	Pressure (mb)	Temperature (deg C)	Relative Humidity (%)	Zonal Wind (m/sec)	Meridional Wind (m/sec)
1.043	897.2	24.85	46.0	-999.00	-999.00
-999.000	-999.0	-999.00	-999.0	-999.00	-999.00
-999.000	-999.0	-999.00	-999.0	-999.00	-999.00
-999.000	-999.0	-999.00	-999.0	-999.00	-999.00
-999.000	-999.0	-999.00	-999.0	-999.00	-999.00
-999.000	-999.0	-999.00	-999.0	-999.00	-999.00
1.514	850.0	21.65	43.0	-3.59	-1.71
2.037	800.0	17.95	50.0	-5.64	-3.23
2.585	750.0	13.55	59.0	-7.10	-3.72
3.162	700.0	8.85	70.0	-5.28	-3.63
3.770	650.0	3.05	95.0	-3.88	-3.43
4.414	600.0	0.25	51.0	-3.43	-0.43
5.110	550.0	-2.05	24.0	-1.78	1.63
5.861	500.0	-5.95	11.0	-3.72	0.13
6.679	450.0	-9.95	9.0	-6.40	-1.30
7.579	400.0	-15.05	14.0	-6.60	-3.10
8.572	350.0	-23.05	15.0	-5.80	-4.30
9.678	300.0	-33.15	34.0	-6.10	-1.40
10.933	250.0	-42.35	67.0	-15.20	10.60
12.402	200.0	-54.25	90.0	-15.60	14.80
14.185	150.0	-68.35	97.0	-13.51	6.60
16.532	100.0	-79.95	86.0	-6.86	-2.90
18.581	70.0	-70.85	-999.0	4.61	-6.83
20.572	50.0	-69.65	-999.0	12.56	-0.76
23.716	30.0	-63.95	-999.0	19.20	-1.60
26.233	20.0	-57.05	-999.0	6.20	9.20
30.650	10.0	-53.35	-999.0	-14.90	6.40

Pressure Reduced to MSL (mb) 1012.9
Pressure @tropopause (mb) 103.4
Altitude @tropopause (km) 16.344
Temperature @tropopause (deg C) -79.45
Column Water (cm) 2.46
Cloud Cover 0.0%

At 2 North 33 East

Altitude (km)	Pressure (mb)	Temperature (deg C)	Relative Humidity (%)	Zonal Wind (m/sec)	Meridional Wind (m/sec)
1.072	894.4	26.55	47.0	-999.00	-999.00
-999.000	-999.0	-999.00	-999.0	-999.00	-999.00
-999.000	-999.0	-999.00	-999.0	-999.00	-999.00
-999.000	-999.0	-999.00	-999.0	-999.00	-999.00
-999.000	-999.0	-999.00	-999.0	-999.00	-999.00
-999.000	-999.0	-999.00	-999.0	-999.00	-999.00
1.513	850.0	20.65	48.0	-5.34	-0.79
2.035	800.0	17.75	53.0	-8.13	-2.88
2.583	750.0	13.75	60.0	-7.45	-3.48

2014-April-20

Atmospheric Profile Summary

User selected to use the profile generated by interpolating between the surrounding four profiles

Profile used:

Altitude (km)	Pressure (mb)	Temperature (C)	Rel Humidity (%)
1.080	889.000	23.860	75.710
1.117	885.661	23.612	76.022
1.618	840.180	20.238	80.268
2.144	792.381	16.691	84.731
2.698	742.035	12.955	89.431
3.285	688.761	9.003	94.405
3.908	638.761	5.535	97.970
4.573	588.761	2.260	95.773
5.287	538.761	-1.913	92.726
6.056	488.761	-6.574	88.745
6.894	438.761	- 11.259	79.744
7.815	388.761	- 16.645	57.416
8.839	338.761	- 23.616	58.783
9.990	288.761	- 32.528	75.280
11.305	238.761	- 43.406	96.851
12.857	188.761	- 55.832	99.148
14.776	138.761	- 70.226	93.676
17.043	93.257	- 80.586	93.382
19.063	65.505	-71.724	1.000
21.303	45.505	-66.677	1.000
24.309	27.752	-58.021	1.000
27.341	17.752	-51.241	1.000
30.883	10.000	-42.522	1.000
50.000	0.683	-7.450	0.000
55.000	0.362	-12.550	0.000
60.000	0.188	-22.350	0.000
70.000	0.047	-42.450	0.000
80.000	0.010	-63.050	0.000
100.000	0.001	-54.550	0.000

Below follow the model profiles for the surrounding integer lat/longs
and for the 2 surrounding times

The following four profiles are for the integer lat/long corners
on 2014-04-20 at GMT 6:00

At 2 North 32 East

Altitude (km)	Pressure (mb)	Temperature (deg C)	Relative Humidity (%)	Zonal Wind (m/sec)	Meridional Wind (m/sec)
1.043	897.2	21.25	93.0	-999.00	-999.00
-999.000	-999.0	-999.00	-999.0	-999.00	-999.00
-999.000	-999.0	-999.00	-999.0	-999.00	-999.00
-999.000	-999.0	-999.00	-999.0	-999.00	-999.00
-999.000	-999.0	-999.00	-999.0	-999.00	-999.00
-999.000	-999.0	-999.00	-999.0	-999.00	-999.00
1.509	850.0	18.45	82.0	-1.14	4.85
2.029	800.0	16.05	83.0	-2.13	4.55
2.575	750.0	12.55	93.0	-4.27	3.55
3.152	700.0	8.95	98.0	-7.16	3.27
3.764	650.0	5.65	100.0	-10.72	1.56
4.417	600.0	2.65	100.0	-10.37	-2.18
5.118	550.0	-1.35	95.0	-8.62	-6.87
5.871	500.0	-5.75	87.0	-9.60	-4.45
6.691	450.0	-9.85	64.0	-7.76	0.07
7.592	400.0	-14.95	72.0	-5.20	3.80
8.588	350.0	-21.75	74.0	-0.60	5.30
9.705	300.0	-30.25	72.0	3.90	4.30
10.972	250.0	-40.75	94.0	3.00	0.90
12.452	200.0	-52.55	96.0	10.73	-6.79
14.248	150.0	-67.25	100.0	13.25	- 7.01
16.586	100.0	-82.45	99.0	4.18	3.09
18.619	70.0	-72.35	-999.0	-0.29	-2.00
20.599	50.0	-69.05	-999.0	13.83	-2.34
23.728	30.0	-59.35	-999.0	10.24	-2.24
26.317	20.0	-52.95	-999.0	-16.32	- 2.53
30.878	10.0	-43.45	-999.0	-26.18	4.87

Pressure Reduced to MSL (mb) 1013.3
Pressure @tropopause (mb) 102.4
Altitude @tropopause (km) 16.455
Temperature @tropopause (deg C) -82.25
Column Water (cm) 4.40
Cloud Cover 0.0%

At 2 North 33 East

Altitude (km)	Pressure (mb)	Temperature (deg C)	Relative Humidity (%)	Zonal Wind (m/sec)	Meridional Wind (m/sec)

999.00
-999.000 -999.0 -999.00 -999.0 -999.00 -999.00
-999.000 -999.0 -999.00 -999.0 -999.00 -999.00
1.523 850.0 19.35 67.0 -4.02 9.26
2.043 800.0 16.55 66.0 -3.11 4.74
2.590 750.0 13.55 68.0 -4.38 -1.14
3.169 700.0 10.35 61.0 -7.01 -6.58
3.782 650.0 6.45 68.0 -8.48 -9.90
4.435 600.0 2.75 65.0 -10.12 -10.40
5.134 550.0 -1.85 72.0 -8.35 -8.14
5.885 500.0 -6.95 89.0 -5.81 -4.33
6.701 450.0 -11.75 97.0 -2.86 0.57
7.595 400.0 -15.85 80.0 -2.10 2.90
8.588 350.0 -23.05 88.0 -1.20 3.20
9.698 300.0 -31.45 91.0 -1.30 5.00
10.960 250.0 -41.85 100.0 1.00 3.30
12.430 200.0 -54.35 100.0 2.60 0.20
14.214 150.0 -66.95 66.0 0.24 0.48
16.581 100.0 -80.05 100.0 -6.74 3.04
18.604 70.0 -75.65 -999.0 -2.91 -0.49
20.565 50.0 -72.45 -999.0 -11.02 -0.40
23.655 30.0 -56.25 -999.0 -30.94 2.12
26.343 20.0 -45.55 -999.0 16.73 -3.09
30.982 10.0 -43.15 -999.0 16.58 -4.12
Pressure Reduced to MSL (mb) 1014.7
Pressure @tropopause (mb) 96.1
Altitude @tropopause (km) 16.804
Temperature @tropopause (deg C) -81.05
Column Water (cm) 3.55
Cloud Cover 0.0%
At 3 North 32 East
Relative Zonal Meridional
Altitude Pressure Temperature
Humidity Wind Wind
(km) (mb) (deg C) (%) (m/sec) (m/sec)
1.020 900.9 22.45 88.0 -999.00 -999.00
-999.000 -999.0 -999.00 -999.0 -999.00 -999.00
-999.000 -999.0 -999.00 -999.0 -999.00 -999.00
-999.000 -999.0 -999.00 -999.0 -999.00 -999.00
-999.000 -999.0 -999.00 -999.0 -999.00 -999.00
1.028 900.0 21.85 85.0 -0.90 2.16
1.523 850.0 20.25 70.0 -2.71 5.82
2.045 800.0 17.15 72.0 -3.48 3.48
2.593 750.0 13.55 71.0 -5.91 -0.13
3.172 700.0 9.65 81.0 -4.21 -4.37
3.784 650.0 5.95 90.0 -5.81 -7.31
4.436 600.0 2.15 80.0 -10.31 -8.73
5.134 550.0 -2.15 76.0 -11.00 -7.95
5.885 500.0 -6.95 85.0 -6.14 -5.64
6.701 450.0 -11.25 97.0 -1.87 1.02
7.597 400.0 -16.65 99.0 -0.80 2.30
8.587 350.0 -23.35 94.0 0.20 3.00
9.697 300.0 -31.55 100.0 -0.90 5.00
10.960 250.0 -41.65 100.0 0.40 5.10
12.430 200.0 -54.35 100.0 2.80 2.90
14.211 150.0 -67.75 89.0 -0.04 0.99
16.578 100.0 -79.15 91.0 -7.02 1.72
18.607 70.0 -76.35 -999.0 -2.96 -0.28
20.566 50.0 -72.15 -999.0 -10.97 -0.60
23.659 30.0 -56.25 -999.0 -29.79 2.29
26.342 20.0 -45.95 -999.0 12.63 -3.80
30.979 10.0 -42.95 -999.0 15.22 -3.78
Pressure Reduced to MSL (mb) 1014.2
Pressure @tropopause (mb) 97.7
Altitude @tropopause (km) 16.711
Temperature @tropopause (deg C) -79.55
Column Water (cm) 4.03
Cloud Cover 0.0%
At 3 North 33 East
Relative Zonal Meridional
Altitude Pressure Temperature
Humidity Wind Wind
(km) (mb) (deg C) (%) (m/sec) (m/sec)
1.027 900.2 22.95 80.0 -999.00 -999.00
-999.000 -999.0 -999.00 -999.0 -999.00 -999.00
-999.000 -999.0 -999.00 -999.0 -999.00 -999.00
-999.000 -999.0 -999.00 -999.0 -999.00 -999.00
1.029 900.0 22.15 77.0 -1.28 1.60
1.523 850.0 19.65 68.0 -3.04 4.98
2.044 800.0 16.85 70.0 -2.54 2.86
2.592 750.0 13.75 71.0 -5.77 -0.29
3.171 700.0 9.95 75.0 -5.91 -5.72
3.783 650.0 6.05 79.0 -8.02 -9.21
4.436 600.0 2.35 74.0 -11.87 -10.59
5.134 550.0 -1.75 70.0 -9.99 -8.31
5.886 500.0 -6.95 86.0 -5.19 -3.49
6.701 450.0 -11.55 97.0 -3.03 0.68
7.596 400.0 -16.45 97.0 -0.20 3.50
8.588 350.0 -22.95 78.0 1.10 2.10
9.699 300.0 -31.55 100.0 1.50 2.90
10.961 250.0 -41.75 100.0 2.20 2.90
12.432 200.0 -54.25 100.0 3.10 1.80
14.214 150.0 -67.45 81.0 -1.12 -0.14
16.582 100.0 -79.45 98.0 -6.48 3.02
18.605 70.0 -76.25 -999.0 -2.74 -0.63
20.566 50.0 -71.95 -999.0 -10.95 -0.35
23.660 30.0 -56.35 -999.0 -30.00 2.23
26.342 20.0 -45.55 -999.0 13.20 -3.60
30.981 10.0 -42.95 -999.0 14.37 -2.63
Pressure Reduced to MSL (mb) 1014.4
Pressure @tropopause (mb) 94.5
Altitude @tropopause (km) 16.903
Temperature @tropopause (deg C) -80.85
Column Water (cm) 3.82
Cloud Cover 0.0%

-999.000 -999.0 -999.00 -999.0 -999.00 -999.00
-999.000 -999.0 -999.00 -999.0 -999.00 -999.00
-999.000 -999.0 -999.00 -999.0 -999.00 -999.00
1.520 850.0 20.65 58.0 1.36 0.61
2.043 800.0 18.05 59.0 1.79 2.83
2.592 750.0 13.75 72.0 1.37 2.81
3.170 700.0 9.45 77.0 -1.68 0.36
3.782 650.0 6.35 59.0 -7.64 -1.54
4.434 600.0 2.65 51.0 -10.49 -3.70
5.133 550.0 -2.05 61.0 -6.53 -4.81
5.884 500.0 -6.65 53.0 -2.71 -3.28
6.700 450.0 -10.75 37.0 -2.72 0.91
7.598 400.0 -14.85 9.0 -5.50 1.40
8.596 350.0 -21.25 9.0 -5.90 0.30
9.712 300.0 -30.25 28.0 -5.60 -0.50
10.979 250.0 -41.35 57.0 -13.20 -1.70
12.451 200.0 -53.95 95.0 -17.10 -4.30
14.236 150.0 -68.15 100.0 -27.20 -5.70
16.604 100.0 -78.55 47.0 -11.61 3.01
18.628 70.0 -77.95 -999.0 -17.46 4.19
20.608 50.0 -63.05 -999.0 -26.18 -4.11
23.823 30.0 -56.75 -999.0 -3.70 -0.60
26.478 20.0 -45.15 -999.0 15.80 1.50
31.083 10.0 -44.75 -999.0 6.30 -0.60
Pressure Reduced to MSL (mb) 1014.5
Pressure @tropopause (mb) 94.0
Altitude @tropopause (km) 16.953
Temperature @tropopause (deg C) -80.05
Column Water (cm) 3.14
Cloud Cover 0.0%
At 3 North 32 East
Relative Zonal Meridional
Altitude Pressure Temperature
Humidity Wind Wind
(km) (mb) (deg C) (%) (m/sec) (m/sec)
1.020 900.7 24.65 75.0 -999.00 -999.00
-999.000 -999.0 -999.00 -999.0 -999.00 -999.00
-999.000 -999.0 -999.00 -999.0 -999.00 -999.00
-999.000 -999.0 -999.00 -999.0 -999.00 -999.00
-999.000 -999.0 -999.00 -999.0 -999.00 -999.00
1.027 900.0 22.85 74.0 -0.70 0.84
1.524 850.0 21.25 59.0 0.19 4.07
2.046 800.0 18.05 58.0 -0.91 5.74
2.596 750.0 13.75 71.0 -0.39 7.03
3.174 700.0 9.45 82.0 -2.63 3.98
3.786 650.0 5.95 72.0 -6.08 -1.22
4.437 600.0 2.05 64.0 -8.75 -3.06
5.134 550.0 -2.55 83.0 -7.00 -1.14
5.885 500.0 -6.75 62.0 -4.89 -1.35
6.701 450.0 -11.05 32.0 -2.90 -1.04
7.597 400.0 -15.55 28.0 -5.10 0.90
8.593 350.0 -21.85 8.0 -9.30 0.80
9.708 300.0 -30.35 24.0 -13.00 -0.50
10.976 250.0 -41.15 55.0 -17.00 -2.90
12.449 200.0 -53.95 97.0 -16.80 -7.00
14.233 150.0 -67.95 99.0 -24.50 -4.40
16.606 100.0 -78.15 40.0 -11.82 3.11
18.633 70.0 -77.55 -999.0 -18.20 4.32
20.616 50.0 -63.65 -999.0 -25.37 -6.09
23.820 30.0 -56.85 -999.0 -7.30 0.20
26.475 20.0 -44.75 -999.0 11.60 1.40
31.084 10.0 -44.15 -999.0 3.00 -0.40
Pressure Reduced to MSL (mb) 1014.1
Pressure @tropopause (mb) 93.6
Altitude @tropopause (km) 16.983
Temperature @tropopause (deg C) -79.55
Column Water (cm) 3.39
Cloud Cover 0.0%
At 3 North 33 East
Relative Zonal Meridional
Altitude Pressure Temperature
Humidity Wind Wind
(km) (mb) (deg C) (%) (m/sec) (m/sec)
1.027 900.1 24.35 77.0 -999.00 -999.00
-999.000 -999.0 -999.00 -999.0 -999.00 -999.00
-999.000 -999.0 -999.00 -999.0 -999.00 -999.00
-999.000 -999.0 -999.00 -999.0 -999.00 -999.00
-999.000 -999.0 -999.00 -999.0 -999.00 -999.00
1.028 900.0 22.25 74.0 -0.54 0.44
1.523 850.0 20.45 65.0 0.07 1.55
2.045 800.0 17.15 75.0 0.07 2.03
2.593 750.0 13.55 78.0 -0.45 1.67
3.172 700.0 10.15 67.0 -2.83 0.48
3.785 650.0 6.55 57.0 -7.08 -1.72
4.437 600.0 2.25 58.0 -9.95 -2.82
5.134 550.0 -2.45 72.0 -8.91 -2.51
5.885 500.0 -6.95 86.0 -6.07 -2.66
6.701 450.0 -10.85 21.0 -3.20 -1.06
7.598 400.0 -15.45 15.0 -5.00 1.10
8.594 350.0 -21.65 12.0 -8.00 -0.30
9.710 300.0 -30.15 27.0 -12.10 0.20
10.978 250.0 -40.95 51.0 -16.60 -2.80
12.453 200.0 -53.65 88.0 -16.30 -4.80
14.238 150.0 -68.05 100.0 -24.40 -4.30
16.607 100.0 -78.55 49.0 -12.23 2.99
18.628 70.0 -77.75 -999.0 -18.66 4.33
20.613 50.0 -63.15 -999.0 -25.99 -5.43
23.824 30.0 -56.65 -999.0 -6.10 0.00
26.475 20.0 -44.95 -999.0 10.80 1.80
31.083 10.0 -44.15 -999.0 2.90 -0.30
Pressure Reduced to MSL (mb) 1014.3
3.160 700.0 8.95 66.0 -4.68 -3.62
3.769 650.0 3.45 74.0 -2.35 -4.22
4.414 600.0 0.95 23.0 -4.40 -1.74
5.111 550.0 -1.25 10.0 -1.21 1.21
5.863 500.0 -5.85 6.0 -2.59 -0.38
6.680 450.0 -10.35 10.0 -6.90 -1.80
7.579 400.0 -15.05 11.0 -8.30 -3.70
8.573 350.0 -23.05 14.0 -6.30 -4.20
9.678 300.0 -33.45 35.0 -8.30 0.00
10.933 250.0 -42.15 58.0 -15.80 11.70
12.402 200.0 -54.05 91.0 -16.50 15.00
14.186 150.0 -68.55 100.0 -14.90 7.05
16.532 100.0 -79.95 88.0 -7.67 -1.84
18.583 70.0 -70.95 -999.0 5.54 -6.72
20.573 50.0 -69.45 -999.0 12.64 -0.20
23.715 30.0 -63.35 -999.0 20.00 -2.10
26.234 20.0 -57.45 -999.0 6.90 10.70
30.654 10.0 -52.35 -999.0 -14.90 6.60
Pressure Reduced to MSL (mb) 1013.0
Pressure @tropopause (mb) 103.7
Altitude @tropopause (km) 16.326
Temperature @tropopause (deg C) -79.45
Column Water (cm) 2.27
Cloud Cover 0.0%
At 3 North 32 East
Relative Zonal Meridional
Altitude Pressure Temperature
Humidity Wind Wind
(km) (mb) (deg C) (%) (m/sec) (m/sec)
0.991 902.6 28.15 38.0 -999.00 -999.00
-999.000 -999.0 -999.00 -999.0 -999.00 -999.00
-999.000 -999.0 -999.00 -999.0 -999.00 -999.00
-999.000 -999.0 -999.00 -999.0 -999.00 -999.00
-999.000 -999.0 -999.00 -999.0 -999.00 -999.00
1.016 900.0 25.05 38.0 -1.08 0.20
1.515 850.0 21.85 40.0 -2.57 -0.57
2.037 800.0 18.15 48.0 -5.69 -2.11
2.586 750.0 13.55 58.0 -7.38 -2.27
3.162 700.0 8.65 70.0 -6.79 -1.40
3.771 650.0 3.45 84.0 -5.59 0.41
4.415 600.0 -0.45 58.0 -5.34 0.89
5.109 550.0 -1.55 10.0 -2.34 1.68
5.860 500.0 -6.35 10.0 -4.22 0.80
6.679 450.0 -9.45 13.0 -6.70 -2.50
7.580 400.0 -14.95 15.0 -6.10 -3.80
8.573 350.0 -22.75 12.0 -6.90 -1.40
9.681 300.0 -32.95 28.0 -3.10 -1.50
10.936 250.0 -42.35 59.0 -13.70 10.40
12.405 200.0 -54.35 97.0 -16.00 14.60
14.187 150.0 -68.75 99.0 -16.42 8.57
16.537 100.0 -80.35 90.0 -4.59 -2.92
18.580 70.0 -71.45 -999.0 5.87 -6.93
20.568 50.0 -69.25 -999.0 13.14 -0.62
23.709 30.0 -64.15 -999.0 19.90 -2.10
26.234 20.0 -56.55 -999.0 5.40 8.90
30.651 10.0 -53.55 -999.0 -15.10 4.40
Pressure Reduced to MSL (mb) 1012.6
Pressure @tropopause (mb) 100.0
Altitude @tropopause (km) 16.539
Temperature @tropopause (deg C) -80.35
Column Water (cm) 2.40
Cloud Cover 0.0%
At 3 North 33 East
Relative Zonal Meridional
Altitude Pressure Temperature
Humidity Wind Wind
(km) (mb) (deg C) (%) (m/sec) (m/sec)
1.020 899.5 28.45 39.0 -999.00 -999.00
-999.000 -999.0 -999.00 -999.0 -999.00 -999.00
-999.000 -999.0 -999.00 -999.0 -999.00 -999.00
-999.000 -999.0 -999.00 -999.0 -999.00 -999.00
-999.000 -999.0 -999.00 -999.0 -999.00 -999.00
1.513 850.0 21.65 44.0 -8.16 -3.06
2.036 800.0 17.95 46.0 -12.64 -1.85
2.584 750.0 13.65 58.0 -10.28 -2.11
3.161 700.0 8.85 67.0 -5.71 -2.46
3.769 650.0 3.75 73.0 -2.56 -2.06
4.414 600.0 0.25 41.0 -4.35 -1.94
5.110 550.0 -1.15 7.0 -2.94 1.05
5.862 500.0 -5.95 7.0 -3.83 1.10
6.680 450.0 -9.75 12.0 -7.30 -1.70
7.581 400.0 -14.75 13.0 -7.50 -2.60
8.575 350.0 -22.95 16.0 -6.90 -0.50
9.681 300.0 -33.45 36.0 -4.90 1.00
10.937 250.0 -41.65 38.0 -14.00 11.90
12.407 200.0 -54.25 88.0 -17.40 14.20
14.190 150.0 -68.85 100.0 -15.10 8.49
16.535 100.0 -80.05 91.0 -6.30 -1.91
18.583 70.0 -71.65 -999.0 6.59 -6.64
20.570 50.0 -69.55 -999.0 13.60 -0.92
23.709 30.0 -63.85 -999.0 19.80 -1.90
26.236 20.0 -56.55 -999.0 7.80 9.20
30.654 10.0 -53.05 -999.0 -14.00 5.30
Pressure Reduced to MSL (mb) 1012.7
Pressure @tropopause (mb) 102.4
Altitude @tropopause (km) 16.402
Temperature @tropopause (deg C) -79.55
Column Water (cm) 2.28
Cloud Cover 0.0%

The following four profiles are for the integer lat/long corners
on 2014-01-14 at GMT 12:00

At 2 North 32 East
Relative Zonal Meridional
Altitude Pressure Temperature
Humidity Wind Wind
(km) (mb) (deg C) (%) (m/sec) (m/sec)
1.043 893.3 32.25 28.0 -999.00 -999.00
1.072 894.0 21.95 89.0 -999.00 -999.00
-999.000 -999.0 -999.00 -999.0 -999.00 -999.00
-999.000 -999.0 -999.00 -999.0 -999.00 -999.00
-999.000 -999.0 -999.00 -999.0 -999.00 -999.00
-999.000 -999.0 -999.00 -999.0 -999.00 -999.00
-999.000 -999.0 -999.00 -999.0 -999.00 -999.00
1.508 850.0 18.45 87.0 -0.23 3.06
2.027 800.0 15.75 89.0 -3.27 0.98
2.575 750.0 13.15 83.0 -7.17 1.43
3.153 700.0 9.85 88.0 -10.10 1.84
3.766 650.0 5.85 100.0 -12.59 -0.19
4.418 600.0 2.25 100.0 -10.64 -2.71
5.118 550.0 -1.25 100.0 -8.00 -6.10
5.873 500.0 -5.45 91.0 -7.96 -4.82
6.693 450.0 -10.25 73.0 -6.82 -0.99
7.592 400.0 -15.35 53.0 -4.70 3.30
8.588 350.0 -21.85 68.0 -1.90 6.00
9.704 300.0 -30.15 69.0 0.10 3.50
10.973 250.0 -40.55 99.0 2.50 0.40
12.454 200.0 -52.55 100.0 9.77 -6.30
14.249 150.0 -67.25 100.0 11.42 -7.06
16.585 100.0 -82.55 96.0 6.03 3.32
18.618 70.0 -72.35 -999.0 0.50 -1.22
20.600 50.0 -69.25 -999.0 14.35 -1.73
23.729 30.0 -59.55 -999.0 10.40 -0.71
26.315 20.0 -53.05 -999.0 -16.70 -2.54
30.877 10.0 -43.25 -999.0 -26.89 5.10
Pressure Reduced to MSL (mb) 1013.1
Pressure @tropopause (mb) 102.6
Altitude @tropopause (km) 16.444
Temperature @tropopause (deg C) -82.25
Column Water (cm) 4.35
Cloud Cover 0.0%
At 3 North 32 East
Relative Zonal Meridional
Altitude Pressure Temperature
Humidity Wind Wind
(km) (mb) (deg C) (%) (m/sec) (m/sec)
0.991 902.2 20.35 98.0 -999.00 -999.00
-999.000 -999.0 -999.00 -999.0 -999.00 -999.00
-999.000 -999.0 -999.00 -999.0 -999.00 -999.00
-999.000 -999.0 -999.00 -999.0 -999.00 -999.00
-999.000 -999.0 -999.00 -999.0 -999.00 -999.00
1.012 900.0 20.05 96.0 -0.68 3.18
1.506 850.0 19.05 85.0 -4.65 6.46
2.026 800.0 15.85 90.0 -7.92 4.57
2.573 750.0 12.75 93.0 -9.34 3.99
3.151 700.0 9.25 99.0 -11.68 3.08
3.764 650.0 6.05 100.0 -13.03 1.11
4.418 600.0 3.05 100.0 -12.03 -1.66
5.120 550.0 -1.05 100.0 -8.85 -4.60
5.874 500.0 -5.85 100.0 -9.58 -5.76
6.694 450.0 -10.15 89.0 -6.69 -3.85
7.593 400.0 -15.35 53.0 -3.30 2.60
8.588 350.0 -22.05 60.0 -0.60 7.00
9.703 300.0 -30.55 77.0 0.30 6.50
10.969 250.0 -41.05 100.0 0.20 2.00
12.450 200.0 -52.45 99.0 8.48 -6.80
14.244 150.0 -67.35 100.0 8.88 -6.31
16.582 100.0 -81.95 93.0 4.53 4.35
18.619 70.0 -72.75 -999.0 -1.66 -2.76
20.600 50.0 -69.05 -999.0 12.79 -3.80
23.727 30.0 -59.25 -999.0 8.75 -2.45
26.317 20.0 -53.65 -999.0 -17.17 -2.19
30.884 10.0 -42.35 -999.0 -26.62 4.58
Pressure Reduced to MSL (mb) 1012.3
Pressure @tropopause (mb) 103.6
Altitude @tropopause (km) 16.386
Temperature @tropopause (deg C) -81.75
Column Water (cm) 4.78
Cloud Cover 0.0%
At 3 North 33 East
Relative Zonal Meridional
Altitude Pressure Temperature
Humidity Wind Wind
(km) (mb) (deg C) (%) (m/sec) (m/sec)
1.020 899.0 23.35 83.0 -999.00 -999.00
-999.000 -999.0 -999.00 -999.0 -999.00 -999.00
-999.000 -999.0 -999.00 -999.0 -999.00 -999.00
-999.000 -999.0 -999.00 -999.0 -999.00 -999.00
-999.000 -999.0 -999.00 -999.0 -999.00 -999.00
1.505 850.0 18.65 85.0 -5.17 2.65
2.025 800.0 15.95 83.0 -9.29 3.88
2.572 750.0 12.95 87.0 -11.36 4.22
3.150 700.0 9.75 97.0 -14.41 2.02
3.764 650.0 6.35 100.0 -13.85 -1.52
4.419 600.0 3.25 99.0 -9.46 -5.61
5.120 550.0 -1.05 97.0 -6.37 -6.38
5.875 500.0 -5.05 81.0 -6.66 -2.51
6.696 450.0 -10.15 70.0 -4.22 1.08
7.594 400.0 -15.45 45.0 -2.80 3.00
8.590 350.0 -21.65 29.0 -1.40 7.00
9.706 300.0 -30.25 53.0 -1.50 4.80
10.974 250.0 -40.85 85.0 1.70 -0.60
12.453 200.0 -52.55 100.0 6.73 -5.37
14.246 150.0 -67.45 100.0 9.22 -5.38

The following four profiles are for the integer lat/long corners
on 2015-04-23 at GMT 12:00

At 2 North 32 East
Relative Zonal Meridional
Altitude Pressure Temperature
Humidity Wind Wind
(km) (mb) (deg C) (%) (m/sec)
(m/sec)
1.115 888.2 27.65 62.0 -999.00 -
999.00
-999.000 -999.0 -999.00 -999.0 -999.00 -
999.00
-999.000 -999.0 -999.00 -999.0 -999.00 -
999.00
-999.000 -999.0 -999.00 -999.0 -999.00 -
999.00
-999.000 -999.0 -999.00 -999.0 -999.00 -
999.00
-999.000 -999.0 -999.00 -999.0 -999.00 -
999.00
1.503 850.0 24.05 56.0 -0.61 1.68
2.030 800.0 18.85 72.0 -1.50 1.84
2.580 750.0 13.55 93.0 -2.80 2.38
3.159 700.0 10.35 77.0 -6.80 -2.79
3.774 650.0 6.85 71.0 -8.94 -7.72
4.427 600.0 2.65 76.0 -9.77 -7.64
5.126 550.0 -1.65 72.0 -8.67 -5.71
5.879 500.0 -6.35 83.0 -6.17 -3.61
6.696 450.0 -10.95 93.0 -2.77 -0.12
7.594 400.0 -15.25 70.0 -1.40 2.30
8.588 350.0 -22.85 86.0 -1.00 2.70
9.700 300.0 -30.75 65.0 -2.00 2.50
10.968 250.0 -40.65 45.0 -0.80 2.10
12.445 200.0 -53.15 70.0 -0.30 2.40
14.236 150.0 -67.15 75.0 -1.81 1.15
16.591 100.0 -81.35 100.0 -5.49 -0.37
18.602 70.0 -76.35 -999.0 -1.78 1.14
20.559 50.0 -72.45 -999.0 -11.34 -0.77
23.663 30.0 -56.35 -999.0 -29.66 0.08
26.329 20.0 -48.15 -999.0 11.67 -2.81
30.958 10.0 -40.75 -999.0 13.91 -3.87
Pressure Reduced to MSL (mb) 1010.0
Pressure @tropopause (mb) 96.0
Altitude @tropopause (km) 16.822
Temperature @tropopause (deg C) -82.25
Column Water (cm) 3.87
Cloud Cover 0.0%
At 2 North 33 East
Relative Zonal Meridional
Altitude Pressure Temperature
Humidity Wind Wind
(km) (mb) (deg C) (%) (m/sec)
(m/sec)
1.059 893.9 30.55 44.0 -999.00 -
999.00
-999.000 -999.0 -999.00 -999.0 -999.00 -
999.00
-999.000 -999.0 -999.00 -999.0 -999.00 -
999.00
-999.000 -999.0 -999.00 -999.0 -999.00 -
999.00
-999.000 -999.0 -999.00 -999.0 -999.00 -
999.00
-999.000 -999.0 -999.00 -999.0 -999.00 -
999.00
1.503 850.0 23.85 54.0 -0.31 3.60
2.029 800.0 18.75 69.0 -1.07 3.25
2.579 750.0 13.45 89.0 -2.16 2.45
3.158 700.0 9.95 82.0 -6.63 -2.05
3.772 650.0 6.85 73.0 -9.23 -7.48
4.425 600.0 2.35 89.0 -8.29 -5.57
5.124 550.0 -1.25 68.0 -7.47 -3.61
5.878 500.0 -6.05 75.0 -5.58 -2.98
6.696 450.0 -10.85 88.0 -1.50 -0.77
7.593 400.0 -15.55 77.0 -1.30 1.00
8.588 350.0 -22.45 75.0 0.00 2.10
9.700 300.0 -30.75 71.0 -0.90 2.00
10.968 250.0 -40.65 37.0 -1.30 1.80
12.445 200.0 -53.45 47.0 -2.90 2.20
14.234 150.0 -67.15 68.0 -1.66 1.46
16.590 100.0 -81.25 100.0 -5.17 0.14
18.602 70.0 -75.95 -999.0 -2.12 0.74
20.558 50.0 -72.75 -999.0 -10.67 -0.74
23.659 30.0 -56.55 -999.0 -30.34 0.08
26.329 20.0 -47.65 -999.0 12.71 -3.00
30.957 10.0 -40.95 -999.0 13.49 -2.76
Pressure Reduced to MSL (mb) 1009.9
Pressure @tropopause (mb) 94.5
Altitude @tropopause (km) 16.905
Temperature @tropopause (deg C) -82.75
Column Water (cm) 3.89
Cloud Cover 0.0%
At 3 North 32 East
Relative Zonal Meridional
Altitude Pressure Temperature
Humidity Wind Wind
(km) (mb) (deg C) (%) (m/sec)
(m/sec)
1.020 897.8 29.55 52.0 -999.00 -
999.00
-999.000 -999.0 -999.00 -999.0 -999.00 -
999.00
-999.000 -999.0 -999.00 -999.0 -999.00 -
999.00
-999.000 -999.0 -999.00 -999.0 -999.00 -
999.00
-999.000 -999.0 -999.00 -999.0 -999.00 -
999.00
-999.000 -999.0 -999.00 -999.0 -999.00 -
999.00
1.503 850.0 23.55 60.0 -1.19 2.81
2.029 800.0 18.45 77.0 -1.97 2.56
2.579 750.0 13.45 95.0 -3.44 2.09
3.158 700.0 10.55 77.0 -5.83 -3.19
3.773 650.0 6.95 73.0 -7.25 -6.56
4.426 600.0 2.55 77.0 -8.15 -7.91
5.125 550.0 -1.85 70.0 -7.72 -7.35
5.878 500.0 -6.35 80.0 -5.20 -3.19
Pressure @tropopause (mb) 92.3
Altitude @tropopause (km) 17.062
Temperature @tropopause (deg C) -80.45
Column Water (cm) 3.40
Cloud Cover 0.0%

The following four profiles are for the integer lat/long corners
on 2015-06-10 at GMT 12:00

At 2 North 32 East
Relative Zonal Meridional
Altitude Pressure Temperature
Humidity Wind Wind
(km) (mb) (deg C) (%) (m/sec) (m/sec)
1.115 888.3 26.75 74.0 -999.00 -999.00
-999.000 -999.0 -999.00 -999.0 -999.00 -
999.00
-999.000 -999.0 -999.00 -999.0 -999.00 -
999.00
-999.000 -999.0 -999.00 -999.0 -999.00 -
999.00
-999.000 -999.0 -999.00 -999.0 -999.00 -
999.00
-999.000 -999.0 -999.00 -999.0 -999.00 -
999.00
1.503 850.0 22.65 67.0 1.29 3.73
2.027 800.0 17.55 82.0 0.90 4.16
2.576 750.0 13.15 91.0 0.80 5.17
3.155 700.0 10.35 67.0 -3.21 2.16
3.769 650.0 7.05 67.0 -8.58 -2.03
4.423 600.0 2.95 78.0 -7.61 -0.96
5.124 550.0 -0.55 53.0 -6.74 -2.08
5.879 500.0 -5.05 48.0 -2.35 -0.79
6.699 450.0 -10.45 62.0 -2.52 0.80
7.596 400.0 -15.85 43.0 -4.20 1.50
8.590 350.0 -22.05 31.0 -6.60 1.60
9.705 300.0 -30.45 41.0 -9.10 0.90
10.972 250.0 -41.05 79.0 -18.80 -1.40
12.447 200.0 -53.55 100.0 -21.10 -5.10
14.233 150.0 -68.15 100.0 -27.40 -4.00
16.606 100.0 -78.25 45.0 -10.95 0.69
18.626 70.0 -77.75 -999.0 -17.01 3.63
20.620 50.0 -63.25 -999.0 -25.37 -4.22
23.815 30.0 -57.05 -999.0 -3.36 1.50
26.461 20.0 -47.95 -999.0 18.90 0.90
31.045 10.0 -43.25 -999.0 4.60 -3.80
Pressure Reduced to MSL (mb) 1010.1
Pressure @tropopause (mb) 91.1
Altitude @tropopause (km) 17.133
Temperature @tropopause (deg C) -80.15
Column Water (cm) 3.68
Cloud Cover 0.0%
At 2 North 33 East
Relative Zonal Meridional
Altitude Pressure Temperature
Humidity Wind Wind
(km) (mb) (deg C) (%) (m/sec) (m/sec)
1.059 893.9 29.45 51.0 -999.00 -999.00
-999.000 -999.0 -999.00 -999.0 -999.00 -
999.00
-999.000 -999.0 -999.00 -999.0 -999.00 -
999.00
-999.000 -999.0 -999.00 -999.0 -999.00 -
999.00
-999.000 -999.0 -999.00 -999.0 -999.00 -
999.00
-999.000 -999.0 -999.00 -999.0 -999.00 -
999.00
1.502 850.0 22.75 61.0 0.46 4.65
2.026 800.0 17.75 76.0 0.13 4.63
2.575 750.0 13.25 84.0 -0.23 3.99
3.154 700.0 10.25 71.0 -1.92 0.12
3.768 650.0 6.75 74.0 -8.00 -2.28
4.422 600.0 3.05 76.0 -8.04 -3.07
5.122 550.0 -0.55 56.0 -6.50 -3.52
5.878 500.0 -4.85 40.0 -1.98 -2.37
6.698 450.0 -10.45 52.0 -1.30 0.10
7.596 400.0 -15.65 47.0 -4.00 1.50
8.590 350.0 -22.05 38.0 -6.40 1.10
9.705 300.0 -30.55 51.0 -9.50 -0.10
10.971 250.0 -41.15 88.0 -18.30 -2.80
12.447 200.0 -53.35 100.0 -21.20 -6.40
14.232 150.0 -68.65 100.0 -25.00 -4.30
16.605 100.0 -77.85 43.0 -10.98 0.24
18.627 70.0 -77.95 -999.0 -16.33 3.89
20.616 50.0 -63.45 -999.0 -25.84 -4.13
23.813 30.0 -56.95 -999.0 -2.89 1.52
26.460 20.0 -47.55 -999.0 19.40 1.20
31.044 10.0 -43.35 -999.0 4.40 -3.60
Pressure Reduced to MSL (mb) 1010.2
Pressure @tropopause (mb) 90.7
Altitude @tropopause (km) 17.162
Temperature @tropopause (deg C) -79.95
Column Water (cm) 3.62
Cloud Cover 0.0%
At 3 North 32 East
Relative Zonal Meridional
Altitude Pressure Temperature
Humidity Wind Wind
(km) (mb) (deg C) (%) (m/sec) (m/sec)
1.020 897.7 29.15 55.0 -999.00 -999.00
-999.000 -999.0 -999.00 -999.0 -999.00 -
999.00
-999.000 -999.0 -999.00 -999.0 -999.00 -
999.00
-999.000 -999.0 -999.00 -999.0 -999.00 -
999.00
-999.000 -999.0 -999.00 -999.0 -999.00 -
999.00
-999.000 -999.0 -999.00 -999.0 -999.00 -
-999.000 -999.0 -999.00 -999.0 -999.00 -999.00
-999.000 -999.0 -999.00 -999.0 -999.00 -999.00
-999.000 -999.0 -999.00 -999.0 -999.00 -999.00
-999.000 -999.0 -999.00 -999.0 -999.00 -999.00
-999.000 -999.0 -999.00 -999.0 -999.00 -999.00
1.483 850.0 26.05 33.0 -1.72 -3.08
2.012 800.0 20.85 42.0 -2.46 -3.07
2.565 750.0 15.55 54.0 -3.22 -3.03
3.145 700.0 9.85 73.0 -4.23 -3.08
3.756 650.0 4.15 96.0 -5.78 -3.46
4.404 600.0 1.45 29.0 -5.87 -1.09
5.101 550.0 -1.45 12.0 -3.95 1.20
5.854 500.0 -4.75 7.0 -5.23 0.98
6.676 450.0 -9.15 10.0 -6.70 -0.10
7.576 400.0 -15.05 12.0 -7.70 -2.10
8.570 350.0 -23.35 17.0 -7.60 -3.30
9.674 300.0 -32.95 32.0 -8.80 0.00
10.933 250.0 -41.75 58.0 -15.40 11.20
12.405 200.0 -53.65 72.0 -15.70 13.90
14.192 150.0 -68.25 97.0 -13.56 6.20
16.530 100.0 -81.55 100.0 -9.96 -2.85
18.585 70.0 -69.45 -999.0 6.65 -5.30
20.573 50.0 -69.85 -999.0 10.87 2.74
23.685 30.0 -65.85 -999.0 17.10 1.00
26.191 20.0 -58.25 -999.0 4.20 2.80
30.654 10.0 -48.75 -999.0 -23.20 8.50
Pressure Reduced to MSL (mb) 1007.2
Pressure @tropopause (mb) 103.6
Altitude @tropopause (km) 16.334
Temperature @tropopause (deg C) -80.85
Column Water (cm) 2.41
Cloud Cover 0.0%
At 2 North 33 East
Relative Zonal Meridional
Altitude Pressure Temperature
Humidity Wind Wind
(km) (mb) (deg C) (%) (m/sec) (m/sec)
1.072 890.1 37.45 25.0 -999.00 -999.00
-999.000 -999.0 -999.00 -999.0 -999.00 -999.00
-999.000 -999.0 -999.00 -999.0 -999.00 -999.00
-999.000 -999.0 -999.00 -999.0 -999.00 -999.00
-999.000 -999.0 -999.00 -999.0 -999.00 -999.00
-999.000 -999.0 -999.00 -999.0 -999.00 -999.00
1.481 850.0 26.45 31.0 -2.94 -1.84
2.011 800.0 21.35 39.0 -3.44 -2.34
2.565 750.0 15.95 51.0 -3.90 -2.88
3.145 700.0 10.35 69.0 -4.43 -3.55
3.757 650.0 4.55 90.0 -5.12 -4.37
4.404 600.0 0.65 57.0 -5.73 -3.11
5.101 550.0 -1.15 10.0 -3.92 0.40
5.854 500.0 -5.45 9.0 -5.66 0.31
6.674 450.0 -9.35 12.0 -8.00 -0.50
7.575 400.0 -14.65 11.0 -8.00 -2.40
8.569 350.0 -23.15 15.0 -7.70 -3.40
9.675 300.0 -32.75 23.0 -10.00 -0.50
10.934 250.0 -41.55 44.0 -14.10 10.00
12.407 200.0 -53.75 85.0 -16.00 14.90
14.191 150.0 -68.45 99.0 -16.09 7.44
16.531 100.0 -80.75 94.0 -7.86 -3.38
18.583 70.0 -70.25 -999.0 5.17 -5.38
20.572 50.0 -70.05 -999.0 10.58 3.70
23.684 30.0 -65.95 -999.0 18.10 0.80
26.190 20.0 -57.65 -999.0 3.60 4.00
30.654 10.0 -48.35 -999.0 -24.40 8.80
Pressure Reduced to MSL (mb) 1007.4
Pressure @tropopause (mb) 103.5
Altitude @tropopause (km) 16.336
Temperature @tropopause (deg C) -80.05
Column Water (cm) 2.39
Cloud Cover 0.0%
At 3 North 32 East
Relative Zonal Meridional
Altitude Pressure Temperature
Humidity Wind Wind
(km) (mb) (deg C) (%) (m/sec) (m/sec)
0.991 898.5 32.15 26.0 -999.00 -999.00
-999.000 -999.0 -999.00 -999.0 -999.00 -999.00
-999.000 -999.0 -999.00 -999.0 -999.00 -999.00
-999.000 -999.0 -999.00 -999.0 -999.00 -999.00
-999.000 -999.0 -999.00 -999.0 -999.00 -999.00
-999.000 -999.0 -999.00 -999.0 -999.00 -999.00
1.484 850.0 26.45 30.0 -2.70 -2.80
2.013 800.0 21.35 39.0 -3.31 -2.73
2.567 750.0 15.95 50.0 -3.89 -2.53
3.148 700.0 10.25 69.0 -4.58 -2.20
3.759 650.0 4.55 93.0 -5.55 -1.57
4.406 600.0 0.45 73.0 -7.02 -0.13
5.102 550.0 -1.35 8.0 -3.90 1.80
5.855 500.0 -5.15 7.0 -5.41 1.44
6.675 450.0 -9.35 12.0 -6.60 -1.10
7.575 400.0 -14.95 14.0 -7.00 -1.50
8.570 350.0 -22.85 14.0 -7.10 -0.60
9.677 300.0 -32.85 23.0 -9.50 1.90
10.935 250.0 -41.85 46.0 -14.30 10.70
12.406 200.0 -53.95 83.0 -15.10 14.50
14.189 150.0 -68.45 100.0 -18.41 9.34
16.532 100.0 -81.65 100.0 -7.85 -2.80
18.585 70.0 -69.25 -999.0 7.85 -5.45
20.570 50.0 -69.65 -999.0 12.56 2.38
23.685 30.0 -64.85 -999.0 18.60 2.70
26.194 20.0 -58.35 -999.0 3.90 3.20
30.659 10.0 -47.45 -999.0 -20.60 7.20
Pressure Reduced to MSL (mb) 1007.1
Pressure @tropopause (mb) 101.4
Altitude @tropopause (km) 16.456
Temperature @tropopause (deg C) -81.15
Column Water (cm) 2.49
Cloud Cover 0.0%
At 3 North 33 East
Relative Zonal Meridional
Altitude Pressure Temperature
Humidity Wind Wind
16.583 100.0 -81.95 90.0 4.74 5.33
18.619 70.0 -72.35 -999.0 -1.19 -2.10
20.601 50.0 -69.45 -999.0 14.30 -2.81
23.728 30.0 -59.85 -999.0 8.19 0.56
26.318 20.0 -53.85 -999.0 -17.14 -
2.71
30.885 10.0 -42.15 -999.0 -26.64 5.75
Pressure Reduced to MSL (mb) 1012.3
Pressure @tropopause (mb) 103.7
Altitude @tropopause (km) 16.378
Temperature @tropopause (deg C) -81.75
Column Water (cm) 4.39
Cloud Cover 0.0%

The following four profiles are for the integer lat/long corners
on 2014-04-20 at GMT 12:00

At 2 North 32 East
Relative Zonal Meridional
Altitude Pressure Temperature
Humidity Wind Wind
(km) (mb) (deg C) (%) (m/sec)
(m/sec)
1.043 893.1 26.55 78.0 -999.00 -
999.00
-999.000 -999.0 -999.00 -999.0 -999.00 -
999.00
-999.000 -999.0 -999.00 -999.0 -999.00 -
999.00
-999.000 -999.0 -999.00 -999.0 -999.00 -
999.00
-999.000 -999.0 -999.00 -999.0 -999.00 -
999.00
-999.000 -999.0 -999.00 -999.0 -999.00 -
999.00
1.477 850.0 21.75 76.0 0.15 3.00
2.000 800.0 16.95 92.0 -0.97 3.33
2.549 750.0 13.55 91.0 -3.91 3.87
3.129 700.0 11.15 76.0 -10.91 2.32
3.746 650.0 7.85 79.0 -12.73 0.03
4.403 600.0 4.05 84.0 -9.89 -3.52
5.106 550.0 -0.15 85.0 -6.89 -4.93
5.863 500.0 -4.85 78.0 -7.31 -2.69
6.686 450.0 -9.35 71.0 -5.26 0.28
7.587 400.0 -14.85 85.0 -3.90 1.90
8.586 350.0 -21.05 73.0 -3.50 4.20
9.705 300.0 -29.45 56.0 1.20 1.50
10.978 250.0 -39.95 75.0 5.50 -2.10
12.462 200.0 -51.95 100.0 5.37 -6.53
14.259 150.0 -67.65 100.0 6.23 -4.55
16.602 100.0 -81.15 87.0 3.25 3.50
18.633 70.0 -74.25 -999.0 3.12 -4.26
20.596 50.0 -69.35 -999.0 13.02 0.91
23.728 30.0 -58.25 -999.0 10.47 -2.52
26.311 20.0 -52.95 -999.0 -15.67 -
3.22
30.873 10.0 -43.05 -999.0 -25.40 2.14
Pressure Reduced to MSL (mb) 1008.2
Pressure @tropopause (mb) 101.7
Altitude @tropopause (km) 16.505
Temperature @tropopause (deg C) -80.95
Column Water (cm) 4.44
Cloud Cover 0.0%
At 2 North 33 East
Relative Zonal Meridional
Altitude Pressure Temperature
Humidity Wind Wind
(km) (mb) (deg C) (%) (m/sec)
(m/sec)
1.072 889.8 28.85 58.0 -999.00 -
999.00
-999.000 -999.0 -999.00 -999.0 -999.00 -
999.00
-999.000 -999.0 -999.00 -999.0 -999.00 -
999.00
-999.000 -999.0 -999.00 -999.0 -999.00 -
999.00
-999.000 -999.0 -999.00 -999.0 -999.00 -
999.00
-999.000 -999.0 -999.00 -999.0 -999.00 -
999.00
1.474 850.0 22.85 65.0 -1.77 1.78
1.999 800.0 18.05 80.0 -3.17 1.61
2.549 750.0 13.45 95.0 -6.39 1.17
3.129 700.0 11.25 75.0 -12.97 0.21
3.746 650.0 8.15 75.0 -11.75 -1.46
4.403 600.0 3.65 94.0 -7.66 -2.68
5.106 550.0 -0.45 88.0 -7.74 -4.96
5.862 500.0 -4.75 80.0 -7.56 -3.59
6.685 450.0 -8.85 51.0 -6.24 0.49
7.588 400.0 -14.15 53.0 -2.80 4.50
8.588 350.0 -21.05 62.0 -1.30 5.40
9.706 300.0 -30.05 75.0 1.90 3.60
10.976 250.0 -40.15 87.0 2.70 0.10
12.459 200.0 -52.15 93.0 7.33 -5.11
14.256 150.0 -67.45 99.0 7.92 -5.65
16.603 100.0 -81.65 90.0 2.45 3.14
18.633 70.0 -73.75 -999.0 5.23 -4.12
20.593 50.0 -69.35 -999.0 14.07 1.81
23.725 30.0 -58.65 -999.0 10.48 -2.40
26.312 20.0 -52.35 -999.0 -15.96 -
2.76
30.872 10.0 -42.85 -999.0 -24.90 1.95
Pressure Reduced to MSL (mb) 1007.1
Pressure @tropopause (mb) 99.6
Altitude @tropopause (km) 16.628
Temperature @tropopause (deg C) -81.65
Column Water (cm) 4.20
Cloud Cover 0.0%
At 3 North 32 East
Relative Zonal Meridional
Altitude Pressure Temperature
Humidity Wind Wind
(km) (mb) (deg C) (%) (m/sec)
(m/sec)
0.991 899.0 27.05 79.0 -999.00 -
999.00
-999.000 -999.0 -999.00 -999.0 -999.00 -
999.00

6.695 450.0 -11.05 93.0 -3.95 1.38
7.592 400.0 -15.35 77.0 -0.60 1.90
8.588 350.0 -22.25 68.0 -0.90 2.60
9.701 300.0 -30.75 69.0 -1.50 3.60
10.968 250.0 -40.95 69.0 0.00 3.00
12.443 200.0 -53.35 65.0 -1.20 2.50
14.236 150.0 -66.65 68.0 -1.70 1.41
16.591 100.0 -81.85 100.0 -3.94 1.40
18.600 70.0 -76.05 -999.0 -1.88 0.76
20.558 50.0 -72.45 -999.0 -11.07 -0.27
23.665 30.0 -56.15 -999.0 -29.02 -0.26
26.326 20.0 -48.35 -999.0 8.30 -2.55
30.953 10.0 -40.45 -999.0 12.40 -3.08
Pressure Reduced to MSL (mb) 1009.3
Pressure @tropopause (mb) 95.8
Altitude @tropopause (km) 16.829
Temperature @tropopause (deg C) -83.05
Column Water (cm) 4.09
Cloud Cover 0.0%
At 3 North 33 East
Relative Zonal Meridional
Altitude Pressure Temperature
Humidity Wind Wind
(km) (mb) (deg C) (%) (m/sec)
(m/sec)
1.027 896.7 30.35 43.0 -999.00 -
999.00
-999.000 -999.0 -999.00 -999.0 -999.00 -
999.00
-999.000 -999.0 -999.00 -999.0 -999.00 -
999.00
-999.000 -999.0 -999.00 -999.0 -999.00 -
999.00
-999.000 -999.0 -999.00 -999.0 -999.00 -
999.00
-999.000 -999.0 -999.00 -999.0 -999.00 -
999.00
1.501 850.0 25.15 47.0 -1.86 1.87
2.029 800.0 19.95 61.0 -2.17 1.70
2.581 750.0 14.45 81.0 -2.49 1.52
3.160 700.0 9.25 100.0 -3.99 -0.57
3.772 650.0 6.35 72.0 -8.86 -8.05
4.425 600.0 2.35 80.0 -8.68 -7.85
5.124 550.0 -1.35 66.0 -7.88 -5.46
5.878 500.0 -5.95 72.0 -5.01 -2.80
6.696 450.0 -10.75 79.0 -2.96 0.18
7.593 400.0 -15.85 79.0 -0.20 1.60
8.588 350.0 -22.15 63.0 -0.10 1.40
9.702 300.0 -30.65 59.0 -1.10 2.00
10.969 250.0 -40.85 52.0 -0.40 0.90
12.445 200.0 -53.35 57.0 -2.30 0.80
14.235 150.0 -67.15 57.0 -3.09 1.42
16.591 100.0 -81.55 100.0 -3.57 1.40
18.603 70.0 -75.85 -999.0 -2.29 0.40
20.558 50.0 -72.75 -999.0 -10.34 -0.31
23.662 30.0 -56.25 -999.0 -29.71 -0.19
26.327 20.0 -47.95 -999.0 9.10 -2.69
30.954 10.0 -40.75 -999.0 11.86 -1.93
Pressure Reduced to MSL (mb) 1009.4
Pressure @tropopause (mb) 95.4
Altitude @tropopause (km) 16.853
Temperature @tropopause (deg C) -82.95
Column Water (cm) 3.83
Cloud Cover 0.0%
Attachments area

999.00
1.501 850.0 23.35 61.0 0.77 4.84
2.027 800.0 18.25 77.0 0.38 5.14
2.577 750.0 13.45 89.0 -0.44 4.57
3.156 700.0 10.55 66.0 -2.99 -0.89
3.770 650.0 6.95 64.0 -6.90 -3.07
4.424 600.0 2.95 75.0 -7.74 -2.35
5.124 550.0 -0.75 62.0 -8.13 -2.23
5.880 500.0 -5.05 44.0 -5.98 -1.87
6.700 450.0 -10.05 23.0 -3.95 -0.70
7.596 400.0 -16.25 23.0 -4.00 1.50
8.589 350.0 -22.45 24.0 -7.30 1.90
9.703 300.0 -30.45 44.0 -12.70 2.20
10.971 250.0 -40.65 75.0 -19.40 -1.60
12.447 200.0 -53.55 100.0 -18.90 -5.90
14.231 150.0 -68.35 99.0 -28.60 -4.00
16.608 100.0 -77.95 49.0 -11.01 0.17
18.627 70.0 -77.65 -999.0 -17.35 4.56
20.621 50.0 -63.65 -999.0 -26.24 -5.53
23.813 30.0 -56.85 -999.0 -5.28 1.75
26.458 20.0 -47.85 -999.0 14.50 1.30
31.047 10.0 -43.05 -999.0 1.70 -3.60
Pressure Reduced to MSL (mb) 1009.6
Pressure @tropopause (mb) 90.1
Altitude @tropopause (km) 17.202
Temperature @tropopause (deg C) -80.35
Column Water (cm) 3.62
Cloud Cover 0.0%
At 3 North 33 East
Relative Zonal Meridional
Altitude Pressure Temperature
Humidity Wind Wind
(km) (mb) (deg C) (%) (m/sec) (m/sec)
1.027 897.2 29.05 62.0 -999.00 -999.00
-999.000 -999.0 -999.00 -999.0 -999.00 -
999.00
-999.000 -999.0 -999.00 -999.0 -999.00 -
999.00
-999.000 -999.0 -999.00 -999.0 -999.00 -
999.00
-999.000 -999.0 -999.00 -999.0 -999.00 -
999.00
1.503 850.0 22.85 62.0 1.25 1.54
2.027 800.0 17.85 78.0 1.01 1.59
2.577 750.0 13.45 88.0 0.74 1.74
3.156 700.0 10.25 74.0 -1.72 0.45
3.769 650.0 6.65 74.0 -6.38 -1.83
4.423 600.0 2.85 82.0 -7.96 -2.37
5.123 550.0 -0.95 73.0 -7.85 -2.19
5.879 500.0 -4.95 52.0 -4.78 -2.30
6.700 450.0 -10.05 38.0 -2.81 -1.10
7.597 400.0 -16.05 49.0 -3.90 0.80
8.590 350.0 -22.15 51.0 -6.90 1.10
9.705 300.0 -30.35 56.0 -14.30 1.10
10.974 250.0 -40.75 76.0 -18.90 -2.20
12.450 200.0 -53.25 100.0 -18.90 -5.20
14.236 150.0 -68.55 100.0 -26.00 -2.80
16.607 100.0 -77.85 47.0 -12.15 -0.66
18.629 70.0 -77.65 -999.0 -16.71 5.02
20.618 50.0 -63.85 -999.0 -26.69 -5.40
23.813 30.0 -56.65 -999.0 -4.93 1.95
26.460 20.0 -47.45 -999.0 14.70 1.80
31.047 10.0 -43.25 -999.0 1.50 -3.40
Pressure Reduced to MSL (mb) 1009.7
Pressure @tropopause (mb) 90.5
Altitude @tropopause (km) 17.172
Temperature @tropopause (deg C) -79.95
Column Water (cm) 3.84
Cloud Cover 0.0%

(km) (mb) (deg C) (%) (m/sec) (m/sec)
1.020 895.3 35.35 23.0 -999.00 -999.00
-999.000 -999.0 -999.00 -999.0 -999.00 -999.00
-999.000 -999.0 -999.00 -999.0 -999.00 -999.00
-999.000 -999.0 -999.00 -999.0 -999.00 -999.00
-999.000 -999.0 -999.00 -999.0 -999.00 -999.00
-999.000 -999.0 -999.00 -999.0 -999.00 -999.00
1.482 850.0 26.95 28.0 -5.29 -2.60
2.012 800.0 21.75 36.0 -5.77 -2.58
2.566 750.0 16.35 47.0 -6.09 -2.44
3.148 700.0 10.65 64.0 -6.29 -2.21
3.759 650.0 4.55 88.0 -6.34 -1.89
4.406 600.0 0.15 76.0 -5.33 -0.71
5.102 550.0 -1.05 8.0 -4.42 1.95
5.855 500.0 -5.45 10.0 -5.80 1.46
6.675 450.0 -9.55 13.0 -7.90 -1.50
7.575 400.0 -14.85 11.0 -7.60 -2.20
8.569 350.0 -23.05 13.0 -7.70 -1.90
9.676 300.0 -32.55 18.0 -12.10 -1.10
10.934 250.0 -41.95 38.0 -13.40 10.10
12.405 200.0 -53.85 86.0 -16.60 15.20
14.189 150.0 -68.45 100.0 -19.17 10.09
16.533 100.0 -81.05 95.0 -7.44 -4.34
18.583 70.0 -69.95 -999.0 8.51 -6.58
20.570 50.0 -70.15 -999.0 12.18 2.92
23.684 30.0 -65.15 -999.0 19.10 3.10
26.193 20.0 -58.25 -999.0 4.20 3.80
30.651 10.0 -47.95 -999.0 -22.80 9.70
Pressure Reduced to MSL (mb) 1007.3
Pressure @tropopause (mb) 101.4
Altitude @tropopause (km) 16.455
Temperature @tropopause (deg C) -80.55
Column Water (cm) 2.39
Cloud Cover 0.0%

-999.000 -999.0 -999.00 -999.0 -999.00 -
999.00
-999.000 -999.0 -999.00 -999.0 -999.00 -
999.00
-999.000 -999.0 -999.00 -999.0 -999.00 -
999.00
-999.000 -999.0 -999.00 -999.0 -999.00 -
999.00
1.480 850.0 20.35 85.0 -0.42 1.99
2.002 800.0 16.35 96.0 -2.01 2.85
2.550 750.0 13.65 88.0 -7.03 3.80
3.130 700.0 10.85 85.0 -12.69 2.60
3.747 650.0 7.55 88.0 -12.03 0.38
4.403 600.0 3.75 93.0 -8.67 -2.35
5.106 550.0 -0.15 81.0 -7.65 -4.73
5.864 500.0 -4.65 70.0 -7.17 -4.45
6.685 450.0 -10.05 78.0 -5.99 0.91
7.584 400.0 -15.45 89.0 -4.00 5.30
8.581 350.0 -21.25 77.0 -2.00 6.90
9.701 300.0 -29.35 70.0 1.80 4.00
10.974 250.0 -39.75 97.0 0.80 1.30
12.459 200.0 -51.85 100.0 2.45 -4.55
14.258 150.0 -67.35 100.0 2.36 -4.58
16.606 100.0 -79.75 67.0 2.95 1.37
18.631 70.0 -75.95 -999.0 -0.06 -4.74
20.595 50.0 -68.65 -999.0 12.08 0.36
23.726 30.0 -57.95 -999.0 10.63 -2.40
26.313 20.0 -53.55 -999.0 -15.85 -
1.93
30.872 10.0 -43.45 -999.0 -25.20 2.97
Pressure Reduced to MSL (mb) 1008.2
Pressure @tropopause (mb) 102.5
Altitude @tropopause (km) 16.468
Temperature @tropopause (deg C) -79.55
Column Water (cm) 4.63
Cloud Cover 0.0%
At 3 North 33 East
Relative Zonal Meridional
Altitude Pressure Temperature
Humidity Wind Wind
(km) (mb) (deg C) (%) (m/sec)
(m/sec)
1.020 895.2 29.25 59.0 -999.00 -
999.00
-999.000 -999.0 -999.00 -999.0 -999.00 -
999.00
-999.000 -999.0 -999.00 -999.0 -999.00 -
999.00
-999.000 -999.0 -999.00 -999.0 -999.00 -
999.00
-999.000 -999.0 -999.00 -999.0 -999.00 -
999.00
-999.000 -999.0 -999.00 -999.0 -999.00 -
999.00
1.475 850.0 23.05 64.0 -5.18 1.37
2.001 800.0 17.95 81.0 -6.46 1.13
2.550 750.0 13.35 97.0 -8.78 0.69
3.130 700.0 10.85 84.0 -12.88 -0.03
3.746 650.0 8.05 78.0 -11.24 -1.20
4.403 600.0 3.75 88.0 -7.93 -2.59
5.106 550.0 -0.25 80.0 -7.11 -4.44
5.863 500.0 -4.75 70.0 -6.60 -4.14
6.685 450.0 -9.75 62.0 -6.14 -1.24
7.585 400.0 -15.05 46.0 -3.70 5.40
8.582 350.0 -21.25 53.0 -0.80 8.30
9.701 300.0 -29.65 67.0 0.00 4.70
10.974 250.0 -39.75 84.0 0.80 -0.70
12.458 200.0 -52.15 100.0 3.51 -3.67
14.255 150.0 -67.15 100.0 5.79 -5.39
16.606 100.0 -80.05 69.0 1.64 1.44
18.630 70.0 -75.65 -999.0 0.18 -3.45
20.591 50.0 -68.45 -999.0 13.05 1.66
23.726 30.0 -58.45 -999.0 10.23 -3.07
26.312 20.0 -52.85 -999.0 -16.43 -
2.09
30.873 10.0 -43.05 -999.0 -24.32 2.50
Pressure Reduced to MSL (mb) 1007.2
Pressure @tropopause (mb) 96.4
Altitude @tropopause (km) 16.810
Temperature @tropopause (deg C) -80.65
Column Water (cm) 4.28
Cloud Cover 0.0%
Attachments area

ANNEX REFERENCES

Monteith, J. L. 1965. “Evaporation and Environment.” In: The state and movement of water in living organism. 19th Symp. Soc. Exptl. Biol. P. 205-234.

Penman, H. L. 1948. “Natural evaporation from open water, bare soil and grass.” Proceedings of the Royal Society of London. Series A, Mathematical and Physical Sciences, Vol. 193, No. 1032, p. 120-145.

Allen, R.G., L.S. Pereira, D. Raes, and M. Smith. 1998. “Crop evapotranspiration: guidelines for computing crop water requirements.” Irrigation and Drainage Paper No. 56, Food and Agriculture Organization of the United Nations, Rome, Italy.

Allen, R. G., Walter, I. A., Elliot, R. L., Howell, T.A., Itenfisu, D., Jensen, M. E. and Snyder, R. 2005. The ASCE standardized reference evapotranspiration equation. ASCE and American Society of Civil Engineers.

Annex FIGURES

Annex TABLES